THE HERZEN STATE PEDAGOGICAL
UNIVERSITY OF RUSSIA

VORONOV YAROSLAV VLADIMIROVICH

THEORETICAL INVESTIGATIONS OF INELASTIC COLLISIONS OF ATOMS AND IONS OF DIFFERENT CHEMICAL ELEMENTS WITH HYDROGEN ATOMS AND IONS

Specialization 1.3.3. Theoretical physics

Thesis is submitted for the degree
of Candidate of Physical and Mathematical Sciences

Translation from Russian

Scientific advisor:
Dr. Sci. (Phys.-Math.), professor
A. K. Belyaev

Saint-Petersburg
2023

Contents

Introduction

Inelastic processes in collisions of atoms, molecules, and ions of various chemical elements determine the properties of gas and plasma media, such as gas laser media, planetary atmospheres, star photospheres, and so on. Astrophysical research plays an important role in modern science because it allows us to learn and understand the laws and evolution of the Universe. The essence of astrophysical research has been and remains unchanged – observation of the spectra in various ranges of electromagnetic waves. Based on the absorption spectra obtained, conclusions can be drawn about the qualitative and quantitative composition of stars.

The main source of spectra is stars. The spectrum of stars is a continuous spectrum with absorption lines. The qualitative composition is quite easy to determine, because each chemical element has a unique spectrum that allows it to be distinguished from other elements. But determining the quantitative composition is a rather difficult. Since only spectra are experimentally observed, the analysis of the quantitative composition is possible based on the study of the characteristics of spectral absorption lines - width, depth, shape. These characteristics are influenced by many factors. Therefore, it is necessary to construct a model spectral lines of the element and, by varying the parameters, obtain a coincidence of the modelled line and the experimentally observed one. Since there are many parameters, and their various combinations can lead to the same result, it is necessary to determine as many unknown parameters as possible by calculating their exact or approximate values in some way.

Such parameters are the rate coefficients of the inelastic processes in collisions of atoms with other particles. Collisions with hydrogen atoms and ions plays the main role, which is due to the high abundance of these particles in the stars photospheres, as well as with electrons. In particular, taking into account inelastic collisions plays an important role for stars of spectral classes F, G, K with a low abundance of heavy elements[1],

[1]So-called low metallicity, metals mean elements heavier than helium.

because for such cases the assumption of local thermodynamic equilibrium in modeling leads to unsatisfactory results (see, for example, recent work [1, 2]). It is necessary to take into account the deviation from the local thermodynamic equilibrium, and the accuracy of the inelastic processes rate coefficients can very significantly affect the final result.

Therefore, the study and analysis of inelastic processes at low-energy (10^{-2} – 10^{2} eV) collisions of certain atoms and ions with hydrogen atoms and ions is important for astrophysical investigations (see, for example, [3–5]). This is confirmed by the great need for such data (see, for example, [3,6]). For the most accurate quantitative determination of the composition of the stars photospheres, the most accurate data on inelastic processes are needed, namely the cross sections and the rate coefficients of these processes. Such data can be obtained both from experiment and from theoretical calculations. However, the level of technical development at the moment does not allow us to obtain complete information about inelastic processes at low collision energies, being limited only to information about ion collisions (see, for example, recent papers [7–10]), while information about neutral atoms collisions is often more important, since the spectral lines of such processes are well observed. Therefore, theoretical studies of inelastic processes in collisions of atoms and ions at low energies are today the main source of information about cross sections and rate coefficients of inelastic processes, and therefore **relevant**.

Often, due to the lack of accurate data on the inelastic processes rate coefficients obtained within the framework of physically correct based quantum methods, astrophysicists use the semi-classical Dravin formula [11,12] in the form proposed by Steenbook and Holweger [13] for estimating the values of rate coefficients. In Barklem et al. [14] it is shown that the use of this formula, which is a modification of the classical Thompson formula for calculations of ionization cross sections at electron impact, for inelastic cross sections in collisions with hydrogen, is not physically justified and leads to differences by several orders of magnitude from the cross sections

obtained by *ab initio* quantum methods (or even to zero cross sections for charge exchange processes, which have the largest cross sections, see, for example, [15–18]). For this reason, the use of physically justified methods for the study of inelastic processes in collisions of atoms and ions of various chemical elements with hydrogen atoms and ions, and obtaining reliable characteristics of inelastic processes is *relevant*.

The most accurate values of the rate coefficients can be obtained by means of a complete quantum calculation. The standard Born-Oppenheimer formalism, proposed in 1927 in [19], was the most widely used in the study of slow inelastic collisions. The main idea of this approach is that due to the large difference in the masses of electrons and nuclei, it is possible to separate the movement of fast-moving electrons and slow-moving nuclei. Within this formalism, the solution of the collision problem is divided into two steps: the calculation of the electronic structure of a quasimolecule with fixed nuclei and the calculation of nuclear dynamics. The big disadvantage of accurate quantum calculations is their time-consuming and large computations required for calculations. For example, an electronic structure calculations can consume a months for elements with a complex electronic structure, such as iron-peak elements (Sc, Ti, V, Cr, Mn, Fe, Co, Ni), which have a significant number of energy levels and a complex fine structure, which together leads to the need to calculate hundreds of molecular potential energy curves (PECs) while calculating even a dozen of PECs using *ab initio* quantum chemical methods is a very resource-intensive and time-consuming task. The nuclear dynamics calculations is also quite complicated and often involves a number of technical difficulties due to numerical methods of solution (see, for example, [20]). For these reasons, there are various model methods for solving both the electronic problem and nuclear dynamics. These model methods allow us to quickly obtain a good estimate of the rate coefficients of inelastic processes with the largest cross sections of inelastic processes with an accuracy of one order of magnitude compared to *ab initio* quantum calculations (see, for exam-

ple, [21, 22]). It is often inelastic processes with the largest cross sections and rate coefficients that are most important for non-Local Thermodynamic Equilibrium (non-LTE) modelling (see, for example, [3]).

This work is devoted to the theoretical study of low-energy inelastic processes in collisions of atoms and ions of various chemical elements with hydrogen atoms and ions by various model methods. **The object** of this study are atoms and ions of various chemical elements. **The subject** of this study is inelastic processes in collisions of atoms and ions of various chemical elements with hydrogen atoms and ions, as well as cross sections and rate coefficients of inelastic processes.

The purpose of the dissertation is to study inelastic processes in collisions of atoms and ions of lithium, calcium, oxygen with hydrogen atoms and ions, calculations of cross sections and rate constants of inelastic processes of excitation, de-excitation, charge exchange, as well as further development of the asymptotic method of accounting for the fine structure in the case of elements of group II of the periodic table of Mendeleev (alkaline earth metals). To achieve these goals, the following **problems were solved**:

1. A search and analysis of the literature concerning previously conducted studies of inelastic processes in collisions of lithium, calcium, oxygen atoms and ions with hydrogen atoms and ions has been carried out, as well as the current literature devoted to the problems of non-LTE modelling of the spectra of lithium, calcium, oxygen atoms and ions has been analyzed.

2. The electronic structures of LiH, OH, CaH quasimolecules, as well as the molecular ion CaH^+, obtained by various research groups using *ab initio* quantum chemical methods from the first principles, are investigated and analyzed.

3. The total probabilities of non-adiabatic transitions (from all possible initial states to all final states among the considered ones) for colli-

sions of lithium, calcium, oxygen atoms and ions with hydrogen atoms and ions by various methods (multichannel formula, the probability current method) are calculated.

4. Cross sections of inelastic processes of excitation, de-excitation, charge exchange are calculated, 1432 inelastic processes in total. In particular, 56 processes for collisions of lithium with hydrogen; 240 for collisions of oxygen with hydrogen, investigated by the probability current method, and 292 processes investigated by the multichannel formula; 110 for collisions of neutral calcium with hydrogen; 272 for collisions of calcium ion with hydrogen in LS representation and 462 in JJ representation.

5. The rate coefficients of all the above inelastic processes are calculated.

6. All the results obtained, namely cross sections and rate coefficients of inelastic processes, are analyzed.

7. Asymptotic method of accounting for the fine structure of energy levels in collisions with hydrogen is generalized for elements of group II of the periodic table.

The statements put forward for defense:

1. The largest values of cross sections and rate coefficients correspond to inelastic neutralization processes into scattering channels with electron binding energy in an atom ≈ 2 eV, which is shown in collisions of lithium, calcium, oxygen with hydrogen, which is consistent with the predictions of the simplified model.

2. The presence of non-adiabatic regions located at small internuclear distances has a significant effect on the values of cross sections and rate coefficients of processes involving highly excited states, while for states with electron binding energy in an atom ≈ 2 eV, this effect is insignificant.

3. Accounting for non-adiabatic transitions in molecular symmetries not generated by ionic states $A^+ + H^-$ practically does not affect the values of cross sections and rate coefficients of processes with large values ($> 10^{-8}$ cms), but it can significantly affect the rate coefficients of processes with values $< 10^{-9}$ cms.

4. For some processes with the values of rate coefficients $< 10^{-9}$ cms, cross sections at low collision energies are mainly determined by non-adiabatic transitions in molecular symmetries other than those of the ionic state.

The results obtained in this scientific research are important for stellar photospheres modelling (especially for stars of spectral classes F, G, K, characterized by low metallicity) under conditions of deviation from local thermodynamic equilibrium.

The scientific novelty of this work is due to:

1. For the first time, the characteristics of inelastic processes, such as cross sections and rate coefficients in slow collisions of oxygen atoms and ions with hydrogen atoms and ions, using the potential energies of a quasi-molecule OH, obtained by *ab initio* quantum chemical methods, are calculated using the quantum probability current method and a multichannel formula.

2. For the first time, the cross sections and rate coefficients for inelastic collisions $Ca + H^+$, $Ca^+ + H$ and $Ca^{2+} + H^-$ are obtained by the quantum probability current method (240 partial processes in total) using the potential energies of the molecular ion CaH^+ obtained using *ab initio* quantum chemical calculations.

3. For the first time, cross sections and rate coefficients for inelastic collisions $Ca^+ + H$ and $Ca^{2+} + H^-$ are obtained using a multichannel formula, taking into account the fine structure of energy levels (462 partial processes in total) using the potential energies of the molecular

ion CaH^+, obtained using *ab initio* quantum chemical calculations and modified within the framework of the asymptotic model of accounting for the fine splitting of energy levels.

4. The quantum probability current method have been used to obtain refined cross sections and rate coefficients of inelastic processes in collisions of lithium atoms and cations with hydrogen atoms and anions. The effect of replacement of lithium isotopes ($^6Li \leftrightarrow {}^7Li$) and hydrogen ($^1H \leftrightarrow {}^2H \leftrightarrow {}^3H$) in collisions on the values of cross sections and rate coefficients of inelastic processes is investigated.

5. The quantum probability current method (stochastic version of the algorithm) obtained the full probabilities of non-adiabatic transitions, cross sections and rate coefficients of inelastic processes in collisions of calcium with hydrogen using the potential energies of the quasimolecule CaH obtained by *ab initio* quantum chemical methods, taking into account the non-adiabatic regions located at relatively small internuclear distances.

6. Modified asymptotic method of accounting for fine structure proposed in [23,24], received a further generalization for collisions with hydrogen of elements of group II of the Periodic table.

The theoretical significance of this work consists in the fact that models based on quantum concepts of atomic collisions are used, as a result of which new knowledge was obtained about the mechanisms of inelastic processes in atomic collisions, data on inelastic processes in collisions of lithium, oxygen, calcium with hydrogen, and a modified asymptotic method was further developed taking into account the fine structure of energy levels in collisions of elements of group II of the Periodic table with hydrogen.

The practical significance of this work is due to the following:

1. The cross sections and rate coefficients of inelastic processes in collisions of lithium, calcium, oxygen atoms and ions with hydrogen

atoms and ions are calculated, which are necessary for further use in the stars photospheres modelling in conditions of deviation from local thermodynamic equilibrium and obtaining more accurate data on the quantitative composition of the stars photospheres.

2. Computer programs designed to calculate the full probabilities of non-adiabatic transitions from the given initial state to a given final state by the probability current method have been written and debugged (deterministic and stochastic versions of the algorithm), as well as cross sections and rate coefficients of inelastic processes. The stochastic version of the algorithm uses CUDA technology designed for parallel calculations on the GPU (which allows to either significantly increase the accuracy while maintaining the same calculation time, or significantly reduce the calculation time while maintaining the accuracy of the results obtained, or get some acceleration of calculations with a slight increase in accuracy compared to calculations on the CPU).

Connection of the topic with the plan of scientific works. This dissertation is a part of the scientific research of the Department of Theoretical Physics and Astronomy and the Laboratory of Atomic and Molecular Physics of the Theoretical Department of the Research Institute of Physics of the Herzen State Pedagogical University.

This work was supported by grants:

1. State assignment of the Ministry of Science and Higher Education No. 3.1738.2017/PCH 2017-2019, head of Prof. Belyaev A. K.

2. RSF Grant no. 17-13-01144 2017-2019, head of Prof. Belyaev A. K.

3. State assignment of the Ministry of Education No. 2020-0026 2020-2022, head of Prof. Gorokhovatsky Yu. A., head of the subgroup prof. Belyaev A. K.

4. Grant of the Foundation for the Development of Theoretical Physics and Mathematics BASIS, head of Prof. Belyaev A. K.

5. RFBR Grant No. 20-33-90047 "Aspirant", head of Prof. Belyaev A. K.

The reliability and scientific validity of the results and conclusions of the dissertation is ensured by a clear formulation of the tasks set, the use of reliable quantum methods for calculating nuclear dynamics, as well as cooperation with international scientific groups engaged in solving problems of quantum chemistry and being experts in this field. In this work, the following theoretical research methods are used: the Born-Oppenheimer approach; the Landau-Zener model; the probability current method; the multichannel formula; the asymptotic method for constructing adiabatic potential energies; the modified asymptotic method that takes into account a fine splitting of the energy levels of atoms.

All these methods are physically justified and correct. The Born-Oppenheimer approach is a fundamental method for studying slow collisions of atoms and ions with each other. The remaining methods used in this scientific work are constructed within the framework of the Born-Oppenheimer approach. The Landau-Zener model is an analytical solution for a system of two interacting diabatic terms and allows to determine the probability of a non-adiabatic transition from one state to another with a single passage of the non-adiabatic region by the system. Within the framework of the Landau-Zener model, the probability current method that allows to calculate the full probability of a non-adiabatic transition from a given initial state to a given final state in the presence of many states was developed. In the particular case of taking into account only the non-adiabatic regions caused by ion-covalent interaction, it becomes possible to obtain an analytical formula for calculating the total probability of a non-adiabatic transition from the given initial state to a given final one within the framework of the probability current method. The asymptotic method allows to calculate adiabatic potential energies, taking into account only the non-adiabatic re-

gions caused by ion-covalent interaction (it has been repeatedly shown that non-adiabatic transitions in the non-adiabatic regions caused by ion-covalent interaction make the greatest contribution to the values of cross sections and rate coefficients of inelastic processes, which is also confirmed in this work).

The author's personal contribution to obtaining the presented scientific results is as follows:

1. The current literature on the subject of the study is analyzed.
2. Quantum chemical data (electronic structure of quasi-molecules OH, LiH, CaH, quasi-molecular ion CaH^+) have been analyzed and prepared for use in calculations.
3. Calculations of the total probabilities of non-adiabatic transitions from each initial state to each final state for all the listed quasimolecules have been carried out.
4. According to the obtained probabilities, the cross sections and rate coefficients of inelastic processes of excitation, de-excitation, and charge exchange are calculated.
5. 9 articles have been prepared and published in international peer-reviewed scientific journals on the subject of the scientific work.
6. The asymptotic model is modified for the case of taking into account the fine structure of energy levels in collisions with hydrogen of elements of group II of the Periodic table.

The main content and results of the scientific work carried out are reflected in the following publications in international peer-reviewed journals:

1. Voronov Ya. V. et. al. Atomic data on inelastic processes in boron-hydrogen collisions with accounting for fine structure / Ya. V. Voronov, S. A. Yakovleva, A. K. Belyaev // Monthly Notices of the Royal Astronomical Society. – 2023 [25].

2. Voronov Ya. V. et. al. Isotopic effects in low-energy lithium-hydrogen collisions / A. K. Belyaev, Ya. V. Voronov // Physical Review A. – 2021. – Vol. 104, No. 2. – Article ID 022812 [26].

3. Voronov Ya. V. et. al. Solar oxygen abundance / M. Bergemann, R. Hoppe, E. Semenova, M. Carlsson, S. A. Yakovleva, Ya. V. Voronov, M. Bautista, A. Nemer, A. K. Belyaev, J. Leenaarts, L. Mashonkina, A. Reiners, M. Ellwarth // Monthly Notices of the Royal Astronomical Society. – 2021. – Vol. 508. – P. 2236–2253 [27].

4. Voronov Ya. V. et. al. Inelastic processes in calcium-hydrogen ionic collisions with account for fine structure / A. K. Belyaev, Ya. V. Voronov, S. A. Yakovleva // Physical Review A. – 2019. – Vol. 100. – Article ID 062710 [24].

5. Voronov Ya. V. et.al. Inelastic excitation and charge transfer processes for oxygen in collision with H atoms / A. Mitrushchenkov, M. Guitou, A. K. Belyaev, Ya. V. Voronov, N. Feautrier // Journal of Chemical Physics. – 2019. – Vol. 150. – Article ID 064312 [28].

6. Voronov Ya. V. et.al. Inelastic processes in oxygen–hydrogen collisions / A. K. Belyaev, Ya. V. Voronov, A. Mitrushchenkov, M. Guitou, N. Feautrier // Monthly Notices of the Royal Astronomical Society. – 2019. – Vol. 487. – P. 5097–5105 [29].

7. Voronov Ya. V. et. al. Data on Inelastic Processes in Low-energy Calcium–Hydrogen Ionic Collisions / A. K. Belyaev, Ya. V. Voronov, F. X. Gadéa // The Astrophysical Journal. – 2018. – Vol. 867. – Article ID 87 (7pp) [30].

8. Voronov Ya. V. et. al. Atomic Data on Inelastic Processes in Low-energy Lithium–Hydrogen Collisions / A. K. Belyaev, Ya. V. Voronov

// The Astrophysical Journal. – 2018. – Vol. 868. – Article ID 86 (6pp) [31].

9. Voronov Ya. V. et. al. Atomic Data on Inelastic Processes in Calcium–Hydrogen Collisions / A. K. Belyaev, Ya. V. Voronov, S. A. Yakovleva, A. Mitrushchenkov, M. Guitou, N. Feautrier // The Astrophysical Journal. – 2017. – Vol. 851. – Article ID 59 (5pp) [32].

The results were also presented at the following international scientific conferences:

1. International Conference "Stars, Planets and Magnetic Fields" (September 17-21, 2018, St. Petersburg, Russia). Poster report "Calculations of atomic data on inelastic processes in collisions of various chemical elements with hydrogen".

2. International Conference "XXI Mendeleev Congress on General and Applied Chemistry", symposium "The Periodic Table through Space and Time" (September 9-13, 2019, St. Petersburg, Russia). Poster report "Application of the probability current method to nuclear dynamic calculations in collisions with hydrogen".

3. International Conference "Physics of Stars and Planets: Atmosphere, activity and magnetic fields" (September 16-20, 2019, N. Tusi Shamakhi Astrophysical Observatory, Shamakhi, Azerbaijan). Poster report "Application of the probability current method to nuclear dynamic calculations in collisions with hydrogen".

Volume and structure of the dissertation. The dissertation consists of an Introduction, 5 substantive chapters and a Conclusion. The full volume is 213 pages, including 48 figures, 11 tables and a List of references (151 sources).

Chapter 1. Theoretical methods for the study of inelastic processes in atomic collisions

§ 1.1 Preliminary remarks

Theoretical methods for studying inelastic processes in slow collisions of atoms and ions play an important role in the physics of gas and plasma media. Despite the fact that in recent decades, technological progress has significantly advanced experimental studies of slow ion collisions (see, for example, investigations of neutralization processes in $Li^+ + D^-$ [7, 8], $Mg^+ + D^-$ [9], $Na^+ + D^-$ [10] collisions, etc.), experimental methods for studying collisions of neutral atoms at low energies (< (1-10) eV) still require further development of technologies and are practically unrealizable at the moment.

Astrophysics is one of the important applications of the slow atomic collisions theory. Observation of the spectra of various stars and numerical modelling of these spectra makes it possible to determine both the qualitative composition of stars and to determine the quantitative content of an element in the photosphere of a star. For this, the assumption of local thermodynamic equilibrium (LTE) is often used, but for certain types of stars, modelling under the assumption of LTE leads to unreliable results. For such stars, it is necessary to use modeling under conditions of deviation from local thermodynamic equilibrium (non-LTE).

When modelling the stars photosphere under non-LTE conditions, it is necessary to take into account the processes of collisions with atoms, ions and electrons. Collisions with hydrogen are of particular importance, since hydrogen is the most abundant element in the Universe. Therefore, the study and analysis of inelastic processes in collisions of certain atoms and ions with hydrogen atoms and ions are important for astrophysical investigations (see, for example, [3–5]). This is confirmed by the great need for such data (see, for example, [3, 6]). Therefore, theoretical studies

of low-energy atomic collisions are currently in high demand for obtaining characteristics of atomic processes.

Often, due to the lack of the most physically reliable data on the rate coefficients of inelastic processes obtained within the framework of quantum methods, astrophysicists use the semi-classical Dravin formula [11–13] for estimating the rate coefficients values, the use of which for hydrogen collision processes is not physically justified [14]. It has been shown repeatedly (see, for example, [3, 14, 15, 33]) that the accuracy of the results obtained is insufficient for the use of these data in modelling the spectra of stars: for excitation/de-excitation processes, the rate coefficients can be either overestimated or underestimated by several orders of magnitude; at the same time, Dravin's formula gives zero values of rate coefficients for charge exchange processes, although quantum calculations show that these processes are characterized by the largest values of rate coefficients (see, for example, [15–18], etc.). At the same time, the modelled spectra are very sensitive to input data. Often astrophysicists introduce a scaling factor that is selected empirically, it is different for different systems. For this reason, the application of physically justified methods for the study of inelastic processes in collisions of atoms and ions of various chemical elements with hydrogen atoms and ions, and obtaining reliable characteristics of inelastic processes is very relevant.

In this dissertation, inelastic processes are considered:

- excitation: $A + B \to A^* + B$;
- de-excitation: $A^* + B \to A + B$;
- charge exchange: $A^+ + B \to A + B^+$.

Separately, we will also highlight two important special cases of charge exchange processes:

- mutual neutralization: $A^+ + B^- \to A^* + B^*$;

- ion-pair formation: $A + B \to A^+ + B^-$.

This chapter provides an overview of various theoretical methods for the study of atomic collisions, which were used by the author in this work. Particular attention is paid to model methods, since all the work was done using various model methods within the framework of the Born-Oppenheimer formalism. Most of the chapter is devoted to the methods of nuclear dynamics research, they are considered in the most detail. Also, in general terms, the methods that the author considers important to mention are considered.

Slow atomic collisions are understood as collisions of atoms with a collision energy in the range from about 0.01 to 100 eV, which corresponds to gas and plasma temperatures in the range from about 10^2 to 10^6 K. Everywhere in the dissertation, unless the opposite is said, an atomic system of units is used, in which the electron charge, the electron mass and the reduced Planck constant are equal to one. Unit of length – Bohr radius $r_B = 0.529\,\text{Å}$.

§ 1.2 The standard Born-Oppenheimer adiabatic approach

Since the exact analytical solution of the Schrödinger equation has only two problems – a quantum harmonic oscillator and a hydrogen atom – then to solve more complex problems it is necessary to use some approximations. In general, when considering atomic or molecular collisions, one has to solve a problem with an arbitrary number of bodies. In the case of molecular collisions, the number of interacting bodies can be measured in tens and hundreds of thousands (for complex organic molecules). For atomic collisions, this number is noticeably less, but it is still measured in tens and even hundreds. The situation with atom-atom collisions (or atom-ion, or ion-ion), which will be further considered, is also simplified by

the fact that, in general, two nuclei and a certain number of electrons are considered.

Consider collisions of two atoms. We will consider a stationary problem, since there is no explicit dependence on time in the operators and wave functions when two atoms collide, although in general the non-stationary Schrödinger equation can also be considered. To solve the stationary problem of atomic collisions, it is necessary to solve the Schrödinger equation:

$$\hat{H}(\vec{r},\vec{R})\Psi^{tot}(\vec{r},\vec{R}) = E_{tot}\Psi^{tot}(\vec{r},\vec{R}) \ , \tag{1.1}$$

where is the total wave function of the system $\Psi^{tot}(\vec{r},\vec{R})$ depends on the coordinates of all electrons $\vec{r}$ ($\vec{r} = \{\vec{r}_1, \vec{r}_2, ..., \vec{r}_N\}$) and the coordinates of all nuclei $\vec{R}$ ($\vec{R} = \{\vec{R}_1, \vec{R}_2, ..., \vec{R}_{\tilde{N}}\}$). We will use Jacobi coordinates to describe colliding atoms. The vector of the internuclear distance $\vec{R}$ is drawn from the center of mass of one core to the center of mass of the other. The first electronic coordinate $\vec{r_1}$ is counted from the center of mass of the system «core» - «core» to the first electron, $\vec{r_2}$ – from the center of mass of the system «center of mass «core» - «core»» - «first electron» to the second electron, and so on, depending on how many bodies are considered. The great advantage of this coordinate system is the ability to consider the problems of many bodies.

One of the most common approximations when considering collision processes is the standard Born-Oppenheimer adiabatic approach [19]. The idea of this approach is that at relatively small energies of atomic motion, a slow-moving subsystem consisting of nuclei and a fast-moving subsystem consisting of electrons can be distinguished. Such an approximation looks justified, since due to the large difference in the masses of the electron and the nucleus (already for the hydrogen atom this difference is about 1800 times), their velocities differ significantly (by about three orders of magnitude). Therefore, for fast-moving electrons, the nuclei look almost

at rest, and with an infinitesimal change in the internuclear distance, the electrons have time to almost instantly rebuild their configuration.

Then the whole initial problem of atomic collisions can be divided into two subtasks:

I: finding electronic wave functions and electronic potential energies at fixed nuclei;

II: solving the problem of nuclear dynamics and finding nuclear wave functions taking into account the electronic wave functions obtained in the first problem.

Let's write down the Hamiltonian of the original equation (1.1) without taking into account the spin-orbit and spin-spin interactions in the center-of-mass system for a system consisting of two nuclei and k electrons:

$$\hat{H} = \hat{T}^M + \hat{T}^\mu + \sum_{i=1}^{k} \hat{T}_i^e + \hat{U}^{nn} + \frac{1}{2}\sum_{i=1}^{k} \sum_{j=1, j=/=i}^{k} \hat{U}_{ij}^{ee} + \sum_{i=1}^{2}\sum_{j=1}^{k} \hat{U}_{ij}^{ne} \ , \quad (1.2)$$

where $\hat{T}^M$ – the kinetic energy operator of the motion of the center of mass, $\hat{T}^\mu$ – the kinetic energy operator of the motion of a fictitious particle with a reduced mass of nuclei $\mu = \frac{M_{n1}M_{n2}}{M_{n1}+M_{n2}}$, $\hat{T}_i^e$ – operators of kinetic energy of electron motion, $\hat{U}^{nn}$ – operator of potential energy of interaction of nuclei, $\hat{U}_{ij}^{ee}$ – operators of the potential energy of interaction of electrons with each other, $\hat{U}_{ij}^{ne}$ – operators of the potential energy of interaction of electrons with nuclei. In the future, we will not consider the motion of the system as a whole, that is, we will not take into account the kinetic energy operator of the motion of the center of mass $\hat{T}^M$, since we will be interested only in the internal states of the system.

In the framework of the Born-Oppenheimer formalism, at the first step it is assumed that the nuclei are at rest. Let us explicitly distinguish the so-called electronic Hamiltonian, consisting of all potential energy operators,

as well as all kinetic energy operators of electron motion:

$$\hat{H}_e = \sum_{i=1}^{k} \hat{T}_i^e + \hat{U}^{nn} + \frac{1}{2}\sum_{i=1}^{k}\sum_{j=1,j=/=i}^{k} \hat{U}_{ij}^{ee} + \sum_{i=1}^{2}\sum_{j=1}^{k} \hat{U}_{ij}^{ne} \ , \qquad (1.3)$$

At the first step of solving the problem of atomic collisions within the framework of the Born-Oppenheimer approach, the problem of eigenvalues and eigenfunctions of the electronic Hamiltonian is solved:

$$\hat{H}_e \phi_j(\vec{r}, R) = U_j(R)\phi_j(\vec{r}, R), \qquad (1.4)$$

moreover, we note that the wave function $\phi_j(\vec{r}, R)$ is called an adiabatic molecular electronic wave function and depends on the internuclear distance R as a parameter. $U_j(R)$ are called adiabatic molecular potential energies, or electronic terms.

At the second step we will solve the original equation (1.1) taking into account the results obtained in the first stage. Write the complete wave function $\Psi^{tot}(\vec{r}, \vec{R})$ in the form of partial wave expansion:

$$\Psi^{tot}(\vec{r}, \vec{R}) = \sum_{J}\sum_{M_J} \Psi_{JM_J}(\vec{r}, \vec{R}) \ , \qquad (1.5)$$

where J and M_J – the quantum numbers of the total angular momentum of the system and its projection onto the internuclear axis. It is possible to decompose each partial wave according to some orthonormal basis set, and in the general case both discrete and continuous states are taken into account. Let's choose the eigenfunctions of the electronic Hamiltonian as the basis (1.3), while neglecting the continuous spectrum[2]. Then the partial wave will be the product of the nuclear $\chi_j(\vec{R})$ and electronic $\phi_j(\vec{r}, R)$ wave functions:

$$\Psi_{JM_J}(\vec{r}, \vec{R}) = \sum_{j} \chi_j(\vec{R})\phi_j(\vec{r}, R) \ . \qquad (1.6)$$

[2]This is justified in this dissertation, since ionization reactions, i.e. with electron separation, are not considered.

From the wave function (1.6), I would like to explicitly isolate the radial nuclear wave function $F_j(R)$. In general, this can be done via generalized spherical harmonics (see, for example, [34]):

$$\Psi_{JM_J}(\vec{r},\vec{R}) = \sum_j \sum_\Lambda \frac{F_{j\Lambda}(R)}{R} I_{j\Lambda}(\vec{r},\vec{R}) \ , \tag{1.7}$$

where are the generalized spherical harmonics $I_{j\Lambda}(\vec{r},\vec{R})$:

$$\begin{aligned} I_{j\Lambda}(\vec{r},\vec{R}) = \cos(M_J\varphi)\Theta_{JM_J\Lambda\mathbf{q}}(\theta)\phi_{j\Lambda\mathbf{s}}(\vec{r},R) + \\ + i\sin(M_J\varphi)\Theta_{JM_J\Lambda\text{-}\mathbf{q}}(\theta)\phi_{j\Lambda\text{-}\mathbf{s}}(\vec{r},R) \ , \end{aligned} \tag{1.8}$$

describing the motion of electrons and the angular part of the nuclear motion, $F_{j\Lambda}(R)$ – the radial nuclear wave function describing the radial motion, and Λ – the modulus of the quantum number of the projection of the orbital moment of the electrons of the molecule on the internuclear axis, $s = \pm 1$ – the parity quantum number of the wave function when reflecting electronic and nuclear coordinates in the plane xz, $q = s \times t = \pm 1$ – the quantum parity number.

For the case of Σ symmetry, spherical harmonics represent angular functions, and then the nuclear wave function can be represented as the product of the radial $F_j(R)/R$ and the angular $Y_{JM_J}(\theta,\varphi)$ wave functions:

$$\chi_j(\vec{R}) = \frac{F_j(R)}{R} Y_{JM_J}(\theta,\varphi) \ . \tag{1.9}$$

Let us consider in more detail the case of Σ molecular symmetry, since in practice this case turns out to be extremely important. Substitute the wave function (1.6) into (1.1) taking into account the nuclear wave function (1.9) and get:

$$(\hat{T}^\mu + \hat{H}_e) \sum_j \frac{F_j(R)}{R} Y_{JM_J}(\theta,\varphi)\phi_j(\vec{r},R) = E_{tot} \sum_j \frac{F_j(R)}{R} Y_{JM_J}(\theta,\varphi)\phi_j(\vec{r},R) \ . \tag{1.10}$$

The kinetic energy operator of the motion of nuclei contains the Laplace operator in spherical coordinates:

$$\begin{aligned}\hat{T}^{\mu} = -\frac{\hbar^2}{2\mu}\nabla^2_{\vec{R}} = -\frac{\hbar^2}{2\mu}\frac{1}{R^2}\frac{\partial}{\partial R}\left(R^2\frac{\partial}{\partial R}\right) - \\ - \frac{\hbar^2}{2\mu}\left\{\frac{1}{R^2\sin(\theta)}\frac{\partial}{\partial\theta}\left(\sin(\theta)\frac{\partial}{\partial\theta}\right) + \frac{1}{R^2\sin^2(\theta)}\frac{\partial^2}{\partial\varphi^2}\right\} .\end{aligned} \tag{1.11}$$

Moreover, the angular part, up to a constant, coincides with the operator of the square of the total angular momentum:

$$\hat{J}^2 = -\hbar^2\left[\frac{1}{\sin(\theta)}\frac{\partial}{\partial\theta}\left(\sin(\theta)\frac{\partial}{\partial\theta}\right) + \frac{1}{\sin^2(\theta)}\frac{\partial^2}{\partial\varphi^2}\right] . \tag{1.12}$$

Then we can write:

$$\hat{T}^{\mu} = -\frac{\hbar^2}{2\mu}\left[\frac{1}{R^2}\frac{\partial}{\partial R}\left(R^2\frac{\partial}{\partial R}\right) - \frac{\hat{J}^2}{\hbar^2R^2}\right] = -\frac{\hbar^2}{2\mu}\frac{1}{R^2}\frac{\partial}{\partial R}\left(R^2\frac{\partial}{\partial R}\right) + \frac{\hat{J}^2}{2\mu R^2} . \tag{1.13}$$

The angular functions $Y_{JM_J}(\theta,\varphi)$ are the eigenfunctions for the operator $\hat{J}^2$:

$$\hat{J}^2Y_{JM_J}(\theta,\varphi) = \hbar^2J(J+1)Y_{JM_J}(\theta,\varphi) . \tag{1.14}$$

Then, acting by the kinetic energy operator on the function (1.6), we get:

$$\begin{aligned}\hat{T}^{\mu}\frac{F_j(R)}{R}Y_{JM_J}(\theta,\varphi) = -\frac{\hbar^2}{2\mu}\Delta_R\frac{F_i(R)}{R}Y_{JM_J}(\theta,\varphi) + \\ + \frac{\hbar^2J(J+1)}{2\mu R^2}\frac{F_i(R)}{R}Y_{JM_J}(\theta,\varphi) .\end{aligned} \tag{1.15}$$

Now, substituting (1.15) in (1.10), multiply on the left by the complex conjugate electronic function $\phi^*_k(\vec{r};R)$ and integrate over all electronic

coordinates $\vec{r}$:

$$\begin{aligned}
&\sum_j \left\langle \phi_k(\vec{r};R) \left| \hat{T}^\mu \right| \frac{F_j(R)}{R} Y_{JM_J}(\theta,\varphi)\phi_j(\vec{r};R) \right\rangle + \\
&+ \sum_j \left\langle \phi_k(\vec{r};R) \left| \hat{H}_e \right| \frac{F_j(R)}{R} Y_{JM_J}(\theta,\varphi)\phi_j(\vec{r};R) \right\rangle = \\
&= E \sum_j \left\langle \phi_k(\vec{r};R) \left| \frac{F_j(R)}{R} Y_{JM_J}(\theta,\varphi)\phi_j(\vec{r};R) \right\rangle
\end{aligned} \tag{1.16}$$

Let's take a closer look at each of the terms and taking into account the orthonormality of the electronic wave functions $\langle \phi_k(\vec{r};R)|\phi_j(\vec{r};R)\rangle = \delta_{kj}$:

1. The term containing the kinetic energy operator of the motion of nuclei:

$$\begin{aligned}
&\sum_j \left\langle \phi_k(\vec{r};R) \left| \hat{T}^\mu \right| \frac{F_j(R)}{R} Y_{JM_J}(\theta,\varphi)\phi_j(\vec{r};R) \right\rangle = \\
&= \sum_j \left\langle \phi_k(\vec{r};R) \left| -\frac{\hbar^2}{2\mu}\Delta_R + \frac{\hat{J}^2}{2\mu R^2} \right| \frac{F_j(R)}{R} Y_{JM_J}(\theta,\varphi)\phi_j(\vec{r};R) \right\rangle .
\end{aligned} \tag{1.17}$$

$$\frac{\hat{J}^2}{2\mu R^2} Y_{JM_J}(\theta,\varphi) = \frac{\hbar^2 J(J+1)}{2\mu R^2} Y_{JM_J}(\theta,\varphi) . \tag{1.18}$$

$$\begin{aligned}
&-\frac{\hbar^2}{2\mu}\frac{\partial^2}{\partial R^2}\left(\frac{F_j(R)}{R}\phi_j(\vec{r};R)\right) = \\
&= -\frac{\hbar^2}{2\mu}\left(\frac{\partial^2 F_j(R)}{\partial R^2}\phi_j(\vec{r};R) + 2\frac{\partial F_j(R)}{\partial R}\frac{\partial \phi_j(\vec{r};R)}{\partial R} + \frac{\partial^2 \phi_j(\vec{r};R)}{\partial R^2}F_j(R)\right) .
\end{aligned} \tag{1.19}$$

Let us introduce notation for radial matrix elements of non-adiabatic coupling:

$$\begin{aligned}\left\langle \phi_k(\vec{r};R) \left| \frac{\partial}{\partial R} \right| \phi_j(\vec{r};R) \right\rangle &= D_{kj}(R)\ , \\ \left\langle \phi_k(\vec{r};R) \left| \frac{\partial^2}{\partial R^2} \right| \phi_j(\vec{r};R) \right\rangle &= DD_{kj}(R)\ .\end{aligned} \tag{1.20}$$

Note that the diagonal matrix element $D_{jj}(R)$ is strictly zero, whereas $DD_{jj}(R)$ is not equal to zero and is called an adiabatic correction. Then we get:

$$\begin{aligned}&\left(-\frac{\hbar^2}{2\mu}\frac{\partial^2}{\partial R^2} + \frac{\hbar^2 J(J+1)}{2\mu R^2} \right) F_k(R) = \\ &= \frac{\hbar^2}{\mu}\sum_j D_{kj}(R)\frac{\partial F_j(R)}{\partial R} + \frac{\hbar^2}{2\mu}\sum_j DD_{kj}(R)F_j(R)\ .\end{aligned} \tag{1.21}$$

2. The term containing the total energy of the system:

$$\begin{aligned}&E\sum_j \left\langle \phi_k(\vec{r};R) \left| \frac{F_j(R)}{R} Y_{JM_J}(\theta,\varphi)\phi_j(\vec{r};R) \right\rangle = \right. \\ &= E\sum_j \left\langle \phi_k(\vec{r};R) \left| \phi_j(\vec{r};R) \right\rangle \frac{F_j(R)}{R} Y_{JM_J}(\theta,\varphi) = E\frac{F_k(R)}{R} Y_{JM_J}(\theta,\varphi)\,.\right.\end{aligned} \tag{1.22}$$

3. The term containing an electronic Hamiltonian:

$$\begin{aligned}
&\sum_j \left\langle \phi_k(\vec{r};R) \left| \hat{H}_e \right| \frac{F_j(R)}{R} Y_{JM_J}(\theta,\varphi)\phi_j(\vec{r};R) \right\rangle = \\
&= \sum_j \left\langle \phi_k(\vec{r};R) \left| \hat{H}_e \right| \phi_j(\vec{r};R) \right\rangle \frac{F_j(R)}{R} Y_{JM_J}(\theta,\varphi) = \\
&= \sum_j \left\langle \phi_k(\vec{r};R) | U_j(R) \phi_j(\vec{r};R) \right\rangle \frac{F_j(R)}{R} Y_{JM_J}(\theta,\varphi) = \\
&= \sum_j \left\langle \phi_k(\vec{r};R) | \phi_j(\vec{r};R) \right\rangle U_j(R) \frac{F_j(R)}{R} Y_{JM_J}(\theta,\varphi) = \\
&= U_k(R) \frac{F_k(R)}{R} Y_{JM_J}(\theta,\varphi)\,.
\end{aligned} \tag{1.23}$$

As a result, we obtain a system of coupled differential equations of the second order:

$$\begin{aligned}
&\left(-\frac{\hbar^2}{2\mu}\frac{\partial^2}{\partial R^2} + \frac{\hbar^2 J(J+1)}{2\mu R^2} + U_k(R) - E \right) F_k(R) = \\
&= \frac{\hbar^2}{\mu} \sum_{j=/=k} D_{kj}(R) \frac{\partial F_j(R)}{\partial R} + \frac{\hbar^2}{2\mu} \sum_j DD_{kj}(R) F_j(R)\,.
\end{aligned} \tag{1.24}$$

Let's introduce the effective potential energy $U_j^{eff}(R)$:

$$U_j^{eff}(R) = U_j(R) + \frac{\hbar^2 J(J+1)}{2\mu R^2} + DD_{jj}(R)\,, \tag{1.25}$$

where $DD_{jj}(R)$ – adiabatic correction. Then the equation (1.24) will take the final form:

$$\begin{aligned}
&\left(-\frac{\hbar^2}{2\mu}\frac{d^2}{dR^2} + U_k^{eff}(R) - E \right) F_k(R) = \\
&= \frac{\hbar^2}{\mu} \sum_{j=/=k} D_{kj}(R) \frac{dF_j(R)}{dR} + \frac{\hbar^2}{2\mu} \sum_{j=/=k} DD_{kj}(R) F_j(R)\,.
\end{aligned} \tag{1.26}$$

Note also that the matrix $D_{kj}(R)$ is antisymmetric.

In general, it is necessary to take the wave function in the form (1.7). Then we can get the system of coupled differential equations of the second order [34] in general form:

$$\begin{aligned}
&\left[-\frac{\hbar^2}{2\mu}\frac{\partial^2}{\partial R^2} + U_{k\Lambda}(R) + \frac{\hbar^2\left(J(J+1)-\Lambda^2\right)}{2\mu R^2} - E_{tot}\right] F_{k\Lambda} = \\
&= \frac{\hbar^2}{\mu}\sum_j \left\langle \phi_{k\Lambda t}(\vec{r};R) \left| \frac{\partial}{\partial R} \right| \phi_{j\Lambda t}(\vec{r};R) \right\rangle \frac{\partial F_{j\Lambda}(R)}{\partial R} + \\
&+ \frac{\hbar^2}{2\mu}\sum_j \left\langle \phi_{k\Lambda t}(\vec{r};R) \left| \frac{\partial^2}{\partial R^2} \right| \phi_{j\Lambda t}(\vec{r};R) \right\rangle F_{j\Lambda}(R) - \\
&- \frac{1}{2\mu R^2}\sum_j \left\langle \phi_{k\Lambda t}(\vec{r};R) \left| \hat{L}_\xi^2 + \hat{L}_\eta^2 \right| \phi_{j\Lambda t}(\vec{r};R) \right\rangle F_{j\Lambda}(R) - \\
&- \frac{\hbar\sqrt{(J+\Lambda+1)(J-\Lambda)}}{\mu R^2}\sum_j \left\langle \phi_{k\Lambda t}(\vec{r};R) \left| -i\hat{L}_\eta \right| \phi_{j\Lambda+1 t}(\vec{r};R) \right\rangle F_{j\Lambda+1}(R) - \\
&- \frac{\hbar\sqrt{(J-\Lambda+1)(J+\Lambda)}}{\mu R^2}\sum_j \left\langle \phi_{k\Lambda t}(\vec{r};R) \left| i\hat{L}_\eta \right| \phi_{j\Lambda-1 t}(\vec{r};R) \right\rangle F_{j\Lambda-1}(R) \ ,
\end{aligned} \tag{1.27}$$

where the first three lines do not differ from the equation (1.24) (except that the term Λ^2 appeared explicitly in the centrifugal term), the fourth, fifth and sixth lines correspond to the matrix elements of the Coriolis interaction as between terms of the same symmetry (fourth line), so it is between terms of different symmetry (fifth and sixth lines). This is true for the adiabatic representation, but in the even more general case of a mixed representation, non-zero matrix elements of the electronic Hamiltonian may appear:

$$\left\langle \phi_{k\Lambda t}(\vec{r};R) \left| \hat{H}_e \right| \phi_{j\Lambda t}(\vec{r};R) \right\rangle F_{j\Lambda}(R) \ .$$

Let us now proceed to a more detailed consideration of the methods for solving both the first and second steps of solving the problem of atomic collisions within the framework of the Born-Oppenheimer approach.

§ 1.3 Methods for calculating the electronic structure of molecules

1.3.1 *Ab initio* (variational) methods

Within the framework of the standard adiabatic approach, the so-called electronic problem (1.4) is solved at the first step of solving the problem of atomic collisions: the equations for eigenvalues and eigenfunctions of the electronic Hamiltonian (1.3) are solved for all the considered states:

$$\hat{H}_e(\vec{r})\phi_j(\vec{r};R) = U_j(R)\phi_j(\vec{r};R)\,, \tag{1.28}$$

where $\hat{H}_e$ – electronic Hamiltonian (1.3), $U_j(R)$ – adiabatic molecular potential energy of the state j, $\phi_j(\vec{r};R)$ – adiabatic molecular electric wave function of the j state, depending on all electronic coordinates $\vec{r}$ and the interniclear distance R (as from the parameter).

The calculation of the electronic structure of atoms and molecules is based on the variational principle, the essence of which is to find, using an iterative procedure, the minimum of the functional G of the form:

$$G_j[\{\Psi(\vec{r},R)\}] = \langle\Psi_j(\vec{r},R)|\hat{H}_e|\Psi_j(\vec{r},R)\rangle\,, \tag{1.29}$$

$$U_j(R) = \min(G_j[\{\Psi(\vec{r},R)\}])\,, \tag{1.30}$$

that is, in the limit, the variation of the functional δG should be zero. In case of numerical calculations, a certain value ε is selected, which determines the accuracy of the calculation, then $\delta G < \varepsilon$. Here Ψ_j –

normalized wave functions of the system state:

$$\langle \Psi_k | \Psi_j \rangle = \delta_{kj} \ , \tag{1.31}$$

where δ_{kj} – the Kronecker symbol.

An important issue is the choice of a trial (initial) wave function. Initially, D. Hartree in [35] proposed to consider the problem of many electrons in the approximation of a self-consistent field, that is, under the assumption that each of the electrons moves in some averaged field of all other electrons and nuclei. The wave function of the system is constructed as the product of the one-electron wave functions of each electron:

$$\Psi^{elec}(\vec{r}) = \phi_1(\vec{r_1})\phi_2(\vec{r_2}) \ ...\phi_N(\vec{r_N}) \ . \tag{1.32}$$

However, such a function is not antisymmetric with respect to permutations of particles, although it is known that the wave functions of fermions are antisymmetric. Therefore, V. Fok proposed to construct a wave function using the Slater determinant [36] so that it would be antisymmetric:

$$\Psi^{elec}(\vec{r}) = \frac{1}{\sqrt{N!}} \begin{vmatrix} \phi_1(\vec{r_1}) & \phi_1(\vec{r_2}) & ... & \phi_1(\vec{r_N}) \\ \phi_2(\vec{r_1}) & \phi_2(\vec{r_2}) & ... & \phi_2(\vec{r_N}) \\ ... & ... & ... & ... \\ \phi_N(\vec{r_1}) & \phi_N(\vec{r_2}) & ... & \phi_N(\vec{r_N}) \end{vmatrix} , \tag{1.33}$$

as a result, the accuracy of calculations has increased due to the appearance of another term – an exchange integral that takes into account the exchange interaction of electrons. Application of the variational principle for the wave function of the form (1.33) is the essence of the Hartree-Fock self-consistent field method. There are also modifications of the Hartree-Fock method, such as the Hartree-Fock-Bogolyubov method (generalization taking into account the wave functions of particle pairs), the Hartree-Fock-Dirac method (generalization for the relativistic case) and others. But

ultimately, all these methods are iterative methods of sequential approximation to the minimum of the functional $G[\{\Psi(\vec{r}, R)\}]$, and require a long calculation time and large computing power.

There are other methods for calculating the electronic structures of molecules, which in some cases are more accurate than the Hartree-Fock methods. These are the so-called post-Hartree-Fock methods that take into account electronic correlations. The following groups of methods can be distinguished here:

1. Configuration Interaction methods (or CI). In these methods, the wave function is constructed not as a Slater determinant, but as a linear combination of Slater determinants corresponding to various electronic configurations in an atom. In this case, using an iterative procedure, the optimal values of the the expansion coefficients on the Slater determinants are found.

2. Self-Consistent Field methods (or SCF). These methods are, in fact, a generalization of the Hartree-Fock method, but take into account the existence of various electronic configurations. Within the framework of this group of methods, the optimal values of both the decomposition coefficients and the electronic configurations themselves are also found using an iterative procedure.

3. Møller-Plesset perturbation theory (or MP). Greatly simplifying, within the framework of these methods, the electronic correlation operator is introduced as a perturbation of the system in addition to the usual undisturbed electronic Hamiltonian. In the null order, the MP theory coincides with the Hartree-Fock method.

4. Coupled Cluster methods (or CC). The main idea of this class of methods is to take into account the electronic correlation using an exponential term multiplying to the wave function, exponent of which there is a special cluster operator.

More about these methods may be found, for example, in the [37, 38].

Separately mention the density functional theory, which is a logical continuation of the Thomas-Fermi model. This method is well described in [39, 40]. Its essence lies in considering the electronic density, that is, the probability density of detecting electrons in a particular region of space. This significantly simplifies the problem, since the consideration of the electronic wave function depending on $3N$ coordinates is replaced by the consideration of the electronic density depending only on three spatial coordinates, which leads to a decrease in the calculation time.

The method originates in 1927, when L. Thomas and E. Fermi first calculated the energy of an atom as the sum of its kinetic energy, represented as an electronic density functional, and the potential energy of the interaction of electrons with the nucleus and with each other. The interaction energy was also expressed in terms of electronic density. However, this approach proved to be insufficient and led to poor quantitative predictions, since the exchange interaction was not taken into account in any way. P. Dirac clarified the energy functional in the Thomas-Fermi model by adding to it a term describing the exchange interaction (this term also had the form of an electronic density functional).

This method is based on two Hohenberg-Cohn theorems. The first of them proves that the properties of the ground state of a multielectronic system are determined only by the electronic density depending on three spatial coordinates. The second theorem proves that the energy of the electronic subsystem, written as the functional of the electronic density, has a minimum equal to the energy of the ground state. Despite the fact that initially these two theorems were formulated only for the ground state, they can be generalized to the case of excited states by introducing a time dependence.

Despite the noticeable progress in the development of the electronic density functional method, this method still has a number of problems with the correct consideration of exchange interaction and electronic correlation,

so it is not universal and is not suitable for all systems. In addition, the density functional method is suitable mainly for calculations of the main and low-lying states.

1.3.2 Asymptotic methods

To study non-adiabatic nuclear dynamics, it is necessary to take into account many states, including highly excited ones, since one of the problems in calculating cross sections is the completeness of the basis of electronic molecular wave functions (for more details, see below, in §1.4.1). All of the above methods face problems when calculating potential energies and molecular electronic wave functions of highly excited states, the solution of which is not always possible. In addition, these calculation methods are inherently iterative methods of sequential approximation to the minimum of the functional, they require large computational power and also time-consuming. In this case, it becomes necessary to use approximate model methods for calculating the electronic structure of molecules.

In this part of the Chapter, some of them will be considered, which have become widely used in practical calculations of collisions of various elements with hydrogen. These methods are asymptotic, that is, they allow us to determine the potential energy of the interaction of atoms at relatively large internuclear distances exceeding the characteristic sizes of atoms. Note that in the monograph of B. M. Smirnov [41] asymptotic methods in the theory of slow atomic collisions are considered in details.

One of the asymptotic methods is the asymptotic approach proposed by A. K. Belyaev in the paper [16] and further developed in the papers [21,42]. This method allows us to calculate the adiabatic molecular potential energies in the approximation of the ion-covalent interaction only, neglecting the covalent-covalent interaction. This method does not allow to obtain molecular electronic wave functions of the states of the molecule.

The essence of this method is as follows. First, the electronic Hamiltonian is constructed as a function of the internuclear distance in the diabatic

basis. The diagonal elements of this Hamiltonian correspond to the energies of molecular states. At large and asymptotic internuclear distances, these are $\approx U_j^{asymp}$ for covalent terms and $\approx -\frac{1}{R} + U_{ion}^{asymp}$ for the ion term[3]. At short distances, Coulomb repulsion is added for both ionic and covalent terms. As mentioned above, taking into account antisymmetrization of electronic wave functions in the Hartree-Fock method leads to the appearance of exchange integrals and exchange interactions that are purely quantum in nature and have no classical analogues. In this method, the exchange interaction is taken into account approximately as an additional term of the form $C_1\exp(-C_2R)$, which increases the accuracy of the calculated electronic structures. It is also possible to take into account the dipole-dipole interaction of atoms, but calculations show that for covalent states, the contribution of these forces for quasimolecules of the form $A+H$ can be neglected, since they noticeably manifest themselves at fairly small distances, i.e. they decrease proportionally to $1/R^6$.

The off-diagonal matrix elements of the electric Hamiltonian responsible for the interaction of terms can be determined using various formulas. One of such formulas is the Olson-Smith-Bayer [43] formula for single-electron charge exchange in the form proposed in the paper [44]:

$$H_{jk}^{OSB}(R) = \beta_{jk}\sqrt{I_{A*}I_{H^-}}\, R\, exp(-0.86\beta_{jk}R)\,, \qquad (1.34)$$

where I_{A^*} is the binding energy of an electron in an excited atom A^*, I_{H^-} is the binding energy of an electron in an ion H^-, R – the internuclear distance, and $\beta_{jk} = \frac{\sqrt{I_{A^*}}+\sqrt{I_{H^-}}}{\sqrt{2}}$. This formula has gained popularity due to the simplicity and good accuracy of the results obtained (see, for example, [16]).

Note that in the work [45] compares the results obtained using various formulas for determining matrix elements of ion-covalent interaction on the example of collisions $\mathrm{H}^- + \mathrm{H}^+$. In this paper, the results of quantum

[3]In the atomic system of units.

ab initio calculations are compared with the Olson-Smith-Bayer formulas (three variants), the Smirnov formula [46,47] and the Janev formula [48]. The authors conclude that Janev's formula gives the closest result to quantum calculations (see Table 1 in [45], the difference is no more than 15%). From Table 1 in [45] it is also seen that the formula (1.34) also allows us to obtain values of both the positions of the centers of the non-adiabatic regions and the values of the matrix elements of non-adiabatic coupling in the centers of the non-adiabatic regions that have reasonable agreement with the quantum data (the difference does not exceed 50%).

Also often arise a situations when a two-electron transition occurs in an inelastic process, and the Olson-Smith-Bayer formula (1.34) cannot be directly applied to evaluate the off-diagonal matrix element. In this case, the formula proposed in [42,49] can be used:

$$H_{jk}^{2e}(R) = [H_{jk}^{OSB}(R)]^2 \times R\,. \qquad (1.35)$$

As a result, the matrix of the electronic Hamiltonian of the system has the form of an arrow: the main diagonal and the elements of the first row and the first column responsible for the ion-covalent interaction are filled (the first state corresponds to the ionic term, the second – the first covalent, the third – the second covalent, etc.). The remaining matrix elements are assumed to be zero, which corresponds to the absence of interaction of covalent terms with each other. To obtain adiabatic molecular terms from diabatic ones, the procedure of diagonalization of the electronic Hamiltonian matrix is carried out. The result is a system of adiabatic molecular terms with one series of sequentially arranged non-adiabatic regions due to ion-covalent interaction.

Another asymptotic method is the method of Linear Combination of Atomic Orbitals (LCAO), proposed and described in the P. Barklem papers [50,51] and being a further generalization of the works of R. Grice, S. A. Adelman, D. R. Herschbach [52,53], S. D. Anstey. The main idea of

this method is to use asymptotic atomic wave functions, which are determined from the known parameters of atoms.

This method is developed in the approximation of two active electrons, one of which is bound to hydrogen before the collision, and the second – to the atom of the collision partner. In the case of hydrogen anions collisions with the collision partner cations – both electrons are bound to the hydrogen anion before the collision. Adiabatic electronic wave functions can be represented as a linear combination of some diabatic functions with expansion coefficients C_{jk}. It is necessary to solve the matrix equation:

$$\underline{\underline{H}}\,\underline{\underline{C}} = \underline{\underline{U}}\,\underline{\underline{S}}\,\underline{\underline{C}}, \tag{1.36}$$

where $\underline{\underline{H}}$ is the matrix of the electronic Hamiltonian, $\underline{\underline{S}}$ is the overlap matrix, $\underline{\underline{C}}$ is the matrix of the coefficients, and $\underline{\underline{U}}$ – diagonal matrix of adiabatic molecular energies.

The molecular wave function in the asymptotic domain can be written in terms of atomic wave functions, following the monograph by E. E. Nikitin and S. Ya. Umansky (see [54], formula (10.6)). The atomic wave function of the ground state of the hydrogen atom is known, the atomic wave function of the hydrogen anion can be approximated by the function:

$$\phi^{H^-}_{long}(r) = \begin{cases} Nexp(-\gamma r)/r, & r \geq r_0 \\ 0, & r \leq r_0 \end{cases} \tag{1.37}$$

where N = 0.333672 a.u., γ = 0.2355885 a.u., r_0 = 2.30986 a.u. (see [50, 51]). The atomic functions of the atoms and ions of the collision partners are represented as the product of unknown radial and known angular functions. Unknown radial wave functions are further calculated numerically and become known. In this case, the matrix elements of the electronic Hamiltonian and the overlap integrals for two different valence states are assumed to be asymptotically small. In other words, within the framework

of this method, only the ion-covalent interaction is taken into account when calculating the electronic structure of molecules.

In this way, an electronic Hamiltonian matrix and the overlap matrix can be constructed, which have the form of an arrow, as in the previous asymptotic method. That is, it is now possible to solve the equation (1.36). Knowing the coefficients, it is possible to determine adiabatic electronic wave functions and adiabatic potential energies. Thus, the electronic problem can be completely solved within the framework of this asymptotic method. It is worth noting, however, that this method is used in conjunction with a multichannel formula within the Landau-Zener model (see §1.4.4), which does not require finding radial non-adiabatic coupling matrix elements.

§ 1.4 Methods of nuclear dynamics investigations

The second step of solving the problem of atomic collisions within the framework of the standard Born-Oppenheimer adiabatic approach – calculation of the dynamics of a system with moving nuclei, using the results obtained at the first step – adiabatic molecular potential energies $U_j(R)$ and adiabatic molecular electronic wave functions $\phi_j(\vec{r}, R)$. Consider again Σ molecular symmetry and a system of equations (1.24), although further reasoning can be applied in the general case of a system of equations (1.27):

$$\left(-\frac{\hbar^2}{2\mu}\frac{d^2}{dR^2} + \frac{\hbar^2 J(J+1)}{2\mu R^2} + U_k(R) - E\right) F_k = \frac{\hbar^2}{\mu}\sum_j D_{kj}\frac{dF_j}{dR} + \frac{\hbar^2}{2\mu}\sum_k DD_{kj}F_j \ .$$

Radial weve function $F_k(R)$ satisfies the following boundary conditions:

$$\begin{aligned} F_k(R) &\longrightarrow 0 \quad at \quad R \to 0 \ , \\ F_k(R) &\longrightarrow \frac{1}{\sqrt{K_k}}\left(a_k^+ \exp(iK_kR) + a_k^- \exp(-iK_kR)\right) \quad at \quad R \to \infty \ , \end{aligned} \tag{1.38}$$

where $K_k = \sqrt{(2\mu/\hbar^2)(E - U_j(\infty))}$ – the wave number kth channel, and $a_j^{\mp}$ – the amplitudes of incident and scattered waves.

A system of coupled channel equations (1.24) is solved numerically. Since the numerical solution does not involve calculating the wave function to an infinite value of the internuclear distance, some finite but sufficiently large internuclear distance R_{asymp} is chosen, at which non-adiabatic transitions no longer occur. This value R_{asymp} defines the second criterion for the convergence of cross sections of inelastic processes (see § 1.5) It is possible to express numerical solutions of the coupled channel equations system through the R-matrix:

$$F_k(R_{asymp}) = \sum_j R_{kj} \frac{dF_j(R_{asymp})}{dR} \ . \tag{1.39}$$

The R-matrix, in turn, allows to find the S-scattering matrix:

$$\begin{aligned} \underline{\underline{S}} = (-1)^J \ exp(-i\underline{\underline{K}}R_{asymp}) \ \sqrt{\underline{\underline{K}}} \ (\underline{\underline{I}} - i\underline{\underline{R}}\,\underline{\underline{K}})^{-1} \times \\ \times \ (\underline{\underline{I}} + i\underline{\underline{R}}\,\underline{\underline{K}}) \ \sqrt{\underline{\underline{K}}}^{-1} \ exp(-i\underline{\underline{K}}R_{asymp}) \ , \end{aligned} \tag{1.40}$$

where $\underline{\underline{K}}$ – diagonal matrix of wave numbers, $\underline{\underline{I}}$ – unit matrix.

The elements of the S-matrix characterize the total probability of a system transition from one state to another:

$$P_{if} = \left|S_{if}\right|^2 \ . \tag{1.41}$$

Knowing the full probability of a non-adiabatic transition from a given initial state to some final one, it is possible to find cross sections of inelastic processes.

However, such a *ab initio* quantum method has some disadvantages. Firstly, accurate quantum calculations require considerable time and large computing power.

Secondly, since in order to perform accurate quantum calculations it is required to know all the non-adiabatic coupling matrix elements, it is impossible to consider a large number of molecular states due to the impossibility of calculating all potential energies and matrix elements of non-adiabatic coupling. While the number of molecular states that need to be taken into account in calculations easily exceeds several tens (see, for example, [55–58]), and matrix elements – several hundred, or even thousands.

Thirdly, there is a fundamental feature of the Born-Oppenheimer approach, also called the Electron Translation problem, which consists in the existence of non-zero matrix elements of non-adiabatic coupling in the asymptotic region. In this case, there is no such asymptotic distance R_{aaymp} at which non-adiabatic transitions stop. This means that the cross sections of the processes increase infinitely and are not convergent for two reasons: the condition for a finite distance R_{asymp} is not fulfilled, since it does not exist; the condition for a finite value of the quantum number of the total angular momentum J_{max} is not fulfilled, that is, the number of partial waves is infinite.

1.4.1 Reprojection method

To solve the last of the above problems, the reprojection method is used, described in detail in the papers [34, 59–62]. The essence of this method is as follows. As part of the standard procedure for solving the nuclear dynamics problem described above, Jacobi molecular coordinates are used, which are not suitable for describing two non-interacting atoms at an infinitely large distance from each other. For a correct description of non-interacting atoms, it is necessary to use atomic Jacobi coordinates, which have a connection with molecular ones. This problem was first brought to the attention of Bates and McCarroll in the paper [63]. For Σ symmetry, the partial wave $\Psi_{JM_J}(\vec{r}, \vec{R})$ in molecular coordinates has the

form (1.6):

$$\Psi_{JM_J}(\vec{r},\vec{R}) = \sum_j \chi_j(\vec{R})\phi_j(\vec{r},R) = \sum_j \frac{F_j(R)}{R} Y_{JM_J}(\theta,\varphi)\phi_j(\vec{r},R)\ . \qquad (1.42)$$

The asymptotic form of the partial wave in this case is:

$$\Psi_{JM_J}(\vec{r},\vec{R}) = \sum_j \frac{1}{\sqrt{K_j}} \left(a_j^+ \psi_j^+(\vec{r},\vec{R}) + a_j^- \psi_j^-(\vec{r},\vec{R}) \right)\ , \qquad (1.43)$$

where

$$\psi_j^{\pm}(\vec{r},\vec{R}) = \frac{\exp(\pm iK_jR)}{R} Y_{JM_J}(\theta,\varphi)\phi_j(\vec{r},R) \qquad (1.44)$$

– incident and scattered waves.

To describe a system of two non-interacting atoms, it is necessary to write the incident and scattered waves $\psi_j^{\pm}(\vec{r},\vec{R})$ in atomic Jacobi coordinates. They have the form:

$$\psi_j^{\pm}(\vec{r},\vec{R}) = \frac{\exp(\pm iK_jR)}{R} Y_{JM_J}(\theta,\varphi) \sum_k t_{jk}^{\pm}\phi_k(\vec{r},R)\ , \qquad (1.45)$$

where $t_{jk}^{\pm}$ – elements of the so-called t-matrix, which are expressed in terms of the asymptotic values of the momentum K_j, potential energies $U_j(\infty), U_k(\infty)$ and the non-adiabatic coupling matrix elements $D_{jk}(\infty)$:

$$t_{jk}^{\pm} = \delta_{jk} \pm \frac{iK_j\hbar^2}{\mu(U_j(\infty) - U_k(\infty))} D_{jk}(\infty)\ , \qquad (1.46)$$

Then the partial wave may be written as:

$$\Psi_{JM_J}(\vec{r},\vec{R}) = \sum_j \frac{F_j(R)}{R} Y_{JM_J}(\theta,\varphi) \sum_k t_{jk}^{\pm}\phi_k(\vec{r},R)\ . \qquad (1.47)$$

In this case, the expression for the S-matrix will change:

$$\begin{aligned}\underline{\underline{S}} = (-1)^J \exp(-i\underline{\underline{K}}R_{asymp}) \sqrt{\underline{\underline{K}}} \, (\underline{\underline{t}}^+ - i\underline{\underline{R}}\,\underline{\underline{t}}^+\,\underline{\underline{K}})^{-1} \times \\ \times (\underline{\underline{t}}^- + i\underline{\underline{R}}\,\underline{\underline{t}}^-\,\underline{\underline{K}}) \sqrt{\underline{\underline{K}}}^{-1} \exp(-i\underline{\underline{K}}R_{asymp}) \, .\end{aligned} \tag{1.48}$$

All the difference between the expression (1.48) and (1.40) is in $t^{\pm}$ matrices. Note that when the values of the non-adiabatic coupling matrix elements $D_{jk}(\infty)$ are zero at infinity, the matrices $t^{\pm}$ turn into unit matrices, and the expression (1.48) turns into (1.40).

Thus, the reprojection method makes it possible to solve the fundamental problem of inelastic processes cross sections convergence in the general case (in the presence of non-zero values at infinity of the non-adiabatic coupling matrix elements).

1.4.2 The Landau-Zener model

Determination of all the necessary data at the first step within the framework of the Born-Oppenheimer approach (adiabatic energies and adiabatic molecular electronic wave functions) is a non-trivial task. It is not uncommon for situations where there are only molecular potential energies, but electronic wave functions are unknown, and in such a situation, the study of nuclear dynamics by solving a coupled channel equations system is impossible due to the impossibility of obtaining non-adiabatic coupling matrix elements. Moreover, solving the coupled channel equations system is a rather complex and time-consuming. In this case, there is a need for reliable model approaches that allow us to estimate with good accuracy the full probability of the transition of the system from a given initial state to a given final one.

In general, non-adiabatic transitions can occur everywhere at small and intermediate internuclear distances. But the largest transition probability occurs in the regions of convergence of terms, in the non-adiabatic regions. Often there are situations of convergence of two terms in the non-adiabatic

region. But there are also situations when three or more terms converge in one non-adiabatic region. To describe most non-adiabatic transitions, it is sufficient to consider the case of two converging terms.

There are several models that describe the probability of a non-adiabatic transition in the case of two terms. For example, the Landau-Zener model [64–66] (linear model), Nikitin model [67,68] (exponential model), Demkov model [69] (a special case of the Nikitin model) and others (see also the book [54]). The Landau-Zener model, which describes the probability of a non-adiabatic transition in the case of two diabatic linear intersecting terms with a constant off-diagonal matrix element, has become quite widespread in model studies of non-adiabatic transitions. This model was first described by Landau in [64, 65] for the case of adiabatic and weak coupling of two terms, and a little later Zener and Stueckelberg in [66, 70] got a solution for strong coupling as well.

The derivation is described in the book [54], and also discussed in the papers [71–73]. In this dissertation, we will limit ourselves to the main results. The Landau-Zener model is formulated as follows: there are two linear intersecting diabatic terms, the coupling between which is constant. The starting point is at the intersection of these terms. Then, when the system moves from $-\infty$ to $+\infty$, the probability of moving from state 1 to state 2 will be described by the following formula:

$$p = exp(-\frac{2\pi H_{jk}^2}{\Delta F\, v}), \tag{1.49}$$

where H_{jk} is the coupling of terms, ΔF – the difference in the slopes of diabatic terms, v – the radial velocity of the nuclei at the intersection of diabatic terms. It is possible to explicitly isolate the dependence on the velocity of the radial motion of the system in the center of the non-adiabatic region by introducing the so-called Landau-Zener parameter ξ_{LZ}:

$$\xi_{LZ}^{diab} = \frac{2\pi H_{jk}^2}{\Delta F}. \tag{1.50}$$

This model allows us to describe a non-adiabatic transition with a single passage of the non-adiabatic region. Since the Landau-Zener model is formulated for two linear intersecting diabatic terms, this model well describes non-adiabatic transitions in the case when adiabatic terms are very close and pseudo-crossing takes place (i.e., the terms almost intersect). This means that the energy splitting in the non-adiabatic region between the two terms is quite small. The criteria for the applicability of the Landau-Zener model can be written as follows:

$$\frac{2H_{jk}}{\Delta U_\infty} << 1, \tag{1.51}$$

$$\frac{\pi H_{jk}^2}{\Delta F} << \xi_\infty, \tag{1.52}$$

where ΔU_∞ is the difference of the asymptotic energies of the terms, ξ_∞ – the Massey parameter for non-adiabatic coupling between terms with splitting ΔU_∞.

Condition (1.51) means that a pseudo-crossing picture is actually reproduced in the non-adiabatic region, that is, the splitting in the center of the non-adiabatic region is significantly less than the energy splitting between terms in the asymptotic region. The condition (1.52) means that the non-adiabatic coupling is localized near this pseudo-crossing point (see [54]).

The first condition describes terms with low energy splitting in the non-adiabatic region, and the second condition describes the localization of the non-adiabatic coupling near the pseudo-crossing point, that is, in the region of the center of the pseudo-crossing point. It is possible to rewrite this formula for the case of an adiabatic basis, which was done in the paper [74] via energy splitting $Z(R) = \Delta U(R)$ and the second derivative by the internuclear distance from it $\frac{d^2 Z(R)}{dR^2}$ in the center of the non-adiabatic region R_C:

$$p = exp\left(-\frac{\pi}{2\hbar v}\sqrt{\frac{Z^3(R_c)}{Z''(R_c)}}\right), \tag{1.53}$$

where the Landau-Zener parameter:

$$\xi_{LZ}^{adiab} = \frac{\pi}{2\hbar}\sqrt{\frac{Z^3(R_c)}{Z''(R_c)}}\,. \qquad (1.54)$$

The use of the formula (1.53) for adiabatic potentials avoids the diabatization procedure, which is not unambiguous (for more information about the problems of diabatization, see, for example, in [20]).

Thus, the Landau-Zener model makes it possible to calculate the probability of a non-adiabatic transition with a single passage of the non-adiabatic region. However, in real systems with a large number of molecular terms, the number of non-adiabatic regions is tens or even hundreds, besides, the system passes each non-adiabatic region at least twice: at moving from ∞ to 0 and at moving from 0 to ∞. Thus, it is necessary to apply methods that allow us to calculate the full probability of a non-adiabatic transition from a given initial state to a given final one. At the same time, the probability of a single passage of each of the non-adiabatic region can be calculated using the Landau-Zener model, the Nikitin model or the Demkov model.

1.4.3 Probability current method

One of the methods of studying nuclear dynamics based on the Landau-Zener model is the probability current method proposed in the paper [75]. This method is similar to the method of classical trajectories developed in [76–79] et al. for the study of dynamics of polyatomic systems.

The solution for the wave function in the asymptotic region is known:

$$\Psi(R \to \infty) \sim sin(KR) = a^{-}\ exp(-iKR) + a^{+}\ exp(iKR)\,, \qquad (1.55)$$

where a^{-} and a^{+} – the amplitudes of incident and scattered waves, K – the wave number, R – the internuclear distance. For the wave function (1.6) decomposition into incident and scattered waves will take the

form:

$$\Psi_{JM_J}(\vec{r},\vec{R}) \sim \sum_j \frac{1}{\sqrt{K_j}} \left(a_j^- \; exp(-iK_jR) + a_j^+ \; exp(iK_jR) \right) , \qquad (1.56)$$

where j – the number of the state, K_j – the wave number of the jth state.

The probability of detecting a system in a particular state before or after a collision is the square of the modulus of the amplitude of the incident or scattered wave, respectively:

$$\tau_j^{\pm} = |a_j^{\pm}|^2 , \qquad (1.57)$$

where $\tau_j^{\pm}$ – the probability currents, incident and scattered. The boundary conditions in the asymptotic region for an incident wave are given as follows:

$$a_i^- = 1, \qquad a_{j=/=i}^- = 0 , \qquad (1.58)$$

that is, only one initial channel i is populated. Then the probability of detecting a system in a particular state after collision in the asymptotic region is defined as the square of the amplitude modulus of the scattered wave of the corresponding state:

$$P_{if}(J,E) = \tau_f^+ = |a_f^+|^2 , \qquad (1.59)$$

with boundary conditions (1.58).

However, the solution for the asymptotic region is not enough to determine the full probability of transition from one state to another, since the dynamics of the system at small and intermediate internuclear distances is unknown, that is, it is not known how non-adiabatic transitions are carried out, and which channels are populated after a collision and with what probability. To solve this problem, the probability current method can be used. Its essence lies in considering the probability current $\tau_j(R)$ as a

function of the internuclear distance to trace its dynamics during the collision. Within the framework of the Demkov-Osherov approach [80] the total probability of a non-adiabatic transition from one state to another $|S_{kj}|^2$ can be represented as products of the probabilities of single transitions in isolated non-adiabatic regions traversed by the system during movement. An important assumption here is that the non-adiabatic regions are considered isolated from each other, although this is not always the case.

The boundary conditions before the collision are set by the condition (1.58), and the probability current $\tau_i(R \to \infty) = 1$ starts moving in the ith channel from the asymptotic region to the region of small internuclear distances to the classical turning point ($R \to 0$). In the process of convergence, the system passes through non-adiabatic regions, where non-adiabatic transitions to other channels are carried out. Having reached the classical turning point, the system begins to move into the region of large internuclear distances $R \to \infty$ and again passes the non-adiabatic regions and makes non-adiabatic transitions. Ultimately, after the expansion in the asymptotic region, all energetically open channels turn out to be populated, and this population can be calculated by knowing the dynamics of the probability current at small internuclear distances. At the same time, the probability of transition with a single passage of each non-adiabatic region is determined within the framework of the Landau-Zener model.

There are two different approaches to considering the evolution of probability currents:

- the branching probability current method (deterministic approach): the probability current is split in each non-adiabatic region into two currents moving in the corresponding channels, proportional to the transition probability. When passing the next non-adiabatic region, each of the split currents is split into two again in accordance with the probability of non-adiabatic transition. Thus, one initial probability current is split into a set of currents that sum up for each jth

channel, and as a result, this one initial probability current inhabits all energetically open scattering channels after collision;

- the hopping probability current method (stochastic approach): the probability current in each non-adiabatic region completely passes into the neighboring channel, or completely remains in this one. This depends on the transition probability in the non-adiabatic region and on the random number generated in the interval [0, 1]. If the probability of transition is greater than the thrown random number, then the probability current will completely hop to the neighboring channel; otherwise, the entire probability current will remain in this channel. Thus, one probability current inhabits only one channel in the asymptotic region. To determine the total transition probability, it is necessary to repeat the calculation procedure for one probability current N_{tot} times, and then the total probability of a non-adiabatic transition is determined as follows:

$$P_{if}(J, E) = \frac{N_f}{N_{tot}}, \tag{1.60}$$

where N_f – the total number of the probability currents, inhabits f th channel at the asymptotic region, N_{tot} – the total number of probability currents.

For the hopping probability current method, the total number of calculated probability currents N_{tot} plays an important role, since it determines the accuracy of the obtained values of the total non-adiabatic transition probabilities. In the practical implementation of this method, the calculation of the probability for the given values of the collision energy E_{col} and the total angular momentum J can take quite a long time, and we have to limit ourselves to the number of probability currents $N = 10^4 - 10^5$.

The situation is facilitated by the fact that the procedure for calculating a single probability current is quite simple and takes little time and computing power, so this method can be implemented using parallel computing

technologies such as CUDA (Compute Unified Device Architecture) [81] for NVidia GPUs and OpenCL (Open Computing Language) [82] for various GPUs and CPUs. As known, the central processing unit (CPU) is designed for efficient sequential execution of a set of commands, while graphics accelerators perform a different role: they must calculate the characteristics of each pixel on the monitor at any given time, such as colour, intensity, and others. At the same time, the parameters of each pixel do not depend on the parameters of other pixels, and these parameters are calculated simultaneously for millions of pixels. It is for this task that the architecture of graphics accelerators has been developed – to process thousands of independent processes at any given time.

The calculation of each probability current is a process independent of other calculations, so it is possible to use graphics accelerators to calculate hundreds and thousands of probability currents at any given time. Although the central processor has a higher command processing speed, the use of graphics accelerators allows us to gain in calculation time due to the number of probability currents calculated simultaneously.

The author of the dissertation has written, optimized and debugged a program in the C++ programming language that implements the algorithm of hopping probability currents, using the paradigm of parallel computing using graphics accelerators (GPU) and CUDA technology. The program effectively implements the hopping probability current algorithm, which is expressed in a significant acceleration of calculations of the full probabilities of non-adiabatic transitions, on average 30 times on NVidia GTX 1060, GTX 1070 graphics accelerators. Also, this program allows us to significantly increase the total number of calculated probability currents while maintaining an acceptable calculation time for all states involved in nuclear dynamics. At the moment, the program can calculate in a few weeks all the full probabilities of non-adiabatic transitions for a system of ≈ 10 states with the number of probability currents $\approx 10^9$ for the values of the quan-

tum number of the total angular momentum J in the range $[0, \approx 3000]$ and in the range of collision energies [0.01,100] eV with an adaptive step.

Note that in numerical calculations there are situations when the calculation takes too long due to the large number of partial waves taken into account, up to tens of thousands of J. In this case, it makes sense to calculate the cross section not with a step by the quantum number of the total angular momentum $\Delta J = 1$, but with a larger step for small values of J. This is justified by the fact that the probability in this situation practically does not change for values, for example, J and $J+1$, so we can assume that $P(J) = P(J+1)$. In order to correctly account for each term in the sum of partial waves, the following formula is used (for more information about cross section calculations, see below, § 1.5):

$$\begin{aligned} &\Delta J = 1 : (2J+1)P_{if}(J,E)\,, \\ &\Delta J > 1 : ((2J+\Delta J)\Delta J + \Delta J(\Delta J - 1))P_{if}(J,E)\,. \end{aligned} \tag{1.61}$$

It is also worth noting that the author of the dissertation wrote, optimized and debugged a program in the C++ programming language that implements the branching probability current algorithm. At first glance, the hopping probability current algorithm is not necessary, since it has a limitation on accuracy, while the branching probability current algorithm allows us to set any accuracy. However, numerical experiment shows that the application of the branching probability current algorithm is best suited for cases when the total energy is higher than the asymptotic energy of the ion channel. In this situation, there are no energetically closed channels and no oscillations occur (see below, in §1.4.4). In the case of oscillations, the calculation time using the branching probability current algorithm increases significantly. At the same time, the hopping probability current algorithm has no problems with calculating the full probabilities of non-adiabatic transitions in the presence of oscillations in closed channels. Therefore, the hopping probability current algorithm should be used in cases where energetically closed channels arise during the calculation,

as well as in general in situations where the application of the branching probability current algorithm leads to a significant calculation time.

1.4.4 Multichannel formula

Another method that allows us to determine the full probability of a non-adiabatic transition of a system from a given initial state to a given final state is the multichannel formula. This method has a number of limitations. Firstly, only the non-adiabatic regions at intermediate and large internuclear distances due to ion-covalent interaction are taken into account. Secondly, using a multichannel formula, it is possible to calculate the full probabilities of non-adiabatic transitions for the processes $i \to f$, where $i > f$, taking into account that the numbering comes from the ground state (i.e. it is possible to calculate the full probabilities only for the processes of de-excitation and neutralization). Thirdly, for the application of the multichannel formula, a certain order of non-adiabatic regions is required: the center of the non-adiabatic region R^C between states i and $i+1$ must be to the left of the center of the non-adiabatic region between states $i+1$ and $i+2$ and to the right of the center of the non-adiabatic region between states $i-1$ and i for all non-adiabatic regions:

$$R^C_{i-1,i} < R^C_{i,i+1} < R^C_{i+1,i+2}\,, \tag{1.62}$$

with the condition, as noted above, the numbering is carried out from the ground state:

$$U(\infty)_{i-1} < U(\infty)_i < U(\infty)_{i+1}\,, \tag{1.63}$$

Despite these disadvantages, the multichannel formula has significant advantages. Firstly, it is an analytical formula that does not require numerical solution of differential equations or numerical calculations of the evolution of probability currents. Secondly, the use of the multichannel formula for the study of non-adiabatic nuclear dynamics allows us to obtain results almost instantly. The study of the nuclear dynamics of a system

of dozens of terms takes a few minutes of estimated time on a computer. Thirdly, the cross sections and rate coefficients obtained by means of a multichannel formula have good accuracy for processes with the largest values of cross sections and rate coefficients. In the papers [18, 21] it was shown that for processes with the largest values of cross sections and rate coefficients, the difference between the values of the rate coefficients obtained using the multichannel formula from the data obtained by accurate *ab initio* quantum calculations does not exceed one order of magnitude for mutual neutralization processes, which it is much more accurate than the results obtained using the Dravin formula. Therefore, the use of the multichannel formula is justified.

Let's consider the derivation of the multichannel formula in more detail. First of all, consider the case of two channels (see Figure 1). We denote the probability of a non-adiabatic transition at a single passage of the non-adiabatic region as p. Then the total probability of a non-adiabatic transition P^{trans} from state 2 to 1 in the presence of one non-adiabatic region is the sum of two probabilities:

- the probabilities of going from state 2 to state 1 at collision and remaining in state 1 at separation – $p(1-p)$;
- the probabilities of remaining in state 2 at collision and going from state 2 to state 1 at separation – $(1-p)p$;

so:

$$P^{trans} = p(1-p) + (1-p)p = 2p(1-p)\ . \qquad (1.64)$$

The multichannel formula is a generalization to the case of many channels. If we consider all possible paths of the system from a given initial state i to a given final state f (and $i > f$, $i = / = ion$), then ultimately we can obtain a formula for the full transition probability in the case when the collision energy is greater than the asymptotic energy of the

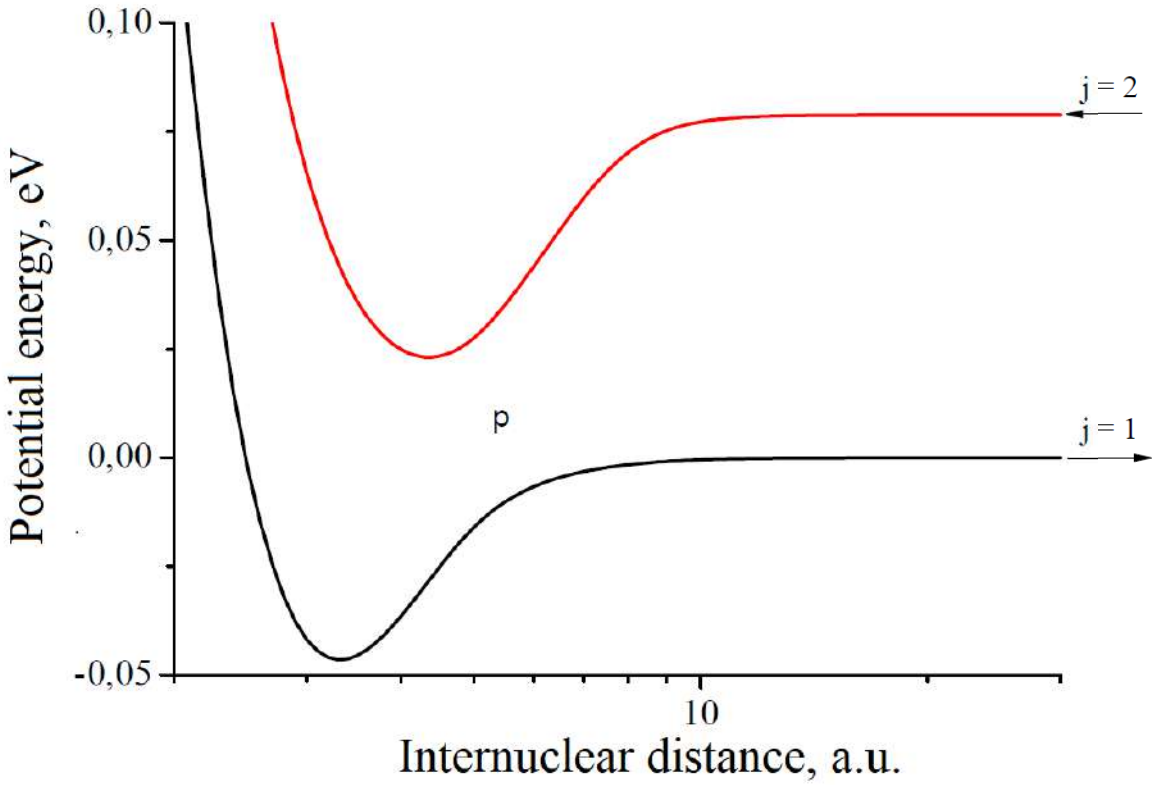

Figure 1. A system of two adiabatic terms.

ion channel:

$$P_{if}^{trans} = 2p_f(1-p_f)(1-p_i)\prod_{k=f+1}^{i-1} p_k \left\{1 + \sum_{m=1}^{2(f-1)} \prod_{k=1}^{m} \left(-p_{f-\left[\frac{k+1}{2}\right]}\right)\right\}, \quad (1.65)$$

where square brackets mean the integer part of the number. The numbering of transition probabilities in non-adiabatic regions begins with the lower term: p_1 corresponds to the probability of transition from state 1 to state 2, p_2 - from 2 to 3... p_k – from k to k+1.

It can be seen that in the case of two channels, this formula turns into the formula (1.64). Let's take a closer look at all the terms in the formula (1.65):

- $2p_f(1-p_f)$ – the transition probability in the case of two terms;

- $1 - p_i$ – the probability that the system will make transitions to the lower states is due to the presence of channels above the ith;
- $\prod_{k=f+1}^{i-1} p_k$ – contribution of channels located between ith and fth states;
- $1 + \sum_{m=1}^{2(f-1)} \prod_{k=1}^{m} (-p_{f-\left[\frac{k+1}{2}\right]})$ – contribution due to the presence of channels below fth.

In the case of neutralization (when $i = ion$) there are no transitions to the higher-lying channels, respectively $p_i = 0$ and $(1 - p_i) = 1$.

If the total energy of the system is less than the asymptotic energy of some higher-lying state, then the system cannot enter this and other higher-lying states. In this case, so-called oscillations occur in the higher-lying states, and such states are called energetically closed. Consider the Figure 2. It can be seen that the system can move into the ionic channel, but there is not enough energy for the system to enter the ion channel at the asymptotic region.

At collision, the system will enter the ionic state, and will reach the classical turning point R_1, will turn around and reach the turning point R_2, and with the probability p_i will enter the underlying channels, and this probability will be redistributed between these channels in the future. At the same time, with a probability of $1 - p_i$, the system will remain in the same ionic channel, again reach the point R_1, will turn around, reach the point R_2, and again with a probability of p_i will move to the lower channels, and with a probability of $1 - p_i$ will again remain in the ionic channel.

By writing down several such steps sequentially, you can make sure that in this case there is a geometric progression [22], and using the formula for the sum of the geometric progression and some simplifications, it is ultimately possible to obtain a formula for finding the full probability of a non-adiabatic transition for the case when energetically closed channels

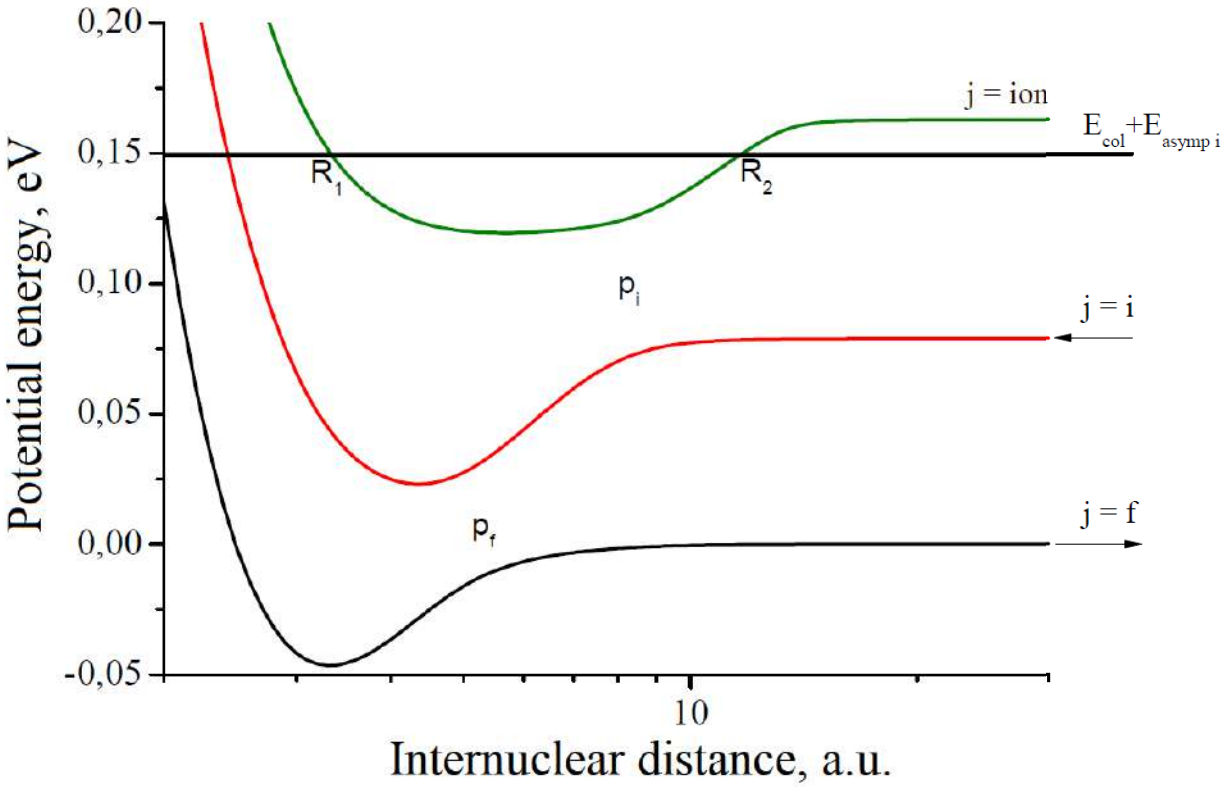

Figure 2. A system of three terms in the case when the ionic channel is energetically closed.

take place:

$$P_{tot\,if}^{trans} = P_{if}^{trans}\left\{1 - \frac{\prod\limits_{k=i}^{F} p_k^2 \left(1 + \sum\limits_{m=1}^{2(i-1)} \prod\limits_{k=1}^{m} \left\{-p_{i-\left[\frac{k+1}{2}\right]}\right\}\right)}{\sum\limits_{m=1}^{2F} \prod\limits_{k=1}^{m} \left(-p_{F+1-\left[\frac{k+1}{2}\right]}\right)}\right\}, \qquad (1.66)$$

where F is the full number of energetically open channels.

Also, when considering inelastic collisions, it is important to take into account the tunnelling effect through a potential barrier that occurs in the non-adiabatic region. The effective potential depends on the quantum number of the total angular momentum of the quasimolecule, see the formula (1.25). Accordingly, with an increase of J, the effective potential may at some point at $J = J_{forbidden}$ become greater than the total col-

lision energy at some point $R = R_{forbidden}$. Then the transitions in the non-adiabatic region will be energetically closed from the classical point of view. At the same time, at $R < R_{forbidden}$, there may be regions in which the total energy is still greater than the effective potential energy. Then there may be sub-barrier transitions, and this effect must be taken into account. At paper [83] consideration was given to the tunnelling effect through a potential barrier. A formula was proposed that allows taking into account sub-barrier transitions in inelastic collisions by simply multiplying the probability of transition in the non-adiabatic region by the passage coefficient, which is calculated by the formula:

$$p_i^{tun} = \left[1 + \exp\left(-\frac{4\left(\mu v_i^2 + Z_i\right)\sqrt{\mu}\,\xi_i}{Z_i^{3/2}}\right)\right]^{-1}. \qquad (1.67)$$

Formula (1.67) allows us to take into account sub-barrier transitions in the case when the energy splitting in the non-adiabatic region is relatively large. In the case of small splitting, this formula is not suitable, and tunnelling must be taken into account otherwise. In general, the passage coefficient can be found by perturbation theory and is expressed in terms of the Airy function [83]. We will write down the final form of the multichannel formula, which will be used in this dissertation in the study of nuclear

dynamics:

$$P_{if}^{tot} = 2p_f(1-p_f)(1-p_i)\prod_{k=f+1}^{i-1} p_k \times$$
$$\times\left\{1+\sum_{m=1}^{2(f-1)}\prod_{k=1}^{m}\left(-p_{f-\left[\frac{k+1}{2}\right]}\right)\right\}\times$$
$$\times\left\{1-\frac{\prod_{k=i}^{F} p_k^2\left(1+\sum_{m=1}^{2(i-1)}\prod_{k=1}^{m}\left\{-p_{i-\left[\frac{k+1}{2}\right]}\right\}\right)}{\sum_{m=1}^{2F}\prod_{k=1}^{m}\left(-p_{F+1-\left[\frac{k+1}{2}\right]}\right)}\right\}. \tag{1.68}$$

§ 1.5 Calculation of cross sections and rate coefficients

Cross sections of inelastic processes are calculated using well-known formulas (see, for example, [84]):

$$\sigma_{if}(K) = \frac{\pi}{K_i^2}\sum_{J=0}^{\infty}(2J+1)|S_{if}^J|^2\,, \tag{1.69}$$

where K – the wave number, J – the quantum number of the total angular momentum, S_{if}^J – the off-diagonal element of the scattering matrix, which, when squared, is nothing more than the total probability of a non-adiabatic transition from the initial state i to the final state f. Let's rewrite this formula in terms of the collision energy, and also take into account the fact that one scattering channel can generate several molecular symmetries, in each of which nuclear dynamics proceeds differently:

$$\sigma_{if}(E) = \frac{\pi\hbar^2 p_i^{stat}}{2\mu E}\sum_{J=0}^{\infty}(2J+1)P_{if}(J,E)\,, \tag{1.70}$$

where E – the total collision energy of the system (the sum of the collision energy and the asymptotic energy of the initial channel i), and p^{stat} – the

statistical weight determining the initial occupancy of the channel in a given molecular symmetry:

$$p_i^{stat} = \frac{N^S N^L}{N_{tot}^S N_{tot}^L}\,, \tag{1.71}$$

where N^S is the number of quantum numbers of full spin projections S that describe the considered ith state in this symmetry, and N_{tot}^S – the total number of quantum numbers of full spin projections that generates this scattering channel in all molecular symmetries; similarly for N^L and N_{tot}^L for the quantum number of the total orbital moment L.

Note that the cross sections of inelastic processes have three requirements in order for them to have finite values, i. e. converge:

1. Completeness of the basis of electronic wave functions.

2. Convergence over the quantum number of the total angular momentum.

3. Convergence over the internuclear distance.

The first condition means that a large number of molecular states, including highly excited molecular states, must be taken into account in non-adiabatic nuclear dynamics. The second condition means that the number of partial waves in the sum (1.70) must be such that all non-zero terms are taken into account (in other words, the summation must go to such a value $J_{max}+1$, at which all inelastic processes stop and only elastic scattering remains). The third condition means that the integration of differential equations must be carried out to such a value R_{asymp}, at which all the non-adiabatic couplings matrix elements turn to zero.

According to the formula (1.70) it is possible to calculate the cross section of any inelastic process, the main thing is to have the entire scattering matrix, or, what is the same thing, to know the full probabilities of a non-adiabatic transition from all initial states to all final ones. But some model methods for studying nuclear dynamics in the framework of

the Landau-Zener model do not allow us to obtain a scattering matrix or complete probabilities of non-adiabatic transitions for all processes. For example, the multichannel formula (1.68) allows us to get only the probabilities of exothermic processes, but not endothermic processes. To obtain cross sections of endothermic processes (excitation, ion-pair formation), it is necessary to use the balance equation:

$$\sigma_{fi}(E) = \sigma_{if}(E - \Delta E_{if}) \, \frac{p_f^{stat}}{p_i^{stat}} \, \frac{E - \Delta E_{if}}{E} \, , \tag{1.72}$$

at the condition $i > f$ $(U(\infty)_i > U(\infty)_j)$.

The cross section, as can be seen from the formulas (1.70) and (1.72), implies summation over the quantum number of the total angular momentum J from 0 to ∞. With numerical calculation, this cannot be done, the summation will go up to some finite value of J_{max}. It is determined from the condition that when the value is $J = J_{max} + 1$ all the total probabilities of non-adiabatic transitions will be zero, that is, only elastic scattering will occur. For model methods in the framework of the Landau-Zener model, this value is determined by the condition that for the value of the total angular momentum quantum number $J_{max} + 1$, the "input" non-adiabatic region (the non-adiabatic region between the input channel and any neighboring one, located at the greatest internuclear distance) becomes closed, that is, the current probability cannot reach any non-adiabatic region in which a non-adiabatic transition could occur, therefore, only elastic scattering is possible. Mathematically, this condition is expressed by the formula (for $R \leq R_C^{init}$):

$$U_j^{eff}(R) > E_{tot} \, . \tag{1.73}$$

In other words, the system cannot pass this non-adiabatic region when moving from right to left (from $R \to \infty$ to $R \to 0$), the system reaches the classical turning point, changes the direction of movement and moves to infinity without making a single non-adiabatic transition.

The rate coefficient is defined as the integral of the cross section over the entire range of collision energies multiplied by the Maxwell energy distribution:

$$k_{if}(T) = \sqrt{\frac{8}{\pi\mu(k_B T)^3}} \int_0^\infty \sigma_{if}(E)\, E\, exp(-\frac{E}{k_B T})\, dE\,, \qquad (1.74)$$

where k_B – Boltzmann constant. For the rate coefficients, the balance equation also can be written and use it to calculate the rate coefficients of endothermic processes through the rate coefficients of exothermic processes:

$$k_{fi}(T) = k_{if}(T)\, \frac{p_f^{stat}}{p_i^{stat}} \exp\left(-\frac{\Delta E_{if}}{k_B T}\right)\,, \qquad (1.75)$$

where $\Delta E_{if} = E_i^{asymp} - E_f^{asymp}$ – the energy difference of the asymptotic channels i and f, again under the condition $i > f$.

The partial rate coefficient $k_{if}(T)$ is hereinafter referred to as the rate coefficient calculated within a single molecular symmetry for an inelastic process $i \to f$ by the formula (1.74) or (1.75). The total rate coefficient $K_{if}(T)$ is hereinafter referred to as the rate coefficient summed over all molecular symmetries generated simultaneously by the channels i, f. For example, for two scattering channels 1, $A^*(np\ ^2P^o) + H(1s\ ^2S)$, and 2, $A^*(nd\ ^2D) + H(1s\ ^2S)$, there are the following possible molecular symmetries within which non-adiabatic transitions can occur (excluding rotational matrix elements): $^{1,3}\Sigma^+$, $^{1,3}\Pi$. Considering non-adiabatic transitions only within the same symmetry, we get that there are 4 partial rate coefficients: $k_{12}^{^1\Sigma^+}(T)$, $k_{12}^{^3\Sigma^+}(T)$, $k_{12}^{^1\Pi}(T)$ and $k_{12}^{^3\Pi}(T)$. The total rate coefficient $K_{12}(T)$ of the inelastic process $1 \to 2$ will then be equal to:

$$K_{12}(T) = k_{12}^{^1\Sigma^+}(T) + k_{12}^{^3\Sigma^+}(T) + k_{12}^{^1\Pi}(T) + k_{12}^{^3\Pi}(T). \qquad (1.76)$$

Thus, calculations of the inelastic transition probabilities, cross sections and rate coefficients of inelastic processes in atomic collisions can be carried

out within the framework of the Born-Oppenheimer approach, using the division the problem of atomic collisions into two steps: calculations of the electronic structures of molecules with fixed nuclei and the study of non-adiabatic nuclear dynamics. There are different methods and approaches for both steps, partially developed in this dissertation (see Chapter 2), which can be used depending on the specific situation.

Chapter 2. Accounting for the fine structure of energy levels in atomic collisions

§ 2.1 Preliminary remarks

Often there are situations when the atomic energy level has a fine splitting. For light atoms, this splitting is quite small, but with increasing atomic number, this splitting increases. For example, collisions of atoms and ions of the iron-peak elements (Sc – Ni) present a great difficulty for the correct calculation of the characteristics of inelastic processes in collisions with hydrogen. The atoms of these elements are characterized by the presence of a fairly large number of energy levels. The values of the fine splitting of atomic terms are comparable to the splits between different atomic terms.

In this situation, it is necessary to consider the Hund coupling type *«c»*, since consideration within the framework of the Hund coupling type *«a»* is not correct. That is, it is necessary to explicitly take into account the fine structure of energy levels when calculating the electronic structure of molecules at the first step of the Born-Oppenheimer approach. Such calculations must be carried out taking into account relativistic effects, which complicates the calculations. Therefore, the development of model approximate methods for calculating the electronic structure of molecules taking into account the fine structure of energy levels is an important goal. Here and further we will call the Hund coupling type *«a»* as LS representation or LS coupling representation [4], and the Hund coupling type *«c»* as JJ representation or JJ coupling representation [5].

Such approach was proposed in the papers [23,24] as a modification of the asymptotic method [75] in case of taking into account the fine structure

[4]The wave functions are described by the quantum numbers of the total orbital moment L, the module of the projection of the total orbital moment on the internuclear axis Λ, the full spin S and the projection of the full spin M_S.

[5]The wave function is described by the quantum number of the total angular momentum of the electrons J, as well as by the module of the projection of the total angular momentum on the internuclear axis Ω.

of energy levels. The original method was proposed and applied to account for the fine structure in collisions with hydrogen for alkali metal atoms, as well as alkali-like ions. This Chapter presents a further generalization for the case of collisions of alkali-earth metal atoms with hydrogen.

§ 2.2 Accounting for fine structure of the energy levels of atoms of group II of the Periodic Table in collisions with hydrogen

The original asymptotic method for calculations of the electronic structure of a collisional quasimolecule A + H, proposed in the paper [75], described in Chapter 1, §1.3.2. This method is formulated in the LS coupling representation and takes into account the presence of only ion-covalent interaction. In the diabatic representation, the electronic Hamiltonian matrix has the form of an arrow: diagonal elements correspond to diabatic potential energies, and non-zero off-diagonal matrix elements (the first column and the first row) are responsible for the ion-covalent interaction calculated by the Olson-Smith-Bayer formula (1.34) [43, 44].

First, we briefly present the main ideas and results of the method of accounting for the fine structure of energy levels in the case of collisions of alkali metals with hydrogen. The essence of the modified asymptotic method of accounting for the fine structure of energy levels proposed in [23, 24], is as follows:

a) it is necessary to change representation from the LS to the JJ one;

b) to do this, it is necessary to take into account relativistic effects, including spin-orbit interaction;

c) then the electronic Hamiltonian, taking into account relativistic operators, will take the following form:

$$\hat{H}_e = \hat{H}_e^{non-rel} + \hat{V}^{rel}\,; \tag{2.1}$$

d) when calculating matrix elements $\langle\phi_k|\,\hat{H}_e\,|\phi_j\rangle$ with an electronic Hamiltonian (2.1), matrix elements of the form $\langle\phi_k|\,\hat{H}_e^{non-rel}ket\phi_j$ and $\langle\phi_k|\,\hat{V}^{rel}\,|\phi_j\rangle$ will arise;

e) for diagonal matrix elements, taking into account $\langle\phi_k|\,\hat{V}^{rel}\,|\phi_k\rangle$ will lead to a fine splitting of energy levels;

f) for off-diagonal matrix elements, the contribution from the relativistic correction $\langle\phi_k|\,\hat{V}^{rel}\,|\phi_j\rangle$ in the first approximation is assumed to be small in comparison with the non-relativistic matrix element $\langle\phi_k|\,\hat{H}_e^{non-rel}\,|\phi_j\rangle$;

g) it remains only to calculate the matrix elements of the ion-covalent interaction H_{kj}^{JJ} in the JJ representation.

To fulfill the last point, it is necessary to find the correspondence between the molecular wave functions in the LS and JJ representations. Let's first consider the LS representation. Following the monograph by E. E. Nikitin and S. Y. Umansky [54], we will represent molecular wave functions in LS representation at large internuclear distances as a linear combination of atomic wave functions:

$$|L\tilde{\Lambda}SM_S\rangle_{AB} = \hat{A}\sum_{M_{L_A}M_{L_B}}\sum_{M_{S_A}M_{S_B}}\begin{bmatrix} L_A & L_B & L \\ M_{L_A} & M_{L_B} & \tilde{\Lambda}\end{bmatrix}\begin{bmatrix} S_A & S_B & S \\ M_{S_A} & M_{S_B} & M_S\end{bmatrix}\times$$
$$\times\,|L_AM_{L_A}S_AM_{S_A}\rangle_A\,|L_BM_{L_B}S_BM_{S_B}\rangle_B\ , \tag{2.2}$$

where $\hat{A}$ is the antisymmetrization operator (containing the normalization coefficient and electron permutation operators), the Clebsch–Gordan coefficients are written in square brackets. Off-diagonal matrix elements of the electronic Hamiltonian in the diabatic representation responsible for the ion-covalent interaction

$$\langle L\tilde{\Lambda}SM_S|\,\hat{H}_e\,|L'\tilde{\Lambda}'S'M'_S\rangle \approx \langle L\tilde{\Lambda}SM_S|\,\hat{H}_e^{non-rel}\,|L'\tilde{\Lambda}'S'M'_S\rangle \tag{2.3}$$

within the framework of the asymptotic method, as previously mentioned, are calculated using the Olson-Smith-Bayer formula:

$$\langle L\tilde{\Lambda}SM_S|\,\hat{H}_e^{non-rel}\,|L'\tilde{\Lambda}'S'M'_S\rangle = H_{kk'}^{OSB,LS}\,. \tag{2.4}$$

In the case of collisions of alkali metal atoms and cations with hydrogen atoms and anions (atom A is an alkali metal atom, atom B is a hydrogen atom), the ionic molecular wave function has only $^1\Sigma^+$ molecular symmetry characterized by the following quantum numbers: $L=0$, $\tilde{\Lambda}=0$, $S=0$, $M_S=0$: $|0000\rangle$. Covalent molecular wave functions in $^1\Sigma^+$ symmetry are written as $|L000\rangle$. Then the matrix element of the ion-covalent interaction of the electronic Hamiltonian will be written in the case of $^1\Sigma^+$ symmetry in the form:

$$\langle 0000|\,\hat{H}_e^{non-rel}\,|L000\rangle = H_{k\,ionic}^{OSB,LS}\,. \tag{2.5}$$

Note that the hydrogen atom is always in the ground state $H(1s\ ^2S_{1/2})$, and the hydrogen anion has a completely filled $(1s^2)$ shell. The quantum number of the total orbital moment L of the molecular wave function is completely determined by the atomic orbital quantum number L_A, since the quantum number of the orbital moment of hydrogen $L_B=0$.

Let us now consider the JJ representation. For the JJ representation, the molecular wave function is written as:

$$|J_AJ_BJ\tilde{\Omega}\rangle_{AB} = \hat{A}\sum_{M_AM_B}\begin{bmatrix} J_A & J_B & J \\ M_A & M_B & \tilde{\Omega}\end{bmatrix}|J_AM_A\rangle_A\,|J_BM_B\rangle_B\,. \tag{2.6}$$

The off-diagonal matrix element of the electronic Hamiltonian in the JJ representation will be written as:

$$H_{kk'}^{JJ} = \langle J_AJ_BJ\tilde{\Omega}|\,\hat{H}_e^{non-rel}\,|J'_AJ'_BJ'\tilde{\Omega}'\rangle\,. \tag{2.7}$$

For collisions of alkali metal atoms and cations with hydrogen atoms and anions, the ionic molecular wave function has only 0^+ molecular symmetry

characterized by the following quantum numbers: $J_1 = 0$, $J_2 = 0$, $J = 0$, $\tilde{\Omega} = 0$: $|0000\rangle$. Covalent molecular wave functions in 0^+ symmetry are written as $|J_A \frac{1}{2} J0\rangle$. Then the matrix element of the ion-covalent interaction of the electronic Hamiltonian will be written in the case of 0^+ symmetry in the form:

$$\langle 0000| \hat{H}_e^{non-rel} |J_A \frac{1}{2} J0\rangle \ . \tag{2.8}$$

It is necessary to find a correspondence between matrix elements in LS and JJ representations. To do this, it is necessary to find the correspondence of molecular wave functions in LS and JJ representations. To do this, we express atomic wave functions, through which molecular wave functions are expressed by the formulas (2.2) and (2.6), through the same one-electron wave functions:

- LS representation: $\psi_{LS}^{atomic}(\vec{r}, \sigma) = \phi_{n\,l\,m_l}(\vec{r}) \chi_{s\,m_s}(\sigma) = |n\,l\,m_l\rangle\, \chi_{\frac{1}{2}\,m_s}$;
- JJ representation: $\psi_{JJ}^{atomic}(\vec{r}, \sigma) = \phi_{j\,m}(\vec{r}) \chi_{s\,m_s}(\sigma) = |jm\rangle\, \chi_{\frac{1}{2}\,m_s}$;

Let's find a correspondence between atomic wave functions in two representations:

$$|jm\rangle = \sum_{m_l\, m_s} \begin{bmatrix} l & s & j \\ m_l & m_s & m \end{bmatrix} |l\, m_l\, s\, m_s\rangle \ . \tag{2.9}$$

Now that it is possible to write down all molecular wave functions through the same one-electron functions, it is possible to find an unambiguous relationship between the off-diagonal matrix elements of the electronic Hamiltonian (see [23, 24]):

$$\langle 0000| \hat{H}_e^{non-rel} |J_A \frac{1}{2} J0\rangle = \langle 0000| \hat{H}_e^{non-rel} |L000\rangle \times$$
$$\times \frac{1}{\sqrt{2}} \left(\begin{bmatrix} J_A & \frac{1}{2} & J \\ \frac{1}{2} & -\frac{1}{2} & 0 \end{bmatrix} \begin{bmatrix} L & \frac{1}{2} & J_A \\ 0 & \frac{1}{2} & \frac{1}{2} \end{bmatrix} - \begin{bmatrix} J_A & \frac{1}{2} & J \\ -\frac{1}{2} & \frac{1}{2} & 0 \end{bmatrix} \begin{bmatrix} L & \frac{1}{2} & J_A \\ 0 & -\frac{1}{2} & -\frac{1}{2} \end{bmatrix} \right) . \tag{2.10}$$

Formula (2.10) allows us to take into account the fine structure of energy levels in collisions with hydrogen of alkali metal atoms and alkali-

like ions (once ionized alkaline earth metals, twice ionized atoms of the third group of the Periodic Table, etc.). The expression in parentheses multiplied by $\frac{1}{\sqrt{2}}$, – the proportionality coefficient C, expressed in terms of the difference of the products of the Clebsch-Gordan coefficients.

Let's now try to generalize this method to the case of two valence electrons on an atom A colliding with hydrogen. I.e., consider collisions of alkali-earth metal atoms with hydrogen and try in the same way to obtain a correspondence between the off-diagonal matrix elements of the electronic Hamiltonian in LS and JJ representations. In this case, the atomic function of the atom A colliding with hydrogen will already be two-electron, and the molecular functions will be three-electron. The basic ionic molecular state always generates only $^2\Sigma^+$ symmetry in the LS representation, and only $\frac{1}{2}$ symmetry in the JJ representation. Further, for clarity, we will consider specific atomic and molecular states on the example of a calcium atom, without detracting from the generality of reasoning.

Let's write down the molecular wave functions in LS and JJ representations, respectively. The ionic molecular wave function of the ground ionic state $\mathrm{Ca}^+(4s\ ^2S_{1/2}) + \mathrm{H}^-(1s^2\ ^1S_0)$, as mentioned above, in the LS representation generates only $^2\Sigma^+$ molecular symmetry and will be written as $|00\frac{1}{2} \pm \frac{1}{2}\rangle$. In JJ representation for the unique symmetry $\Omega = \frac{1}{2}$, this function is written as $|0\frac{1}{2}\frac{1}{2} \pm \frac{1}{2}\rangle$. Both of these functions can be expressed in terms of atomic wave functions of hydrogen and calcium:

- LS: $|00\frac{1}{2} \pm \frac{1}{2}\rangle = \hat{A}\,|00\frac{1}{2} \pm \frac{1}{2}\rangle^{Ca^+}\,|0000\rangle^{H^-}$;
- JJ: $|0\frac{1}{2}\frac{1}{2} \pm \frac{1}{2}\rangle = \hat{A}\,|\frac{1}{2} \pm \frac{1}{2}\rangle^{Ca^+}\,|00\rangle^{H^-}$.

Let's write down explicitly how atomic wave functions are related in JJ and LS representations, following the formula (2.9), for the case of ion wave functions:

- LS: $|00\rangle = \begin{bmatrix} 0 & 0 & 0 \\ 0 & 0 & 0 \end{bmatrix} |0000\rangle = |0000\rangle$;

- JJ: $|\frac{1}{2}\pm\frac{1}{2}\rangle = \begin{bmatrix} 0 & \frac{1}{2} & \frac{1}{2} \\ 0 & \pm\frac{1}{2} & \pm\frac{1}{2} \end{bmatrix} |00\frac{1}{2}\pm\frac{1}{2}\rangle = |00\frac{1}{2}\pm\frac{1}{2}\rangle\,.$

Let's write down the final form of the ionic wave functions in two representations expressed in terms of the same atomic wave functions in the LS representation:

- LS: $|00\frac{1}{2}\pm\frac{1}{2}\rangle = \hat{A}\,|00\frac{1}{2}\pm\frac{1}{2}\rangle^{Ca^+}\,|0000\rangle^{H^-}$;
- JJ: $|\frac{1}{2}0\frac{1}{2}\pm\frac{1}{2}\rangle = \hat{A}\,|00\frac{1}{2}\pm\frac{1}{2}\rangle^{Ca^+}\,|0000\rangle^{H^-}$.

Let us now write down the molecular wave functions of the covalent states $\mathrm{Ca}(nl\,n'l'\,{}^{1,3}L_J) + \mathrm{H}(1s\,{}^2S_{1/2})$ in symmetries ${}^2\Sigma^+$ and $\frac{1}{2}$. They are given in the Table 1.

Then we write out all the molecular functions in the LS and JJ representations also through the same atomic functions in the LS representation using the formulas (2.2), (2.6), (2.9), leaving the antisymmetrization operator $\hat{A}$ in an implicit form. We will also limit ourselves to considering only those functions that have a positive projection of the full spin $M_S = \frac{1}{2}$, since for negative projections the result will be the same.

Let us first consider the simplest case, namely the singlet S states of the calcium atom. In this case, there will be no separation at all, and the matrix element H^{JJ}_{kj} in the JJ representation exactly coincides with the matrix element in the LS representation H^{LS}_{kj}. We will also consider further the singlet states of the calcium atom, but different from S. Take, for example, the state of the calcium atom ${}^1D$, which corresponds to the molecular state $\mathrm{Ca}(4s3d\,{}^1D_2) + \mathrm{H}(1s\,{}^2S_{1/2})$:

- LS:

$$|20\frac{1}{2}\frac{1}{2}\rangle = \hat{A} \begin{bmatrix} 2 & 0 & 2 \\ 0 & 0 & 0 \end{bmatrix} \begin{bmatrix} 0 & \frac{1}{2} & \frac{1}{2} \\ 0 & \frac{1}{2} & \frac{1}{2} \end{bmatrix} |2000\rangle^{Ca}\,|00\frac{1}{2}\frac{1}{2}\rangle^{H} = \hat{A}\,|2000\rangle^{Ca}\,|00\frac{1}{2}\frac{1}{2}\rangle^{H}\,.$$

Table 1. Explicit form of molecular wave functions in LS and JJ representations in $^2\Sigma^+$ and $\frac{1}{2}$ symmetries, respectively.

State	LS	JJ
	$\|L\tilde{\Lambda}SM_S\rangle$	$\|J_{Ca}J_H J\tilde{\Omega}\rangle$
$\mathrm{Ca}(4s^2\ ^1S_0) + \mathrm{H}(1s\ ^2S_{1/2})$	$\|00\frac{1}{2}\pm\frac{1}{2}\rangle$	$\|0\frac{1}{2}\frac{1}{2}\pm\frac{1}{2}\rangle$
$\mathrm{Ca}(4s4p\ ^1P_1) + \mathrm{H}(1s\ ^2S_{1/2})$	$\|10\frac{1}{2}\pm\frac{1}{2}\rangle$	$\|1\frac{1}{2}\frac{1}{2}\pm\frac{1}{2}\rangle$, $\|1\frac{1}{2}\frac{3}{2}\pm\frac{1}{2}\rangle$
$\mathrm{Ca}(4s4p\ ^3P_0) + \mathrm{H}(1s\ ^2S_{1/2})$	$\|10\frac{1}{2}\pm\frac{1}{2}\rangle$	$\|0\frac{1}{2}\frac{1}{2}\pm\frac{1}{2}\rangle$
$\mathrm{Ca}(4s4p\ ^3P_1) + \mathrm{H}(1s\ ^2S_{1/2})$		$\|1\frac{1}{2}\frac{1}{2}\pm\frac{1}{2}\rangle$, $\|1\frac{1}{2}\frac{3}{2}\pm\frac{1}{2}\rangle$
$\mathrm{Ca}(4s4p\ ^3P_2) + \mathrm{H}(1s\ ^2S_{1/2})$		$\|2\frac{1}{2}\frac{3}{2}\pm\frac{1}{2}\rangle$, $\|2\frac{1}{2}\frac{5}{2}\pm\frac{1}{2}\rangle$
$\mathrm{Ca}(4s3d\ ^1D_2) + \mathrm{H}(1s\ ^2S_{1/2})$	$\|20\frac{1}{2}\pm\frac{1}{2}\rangle$	$\|2\frac{1}{2}\frac{3}{2}\pm\frac{1}{2}\rangle$, $\|2\frac{1}{2}\frac{5}{2}\pm\frac{1}{2}\rangle$
$\mathrm{Ca}(4s3d\ ^3D_1) + \mathrm{H}(1s\ ^2S_{1/2})$	$\|20\frac{1}{2}\pm\frac{1}{2}\rangle$	$\|1\frac{1}{2}\frac{1}{2}\pm\frac{1}{2}\rangle$, $\|1\frac{1}{2}\frac{3}{2}\pm\frac{1}{2}\rangle$
$\mathrm{Ca}(4s3d\ ^3D_2) + \mathrm{H}(1s\ ^2S_{1/2})$		$\|2\frac{1}{2}\frac{3}{2}\pm\frac{1}{2}\rangle$, $\|2\frac{1}{2}\frac{5}{2}\pm\frac{1}{2}\rangle$
$\mathrm{Ca}(4s3d\ ^3D_3) + \mathrm{H}(1s\ ^2S_{1/2})$		$\|3\frac{1}{2}\frac{5}{2}\pm\frac{1}{2}\rangle$, $\|3\frac{1}{2}\frac{7}{2}\pm\frac{1}{2}\rangle$
$\mathrm{Ca}(4s5s\ ^1S_0) + \mathrm{H}(1s\ ^2S_{1/2})$	$\|00\frac{1}{2}\pm\frac{1}{2}\rangle$	$\|0\frac{1}{2}\frac{1}{2}\pm\frac{1}{2}\rangle$
$\mathrm{Ca}(4s5s\ ^3S_1) + \mathrm{H}(1s\ ^2S_{1/2})$	$\|00\frac{1}{2}\pm\frac{1}{2}\rangle$	$\|1\frac{1}{2}\frac{1}{2}\pm\frac{1}{2}\rangle$, $\|1\frac{1}{2}\frac{3}{2}\pm\frac{1}{2}\rangle$
$\mathrm{Ca}(4s5p\ ^1P_1) + \mathrm{H}(1s\ ^2S_{1/2})$	$\|10\frac{1}{2}\pm\frac{1}{2}\rangle$	$\|1\frac{1}{2}\frac{1}{2}\pm\frac{1}{2}\rangle$, $\|1\frac{1}{2}\frac{3}{2}\pm\frac{1}{2}\rangle$
$\mathrm{Ca}(4s5p\ ^3P_0) + \mathrm{H}(1s\ ^2S_{1/2})$	$\|10\frac{1}{2}\pm\frac{1}{2}\rangle$	$\|0\frac{1}{2}\frac{1}{2}\pm\frac{1}{2}\rangle$
$\mathrm{Ca}(4s5p\ ^3P_1) + \mathrm{H}(1s\ ^2S_{1/2})$		$\|1\frac{1}{2}\frac{1}{2}\pm\frac{1}{2}\rangle$, $\|1\frac{1}{2}\frac{3}{2}\pm\frac{1}{2}\rangle$
$\mathrm{Ca}(4s5p\ ^3P_2) + \mathrm{H}(1s\ ^2S_{1/2})$		$\|2\frac{1}{2}\frac{3}{2}\pm\frac{1}{2}\rangle$, $\|2\frac{1}{2}\frac{5}{2}\pm\frac{1}{2}\rangle$
$\mathrm{Ca}(3d4p\ ^3F_2) + \mathrm{H}(1s\ ^2S_{1/2})$	$\|30\frac{1}{2}\pm\frac{1}{2}\rangle$	$\|2\frac{1}{2}\frac{3}{2}\pm\frac{1}{2}\rangle$, $\|2\frac{1}{2}\frac{5}{2}\pm\frac{1}{2}\rangle$
$\mathrm{Ca}(3d4p\ ^3F_3) + \mathrm{H}(1s\ ^2S_{1/2})$		$\|3\frac{1}{2}\frac{5}{2}\pm\frac{1}{2}\rangle$, $\|3\frac{1}{2}\frac{7}{2}\pm\frac{1}{2}\rangle$
$\mathrm{Ca}(3d4p\ ^3F_4) + \mathrm{H}(1s\ ^2S_{1/2})$		$\|4\frac{1}{2}\frac{7}{2}\pm\frac{1}{2}\rangle$, $\|4\frac{1}{2}\frac{9}{2}\pm\frac{1}{2}\rangle$

- JJ:

$$|2\frac{1}{2}\frac{3}{2}\frac{1}{2}\rangle = \hat{A}\begin{bmatrix} 2 & \frac{1}{2} & \frac{3}{2} \\ M_1 & M_2 & \frac{1}{2} \end{bmatrix} |2M_1\rangle^{Ca} |\frac{1}{2}M_2\rangle^{H} =$$
$$= \hat{A}\left(\sqrt{\frac{3}{5}}\,|21\rangle^{Ca}\,|\frac{1}{2}-\frac{1}{2}\rangle^{H} - \sqrt{\frac{2}{5}}\,|20\rangle^{Ca}\,|\frac{1}{2}\frac{1}{2}\rangle^{H}\right) =$$
$$= \hat{A}\left(\sqrt{\frac{3}{5}}\,|2100\rangle^{Ca}\,|00\frac{1}{2}-\frac{1}{2}\rangle^{H} - \sqrt{\frac{2}{5}}\,|2000\rangle^{Ca}\,|00\frac{1}{2}\frac{1}{2}\rangle^{H}\right) .$$

$$|2\frac{1}{2}\frac{5}{2}\pm\frac{1}{2}\rangle = \hat{A}\begin{bmatrix} 2 & \frac{1}{2} & \frac{5}{2} \\ M_1 & M_2 & \frac{1}{2} \end{bmatrix} |2M_1\rangle^{Ca} |\frac{1}{2}M_2\rangle^{H} =$$
$$= \hat{A}\left(\sqrt{\frac{2}{5}}\,|21\rangle^{Ca}\,|\frac{1}{2}-\frac{1}{2}\rangle^{H} + \sqrt{\frac{3}{5}}\,|20\rangle^{Ca}\,|\frac{1}{2}\frac{1}{2}\rangle^{H}\right) =$$
$$= \hat{A}\left(\sqrt{\frac{2}{5}}\,|2100\rangle^{Ca}\,|00\frac{1}{2}-\frac{1}{2}\rangle^{H} + \sqrt{\frac{3}{5}}\,|2000\rangle^{Ca}\,|00\frac{1}{2}\frac{1}{2}\rangle^{H}\right) .$$

The multipliers $\pm\sqrt{\frac{2}{5}}, \sqrt{\frac{3}{5}}$ were obtained from the Klebsch-Gordan coefficients. We now write down the matrix element of the electron Hamiltonian in LS and JJ representations, calculated on these molecular wave functions, as well as on the functions of the ionic state. In this case, we denote the ionic state $|00\frac{1}{2}\frac{1}{2}\rangle$ as k, the covalent state $|20\frac{1}{2}\frac{1}{2}\rangle$ in LS representation as j, and the covalent states in JJ representation $|2\frac{1}{2}\frac{3}{2}\frac{1}{2}\rangle$ and $|2\frac{1}{2}\frac{5}{2}\frac{1}{2}\rangle$ as j_1 and j_2 respectively:

- LS:

$$H_{kj}^{OSB,LS} = \langle 00\frac{1}{2}\frac{1}{2}|\,\hat{H}_e\,|20\frac{1}{2}\frac{1}{2}\rangle =$$
$$= \left\langle \hat{A}\,\langle 00\frac{1}{2}\frac{1}{2}|^{Ca^+}\,\langle 0000|^{H^-}\,\left|\hat{H}_e\right|\,\hat{A}\,|2000\rangle^{Ca}\,|00\frac{1}{2}\frac{1}{2}\rangle^{H}\right\rangle .$$

- JJ:

$$H^{JJ}_{kj_1} = \langle \frac{1}{2}0\frac{1}{2}\frac{1}{2}| \hat{H}_e |2\frac{1}{2}\frac{3}{2}\frac{1}{2}\rangle = \sqrt{\frac{3}{5}}\tilde{H}^{JJ}_{kj_1} - \sqrt{\frac{2}{5}}H^{OSB,LS}_{kj} =$$
$$= \left\langle \hat{A}\,\langle 00\frac{1}{2}\frac{1}{2}|^{Ca^+}\,\langle 0000|^{H^-}\left|\hat{H}_e\right|\sqrt{\frac{3}{5}}\hat{A}\,|2100\rangle^{Ca}\,|00\frac{1}{2}-\frac{1}{2}\rangle^{H}\right\rangle -$$
$$- \left\langle \hat{A}\,\langle 00\frac{1}{2}\frac{1}{2}|^{Ca^+}\,\langle 0000|^{H^-}\left|\hat{H}_e\right|\sqrt{\frac{2}{5}}\hat{A}\,|2000\rangle^{Ca}\,|00\frac{1}{2}\frac{1}{2}\rangle^{H}\right\rangle .$$

$$H^{JJ}_{kj_2} = \langle \frac{1}{2}0\frac{1}{2}\frac{1}{2}| \hat{H}_e |2\frac{1}{2}\frac{5}{2}\frac{1}{2}\rangle = \sqrt{\frac{2}{5}}\tilde{H}^{JJ}_{kj_2} + \sqrt{\frac{3}{5}}H^{OSB,LS}_{kj} =$$
$$= \left\langle \hat{A}\,\langle 00\frac{1}{2}\frac{1}{2}|^{Ca^+}\,\langle 0000|^{H^-}\left|\hat{H}_e\right|\sqrt{\frac{2}{5}}\hat{A}\,|2100\rangle^{Ca}\,|00\frac{1}{2}-\frac{1}{2}\rangle^{H}\right\rangle +$$
$$+ \left\langle \hat{A}\,\langle 00\frac{1}{2}\frac{1}{2}|^{Ca^+}\,\langle 0000|^{H^-}\left|\hat{H}_e\right|\sqrt{\frac{3}{5}}\hat{A}\,|2000\rangle^{Ca}\,|00\frac{1}{2}\frac{1}{2}\rangle^{H}\right\rangle .$$

It can be seen that in the JJ representation, the matrix elements of the ion-covalent interaction $H^{JJ}_{kj_1,kj_2}$ will be the sum of two matrix elements $\tilde{H}^{JJ}_{kj_1,kj_2}$ and $H^{OSB,LS}_{kj}$ multiplied by some coefficients calculated from the Klebsch-Gordan coefficients. Matrix elements $\tilde{H}^{JJ}_{kj_1,kj_2}$ represent the contribution from the interaction of the ionic state with the state described by the molecular wave function $\hat{A}\,|2100\rangle^{Ca}\,|00\frac{1}{2}-\frac{1}{2}\rangle^{H}$ corresponding to the $^2\Pi$ symmetry representation in LS. Within the framework of the asymptotic method, only the interaction between the ionic state and all covalent ones in the same molecular symmetry is calculated, that is, such matrix elements $\tilde{H}^{JJ}_{kj_1,kj_2}$ are assumed to be zero. As a result, we obtain the following relationship between the matrix elements of the ion-covalent interaction in LS and JJ representations:

$$\begin{aligned} H^{JJ}_{kj_1} &= -\sqrt{\frac{2}{5}}H^{OSB,LS}_{kj}\,, \\ H^{JJ}_{kj_2} &= \sqrt{\frac{3}{5}}H^{OSB,LS}_{kj}\,, \end{aligned} \tag{2.11}$$

which coincides with the results obtained to account for the fine structure in collisions with hydrogen of elements of the first group of the Periodic table, namely for the states $\mathrm{Elem}(nd\ ^2D_{3/2,5/2}) + \mathrm{H}(1s\ ^2S)$. Note that in the case of alkali metals, the molecular states are not doubly degenerate, as in the case of alkaline earth metals. Similar results can be obtained for the atomic terms ^1P, ^1F and so on, with the corresponding coefficients $\left(-\sqrt{\frac{1}{3}}, \sqrt{\frac{2}{3}}\right)$ and $\left(-\sqrt{\frac{3}{7}}, \sqrt{\frac{4}{7}}\right)$ and so on, according to the results for alkali metals.

Let us now consider a more complex case, namely triplet states. To begin with, consider the state of calcium ^3S. Let's write down the wave functions of the corresponding covalent states $\mathrm{Ca}(4s5s\ ^3S_1) + \mathrm{H}(1s\ ^2S_{1/2})$:

- LS:

$$|00\frac{1}{2}\frac{1}{2}\rangle = \hat{A} \begin{bmatrix} 0 & 0 & 0 \\ 0 & 0 & 0 \end{bmatrix} \begin{bmatrix} 1 & \frac{1}{2} & \frac{1}{2} \\ M_S^{Ca} & M_S^H & \frac{1}{2} \end{bmatrix} |001M_S^{Ca}\rangle^{Ca} |00\frac{1}{2}M_S^H\rangle^H =$$
$$= \hat{A} \left(\sqrt{\frac{2}{3}} |0011\rangle^{Ca} |00\frac{1}{2} - \frac{1}{2}\rangle^H - \sqrt{\frac{1}{3}} |0010\rangle^{Ca} |00\frac{1}{2}\frac{1}{2}\rangle^H \right) .$$

- JJ:

$$|1\frac{1}{2}\frac{1}{2}\frac{1}{2}\rangle = \hat{A} \begin{bmatrix} 1 & \frac{1}{2} & \frac{1}{2} \\ M_1 & M_2 & \frac{1}{2} \end{bmatrix} |1M_1\rangle^{Ca} |\frac{1}{2}M_2\rangle^H =$$
$$= \hat{A} \left(\sqrt{\frac{2}{3}} |11\rangle^{Ca} |\frac{1}{2} - \frac{1}{2}\rangle^H - \sqrt{\frac{1}{3}} |10\rangle^{Ca} |\frac{1}{2}\frac{1}{2}\rangle^H \right) =$$
$$= \hat{A} \left(\sqrt{\frac{2}{3}} |0011\rangle^{Ca} |00\frac{1}{2} - \frac{1}{2}\rangle^H - \sqrt{\frac{1}{3}} |0010\rangle^{Ca} |00\frac{1}{2}\frac{1}{2}\rangle^H \right) .$$

$$|1\frac{1}{2}\frac{3}{2}\frac{1}{2}\rangle = \hat{A}\begin{bmatrix} 1 & \frac{1}{2} & \frac{3}{2} \\ M_1 & M_2 & \frac{1}{2} \end{bmatrix} |1M_1\rangle^{Ca} |\frac{1}{2}M_2\rangle^{H} =$$
$$= \hat{A}\left(\sqrt{\frac{1}{3}}\,|11\rangle^{Ca}\,|\frac{1}{2}-\frac{1}{2}\rangle^{H} + \sqrt{\frac{2}{3}}\,|10\rangle^{Ca}\,|\frac{1}{2}\frac{1}{2}\rangle^{H}\right) =$$
$$= \hat{A}\left(\sqrt{\frac{1}{3}}\,|0011\rangle^{Ca}\,|00\frac{1}{2}-\frac{1}{2}\rangle^{H} + \sqrt{\frac{2}{3}}\,|0010\rangle^{Ca}\,|00\frac{1}{2}\frac{1}{2}\rangle^{H}\right) .$$

As in the previous case, we will write down the matrix element of the electron Hamiltonian in LS and JJ representations, calculated on these molecular wave functions and the ionic state wave functions. We also denote the ionic state $|00\frac{1}{2}\frac{1}{2}\rangle$ as k, the covalent state $|00\frac{1}{2}\frac{1}{2}\rangle$ in LS representation as j, and the covalent states in JJ representation $|1\frac{1}{2}\frac{1}{2}\frac{1}{2}\rangle$ and $|1\frac{1}{2}\frac{3}{2}\frac{1}{2}\rangle$ as j_1 and j_2 respectively:

- LS:

$$H_{kj}^{OSB,LS} = \langle 00\frac{1}{2}\frac{1}{2}|\,\hat{H}_e\,|00\frac{1}{2}\frac{1}{2}\rangle =$$
$$= \left\langle \hat{A}\,\langle 00\frac{1}{2}\frac{1}{2}|^{Ca^+}\,\langle 0000|^{H^-}\left|\hat{H}_e\right|\sqrt{\frac{2}{3}}\hat{A}\,|0011\rangle^{Ca}\,|00\frac{1}{2}-\frac{1}{2}\rangle^{H}\right\rangle -$$
$$- \left\langle \hat{A}\,\langle 00\frac{1}{2}\frac{1}{2}|^{Ca^+}\,\langle 0000|^{H^-}\left|\hat{H}_e\right|\sqrt{\frac{1}{3}}\hat{A}\,|0010\rangle^{Ca}\,|00\frac{1}{2}\frac{1}{2}\rangle^{H}\right\rangle .$$

- JJ:

$$H_{kj_1}^{JJ} = \langle\frac{1}{2}0\frac{1}{2}\frac{1}{2}|\,\hat{H}_e\,|1\frac{1}{2}\frac{1}{2}\frac{1}{2}\rangle = H_{kj}^{OSB,LS} =$$
$$= \left\langle \hat{A}\,\langle 00\frac{1}{2}\frac{1}{2}|^{Ca^+}\,\langle 0000|^{H^-}\left|\hat{H}_e\right|\sqrt{\frac{2}{3}}\hat{A}\,|0011\rangle^{Ca}\,|00\frac{1}{2}-\frac{1}{2}\rangle^{H}\right\rangle -$$
$$- \left\langle \hat{A}\,\langle 00\frac{1}{2}\frac{1}{2}|^{Ca^+}\,\langle 0000|^{H^-}\left|\hat{H}_e\right|\sqrt{\frac{1}{3}}\hat{A}\,|0010\rangle^{Ca}\,|00\frac{1}{2}\frac{1}{2}\rangle^{H}\right\rangle .$$

$$H^{JJ}_{kj_2} = \langle \frac{1}{2} 0 \frac{1}{2}\frac{1}{2}| \, \hat{H}_e \, |1\frac{1}{2}\frac{3}{2}\frac{1}{2}\rangle =$$
$$= \left\langle \hat{A} \, \langle 00\frac{1}{2}\frac{1}{2}|^{Ca^+} \, \langle 0000|^{H^-} \left|\hat{H}_e\right| \sqrt{\frac{1}{3}}\hat{A} \, |0011\rangle^{Ca} \, |00\frac{1}{2} - \frac{1}{2}\rangle^{H} \right\rangle +$$
$$+ \left\langle \hat{A} \, \langle 00\frac{1}{2}\frac{1}{2}|^{Ca^+} \, \langle 0000|^{H^-} \left|\hat{H}_e\right| \sqrt{\frac{2}{3}}\hat{A} \, |0010\rangle^{Ca} \, |00\frac{1}{2}\frac{1}{2}\rangle^{H} \right\rangle \, .$$

In this case, it is not enough to consider only molecular functions expressed in terms of atomic ones, although it is clear that the matrix element in the JJ representation of $H^{JJ}_{kj_1}$ exactly coincides with the matrix element of $H^{OSB,LS}_{kj}$ in the LS representation. In order to deal with the matrix element $H^{JJ}_{kj_2}$, it is necessary to express all atomic functions (calcium and hydrogen) through one-electron wave functions, and when calculating the matrix element, integrate over all coordinates and sum over the spin variable. Omitting the rather cumbersome calculations, which occupy about 8 A4 pages for one of this matrix element, we will only give the final result. Let's introduce the notation:

$$\tilde{H}_1 = \left\langle \hat{A} \, \langle 00\frac{1}{2}\frac{1}{2}|^{Ca^+} \, \langle 0000|^{H^-} \left|\hat{H}_e\right| \hat{A} \, |0011\rangle^{Ca} \, |00\frac{1}{2} - \frac{1}{2}\rangle^{H} \right\rangle \, ,$$
$$\tilde{H}_2 = \left\langle \hat{A} \, \langle 00\frac{1}{2}\frac{1}{2}|^{Ca^+} \, \langle 0000|^{H^-} \left|\hat{H}_e\right| \hat{A} \, |0010\rangle^{Ca} \, |00\frac{1}{2}\frac{1}{2}\rangle^{H} \right\rangle \, . \qquad (2.12)$$

In these notations , matrix elements in LS and JJ representation will be written as:

$$\text{LS} : H^{OSB,LS}_{kj} = \sqrt{\frac{2}{3}}\tilde{H}_1 - \sqrt{\frac{1}{3}}\tilde{H}_2 \, ,$$
$$\text{JJ} : H^{JJ}_{kj_1} = \sqrt{\frac{2}{3}}\tilde{H}_1 - \sqrt{\frac{1}{3}}\tilde{H}_2 \, , \qquad (2.13)$$
$$H^{JJ}_{kj_2} = \sqrt{\frac{1}{3}}\tilde{H}_1 + \sqrt{\frac{2}{3}}\tilde{H}_2; .$$

Further, it can be shown that both matrix elements $\tilde{H}_1, \tilde{H}_2$, when expressed in terms of the same one-electron functions, can be expressed in terms of the same matrix element $\tilde{H}$:

$$\begin{aligned} \tilde{H}_1 &= \tilde{H} \ , \\ \tilde{H}_2 &= -\sqrt{\frac{1}{2}}\tilde{H} \ . \end{aligned} \tag{2.14}$$

Finally (2.13) will be written as:

$$\begin{aligned} \text{LS} : H_{kj}^{OSB,LS} &= \sqrt{\frac{2}{3}}\tilde{H} + \sqrt{\frac{1}{6}}\tilde{H} = H_{kj}^{OSB,LS} \ , \\ \text{JJ} : H_{kj_1}^{JJ} &= \sqrt{\frac{2}{3}}\tilde{H} + \sqrt{\frac{1}{6}}\tilde{H} = H_{kj}^{OSB,LS} \ , \\ H_{kj_2}^{JJ} &= \sqrt{\frac{1}{3}}\tilde{H} - \sqrt{\frac{1}{3}}\tilde{H} = 0 \ . \end{aligned} \tag{2.15}$$

Thus, despite the fact that in collisions $\mathrm{Ca}(4s5s\ ^3S_1) + \mathrm{H}(1s\ ^2S_{1/2})$ in the JJ representation, two states are obtained in symmetry $\frac{1}{2}$, only one of them participates in nuclear dynamics, while the matrix elements are identically equal to each other in LS and JJ representations.

Finally, consider the triplet states of the calcium atom other than S. For example, consider the ^3P state. This atomic state in collisions with hydrogen in the ground state generates five molecular states in JJ representation (which we will denote j_1, j_2, j_3, j_4, j_5, respectively). Let's write down the wave functions of the covalent states $\mathrm{Ca}(4s4p\ ^3P_{1/2,3/2,5/2}) + rmH(1s\ ^2S_{1/2})$:

- LS:

$$|10\frac{1}{2}\frac{1}{2}\rangle = \hat{A} \begin{bmatrix} 1 & 0 & 1 \\ 0 & 0 & 0 \end{bmatrix} \begin{bmatrix} 1 & \frac{1}{2} & \frac{1}{2} \\ M_S^{Ca} & M_S^H & \frac{1}{2} \end{bmatrix} |100M_S^{Ca}\rangle^{Ca} |00\frac{1}{2}M_S^H\rangle^H =$$

$$= \hat{A} \left(\sqrt{\frac{2}{3}} |1011\rangle^{Ca} |00\frac{1}{2} - \frac{1}{2}\rangle^H - \sqrt{\frac{1}{3}} |1010\rangle^{Ca} |00\frac{1}{2}\frac{1}{2}\rangle^H \right) \ .$$

- JJ:

$$|0\frac{1}{2}\frac{1}{2}\frac{1}{2}\rangle = \hat{A}\begin{bmatrix} 0 & \frac{1}{2} & \frac{1}{2} \\ 0 & \frac{1}{2} & \frac{1}{2} \end{bmatrix} |00\rangle^{Ca} |\frac{1}{2}\frac{1}{2}\rangle^{H} =$$

$$= \hat{A}\left(\sqrt{\frac{1}{3}}\,|111-1\rangle^{Ca}\,|00\frac{1}{2}\frac{1}{2}\rangle^{H} + \sqrt{\frac{1}{3}}\,|1-111\rangle^{Ca}\,|00\frac{1}{2}\frac{1}{2}\rangle^{H} -\right.$$

$$\left. - \sqrt{\frac{1}{3}}\,|1010\rangle^{Ca}\,|00\frac{1}{2}\frac{1}{2}\rangle^{H}\right) .$$

$$|1\frac{1}{2}\frac{1}{2}\frac{1}{2}\rangle = \hat{A}\begin{bmatrix} 1 & \frac{1}{2} & \frac{1}{2} \\ M_1 & M_2 & \frac{1}{2} \end{bmatrix} |1M_1\rangle^{Ca} |\frac{1}{2}M_2\rangle^{H} =$$

$$= \hat{A}\left(\sqrt{\frac{2}{3}}\,|11\rangle^{Ca}\,|\frac{1}{2}-\frac{1}{2}\rangle^{H} - \sqrt{\frac{1}{3}}\,|10\rangle^{Ca}\,|\frac{1}{2}\frac{1}{2}\rangle^{H}\right) =$$

$$= \hat{A}\left(-\sqrt{\frac{2}{3}}\sqrt{\frac{1}{2}}\,|1011\rangle^{Ca}\,|00\frac{1}{2}-\frac{1}{2}\rangle^{H} + \sqrt{\frac{2}{3}}\sqrt{\frac{1}{2}}\,|1110\rangle^{Ca}\,|00\frac{1}{2}-\frac{1}{2}\rangle^{H} -\right.$$

$$\left. - \sqrt{\frac{1}{3}}\sqrt{\frac{1}{2}}\,|111-1\rangle^{Ca}\,|00\frac{1}{2}\frac{1}{2}\rangle^{H} + \sqrt{\frac{1}{3}}\sqrt{\frac{1}{2}}\,|1-111\rangle^{Ca}\,|00\frac{1}{2}\frac{1}{2}\rangle^{H}\right) .$$

$$|1\frac{1}{2}\frac{3}{2}\frac{1}{2}\rangle = \hat{A}\begin{bmatrix} 1 & \frac{1}{2} & \frac{3}{2} \\ M_1 & M_2 & \frac{1}{2} \end{bmatrix} |1M_1\rangle^{Ca} |\frac{1}{2}M_2\rangle^{H} =$$

$$= \hat{A}\left(\sqrt{\frac{1}{3}}\,|11\rangle^{Ca}\,|\frac{1}{2}-\frac{1}{2}\rangle^{H} + \sqrt{\frac{2}{3}}\,|10\rangle^{Ca}\,|\frac{1}{2}\frac{1}{2}\rangle^{H}\right) =$$

$$= \hat{A}\left(-\sqrt{\frac{1}{3}}\sqrt{\frac{1}{2}}\,|1011\rangle^{Ca}\,|00\frac{1}{2}-\frac{1}{2}\rangle^{H} + \sqrt{\frac{1}{3}}\sqrt{\frac{1}{2}}\,|1110\rangle^{Ca}\,|00\frac{1}{2}-\frac{1}{2}\rangle^{H} -\right.$$

$$\left. - \sqrt{\frac{2}{3}}\sqrt{\frac{1}{2}}\,|111-1\rangle^{Ca}\,|00\frac{1}{2}\frac{1}{2}\rangle^{H} + \sqrt{\frac{2}{3}}\sqrt{\frac{1}{2}}\,|1-111\rangle^{Ca}\,|00\frac{1}{2}\frac{1}{2}\rangle^{H}\right) .$$

$$|2\frac{1}{2}\frac{3}{2}\frac{1}{2}\rangle = \hat{A}\begin{bmatrix} 2 & \frac{1}{2} & \frac{3}{2} \\ M_1 & M_2 & \frac{1}{2} \end{bmatrix} |1M_1\rangle^{Ca} |\frac{1}{2}M_2\rangle^{H} =$$

$$= \hat{A}\left(\sqrt{\frac{3}{5}}\,|21\rangle^{Ca}\,|\frac{1}{2}-\frac{1}{2}\rangle^{H} - \sqrt{\frac{2}{5}}\,|20\rangle^{Ca}\,|\frac{1}{2}\frac{1}{2}\rangle^{H}\right) =$$

$$= \hat{A}\left(\sqrt{\frac{3}{5}}\sqrt{\frac{1}{2}}\,|1011\rangle^{Ca}\,|00\frac{1}{2}-\frac{1}{2}\rangle^{H} + \sqrt{\frac{3}{5}}\sqrt{\frac{1}{2}}\,|1110\rangle^{Ca}\,|00\frac{1}{2}-\frac{1}{2}\rangle^{H} -\right.$$

$$- \sqrt{\frac{2}{5}}\sqrt{\frac{1}{6}}\,|111-1\rangle^{Ca}\,|00\frac{1}{2}\frac{1}{2}\rangle^{H} - \sqrt{\frac{2}{5}}\sqrt{\frac{1}{6}}\,|1-111\rangle^{Ca}\,|00\frac{1}{2}\frac{1}{2}\rangle^{H} -$$

$$\left. - \sqrt{\frac{2}{5}}\sqrt{\frac{2}{3}}\,|1010\rangle^{Ca}\,|00\frac{1}{2}\frac{1}{2}\rangle^{H}\right) .$$

$$|2\frac{1}{2}\frac{5}{2}\frac{1}{2}\rangle = \hat{A}\begin{bmatrix} 2 & \frac{1}{2} & \frac{5}{2} \\ M_1 & M_2 & \frac{1}{2} \end{bmatrix} |1M_1\rangle^{Ca} |\frac{1}{2}M_2\rangle^{H} =$$

$$= \hat{A}\left(\sqrt{\frac{2}{5}}\,|21\rangle^{Ca}\,|\frac{1}{2}-\frac{1}{2}\rangle^{H} + \sqrt{\frac{3}{5}}\,|20\rangle^{Ca}\,|\frac{1}{2}\frac{1}{2}\rangle^{H}\right) =$$

$$= \hat{A}\left(\sqrt{\frac{2}{5}}\sqrt{\frac{1}{2}}\,|1011\rangle^{Ca}\,|00\frac{1}{2}-\frac{1}{2}\rangle^{H} + \sqrt{\frac{2}{5}}\sqrt{\frac{1}{2}}\,|1110\rangle^{Ca}\,|00\frac{1}{2}-\frac{1}{2}\rangle^{H} +\right.$$

$$+ \sqrt{\frac{3}{5}}\sqrt{\frac{1}{6}}\,|111-1\rangle^{Ca}\,|00\frac{1}{2}\frac{1}{2}\rangle^{H} + \sqrt{\frac{3}{5}}\sqrt{\frac{1}{6}}\,|1-111\rangle^{Ca}\,|00\frac{1}{2}\frac{1}{2}\rangle^{H} -$$

$$\left. + \sqrt{\frac{3}{5}}\sqrt{\frac{2}{3}}\,|1010\rangle^{Ca}\,|00\frac{1}{2}\frac{1}{2}\rangle^{H}\right) .$$

For further consideration, in order to associate the matrix elements in the JJ representation with the only one matrix element of the $^2\Sigma^+$ molecular symmetry in the LS representation, we will leave only those wave functions on which the matrix element in the LS representation is

calculated, and also introduce the designation:

$$\begin{aligned} \tilde{HH}_1 &= \left\langle \hat{A}\,\langle 00\frac{1}{2}\frac{1}{2}|^{Ca^+}\ \langle 0000|^{H^-}\ \left|\hat{H}_e\right|\ \hat{A}\,|1011\rangle^{Ca}\,|00\frac{1}{2}-\frac{1}{2}\rangle^{H}\right\rangle\ , \\ \tilde{HH}_2 &= \left\langle \hat{A}\,\langle 00\frac{1}{2}\frac{1}{2}|^{Ca^+}\ \langle 0000|^{H^-}\ \left|\hat{H}_e\right|\ \hat{A}\,|1010\rangle^{Ca}\,|00\frac{1}{2}\frac{1}{2}\rangle^{H}\right\rangle\ . \end{aligned} \tag{2.16}$$

Then the matrix elements calculated on the above-mentioned molecular wave functions in LS and JJ representations will be written in the following form:

$$\begin{aligned} \text{LS}: H_{kj}^{OSB,LS} &= \sqrt{\frac{2}{3}}\tilde{HH}_1 - \sqrt{\frac{1}{3}}\tilde{HH}_2\ , \\ \text{JJ}: H_{kj_1}^{JJ} &= -\sqrt{\frac{1}{3}}\tilde{HH}_2\ , \\ H_{kj_2}^{JJ} &= -\sqrt{\frac{1}{3}}\tilde{HH}_1\ , \\ H_{kj_3}^{JJ} &= -\sqrt{\frac{1}{6}}\tilde{HH}_1\ , \\ H_{kj_4}^{JJ} &= \sqrt{\frac{3}{10}}\tilde{HH}_1 - \sqrt{\frac{4}{15}}\tilde{HH}_2\ , \\ H_{kj_5}^{JJ} &= \sqrt{\frac{1}{5}}\tilde{HH}_1 + \sqrt{\frac{2}{5}}\tilde{HH}_2\ . \end{aligned} \tag{2.17}$$

Again, it can be shown that both matrix elements $\tilde{HH}_1, \tilde{HH}_2$, when expressed in terms of the same one-electron functions, can be expressed in terms of the same matrix element $\tilde{HH}$:

$$\begin{aligned} \tilde{HH}_1 &= \tilde{HH}\ , \\ \tilde{HH}_2 &= -\sqrt{\frac{1}{2}}\tilde{HH}\ . \end{aligned} \tag{2.18}$$

Finally (2.17) can be written as:

$$\begin{aligned}
\text{LS} : H_{kj}^{OSB,LS} &= \sqrt{\frac{2}{3}}\tilde{HH} + \sqrt{\frac{1}{6}}\tilde{HH} = \sqrt{\frac{9}{6}}\tilde{HH} \ , \\
\text{JJ} : H_{kj_1}^{JJ} &= \sqrt{\frac{1}{6}}\tilde{HH} \ , \\
H_{kj_2}^{JJ} &= -\sqrt{\frac{2}{6}}\tilde{HH} \ , \\
H_{kj_3}^{JJ} &= -\sqrt{\frac{1}{6}}\tilde{HH} \ , \\
H_{kj_4}^{JJ} &= \sqrt{\frac{9}{30}}\tilde{HH} + \sqrt{\frac{4}{30}}\tilde{HH} = \sqrt{\frac{5}{6}}\tilde{HH} \ , \\
H_{kj_5}^{JJ} &= \sqrt{\frac{1}{5}}\tilde{HH} - \sqrt{\frac{1}{5}}\tilde{HH} = 0 \ .
\end{aligned} \tag{2.19}$$

Expressing (2.19) through $H_{kj}^{OSB,LS}$, we get the final relationship between matrix elements in LS and JJ representations:

$$\begin{aligned}
H_{kj_1}^{JJ} &= \sqrt{\frac{1}{9}}H_{kj}^{OSB,LS} \ , \\
H_{kj_2}^{JJ} &= -\sqrt{\frac{2}{9}}H_{kj}^{OSB,LS} \ , \\
H_{kj_3}^{JJ} &= -\sqrt{\frac{1}{9}}H_{kj}^{OSB,LS} \ , \\
H_{kj_4}^{JJ} &= \sqrt{\frac{5}{9}}H_{kj}^{OSB,LS} \ , \\
H_{kj_5}^{JJ} &= 0 \ .
\end{aligned} \tag{2.20}$$

Similarly, expressions can be obtained for all matrix elements. Finally, it can be possible to collect all the results into a single table 2.

Let's analyze the results given in the Table 2. Firstly, it can be seen that the sum of the squares of the matrix elements in the JJ representation is exactly equal to the square of the matrix element in the LS representation, as it should be, following [23, 24]. Secondly, it can be noted that each coefficient C_{j_i} is the square root of a fraction, and the denominator of the

Table 2. Coefficients C_{j_i} of relationship of matrix elements in LS and JJ representations: $H^{JJ}_{kj_i} = C_{j_i} H^{OSB,LS}_{kj}$.

j	State	Coefficient C_{j_i}	
		$J^{Ca} - \frac{1}{2}$	$J^{Ca} + \frac{1}{2}$
1	$\mathrm{Ca}(4s^2\ ^1S_0) + \mathrm{H}(1s\ ^2S_{1/2})$	–	1.0
2	$\mathrm{Ca}(4s4p\ ^1P_1) + \mathrm{H}(1s\ ^2S_{1/2})$	$-\sqrt{\frac{1}{3}}$	$\sqrt{\frac{2}{3}}$
3	$\mathrm{Ca}(4s4p\ ^3P_0) + \mathrm{H}(1s\ ^2S_{1/2})$	–	$\sqrt{\frac{1}{9}}$
	$\mathrm{Ca}(4s4p\ ^3P_1) + \mathrm{H}(1s\ ^2S_{1/2})$	$-\sqrt{\frac{2}{9}}$	$-\sqrt{\frac{1}{9}}$
	$\mathrm{Ca}(4s4p\ ^3P_2) + \mathrm{H}(1s\ ^2S_{1/2})$	$\sqrt{\frac{5}{9}}$	0.0
4	$\mathrm{Ca}(4s3d\ ^1D_2) + \mathrm{H}(1s\ ^2S_{1/2})$	$-\sqrt{\frac{2}{5}}$	$\sqrt{\frac{3}{5}}$
5	$\mathrm{Ca}(4s3d\ ^3D_1) + \mathrm{H}(1s\ ^2S_{1/2})$	0.0	$\sqrt{\frac{3}{15}}$
	$\mathrm{Ca}(4s3d\ ^3D_2) + \mathrm{H}(1s\ ^2S_{1/2})$	$-\sqrt{\frac{3}{15}}$	$-\sqrt{\frac{2}{15}}$
	$\mathrm{Ca}(4s3d\ ^3D_3) + \mathrm{H}(1s\ ^2S_{1/2})$	$\sqrt{\frac{7}{15}}$	0.0
6	$\mathrm{Ca}(4s5s\ ^1S_0) + \mathrm{H}(1s\ ^2S_{1/2})$	–	1.0
7	$\mathrm{Ca}(4s5s\ ^3S_1) + \mathrm{H}(1s\ ^2S_{1/2})$	1.0	0.0
8	$\mathrm{Ca}(4s5p\ ^1P_1) + \mathrm{H}(1s\ ^2S_{1/2})$	$-\sqrt{\frac{1}{3}}$	$\sqrt{\frac{2}{3}}$
9	$\mathrm{Ca}(4s5p\ ^3P_0) + \mathrm{H}(1s\ ^2S_{1/2})$	–	$\sqrt{\frac{1}{9}}$
	$\mathrm{Ca}(4s5p\ ^3P_1) + \mathrm{H}(1s\ ^2S_{1/2})$	$-\sqrt{\frac{2}{9}}$	$-\sqrt{\frac{1}{9}}$
	$\mathrm{Ca}(4s5p\ ^3P_2) + \mathrm{H}(1s\ ^2S_{1/2})$	$\sqrt{\frac{5}{9}}$	0.0
10	$\mathrm{Ca}(3d4p\ ^3F_2) + \mathrm{H}(1s\ ^2S_{1/2})$	0.0	$\sqrt{\frac{5}{21}}$
	$\mathrm{Ca}(3d4p\ ^3F_3) + \mathrm{H}(1s\ ^2S_{1/2})$	$-\sqrt{\frac{4}{21}}$	$-\sqrt{\frac{3}{21}}$
	$\mathrm{Ca}(3d4p\ ^3F_4) + \mathrm{H}(1s\ ^2S_{1/2})$	$\sqrt{\frac{9}{21}}$	0.0

fraction is exactly equal to the sum of the terms $2J^{at.state}+1$ through all fine structure levels. That is, for example, for the state of the calcium atom $^3P_{0,1,2}$ we have the sum $(2*0+1)+(2*1+1)+(2*2+1)=9$. It is also worth noting that for the minimum and maximum values of the total angular momentum of the calcium atom $J_{min}^{at.state}$ and $J_{max}^{at.state}$, the relationship coefficient C_{j_i} has a non-zero value for only one of two possible molecular states in the symmetry $\frac{1}{2}$ (or only one non-zero value if $J^{at.state}=0$ and only one molecular state is generated in the symmetry $\frac{1}{2}$). At the same time, these coefficients are positive, while the coefficients for the total angular momentum $J_{min}^{at.state}<J<J_{max}^{at.state}$ are negative. In the case of singlet states of the atom, the minus sign always stands before the smaller coefficient, while the plus sign always stands before the larger coefficient. Thirdly, the sum of the numerators values of the coefficients C_{j_i}, excluding the square root and the signs before it, is equal to the value of $2J^{at.state}+1$ for each level of the fine structure.

§ 2.3 Concluding remarks

In this Chapter, an asymptotic method for taking into account the fine structure in collisions of alkali atoms and alkali-like metal ions with hydrogen, proposed in [23,24], was further generalized to the case of atoms of elements of II group of the Periodic table (alkaline earth metals), as well as ions with a similar structure. It is shown that the matrix elements in the JJ representation are related to the matrix elements in the LS representation through the coefficients C_{j_i}, which obey the same laws as in the case of alkali metal atoms or alkali-like ions.

The results of the method of accounting for the fine structure of energy levels in collisions of potassium and calcium ions Ca^+ with hydrogen were tested in [85]. In this paper, it is shown that in the case of potassium, taking into account the fine structure in collisions of potassium with hydrogen by the method proposed in [23, 24], leads to a better agreement of the

potassium abundance for the Sun with the meteoritic potassium abundance than in the case of not taking into account the fine structure. For Ca^+, the consideration of the influence of the fine structure turned out to be less pronounced.

Also, this method can be generalized to the case of elements of III group of the Periodic table. The calculation of the electronic structure by a modified asymptotic method was carried out for collisions of boron with hydrogen. The cross sections and rate coefficients of the processes of excitation, de-excitation, ion-pair formation and mutual neutralization calculated using a multichannel formula are published in [25], which also presents a comparison of the results obtained with (see [25]) and without taking into account (see [86]) fine structure. In this work it is shown that from the rate coefficients obtained without taking into account the fine structure, it is impossible to obtain the rate coefficients of processes with taking into account the fine structure by means of any simple formula.

This research was supported by the RFBR grant Graduate Students No. 20-33-90047, head of Prof. Belyaev A. K.

Chapter 3. Investigation of inelastic processes in collisions of oxygen atoms and ions with hydrogen atoms and ions

§ 3.1 Preliminary remarks

Oxygen is the third most abundant element in the Universe after hydrogen and helium (see, for example, [3, 29]). The determination of oxygen abundance plays an important role in understanding the formation and evolution of planets, stars and galaxies (see, for example, [87–92]). The ratio of oxygen to iron abundances is a widely used indicator for determining the stages of the chemical evolution of stars (see [87, 93, 94]). It is believed that the main source of oxygen is collapsing supernova nuclei formed from massive stars, so a detailed study of the oxygen abundance allows us to understand the history of star formation [95].

As mentioned in [95], the main source of the data on the evolution of oxygen abundance in our Galaxy is the data on the oxygen abundance in the atmospheres of cold stars (spectral classes F, G, K). Based on the above, it can be concluded that it is necessary to determine oxygen abundance in the photospheres of cold stars as accurately as possible. Unfortunately, different methods of spectral analysis lead to different results (see [95–99]). For these reasons, the most accurate atomic data, such as data on collisions of oxygen with hydrogen, electrons, photoionization data, and so on, are needed to modelling of the oxygen spectra in the stars photospheres.

Most often, the triplet O I 777 nm, corresponding to the transitions between the fine structure levels $O(2p^3 3p\,^5P_{3,2,1}) \leftrightarrow O(2p^3 3s\,^5S_2^\circ)$, is used for analysis. In many papers (see, for example, [87, 92, 100, 101]) it was shown that this line is formed under conditions of deviation from local thermodynamic equilibrium. In the paper [92] it is shown that the accuracy of the rate coefficients of inelastic processes in collisions with hydrogen

have the greatest impact on the accuracy of modelling spectral lines under conditions of deviation from local thermodynamic equilibrium for stars of spectral classes F, G, K.

As discussed earlier, the Dravin formula [11–13] is often used to determine the values of the rate coefficients of inelastic processes in collisions with hydrogen, due to the complexity and time-consuming of the *ab initio* calculations. In this case, a scaling factor is used, the value of which is selected for some reasons and varies from element to element. However, it has been shown repeatedly (see, for example, [3, 14, 15, 33]) that the accuracy of the results obtained by the Drawin formula is insufficient for the use of these data in modelling the spectra of stars: for excitation/de-excitation processes, the rate coefficients can be either overestimated or underestimated by several orders of magnitude; at the same time, for charge-exchange processes, Dravin's formula gives zero values of the rate coefficients, although quantum calculations show that these processes are characterized by the largest values of the rate coefficients.

This Chapter is devoted to the study of the characteristics of inelastic processes (cross sections and rate coefficients) in collisions of oxygen atoms and ions with hydrogen atoms and ions for astrophysical applications in the field of modelling of oxygen spectra in the photospheres of stars under conditions of deviation from local thermodynamic equilibrium. The use of the most accurate quantum reprojection method for calculating the cross sections of inelastic processes requires the presence of calculated non-adiabatic couplings, which currently do not exist. Nevertheless, there is a set of molecular adiabatic potential energies calculated in the paper [28] by the Multireference Configuration Interaction method (or MRCI) for 13 scattering channels. Up to date, these data are the most complete. Using them, it is possible to calculate the full probabilities of non-adiabatic transitions from a given initial state to a given final state within the framework of model methods based on the two-channel Landau-Zener model.

In this part of the dissertation, the full probabilities of non-adiabatic transitions from all initial states to all final ones are calculated by two model methods of nuclear dynamics investigation based on the Landau-Zener model: the probability current method and the multichannel formula. The cross sections of all inelastic processes in the collision energy range 0.01 – 100 eV (the probability current method) and 0.0001 – 100 eV (the multichannel formula) were calculated from the calculated total probabilities of non-adiabatic transitions. All the rate coefficients of inelastic processes in the temperature range 1000 – 10000 K are calculated through the cross sections. The analysis of the obtained cross sections and rate coefficients was carried out.

§ 3.2 Adiabatic potential energies of the OH molecule

The OH molecule is one of the most studied molecules at the moment (see papers [28, 102], as well as references therein). The electronic structure of this molecule was calculated for various states in [102–105] etc. Inelastic processes in collisions of oxygen with hydrogen were previously investigated in [106] by the LCAO model method for calculation of the potential energies and the multichannel formula for nuclear dynamics investigation. In [28], the adiabatic potential energy curves of the OH molecule were obtained for the first time using the MRCI quantum chemical method for a sufficiently large number of scattering channels, namely for 13 scattering channels, two of which correspond to closely spaced ionic states $O^+ + H^-$ and $O^- + H^+$. This makes it possible for the first time to study non-adiabatic nuclear dynamics with potentials obtained by *ab initio* quantum chemical methods, and to calculate cross sections and rate coefficients of inelastic processes with a more complete basis of states than before.

In [28], 43 molecular adiabatic PECs (40 covalent and three ionic) were calculated in ten molecular symmetries, namely: 11 PECs in $^4\Sigma^-$ molecular

symmetry (Figure 3), 7 in $^2\Pi$ symmetry (Figure 5), 4 in $^2\Sigma^+$ symmetry (Figure 4), 3 in $^6\Sigma^-$ symmetry (Figure 8), 7 in $^2\Sigma^-$ symmetry (Figure 6), 6 in $^4\Pi$ symmetry (Figure 7), 2 in $^2\Delta$ symmetries and one term each in $^4\Delta$, $^6\Pi$, $^4\Sigma^+$ symmetries. The Table 3 shows all the scattering channels of the OH molecule taken into account in this study: the PECs of the 11 lower atomic scattering channels, as well as two ionic scattering channels, were obtained by the MRCI method, atomic scattering channels j = 12-16 were taken into account within the asymptotic model. For each scattering channel, all molecular symmetries generated by this scattering channel are given, as well as the asymptotic energies calculated from the ground state $O(2p^4\,^3P) + H(1s\,^2S)$, in the Table 4 presents statistical populations of all molecular channels calculated by the MRCI method in [28].

Simplified model [107,108] predicts that the maximum of the so-called "optimal window" located at the value of the excitation energy of the oxygen atom approximately 11.62 eV. This indicates that the maximum rate coefficients will correspond to neutralization processes into scattering channels, for which the excitation energy of the oxygen atom lies approximately in the range of 11.0 – 12.2 eV. Quantum chemical calculations end, however, at the state $O(2p^3 4s\,^3S^o)+H(1s)$ with an asymptotic energy of 11.9304 eV according to NIST (The National Institute of Standards and Technology) (12.07 eV according to calculations in the paper [28]). In addition to the PECs obtained in [28], five additional scattering channels (states 12-16 in the Table 3) were also taken into account when calculating cross sections using the multichannel formula within the framework of the asymptotic model. For these additional channels, the nuclear dynamics was investigated only for $^4\Sigma^-$ molecular symmetry, since the asymptotic model allows us to determine only the non-adiabatic regions due to ion-covalent interaction, that is, for $^4\Sigma^-$, $^2\Sigma^+$ and $^2\Pi$ symmetries, but none of these states generates $^2\Sigma^+$ symmetry, and for $^2\Pi$ symmetry, the non-adiabatic regions is located at a relatively large internuclear distance (greater than 100 a.u.), as a result, the energy splitting in the centers of these non-adiabatic regions

is very small, and the nature of the passage of these non-adiabatic regions by the system is practically diabatic. In turn, this leads to a negligible (within the framework of the multichannel formula) probabilities of non-adiabatic transitions from some initial channel to the final channels 12-16, and, consequently, negligible values of cross sections and rate coefficients of inelastic processes involving these scattering channels in molecular symmetry $^2\Pi$.

§ 3.3 Non-adiabatic nuclear dynamics investigation

As stated above, non-adiabatic couplings in the paper [28] were not presented, and therefore the study of non-adiabatic nuclear dynamics cannot be carried out within the framework of the most accurate quantum reprojection method. Nevertheless, the nuclear dynamics can be calculated within the framework of model methods based on the Landau-Zener model [64–66], which is the probability of a non-adiabatic transition in a single passage of the non-adiabatic region. For convenience, the calculations in this work used the Landau-Zener formula, rewritten for adiabatic representation in terms of energy splitting and its second derivative in the center of the non-adiabatic region [74] (see the formula (1.53)).

Since the Landau-Zener model allows us to consider non-adiabatic transitions only between states with the same molecular symmetry, and the rotational couplings for theconsidered OH molecule were also not calculated in the paper [28], non-adiabatic transitions between different symmetries were not taken into account in this study. This solution is justified by the fact that the contribution to the partial cross sections of inelastic processes from non-adiabatic transitions between different molecular symmetries is less than the contribution from transitions within the same molecular symmetry (see, for example, [20, 110]) at low collision energies (less than a few eV). The cross sections in this range mainly determine the values of

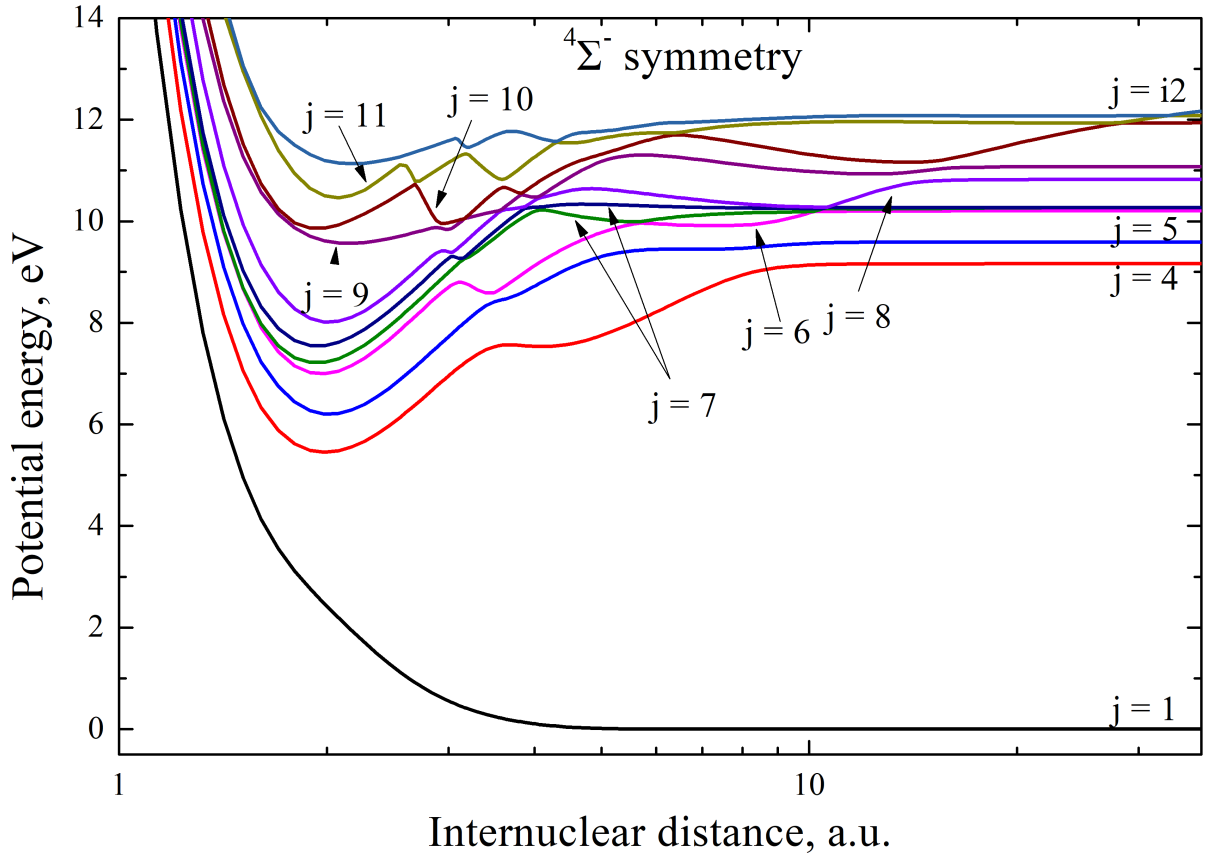

Figure 3. Adiabatic potential energy curves U_j of the OH quasimolecule depending on the internuclear distance R for molecular symmetry $^4\Sigma^-$, calculated in [28]. For the notation, see the Table 3.

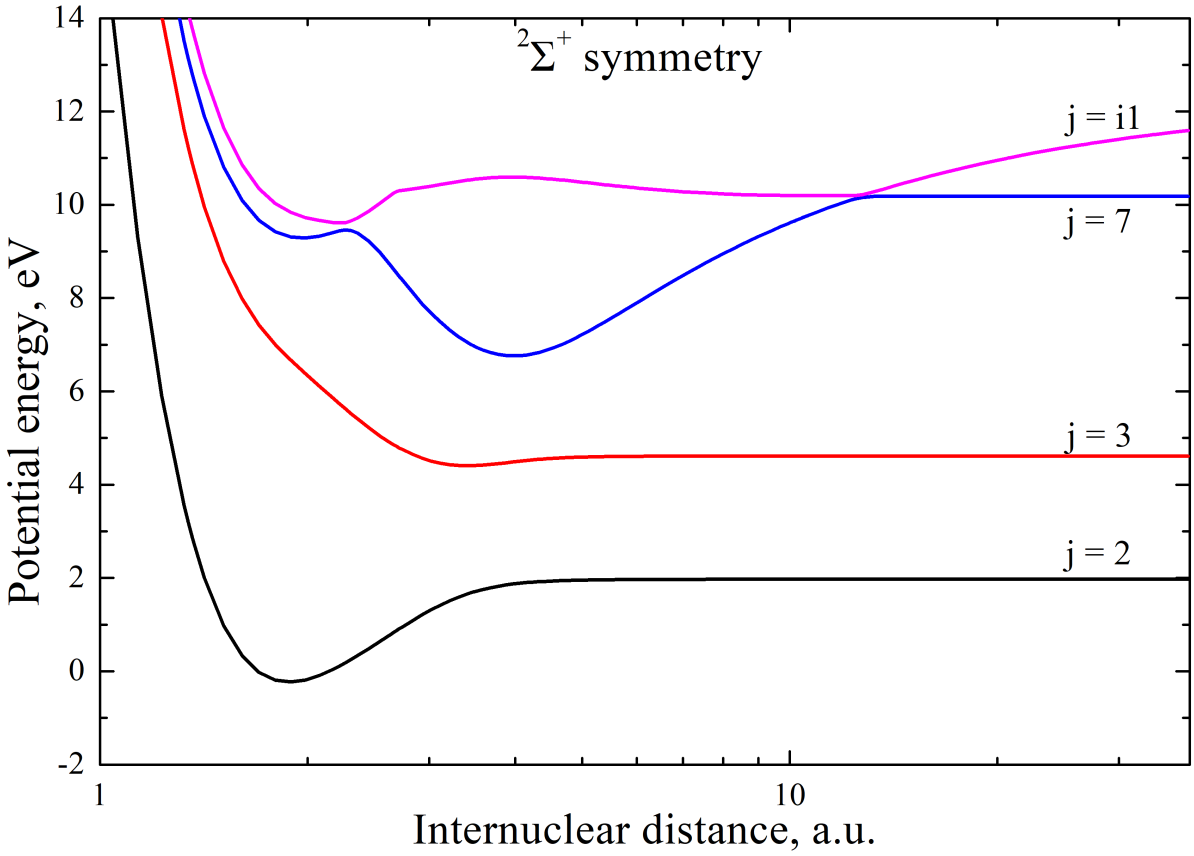

Figure 4. Adiabatic potential energy curves U_j of the OH quasimolecule depending on the internuclear distance R for molecular symmetry $^2\Sigma^+$, calculated in [28]. For the notation, see the Table 3.

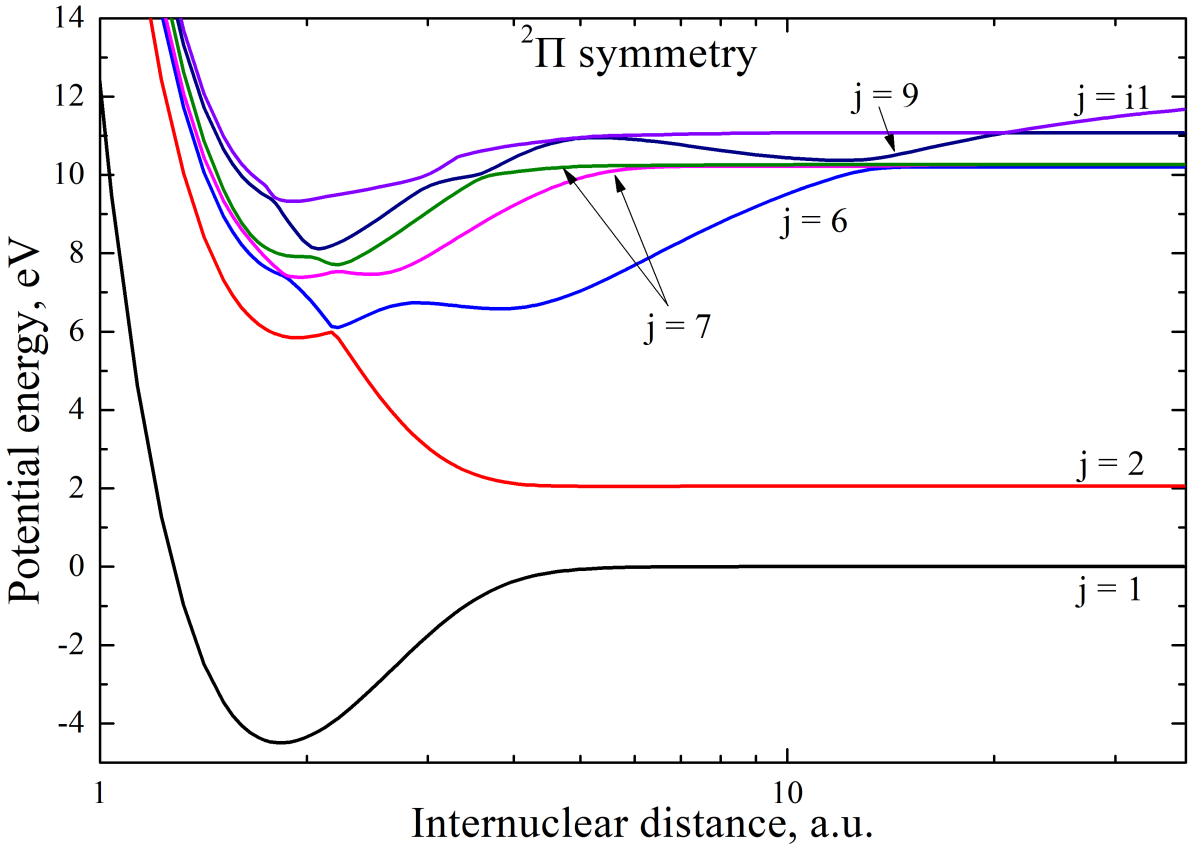

Figure 5. Adiabatic potential energy curves U_j of the OH quasimolecule depending on the internuclear distance R for molecular symmetry $^2\Pi$, calculated in [28]. For the notation, see the Table 3.

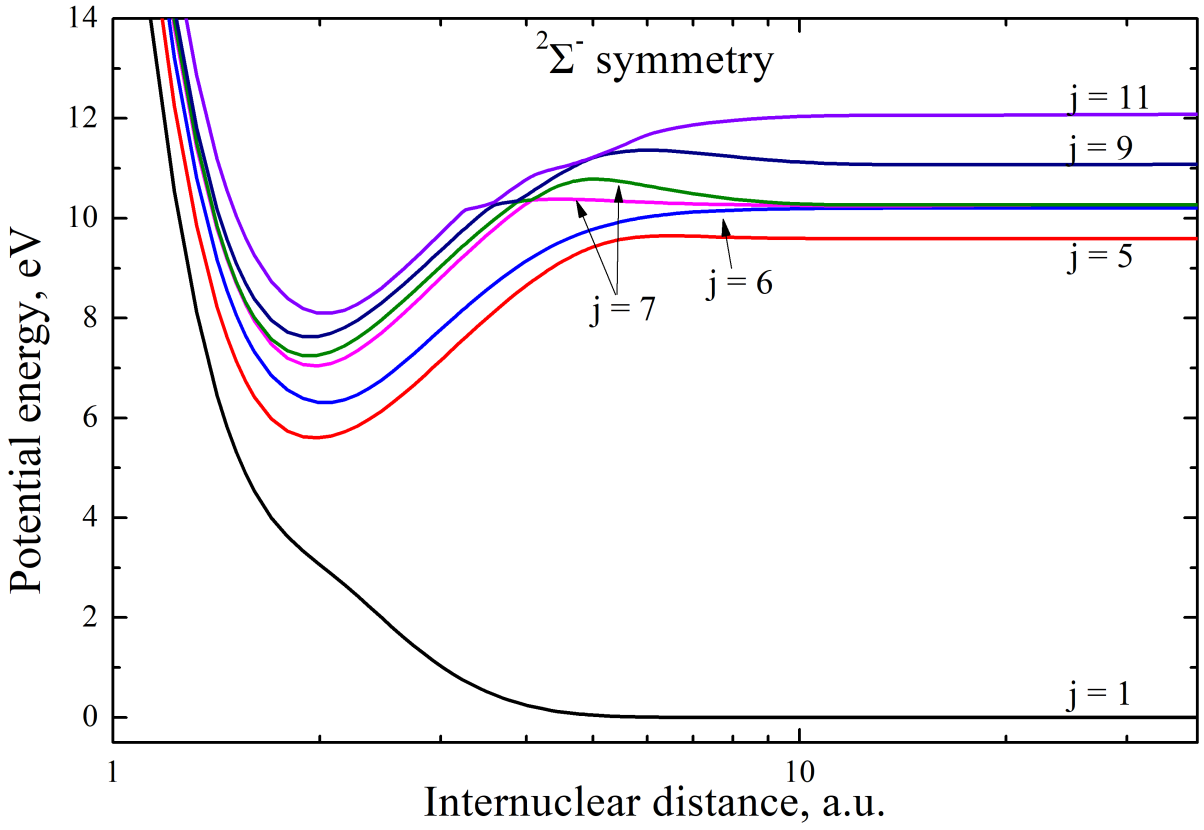

Figure 6. Adiabatic potential energy curves U_j of the OH quasimolecule depending on the internuclear distance R for molecular symmetry $^2\Sigma^-$, calculated in [28]. For the notation, see the Table 3.

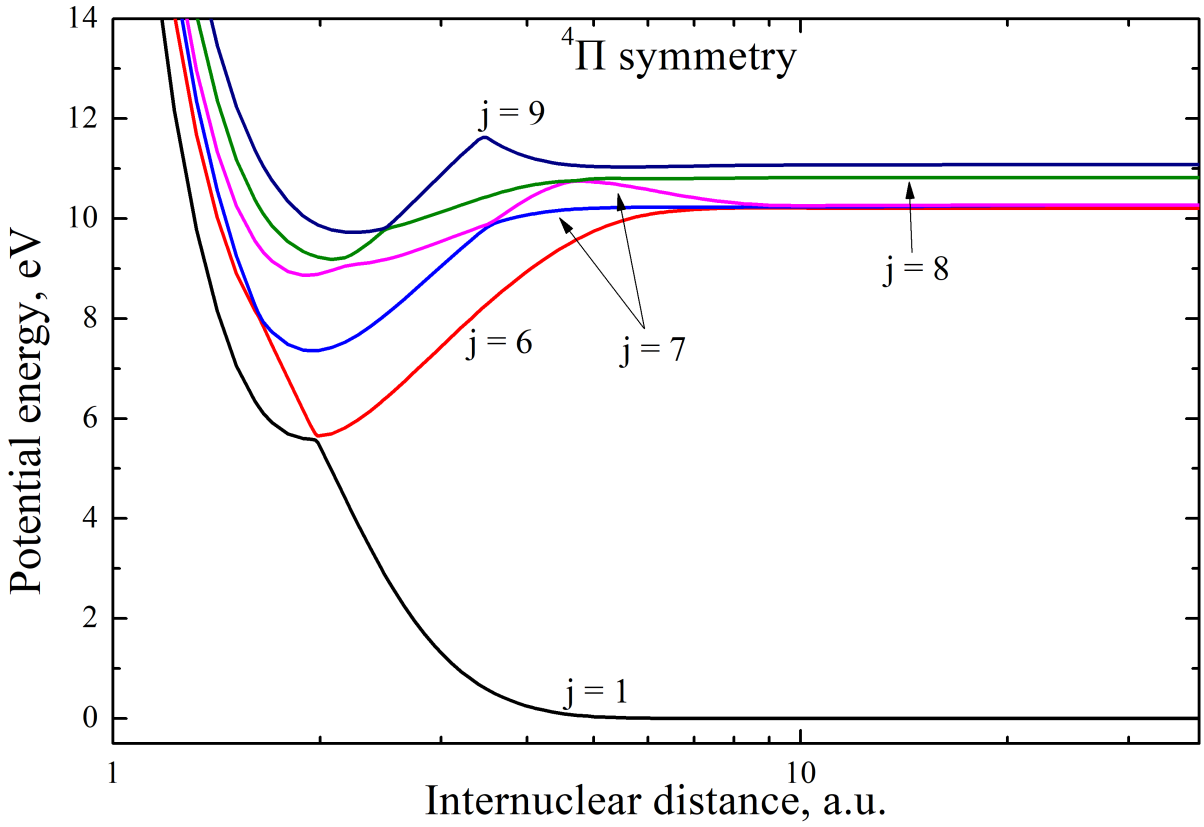

Figure 7. Adiabatic potential energy curves U_j of the OH quasimolecule depending on the internuclear distance R for molecular symmetry $^4\Pi$, calculated in [28]. For the notation, see the Table 3.

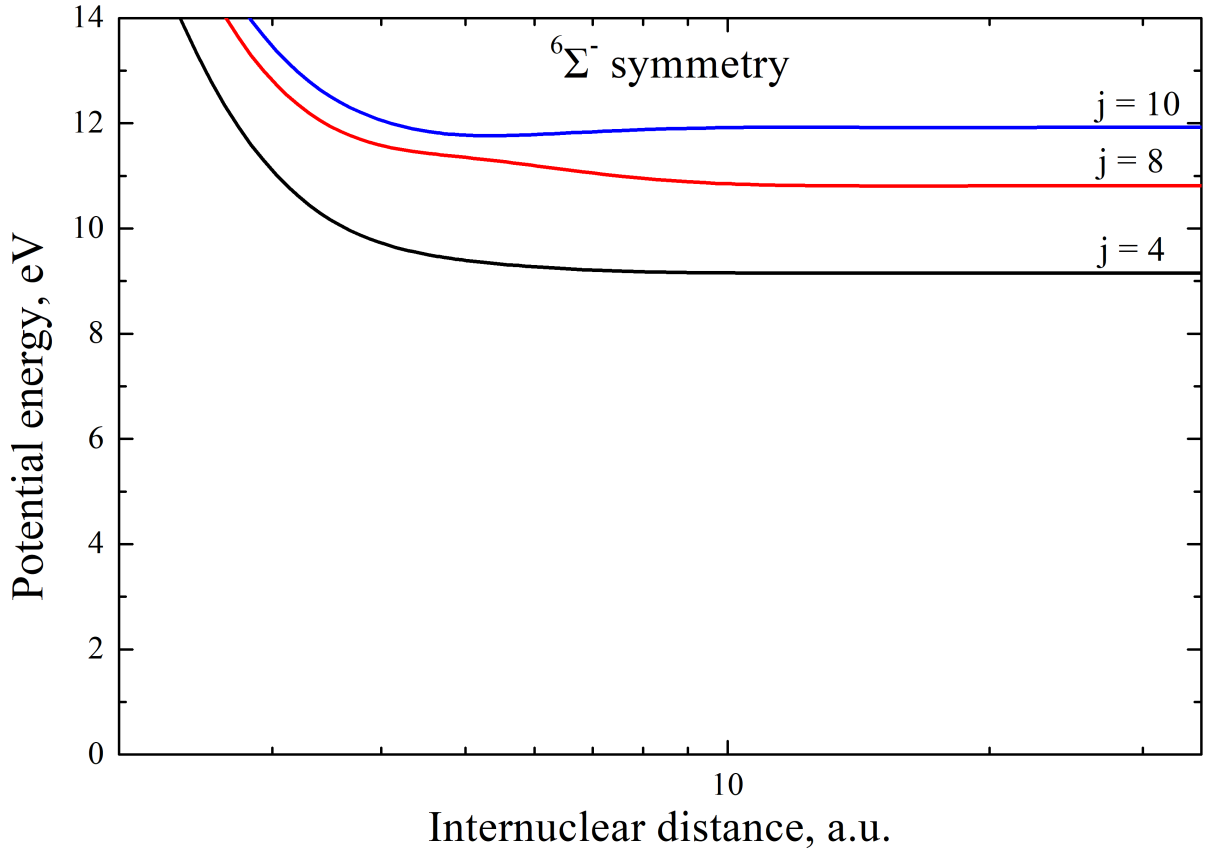

Figure 8. Adiabatic potential energy curves U_j of the OH quasimolecule depending on the internuclear distance R for molecular symmetry $^6\Sigma^-$, calculated in [28]. For the notation, see the Table 3.

Table 3. The molecular states of the OH molecule, their corresponding atomic scattering channels, all possible molecular symmetries of each molecular state, the asymptotic energies of the states of the OH molecule presented in [28] and the asymptotic energies taken from the NIST [109] database. The asymptotic energies are calculated from the ground state of the OH molecule $O\,(2p^4\,{}^3P)$+H$(1s\,{}^2S)$.

j	Scattering channel	Molecular state	Asymptotic energy (eV)	Asymptotic energy (NIST, eV)
1	$O(2p^4\,{}^3P)$ +H$(1s\,{}^2S)$	${}^2\Sigma^-,{}^2\Pi,{}^4\Sigma^-,{}^4\Pi$	0	0.0000
2	$O(2p^4\,{}^1D)$ +H$(1s\,{}^2S)$	${}^2\Sigma^+,{}^2\Pi,{}^2\Delta$	2.05	1.9674
3	$O(2p^4\,{}^1S)$ +H$(1s\,{}^2S)$	${}^2\Sigma^+$	4.69	4.1897
4	$O(2p^3 3s\,{}^5S^o)$ +H$(1s\,{}^2S)$	${}^4\Sigma^-,{}^6\Sigma^-$	9.16	9.1461
5	$O(2p^3 3s\,{}^3S^o)$ +H$(1s\,{}^2S)$	${}^2\Sigma^-,{}^4\Sigma^-$	9.59	9.5214
6	$O(2p^4\,{}^3P)$ +H$(2s\,{}^2S)$	${}^2\Sigma^-,{}^2\Pi,{}^4\Sigma^-,{}^4\Pi$	10.20	10.2000
7	$O(2p^4\,{}^3P)$ +H$(2p\,{}^2P)$	${}^2\Sigma^+,{}^2\Sigma^-(\times2),{}^2\Pi(\times2),{}^2\Delta$ ${}^4\Sigma^+,{}^4\Sigma^-(\times2),{}^4\Pi(\times2),{}^4\Delta$	10.27	10.2000
8	$O(2p^3 3p\,{}^5P)$ +H$(1s\,{}^2S)$	${}^4\Sigma^-,{}^4\Pi,{}^6\Sigma^-,{}^6\Pi$	10.82	10.7406
9	$O(2p^3 3p\,{}^3P)$ +H$(1s\,{}^2S)$	${}^2\Sigma^-,{}^2\Pi,{}^4\Sigma^-,{}^4\Pi$	11.07	10.9888
10	$O(2p^3 4s\,{}^5S^o)$ +H$(1s\,{}^2S)$	${}^4\Sigma^-,{}^6\Sigma^-$	11.93	11.8376
11	$O(2p^3 4s\,{}^3S^o)$ +H$(1s\,{}^2S)$	${}^2\Sigma^-,{}^4\Sigma^-$	12.07	11.9304
12	$O(2p^3 3d\,{}^5D^o)$ +H$(1s\,{}^2S)$	${}^4\Sigma^-,{}^4\Pi,{}^4\Delta,{}^6\Sigma^-,{}^6\Pi,{}^6\Delta$	–	12.0786
13	$O(2p^3 3d\,{}^3D^o)$ +H$(1s\,{}^2S)$	${}^2\Sigma^-,{}^2\Pi,{}^2\Delta,{}^4\Sigma^-,{}^4\Pi,{}^4\Delta$	–	12.0870
14	$O(2p^3 4p\,{}^5P)$ +H$(1s\,{}^2S)$	${}^4\Sigma^-,{}^4\Pi,{}^6\Sigma^-,{}^6\Pi$	–	12.2861
15	$O(2p^3 4p\,{}^3P)$ +H$(1s\,{}^2S)$	${}^2\Sigma^-,{}^2\Pi,{}^4\Sigma^-,{}^4\Pi$	–	12.3589
16	$O(2p^3 3s\,{}^3D^o)$ +H$(1s\,{}^2S)$	${}^2\Sigma^-,{}^2\Pi,{}^2\Delta,{}^4\Sigma^-,{}^4\Pi,{}^4\Delta$	–	12.5402
i1	$O^-(2p^5\,{}^2P)$ +H^+	${}^2\Sigma^+,{}^2\Pi$	12.39	12.1500
i2	$O^+(2p^3\,{}^4S^o)$ +$H^-(1s^2\,{}^1S)$	${}^4\Sigma^-$	12.90	12.8641

Table 4. Statistical populations of all 43 molecular adiabatic states calculated in paper [28].

j	Scattering channel	${}^4\Sigma^-$	${}^2\Sigma^+$	${}^2\Pi$	${}^2\Sigma^-$	${}^4\Pi$	${}^6\Sigma^-$	${}^2\Delta$	${}^4\Delta$	${}^6\Pi$	${}^4\Sigma^+$
1	$O(2p^4\,{}^3P)$+H$(1s)$	4/18	-	4/18	2/18	8/18	-	-	-	-	-
2	$O(2p^4\,{}^1D)$+H$(1s)$	-	1/5	2/5	-	-	-	2/5	-	-	-
3	$O(2p^4\,{}^1S)$+H$(1s)$	-	1	-	-	-	-	-	-	-	-
4	$O(2p^3 3s\,{}^5S^o)$+H$(1s)$	4/10	-	-	-	-	6/10	-	-	-	-
5	$O(2p^3 3s\,{}^3S^o)$+H$(1s)$	4/6	-	-	2/6	-	-	-	-	-	-
6	$O(2p^4\,{}^3P)$+H$(2s)$	4/18	-	4/18	2/18	8/18	-	-	-	-	-
7	$O(2p^4\,{}^3P)$+H$(2p)$	4/54	2/54	4/54	2/54	8/54	-	4/54	8/54	-	4/54
		4/54	-	4/54	2/54	8/54	-	-	-	-	-
8	$O(2p^3 3p\,{}^5P)$+H$(1s)$	4/30	-	-	-	8/30	6/30	-	-	12/30	-
9	$O(2p^3 3p\,{}^3P)$+H$(1s)$	4/18	-	4/18	2/18	8/18	-	-	-	-	-
10	$O(2p^3 4s\,{}^5S^o)$+H$(1s)$	4/10	-	-	-	-	6/10	-	-	-	-
11	$O(2p^3 4s\,{}^3S^o)$+H$(1s)$	4/6	-	-	2/6	-	-	-	-	-	-
i1	$O^-(2p^5\,{}^2P)$+H^+	-	1/3	2/3	-	-	-	-	-	-	-
i2	$O^+(2p^3\,{}^4S^o)$+$H^-({}^1S)$	1	-	-	-	-	-	-	-	-	-

the rate coefficients for the temperature range of 1000 – 10000 K studied in this work.

In this regard, in this work, the study of nuclear dynamics was carried out only in six molecular symmetries, namely: $^4\Sigma^-$, $^2\Pi$, $^2\Sigma^+$, $^6\Sigma^-$, $^2\Sigma^-$, $^4\Pi$. The molecular symmetries $^4\Delta$, $^6\Pi$, $^4\Sigma^+$ were not considered due to the fact that only one molecular term was calculated in these symmetries, therefore, within the framework of the chosen approach, non-adiabatic transitions in these symmetries were not taken into account. The molecular symmetry $^2\Delta$ was also not taken into account due to the fact that there is a significant energy splitting (about 2.8 eV) between the two calculated PECs in the center of the non-adiabatic region, which leads to an extremely small probability of non-adiabatic transition within the Landau-Zener model and negligibly small cross sections of inelastic processes. Thus, in this study, non-adiabatic transitions between states of the same molecular symmetry were considered independently for six molecular symmetries.

To calculate the total probability of non-adiabatic transitions from one initial state to all final states for all states with the same molecular symmetry, two quantum model methods were used for all six considered symmetries: the multichannel formula (see §1.4.4) and the probability current method (see §1.4.3) in its stochastic version. At the same time, the total number of calculated probability currents for each symmetry in this study is $N^{tot} = 2.62144 \times 10^8$, which allows us to calculate the total inelastic transition probability with a minimum value of the order of 4.0×10^{-9} and an accuracy of the order of $\frac{1}{\sqrt{N^{tot}}} = 6.3 \times 10^{-5}$. For each non-adiabatic region, the parameters necessary for calculation were determined, such as the position of the center of the non-adiabatic region R_c, the energy splitting Z in the center of the non-adiabatic region, the average potential energy $< E >$ in the center of the non-adiabatic region and the Landau-Zener parameter ξ (see the formula (1.54)).

240 inelastic processes were investigated in total by the of probability current method: 108 in symmetry $^4\Sigma^-$, 42 in symmetry $^2\Pi$, 12 in symme-

try $^2\Sigma^+$, 6 in symmetry $^6\Sigma^-$, 42 in symmetry $^2\Sigma^-$ and 30 in symmetry $^4\Pi$. 292 inelastic processes were studied by the multichannel formula: 238 in symmetry $^4\Sigma^-$, 42 in symmetry $^2\Pi$, 12 in symmetry $^2\Sigma^+$. Cross sections of inelastic processes were calculated by the formula (1.70). The cross sections calculated from probabilities obtained by the probability current method are calculated in the collision energy range 0.01 - 100 eV, by the multichannel formula – in the range 0.0001 - 100 eV. The partial rate coefficients were calculated from the cross sections according to the formula (1.74) for exothermic processes and according to the balance equation (1.75) for endothermic processes in the temperature range 1000 – 10000 K. The total rate coefficients of inelastic processes are obtained by summing the partial rate coefficients over all molecular symmetries (see formula (1.76)).

§ 3.4 Analysis of cross sections of inelastic processes in O+H collisions

Let's analyze the results obtained, starting with the analysis of cross sections of inelastic processes. The following question is relevant: which cross sections in collisions in various molecular symmetries have the largest values and, accordingly, make the greatest contribution to the value of the total partial cross section of the inelastic process (meaning the cross section summed over all molecular symmetries)? The oxygen-hydrogen collision system is a pretty good system for investigating this issue, since inelastic transitions occur in a variety of molecular symmetries: $^2\Sigma^+$, $^2\Sigma^-$, $^4\Sigma^+$, $^4\Sigma^-$, $^6\Sigma^-$, $^2\Pi$, $^4\Pi$, $^6\Pi$, $^2\Delta$, $^4\Delta$, $^6\Delta$. As mentioned earlier, in this study, only transitions within the same molecular symmetry were considered, therefore cross sections of inelastic processes for molecular symmetries $^4\Sigma^-$, $^2\Pi$, $^2\Sigma^+$, $^6\Sigma^-$, $^2\Sigma^-$, $^4\Pi$, obtained in this investigation by the probability current method as more accurate in comparison with the multichannel formula, will be considered.

Let's consider some specific inelastic processes. Figure 9 shows the de-excitation cross sections of the process $O(2p^3 3p\,^5P) + H(1s\,^2S) \rightarrow O(2p^3 3s\,^5S^o) + H(1s\,^2S)$, obtained in the molecular symmetries $^4\Sigma^-$ and $^6\Sigma^-$. It can be seen from the figure that, over the entire studied range of collision energies, the dominant contribution to the total partial cross section is made by transitions within the $^4\Sigma^-$ symmetry, while in the $^6\Sigma^-$ symmetry, the cross section value is negligible at collision energies < 10 eV (not less than five orders of magnitude less). Hence, it can be concluded that for this inelastic process in the studied range of collision energies, the dominant mechanism is the ion-covalent interaction, which causes transitions within the $4\Sigma^-$ molecular symmetry.

Figure 10 shows the de-excitation cross sections of the process $O(2p^3 3p\,^3P) + H(1s\,^2S) \rightarrow O(2p^4\,^3P) + H(2s\,^2S)$ calculated in the molecular symmetries $^2\Sigma^-$, $^4\Sigma^-$, $^2\Pi$ and $^4\Pi$. As can be seen in comparison with the figure 9, the situation for this process is different. At collision energies less than 0.2 eV, the processes in $^2\Sigma^-$ and $^4\Sigma^-$ symmetries can practically be neglected, while the main contribution is made by the cross section in $^4\Pi$ symmetry, the cross section in $^2\Pi$ symmetry on average three to four times lower than the cross section in symmetry $^4\Pi$. With a further increase of the collision energy, the contribution of $^4\Sigma^-$ symmetry begins to grow, and the contribution of $^4\Pi$ steadily decreases. In the range of 1 – 10 eV, the cross section in the $^2\Pi$ symmetry dominates, and at 10 eV, the contribution of $^2\Pi$ and $^4\Sigma^-$ becomes approximately equal, while the contribution of the cross section in the $^2\Sigma^-$ symmetry is at least less by an order of magnitude and is comparable to the contribution of the cross section in the $^4\Pi$ symmetry. With a further increase of the collision energy, the main contribution to the value of the total partial cross section is already made by transitions in the symmetries $^4\Sigma^-$ and $^2\Pi$. This suggests that for this inelastic process at low collision energies, not only the ion-covalent interaction makes a great contribution to the final value of the total partial cross section, but also the covalent-covalent interaction at

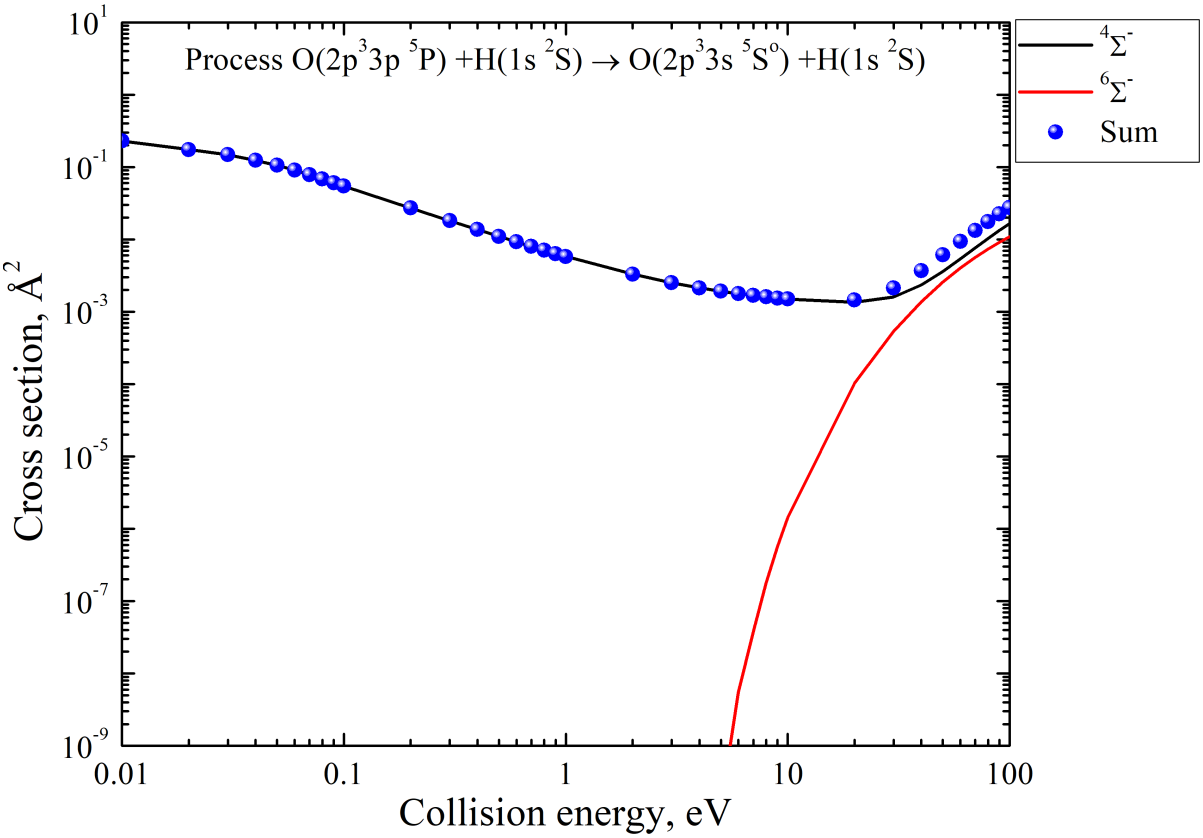

Figure 9. Cross sections of the inelastic process $O(2p^3 3p\,^5P) + H(1s\,^2S) \to O(2p^3 3s\,^5S^o) + H(1s\,^2S)$ as a function of the collision energy. The black solid line corresponds to the cross section obtained in the molecular symmetry $^4\Sigma^-$, the red solid line corresponds to the cross section obtained in the molecular symmetry $^6\Sigma^-$, the symbols denote the sum of two partial cross sections.

small internuclear distances in molecular symmetries other than the symmetries of ionic states plays an important role. It should be noted that the $^2\Pi$ symmetry is generated by the ionic state $O^- + H^+$, which indicates the importance of taking into account this ionic state when considering at least some inelastic processes in collisions of oxygen with hydrogen.

Another interesting question is: which of the two main mechanisms of non-adiabatic interaction – ion-covalent interaction or covalent-covalent interaction – is decisive for certain processes. As mentioned earlier, it is the ion-covalent interaction that most often leads to the largest cross sections of inelastic processes. Taking into account the covalent-covalent interaction may be important for processes with not the largest cross sections ($<10 Å^2$). In order to clarify this issue in the case of collisions of oxygen and hydrogen, we will analyze the results obtained by two different methods: the multichannel formula (taking into account only the non-adiabatic regions due to ion-covalent interaction) and the probability current method (taking into account both the non-adiabatic regions due to ion-covalent interaction and the regions due to covalent-covalent interaction).

Consider the molecular symmetries generated by the ionic states $O^+ + H^-$ and $O^- + H^+$, namely $^4\Sigma^-$, $^2\Sigma^+$ and $^2\Pi$. Figure 11 shows cross sections of mutual neutralization processes $O^+(2p^3\,{}^4S^o) + H^-(1s^2\,{}^1S) \rightarrow O^* + H^*$ as a function of the collision energy for molecular symmetry $^4\Sigma^-$ calculated by the multichannel formula (solid lines) and the probability current method (symbols). It can be seen that for cross sections with the largest values (processes $i2 \rightarrow 8$, 9, 10, 11, see Table 3 with characteristic values of cross sections $10 - 10^4$ AA^2) both methods have a good agreement in the considered energy range 0.01 – 100 eV. For cross sections of inelastic processes corresponding to transitions from the ionic state to low-lying states 4 and 5, the cross sections agree well at collision energies exceeding 10 eV, and at lower collision energies, the multichannel formula gives values several orders of magnitude lower than the values obtained using the probability current method, which indicates a significant role

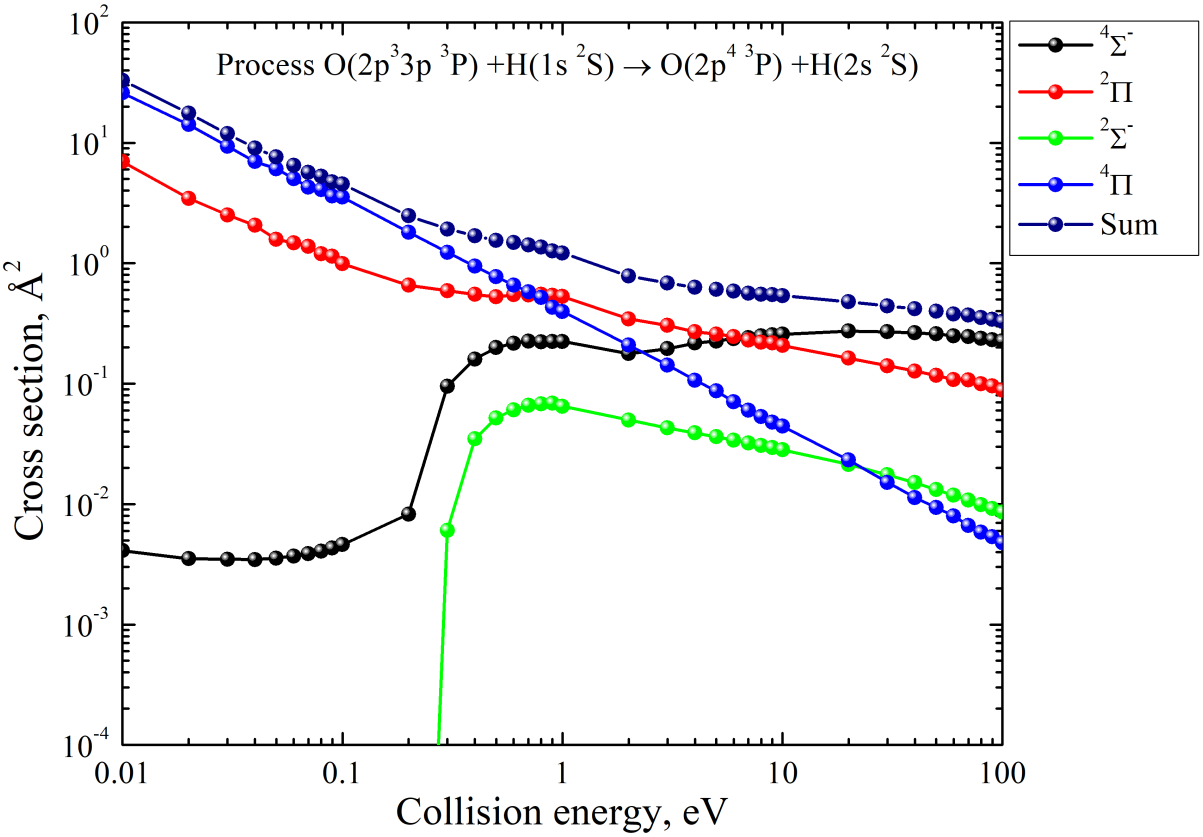

Figure 10. Cross sections of the inelastic process $O(2p^3 3p\,^3P) + H(1s\,^2S) \rightarrow O(2p^4\,^3P) + H(2s\,^2S)$ as a function of the collision energy. The black line corresponds to the partial cross section obtained in the molecular symmetry $^4\Sigma^-$, the red line corresponds to the partial cross section obtained in the molecular symmetry $^2\Pi$, the green line corresponds to the partial cross section obtained in the molecular symmetry $^2\Sigma^-$, the blue line is the partial cross section obtained in molecular symmetry $^4\Pi$, the purple line is the sum of all four partial sections.

covalent-covalent interaction at low collision energies. The cross sections calculated for processes involving the excited states of the hydrogen atom H(2s) and H(2p) (processes i2 $\rightarrow$ 6, 7(a,b), see Table 3) do not agree well in the entire studied range of collision energies. This suggests that the main mechanism of non-adiabatic transitions for these processes is due not to ion-covalent interaction, but to covalent-covalent interaction at relatively short distances, which are not taken into account when calculating using the multichannel formula.

The Figure 12 shows cross sections of mutual neutralization processes $O^-(2p^5\,^2\,\mathrm{rmP}) + H^+ \rightarrow O^* + H^*$ as a function of the collision energy for molecular symmetry $^2\Sigma^+$, calculated by the multichannel formula (solid lines) and by the probability current method (symbols). It can be seen that the cross sections obtained by two different methods are almost identical, which suggests that for the molecular symmetry $^2\Sigma^+$, the ion-covalent interaction is the dominant mechanism causing non-adiabatic transitions, while the covalent-covalent interaction does not give any noticeable contribution to the values of the cross sections.

The Figure 13 shows cross sections of mutual neutralization processes $O^-(2p^5\,^2\,\mathrm{rmP}) + H^+ \rightarrow O^* + H^*$ as a function of the collision energy for molecular symmetry $^2\Pi$, calculated by the multichannel formula (solid lines) and by the probability current method (symbols). It can be seen that for processes whose cross section values are the largest (in the range 10 – 10^4 Å^2, processes i1 $\rightarrow$ 2, 6, 7(a, b), see Table 3), the results obtained by the two methods agree quite well. However, it can be seen that if we take into account the non-adiabatic regions at short distances (by the probability current method), the cross sections of the processes i1 $\rightarrow$ 6, 7(a, b) decrease somewhat relative to the situation when only the non-adiabatic regions due to ion-covalent interaction are taken into account. At the same time, for the process i1 $\rightarrow$ 9, the difference in the values of the cross sections is about six orders of magnitude. For this process, the characteristic values of the cross section obtained by the probability current method are 0.1 – 100 Å^2,

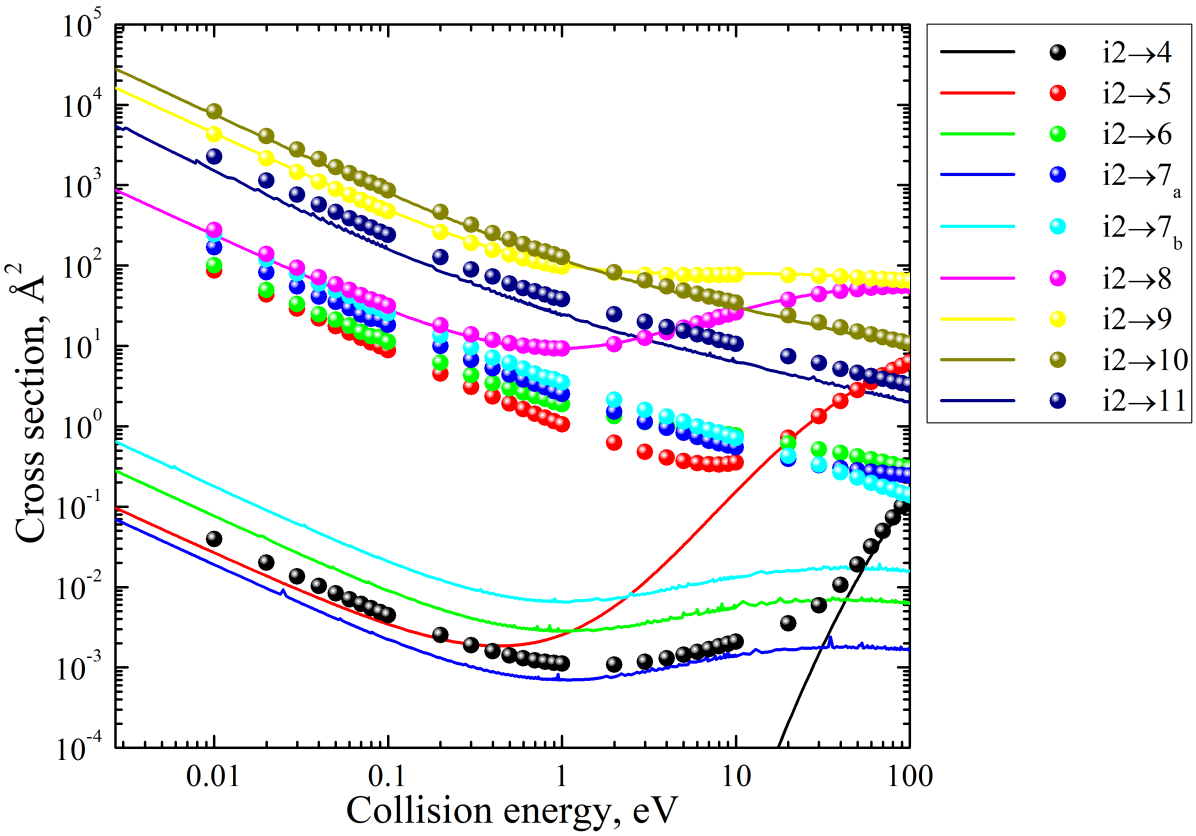

Figure 11. Cross sections of mutual neutralization processes $O^+ + H^- \to O^* + H^*$ as a function of the collision energy for molecular symmetry $^4\Sigma^-$. Solid lines denote cross sections calculated by the multichannel formula, symbols – cross sections calculated within the framework of the probability current method. For a description of the legend, see the Table 3.

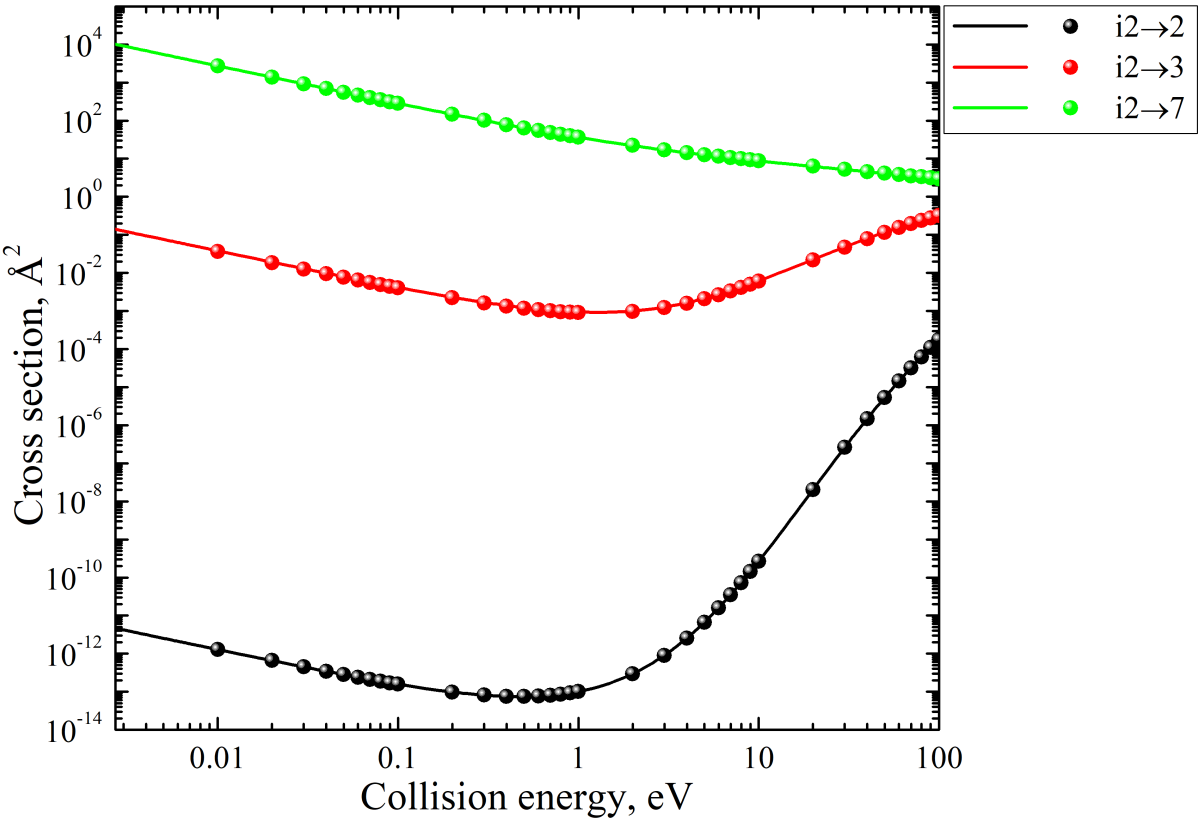

Figure 12. Cross sections of mutual neutralization processes $O^- + H^+ \to O^* + H^*$ as a function of the collision energy for molecular symmetry $^2\Sigma^+$. Solid lines denote cross sections calculated by the multi-channel formula, symbols – cross sections calculated within the framework of the probability current method. For a description of the legend, see the Table 3.

while the results obtained by the multichannel formula give the values 10^{-7} – 10^{-4} Å^2, which says about the dominant contribution of the covalent-covalent interaction. It is obvious that in the non-adiabatic regions located at short distances, the probability is redistributed in a non-trivial way, due to which the cross sections of processes $i1 \to 6$, 7(a, b) decrease and the cross section of the process $i1 \to 9$ increases greatly. This situation is often found for processes involving highly excited states, which was previously shown in the paper [30] and will be discussed in Chapter 4.

Let us now consider molecular symmetries generated only by covalent states. In this case, the application of a multichannel formula becomes impossible, since a series of consecutive non-adiabatic regions is not formed in these molecular symmetries, therefore, the study of non-adiabatic nuclear dynamics in this situation is possible only by the probability current method. Figures 14, 15 and 16 show cross sections of de-excitation processes as a functions of the collision energy for various initial channels for molecular symmetries $^6\Sigma^-$, $^4\Pi$ and $^2\Sigma^-$ respectively. The presented cross sections have the largest values, so these processes were chosen. The excitation processes have smaller cross sections than the cross sections of the de-excitation processes. From the Figures 14, 15 and 16, as well as Figures 9 and 10 it can be seen that the largest values of the cross sections over the entire studied range of collision energies do not exceed 100Å^2, and moreover, rarely exceed the value of 10 Å^2. Consequently, the thesis that the largest cross sections and, consequently, the rate coefficients are correspond to processes in those molecular symmetries that are generated by ionic states is again confirmed. Nevertheless, non-adiabatic transitions in molecular symmetries not generated by ionic states can make a non-negligible contribution to the final values of the cross sections of inelastic processes. This is of great importance from an applied point of view, since processes with the largest cross sections and rate coefficients mainly determine the parameters of gas and plasma media, and the correct definition of

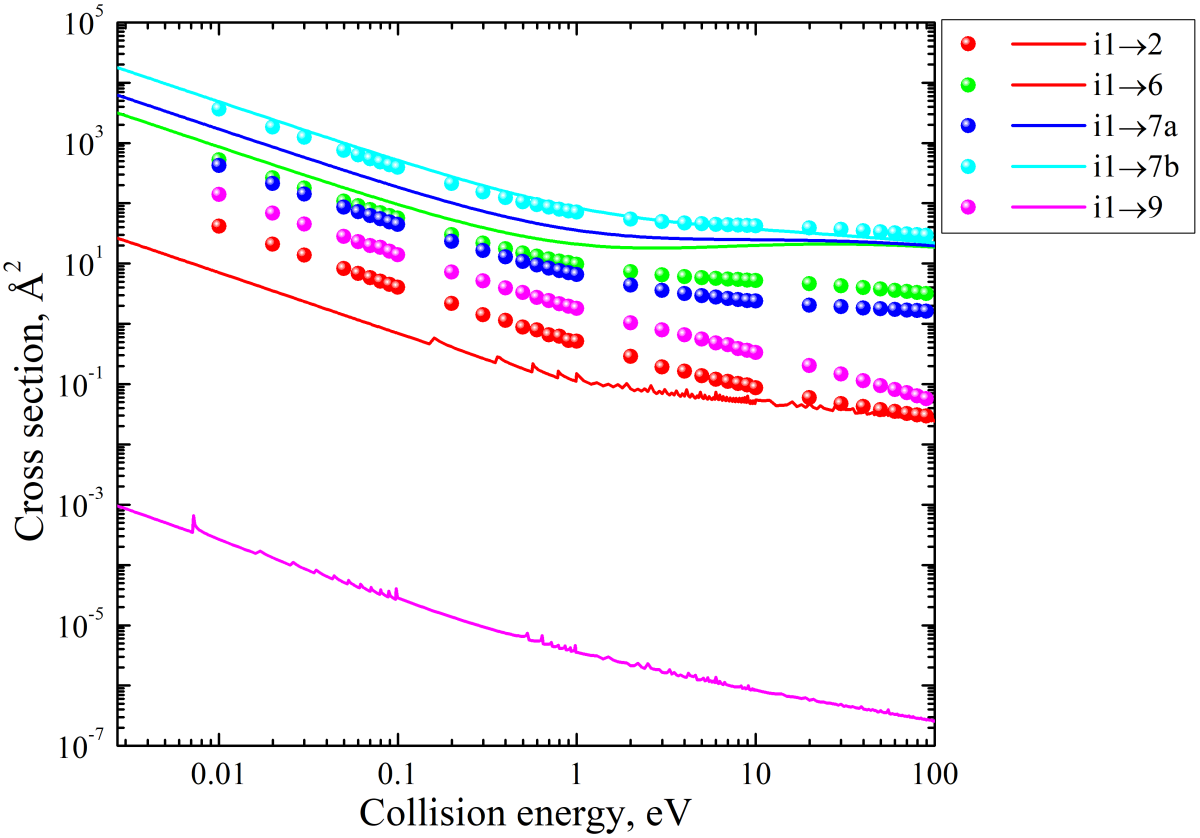

Figure 13. Cross sections of mutual neutralization processes $O^- + H^+ \rightarrow O^* + H^*$ as a function of the collision energy for molecular symmetry $^2\Pi$. Solid lines denote cross sections calculated by the multichannel formula, symbols – cross sections calculated within the framework of the probability current method. For a description of the legend, see the Table 3.

processes with the largest cross sections is important for physically correct modelling of gas and plasma media.

§ 3.5 Analysis of the rate coefficients of inelastic processes in O+H collisions

Let us now proceed to the analysis of the rate coefficients of the studied processes, as well as the comparison of the results obtained within the framework of this study with the results of other previous studies. For all inelastic processes, the rate coefficients are calculated in this paper using the formulas (1.74) and (1.75) in the temperature range 1000 – 10000 K. In general, all calculated rate coefficients can be divided into three groups, according to their values:

- group I: the processes with a rate coefficient exceeding 10^{-8} cm^3/s;
- group II: the processes with a rate coefficient lying in the range $10^{-8} - -10^{-12}$ cm^3/s;
- group III: the processes with a rate coefficient smaller than 10^{-12} cm^3/s.

Here are some concrete examples of rate coefficients for temperature T = 6000 K:

- group I includes the processes of mutual neutralization $\mathrm{O}^+(2p^3\ {}^4S^\circ) + \mathrm{H}^-(1s^2\ {}^1S) \rightarrow \mathrm{O}(2p^3 4s\ {}^5S^o) + \mathrm{H}(1s\ {}^2S)$, $\mathrm{O}^-(2p^5\ {}^2P) + \mathrm{H}^+ \rightarrow \mathrm{O}(2p^4\ {}^3P) + \mathrm{H}(2p^2P)$ and $\mathrm{O}^+(2p^3\ {}^4S^\circ) + \mathrm{H}^-(1s^2\ {}^1S) \rightarrow \mathrm{O}(2p^3 3p\ {}^3P) + \mathrm{H}(1s\ {}^2S)$ with the values of the rate coefficients (2.95, 2.56, 1.98) $\times 10^{-8}$ cm^3/s respectively;
- group II includes many processes of excitation/de-excitation, as well as the processes of ion-pair formation and mutual neutralization; among the processes of excitation/de-excitation, the highest value of

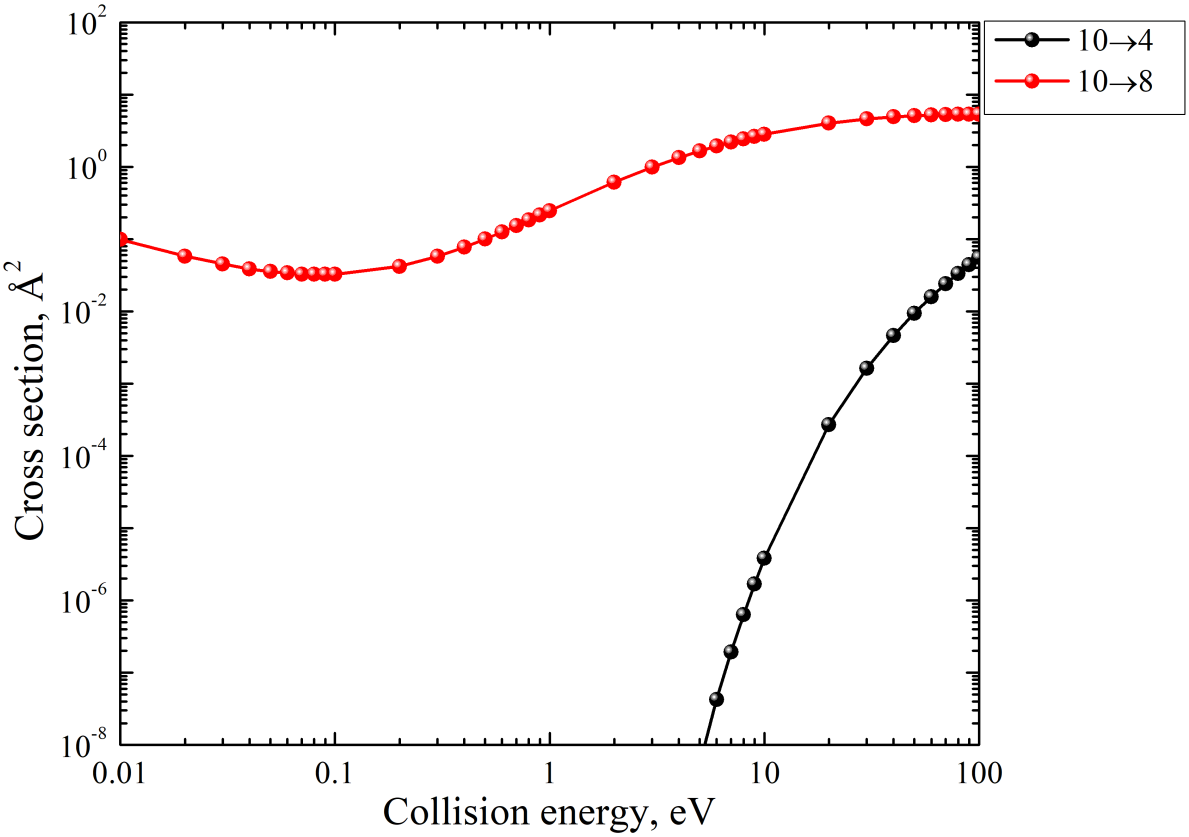

Figure 14. Cross sections of de-excitation processes for the initial state $O(2p^3 4s\,^5S^o) + H(1s\,^2S)$ as a function of the collision energy for molecular symmetry $^6\Sigma^-$. Lines and symbols denote the cross sections obtained within the framework of the probability current method. For a description of the legend, see the Table 3.

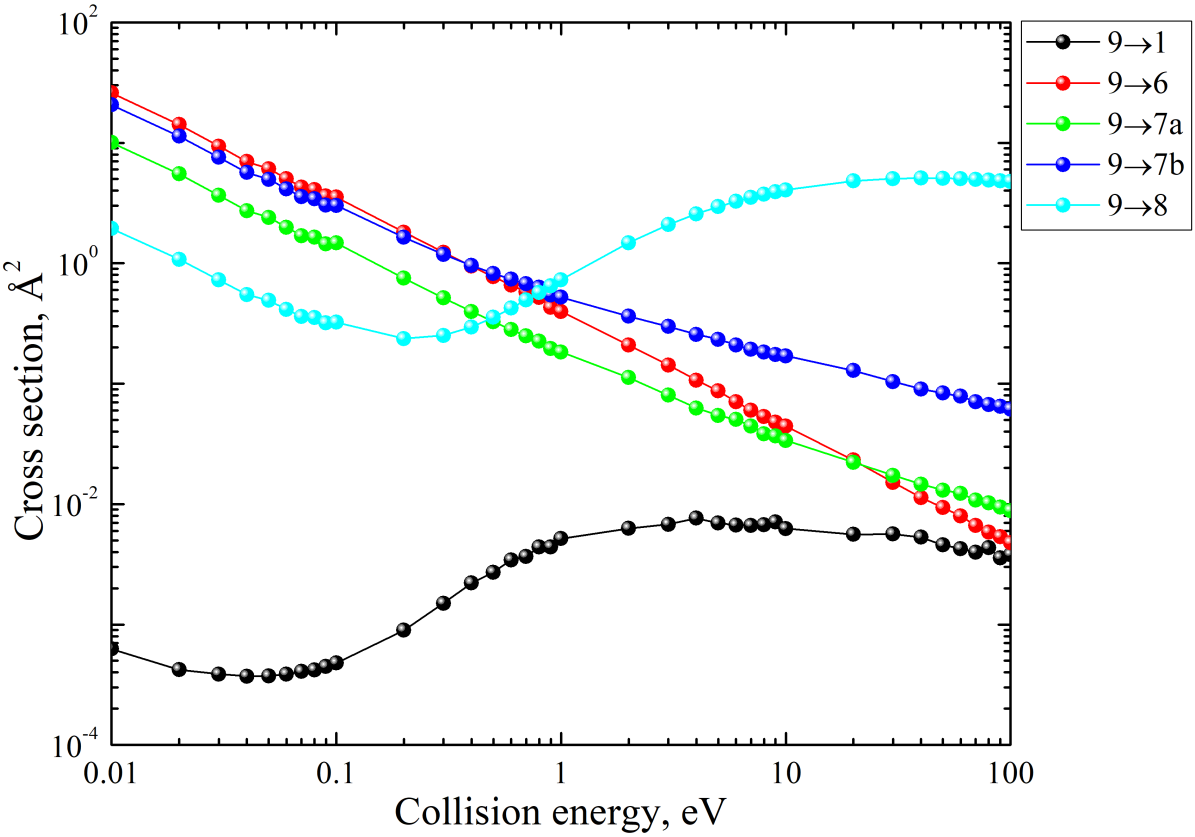

Figure 15. Cross sections of de-excitation processes for the initial state $O(2p^3 3p\,^3P) + H(1s\,^2S)$ as a function ofthe collision energy for molecular symmetry $^4\Pi$. Lines and symbols denote the cross sections obtained within the framework of the probability current method. For a description of the legend, see the Table 3.

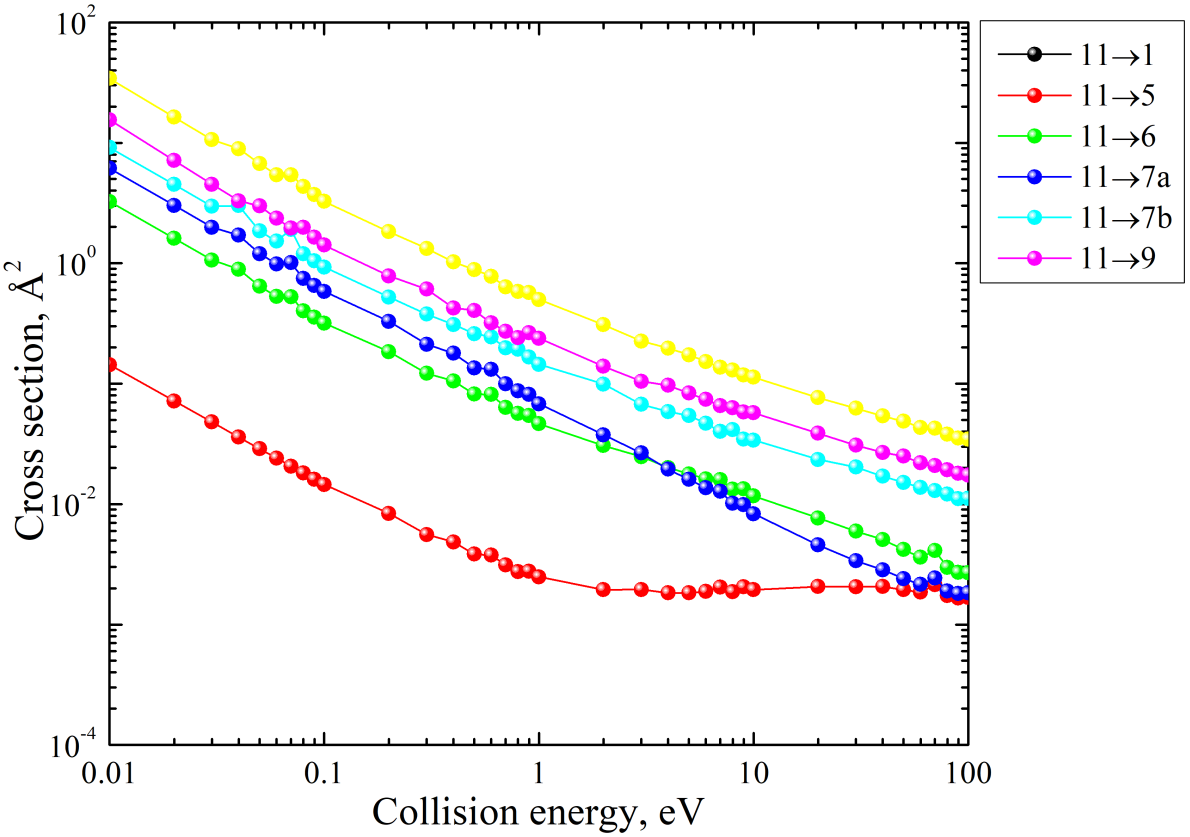

Figure 16. Cross sections of de-excitation processes for the initial state $O(2p^3 4s\,^3S^o) + H(1s\,^2S)$ as a function of the collision energy for molecular symmetry $^2\Sigma^-$. Lines and symbols denote the cross sections obtained within the framework of the probability current method. For a description of the legend, see the Table 3.

the rate coefficient corresponds to the process $O(2p^4\,^3P)+H(2s) \rightarrow O(2p^4\,^3P)+H(2p)$ with the value 3.91×10^{-9} cm^3/s;

- group III includes some processes of excitation, de-excitation, ion-pair formation and mutual neutralization; for example, all processes of excitation from the three lower states do not exceed 1.63×10^{-16} cm^3/s, and the processes of de-excitation in these three states do not exceed the magnitude 4.88×10^{-11} cm^3/s.

The analysis of partial rate coefficients obtained for the same process, but in different molecular symmetries, shows that the rate coefficients calculated for symmetries generated by ionic states make the greatest contribution to the values of the total rate coefficients. For example, the contribution to the values of the rate coefficients for processes involving the channel $O(2p^3 3s\ ^5S^o) + H(1s)$ give inelastic transitions within two symmetries – $^4\Sigma^-$ and $^6\Sigma^-$; at the same time, the values of the partial rate coefficients for $^6\Sigma^-$ symmetries are at least six orders of magnitude less than for $^4\Sigma^-$.

At the same time, for processes involving the channel $O(2p^3 3p\ ^5P) + H(1s)$ the situation is different: of the possible four molecular symmetries, this work takes into account transitions within three of them – $^4\Sigma^-$, $^4\Pi$ and $^6\Sigma^-$. The main contribution to the value of the total rate coefficient is also made by the $^4\Sigma^-$ symmetry rate coefficients, however, for the process $O(2p^3 3p\,^5P) + H(1s) \rightarrow O(2p^3 4s\,^5S^o) + H(1s)$ at a temperature of 6000 K the value of the rate coefficient in symmetry $^6\Sigma^-$ reaches $\approx$30% of the value of the constant $^4\Sigma^-$ (1.51×10^{-12} and 4.45×10^{-12} cm^3/s respectively). At the same time, for other processes, the values of the rate coefficients in the $^4\Pi$ symmetry reach $\approx$66% of the value of the rate coefficients in the $^4\Sigma^-$ symmetry.

It is also of interest to compare the total partial rate coefficients, that is, summed over all molecular symmetries (see the formula (1.76)) calculated by various methods. Since the available quantum-chemical data

obtained by *ab initio* methods of calculating the electronic structure are currently insufficient for nuclear dynamics calculations within the framework of the reprojection method, and experimental data are also missing, then a comparison of the results obtained in this study by the probability current method and by the multichannel formula using potential energies obtained by *ab initio* calculations by the MRCI method in the work [28], will be conducted only with the available data, obtained by various model methods, namely:

- simplified model [107, 108];
- the multichannel formula using the electronic structure of the OH quasimolecule obtained by a Linear Combination of Atomic Orbitals (hereinafter referred to as LCAO+multichannel formula) [106].

Consider the behavior of the rate coefficients as a function of temperature in the studied range of 1000 – 10000 K. The Figures 17 and 18 show the dependences of the rate coefficients of the processes of de-excitation/neutralization and excitation/ion-pair formation, respectively, on temperature. The presented neutralization processes from both ion channels in Figure 17 have the largest values in the entire temperature range studied. The de-excitation process $O(2p^3 4s\,^5S^o) + H(1s^2S) \rightarrow O(2p^3 3p\,^3P) + H(1s^2S)$ has a value exceeding 10^{-9} cm^3/sover the entire temperature range. Figure 17 shows that the rate coefficients of exothermic neutralization and de-excitation processes are practically independent of temperature, while Figure 18 shows that endothermic processes of excitation and ion-pair formation strongly depend on temperature, especially in the region of T < 5000 K. It is also seen that for exothermic processes, the rate coefficients in the entire studied temperature range exceed the rate coefficients of endothermic processes by at least an order of magnitude, even at a temperature of T = 10000 K. The strong dependence of endothermic processes on temperature is due to the fact that the cross sections of endothermic processes (excitation and ion-pair formation) have a reaction threshold. For

this reason, it is better to compare and analyze the rate coefficients of exothermic processes, since they do not have a reaction threshold.

Since the modelling of stellar photospheres under conditions of deviation from local thermodynamic equilibrium is important for stars of spectral classes F, G, K, which are characterized by temperatures less than 10000 K, further comparison of the values of the rate coefficients obtained by different methods will be carried out for a temperature of 6000 K. Figures 19 and 20 show the rate coefficients of mutual neutralization processes as a function of the excitation energy of the oxygen atom, obtained by different methods:

- by the probability current method using potentials obtained by the MRCI quantum method (black balls are marked in both figures);
- by the multichannel formula using potentials obtained by the MRCI quantum method (marked with red asterisks in both figures);
- by the multichannel formula using model potentials obtained by the LCAO method (marked with green diamonds in all figures);
- by the simplified model (marked with a black solid line in both figures).

For processes involving the ion channel $O^- + H^+$, the calculation of cross sections and rate coefficients was performed for the first time in this work, calculations by other methods have not been carried out before, so in the Figure 20 the rate coefficients obtained by the multichannel formula and the probability current method, as well as the predictions of the simplified model, are presented. It can be seen that for the processes $i1 \to 6, 7$, the results agree well with each other, but there is a difference several times with respect to the predictions of the simplified model. But for the process $i1 \to 9$, the rate coefficients obtained by the probability current method and by the multichannel formula differ by about six orders of magnitude, and the predictions of the simplified model give a value greater

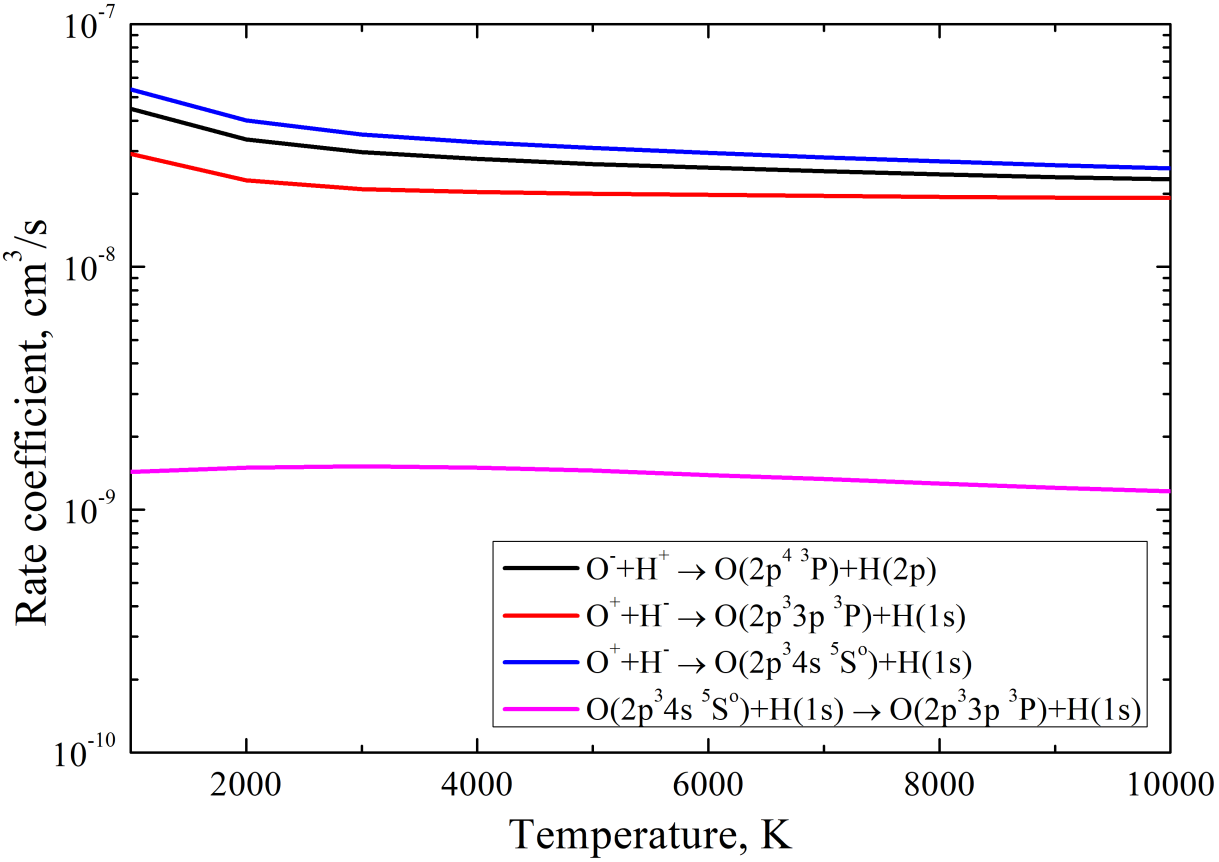

Figure 17. The dependence of the rate coefficients of some neutralization and de-excitation processes on temperature.

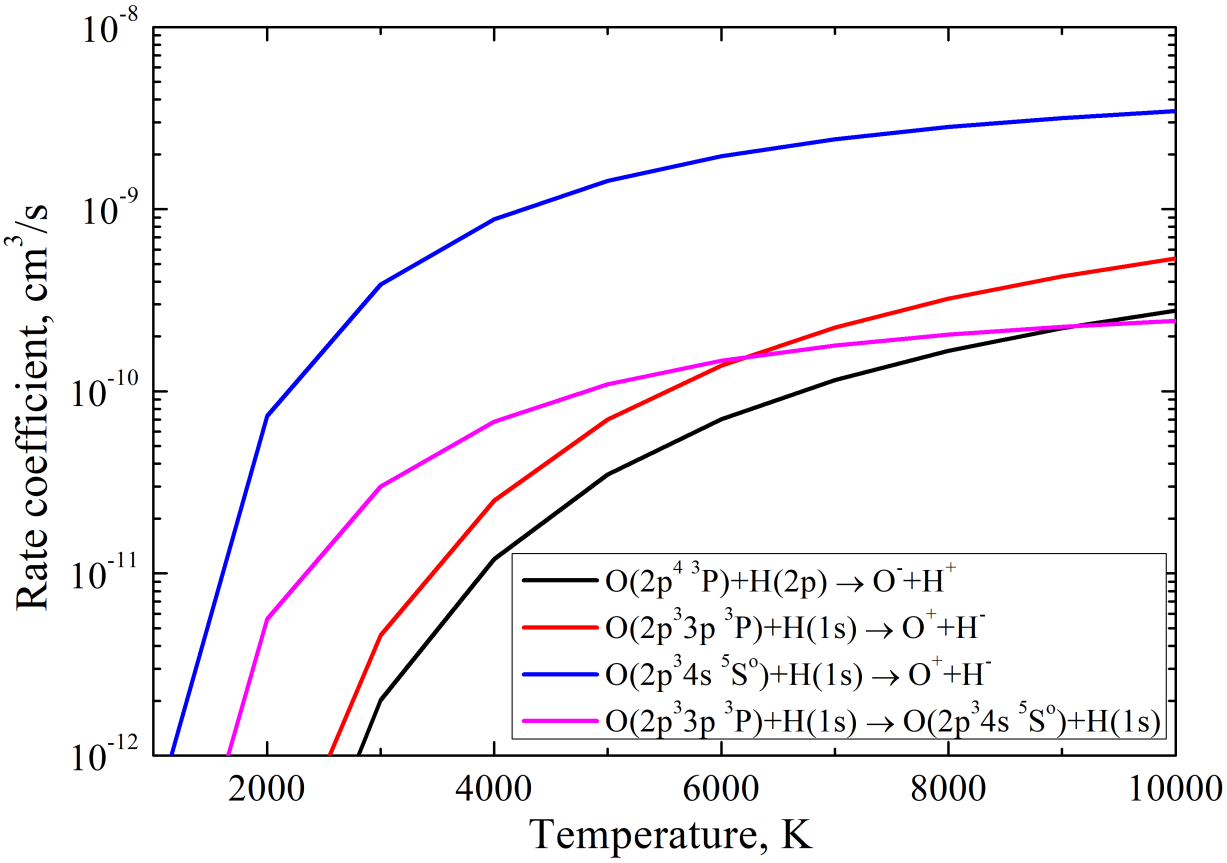

Figure 18. The dependence of the rate coefficients of some processes of ion-pair formation and excitation on temperature.

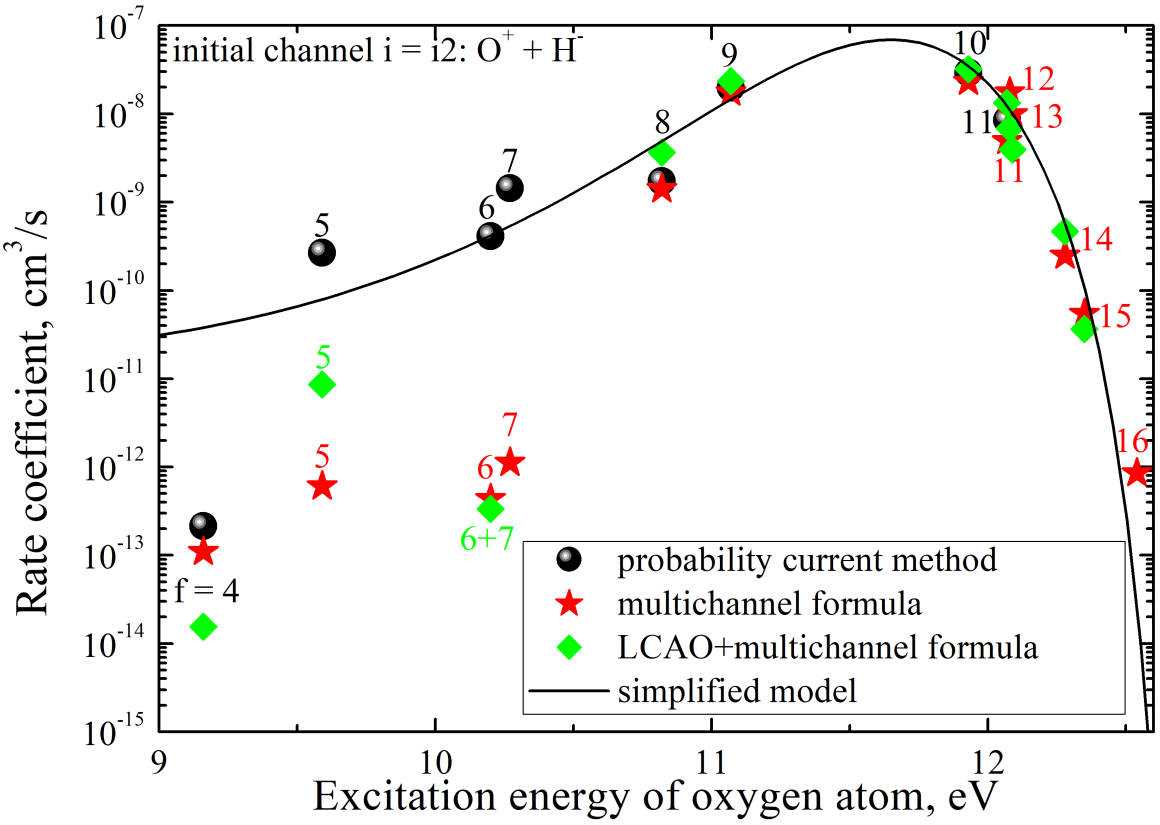

Figure 19. The dependence of the total partial rate coefficients of the mutual neutralization processes for the initial channel $O^+ + H^-$ on the excitation energy of the oxygen atom. Black circles corresponds to the rate coefficients obtained from the cross sections calculated by the probability current method; red asterisks – the rate coefficients obtained from the cross sections calculated by the multichannel formula; green diamonds – the rate coefficients obtained in the work [106] by the multichannel formula using potentials obtained by the LCAO method; the black solid line corresponds to the predictions of the simplified model. For the notation, see the Table 3.

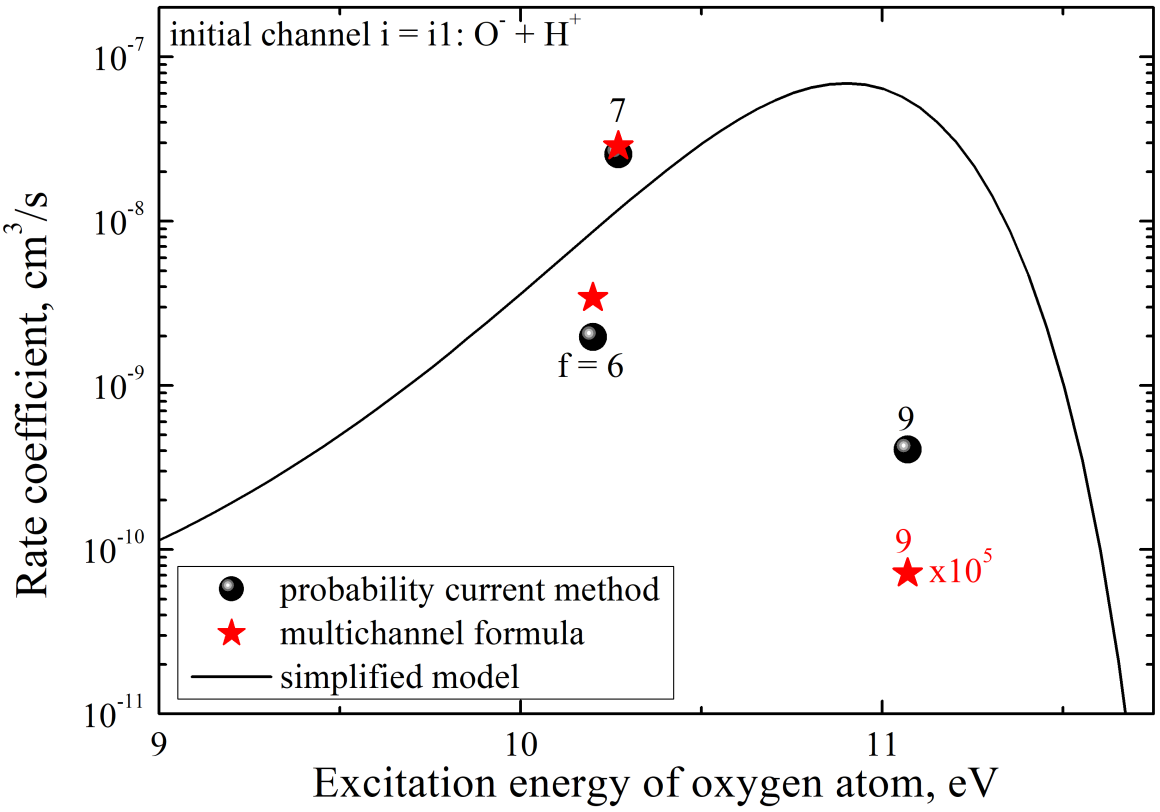

Figure 20. The dependence of the total partial rate coefficients of the mutual neutralization processes for the initial channel $O^- + H^+$ on the excitation energy of the oxygen atom. Black circles corresponds to the rate coefficients obtained from the cross sections calculated by the probability current method; red asterisks – the rate coefficients obtained from the cross sections calculated by the multichannel formula; black solid line corresponds to the predictions of the simplified model. For the notation, see the Table 3. The rate coefficient of the process $i1 \to 9$, obtained by the multichannel formula, is multiplied by 10^5.

by about two orders of magnitude than the value of the rate coefficient obtained by the probability current method. It is worth remembering that the simplified model describes neutralization processes for a situation where the ion channel corresponds to the collision of the cation of the considered element with the hydrogen anion, and not vice versa. Nevertheless, it can be said that this process is greatly influenced by transitions in non-adiabatic regions due to covalent-covalent interaction and located at short distances, see Figures 4 and 5, since taking into account these regions by the probability current method leads to an increase in the rate coefficient of this process by about six orders of magnitude.

For neutralization processes involving the ion channel $O^+ + H^-$ (Figure 19) the situation is different. The Table 5 shows the values of all the values of the rate coefficients obtained by all four methods. For processes $i2 \to 8, 9, 10, 11$, the values of the rate coefficients obtained by four different methods agree well with each other. These processes fall into the so-called "optimal window" of the simplified model and have the highest values of the rate coefficients. The processes falling into the optimal window are mainly determined by non-adiabatic transitions in the non-adiabatic regions due to ion-covalent interaction. At the same time, the rate coefficients obtained by the multichannel formula on the LCAO model potentials and on the MRCI *ab initio* potentials for the processes $i2 \to 4, 5, 6, 7$ agree with each other up to about one order of magnitude, and do not exceed the values of 10^{-11} cm^3/s. But the values of the rate coefficients obtained by the probability current method are significantly greater than the values of the rate coefficients obtained by the multichannel formula, and at the same time these rate coefficients are significantly better consistent with the predictions of the simplified model. This suggests that for these processes, the influence of non-adiabatic transitions in the non-adiabatic regions at short distances due to covalent-covalent interaction is significant. Taking into account transitions at small internuclear distances leads to an increase in

Table 5. Comparison of the rate coefficient values of the mutual neutralization processes $O^+ + H^- \to O^* + H^*$ at the temperature T = 6000 K obtained by four different methods: the probability current method + *ab initio* potentials from the paper [28] (PC-MRCI, this study), the multichannel formula + *ab initio* potentials from the paper [28](MC-MRCI, this study), the multichannel formula + model LCAO potentials [106] (MC-LCAO), the simplified model [107] (SM). All rate coefficient have dimension cm^3/s. E denotes the power of ten.

j	Scattering channel	Excitation energy, eV	PC-MRCI	MC-MRCI	MC-LCAO	SM
4	$O(2p^3 3s\,^5S^o) + H(1s^2S)$	9.1461	2.15E-13	1.1E-13	1.55E-14	3.76E-11
5	$O(2p^3 3s\,^3S^o) + H(1s^2S)$	9.5214	2.68E-10	6.04E-13	8.6E-12	6.84E-11
6	$O(2p^4\,^3P) + H(2s^2S)$	10.2000	4.14E-10	4.35E-13	3.34E-13	4.36E-10
7	$O(2p^4\,^3P) + H(2p^2P)$	10.2000	1.44E-9	1.12E-12		4.36E-10
8	$O(2p^3 3p\,^5P) + H(1s^2S)$	10.7406	1.73E-9	1.41E-9	3.65E-9	3.45E-9
9	$O(2p^3 3p\,^3P) + H(1s^2S)$	10.9888	1.98E-8	1.75E-8	2.34E-8	1.04E-8
10	$O(2p^3 4s\,^5S^o) + H(1s^2S)$	11.8376	2.95E-8	2.32E-8	3.2E-8	5.11E-8
11	$O(2p^3 4s\,^3S^o) + H(1s^2S)$	11.9304	8.48E-9	4.94E-9	1.33E-8	3.36E-8
12	$O(2p^3 3d\,^5D^o) + H(1s^2S)$	12.0786	–	1.76E-8	6.85E-9	1.14E-8
13	$O(2p^3 3d\,^3D^o) + H(1s^2S)$	12.0870	–	9.96E-9	3.95E-9	1.08E-8
14	$O(2p^3 4p\,^5P) + H(1s^2S)$	12.2861	–	2.49E-10	4.65E-10	5.04E-10
15	$O(2p^3 4p\,^3P) + H(1s^2S)$	12.3589	–	5.46E-11	3.65E-11	7.10E-11
16	$O(2p^3 3s\,^3D^o) + H(1s^2S)$	12.5402	–	8.53E-13	–	3.06E-14

the final value of the rate coefficients for these processes by several orders of magnitude, up to the value of 10^{-9} cm^3/s.

It is also worth noting that in Chapter 4, a comparison of the results obtained by the probability current method using potentials obtained by *ab initio* methods with the results obtained by the reprojection method for Ca+H collisions will be considered. Good agreement of the results of the most accurate quantum calculations with predictions of the simplified model will be shown, which suggests that the comparison of the results obtained by various theoretical methods with the predictions of the simplified model allows us to judge the correctness of these results.

In the figures 21, 22, 23, 24 the dependences of the rate coefficients values of the excitation and de-excitation processes on the excitation energy of the oxygen atom for the initial channels $O(2p^4\,^3P)+H(2p\,^2P), O(2p^3 3p\,^5P)+$

$H(1s^2S), O(2p^3 4s\,^5S^o) + H(1s^2S), O(2p^3 4s\,^3S^o) + H(1s^2S)$ (7, 8, 10 and 11), respectively, are shown. It can be seen from the figures that for almost all processes, the values of the rate coefficients obtained within the framework of the probability current method exceed the values of the rate coefficients obtained by the multichannel formula, regardless of whether model potentials are used or obtained by the MRCI method. At the same time, the data obtained by the probability current method agree with the predictions of the simplified model better than the data obtained by other methods. The rate coefficients obtained by the multichannel formula have particularly small values (not exceeding 10^{-13} cm^3/s) in the region of the excitation energies of the oxygen atom < 10.5 eV, with the exception of several processes for which channel 8 is the initial channel (processes $8 \rightarrow 5$, 6, 7, see Figure 22), as well as process $7 \rightarrow 6$ (see Figure 21). This result confirms the thesis that the largest cross sections and rate coefficients are determined by non-adiabatic transitions in the non-adiabatic regions caused by ion-covalent interaction and usually located at distances of 20-40 atomic units. At the same time, taking into account the non-adiabatic regions caused by covalent-covalent interaction and located at distances less than 10 – 15 atomic units can lead to an increase in the values of the rate coefficients for processes having values less than 10^{-12} cm^3/s.

Thus, the conducted research shows the importance of taking into account all possible molecular symmetries when calculating non-adiabatic nuclear dynamics, since they can have a significant impact on the values of the rate coefficients of the excitation/de-excitation processes, despite the fact that such accounting affects only the values of constants from groups II and III.

§ 3.6 Concluding remarks

In this study, the processes of excitation, de-excitation, ion-pair formation and mutual neutralization in collisions of oxygen atoms and ions

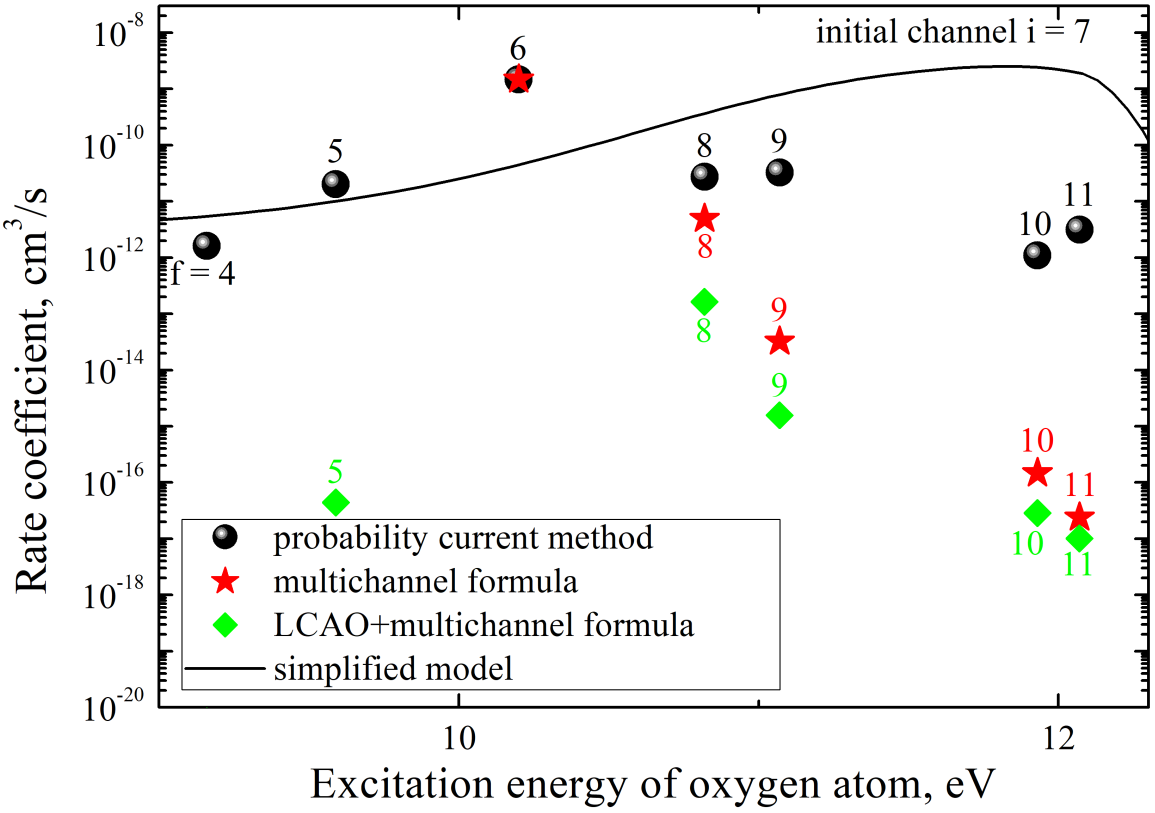

Figure 21. The dependence of the values of the total partial rate coefficients of the excitation and de-excitation processes for the initial channel 7 on the excitation energy of the oxygen atom. Black circles corresponds to the rate coefficients obtained from the cross sections calculated by the probability current method; red asterisks – the rate coefficients obtained from the cross sections calculated by the multichannel formula; green diamonds – the rate coefficients obtained in the work [106] by the multichannel formula using potentials obtained by the LCAO method; black solid line corresponds to the predictions of the simplified model. For the notation, see the Table 3.

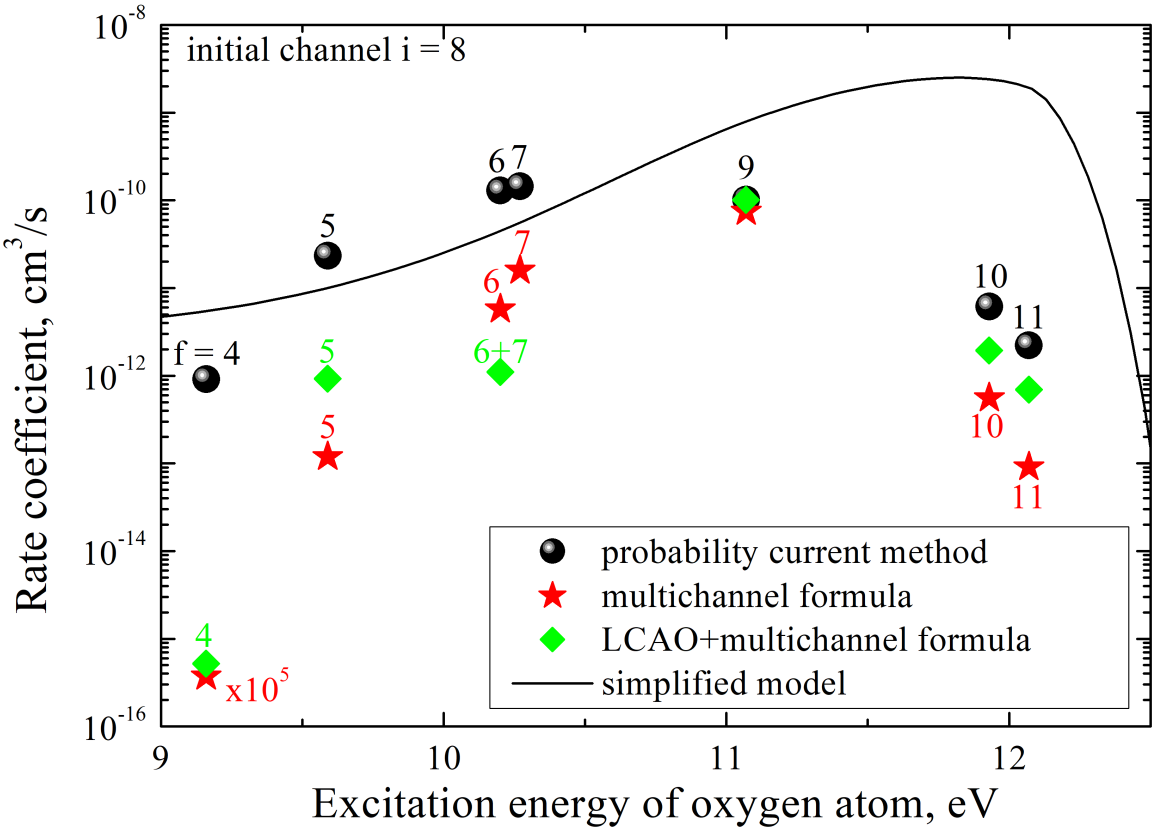

Figure 22. The dependence of the values of the total partial rate coefficients of the excitation and de-excitation processes for the initial channel 8 on the excitation energy of the oxygen atom. Black circles corresponds to the rate coefficients obtained from the cross sections calculated by the probability current method; red asterisks – the rate coefficients obtained from the cross sections calculated by the multichannel formula; green diamonds – the rate coefficients obtained in the work [106] by the multichannel formula using potentials obtained by the LCAO method; black solid line corresponds to the predictions of the simplified model. For the notation, see the Table 3.

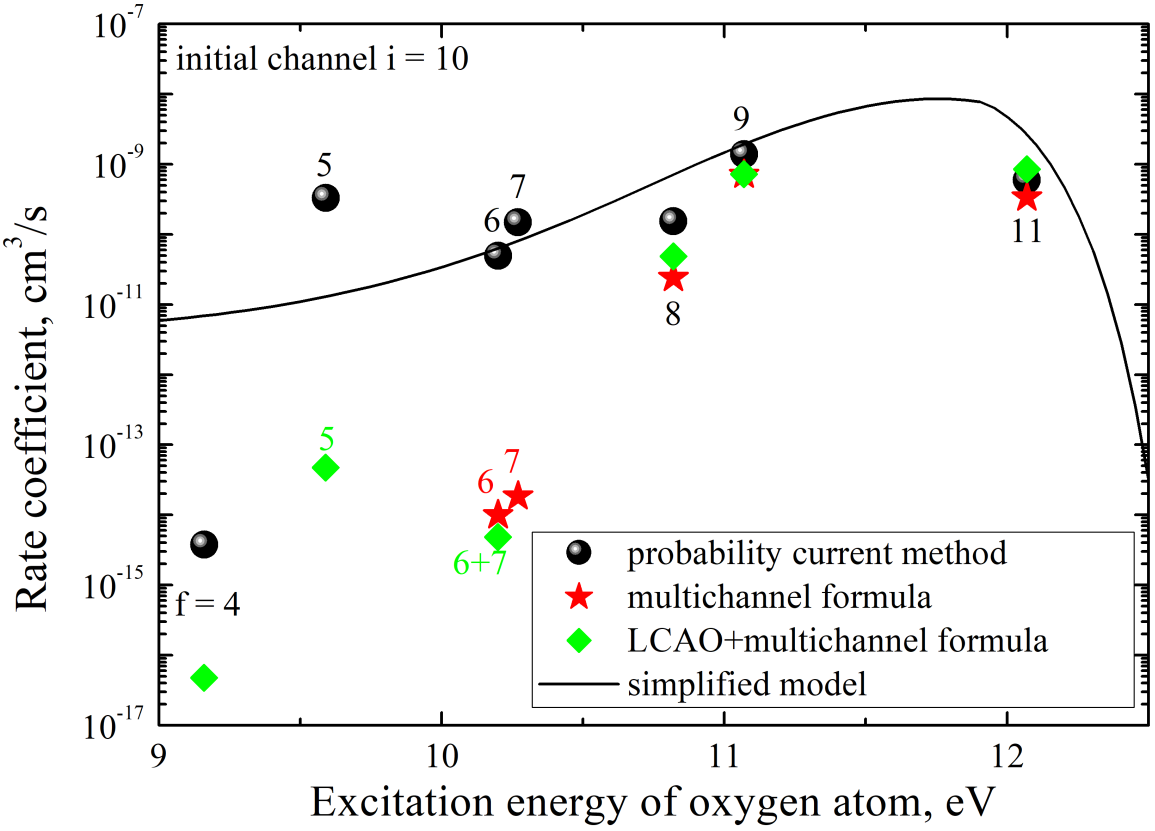

Figure 23. The dependence of the values of the total partial rate coefficients of the excitation and de-excitation processes for the initial channel 10 on the excitation energy of the oxygen atom. Black circles corresponds to the rate coefficients obtained from the cross sections calculated by the probability current method; red asterisks – the rate coefficients obtained from the cross sections calculated by the multichannel formula; green diamonds – the rate coefficients obtained in the work [106] by the multichannel formula using potentials obtained by the LCAO method; black solid line corresponds to the predictions of the simplified model. For the notation, see the Table 3.

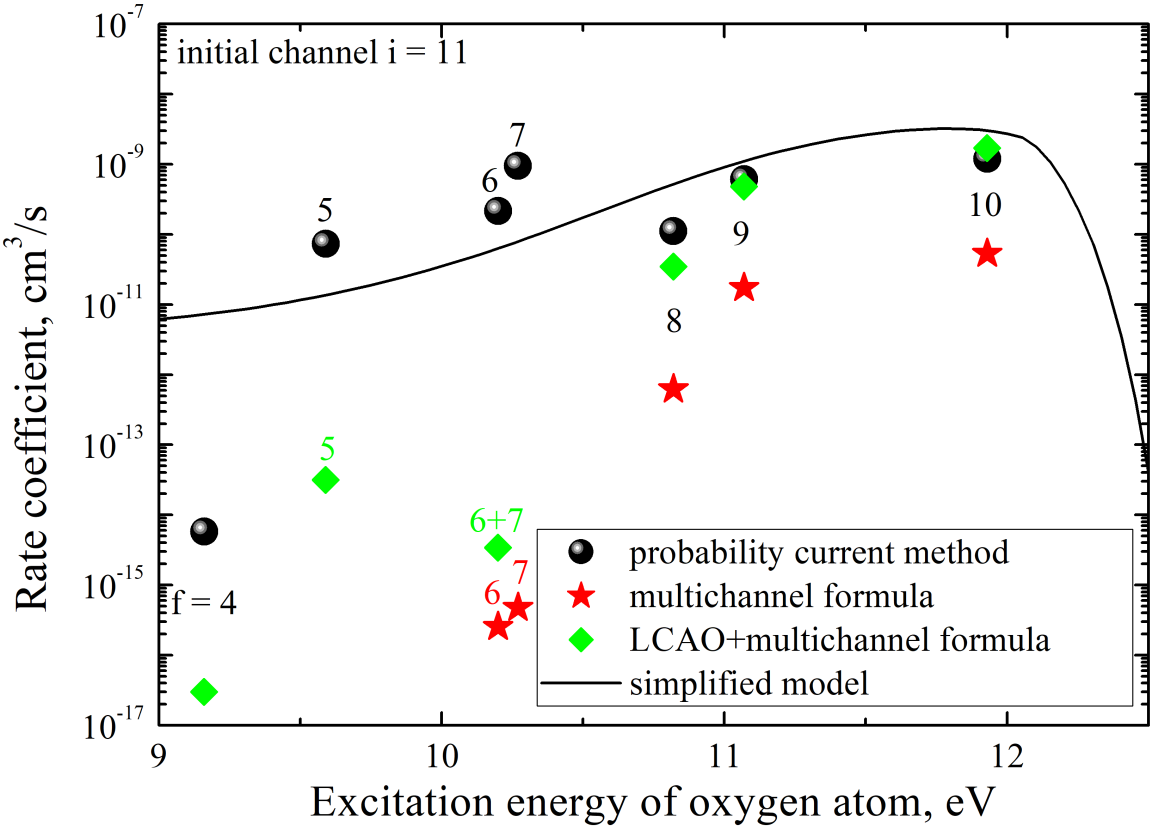

Figure 24. The dependence of the values of the total partial rate coefficients of the de-excitation processes for the initial channel 11 on the excitation energy of the oxygen atom. Black circles corresponds to the rate coefficients obtained from the cross sections calculated by the probability current method; red asterisks – the rate coefficients obtained from the cross sections calculated by the multichannel formula; green diamonds – the rate coefficients obtained in the work [106] by the multichannel formula using potentials obtained by the LCAO method; black solid line corresponds to the predictions of the simplified model. For the notation, see the Table 3.

with hydrogen atoms and ions were considered. Inelastic processes for 11 covalent states and two ionic states in six molecular symmetries have been studied by the hopping probability current method (stochastic version), for a total of 240 processes. By the multichannel formula, processes for 16 covalent states and two ionic ones for three molecular symmetries were studied, a total of 292 processes. In the study of nuclear dynamics, molecular adiabatic potential energies were used, obtained in paper [28] by the MRCI method for 11 lower covalent states and two ionic ones, as well as obtained within the framework of the asymptotic method for 5 high-lying covalent states.

It is shown that:

- rate coefficients with the largest values correspond to the neutralization processes $O^+(2p^3\ ^4S^\circ) + H^-(1s^2\ ^1S) \to O(2p^3 4s\ ^5S^o) + H(1s\ ^2S)$, $O^-(2p^5\ ^2P) + H^+ \to O(2p^4\ ^3P) + H(2p^2P)$ and $O^+(2p^3\ ^4S^\circ) + H^-(1s^2\ ^1S) \to O(2p^3 3p\ ^3P) + H(1s\ ^2S)$; these processes, as well as processes with the rate coefficients values greater than 10^{-12} cm^3/s, that is, processes belonging to groups I and II, are the most important to take into account in modelling stellar spectra under conditions of deviation from local thermodynamic equilibrium;

- taking into account non-adiabatic transitions in molecular symmetries not generated by ionic states practically does not affect the values of cross sections and rate coefficients of processes belonging to group I, but can significantly affect processes belonging to groups II and III; in particular, for some processes, the values of cross sections at low collision energies are mainly determined by the contribution of non-adiabatic transitions in molecular symmetries not generated by ionic states;

The results obtained in this Chapter are published in the following articles:

- Mitrushchenkov A. et al. Inelastic excitation and charge transfer processes for oxygen in collision with H atoms / A. Mitrushchenkov, M. Guitou, A. K. Belyaev, **Ya. V. Voronov**, N. Feautrier // The Journal of chemical physics. – 2019. – Vol. 150. – No. 6. – P. 064312 [28];

- Belyaev A. K. et al. Inelastic processes in oxygen–hydrogen collisions / A. K. Belyaev, **Ya. V. Voronov**, A. Mitrushchenkov, M. Guitou and N. Feautrier // Monthly Notices of the Royal Astronomical Society. – 2019. – Vol. 487. – No. 4. – P. 5097-5105 [29];

- Bergemann M. et al. Solar oxygen abundance / M. Bergemann, R. Hoppe, E. Semenova, M. Carlsson, S. A. Yakovleva, **Ya. V. Voronov**, M. Bautista, A. Nemer, A. K. Belyaev, J. Leenaarts, L. Mashonkina, A. Reiners, M. Ellwarth // Monthly Notices of the Royal Astronomical Society. – 2021. – Vol. 508. – No. 2. – P. 2236-2253 [27].

Also, the results of this study were presented at two international scientific conferences in the form of poster presentations:

- XXI Mendeleev Congress on General and Applied Chemistry, Symposium "The Periodic Table through Space and Time" (9-13 September, 2019, Saint-Petersburg, Russia). Poster "**Application of the probability current method to nuclear dynamical calculations in collisions with hydrogen**";

- Physics of Stars and Planets: atmospheres, activity and magnetic fields (16-20 September, 2019, N. Tusi Shamakhi Astrophysical Observatory, Shamakhi, Azerbaijan). Poster "**Application of the probability current method to nuclear dynamical calculations in collisions with hydrogen**".

This research was supported by grants:

- the Ministry of Science and Higher Education grant No. 3.1738.2017/PCH 2017-2019, the head of Prof. Belyaev A. K.

- the Ministry of Education grant No. 2020-0026 2020-2022, the head of Prof. Belyaev A. K.

Chapter 4. Investigation of inelastic processes in collisions of calcium atoms and ions with hydrogen atoms and ions

§ 4.1 Preliminary remarks

Calcium, along with other alkaline earth metals, as well as their ions, is of great importance for astrophysical applications and for spectroscopy (see, for example, papers [3–5, 111–115] and references therein). It is one of the best observed chemical elements in late-type stars [113, 116, 117]. In the paper [116] noted: "In very metal-poor stars with metallicity [Fe/H] < -5, calcium is the only chemical element visible in two ionized states, and the Ca I and Ca II lines can also be a powerful tool for obtaining accurate values of the fundamental parameters of stars and the Ca abundance itself."[6]

Calcium belongs to the group of α-elements and is of particular importance for astrophysics. For example, calcium is well suited for distinguishing stellar populations in the galactic disk and halo, and also allows us to understand the relationship with dwarf spheroidal galaxies (see [113, 118, 119] and references therein).

The main mechanism of calcium formation is explosive nucleosynthesis in supernovae, with the yield coefficient [Ca/Fe] depending on the mass and energy of the explosion [120]. However, it has been suggested that a certain amount of calcium may also be synthesized during hydrostatic combustion in the hot CNO cycle in stars belonging to stellar population III (for example, [121]). Observations of the calcium content in stars with low metallicity can help distinguish between these two mechanisms of calcium formation.

Previously using the classical Drawin formula [11–13] several studies have been conducted to model calcium spectral lines under condi-

[6] [Fe/H] $= log_{10}(N_{Fe}/N_H)_{stars} - log_{10}(N_{Fe}/N_H)_{Sun}$, where N is the concentration of atoms of an element.

tions of deviation from local thermodynamic equilibrium (see, for example, [116, 122–124]), although it has been repeatedly shown (see, for example, [3, 14, 15]) that Drawin's formula gives incorrect results. There are also more accurate calculations of cross sections and rate coefficients of inelastic processes in collisions of Ca+H and $Ca^+ + H^-$, carried out by quantum model methods within the framework of the Landau-Zener model [50, 125, 126]. Then the obtained quantum data were used to simulate the formation of Ca I lines under conditions of deviation from local thermodynamic equilibrium in the works [113, 117]. The availability of these data has eliminated the main source of uncertainty in the formation of the Ca I line associated with the deviation from the local thermodynamic equilibrium, so it is also important to expand the work on Ca II.

Thus, knowledge of the characteristics of inelastic processes in collisions of calcium atoms and ions with hydrogen is of great importance for astrophysical applications. This study is aimed at obtaining more accurate values of cross sections and rate coefficients of inelastic processes in collisions of Ca+H and $Ca^+ + H^-$ within the framework of the probability current method by taking into account non-adiabatic transitions at small internuclear distances, as well as obtaining new collision data $Ca^+ + H$, $Ca + H^+$ and $Ca^{2+} + H^-$. Moreover, the study of inelastic processes for the quasimolecular ion CaH^+ was carried out both without taking into account the fine splitting of energy levels, and taking it into account, that is, in the LS- and JJ representation, respectively. The account for the fine structure is carried out within the framework of the approach proposed in [23, 24].

Relatively recently, the paper of A. K. Belyaev et al. [18] was published, in which nuclear dynamics was investigated within the framework of the quantum reprojection method. In this regard, it is possible to analyze the accuracy of the probability current method.

§ 4.2 Investigation of inelastic processes in atom-atomic collisions of Ca+H, as well as ion-ion collisions of $Ca^+ + H^-$

Let us proceed directly to the study of inelastic processes in collisions of Ca+H and $Ca^+ + H^-$. The study was conducted within the framework of the Born-Oppenheimer approach [19]. The electronic structure of the CaH quasimolecule used in this work was obtained by the MRCI method in [126]. Nuclear dynamics is investigated by the probability current method (stochastic version of the algorithm). The cross sections of all inelastic processes are calculated in the collision energy range 0.01 – 100 eV according to the formulas (1.70) and (1.72). The rate coefficients are calculated in the temperature range 1000 – 10000 K according to the formula (1.74) for exothermic processes and according to the balance equation (1.75) for endothermic processes.

4.2.1 Adiabatic potential energies of a CaH quasimolecule

The adiabatic molecular potential energies used in this study were calculated in the paper [126] by the MRCI quantum chemical method. In total, 11 molecular states corresponding to 10 covalent and one ion scattering channel in the molecular symmetry $^2\Sigma^+$ were taken into account. All the states taken into account in the study of nuclear dynamics are given in the Table 6. Figure 25 shows the adiabatic molecular potential energies of all the considered states, as a function of the internuclear distance.

4.2.2 Investigation of non-adiabatic nuclear dynamics by the hopping probability current method

Non-adiabatic nuclear dynamics in this study is investigated by the probability current method (see §1.4.3), namely the stochastic version of the algorithm. To calculate the full probabilities of a non-adiabatic transition

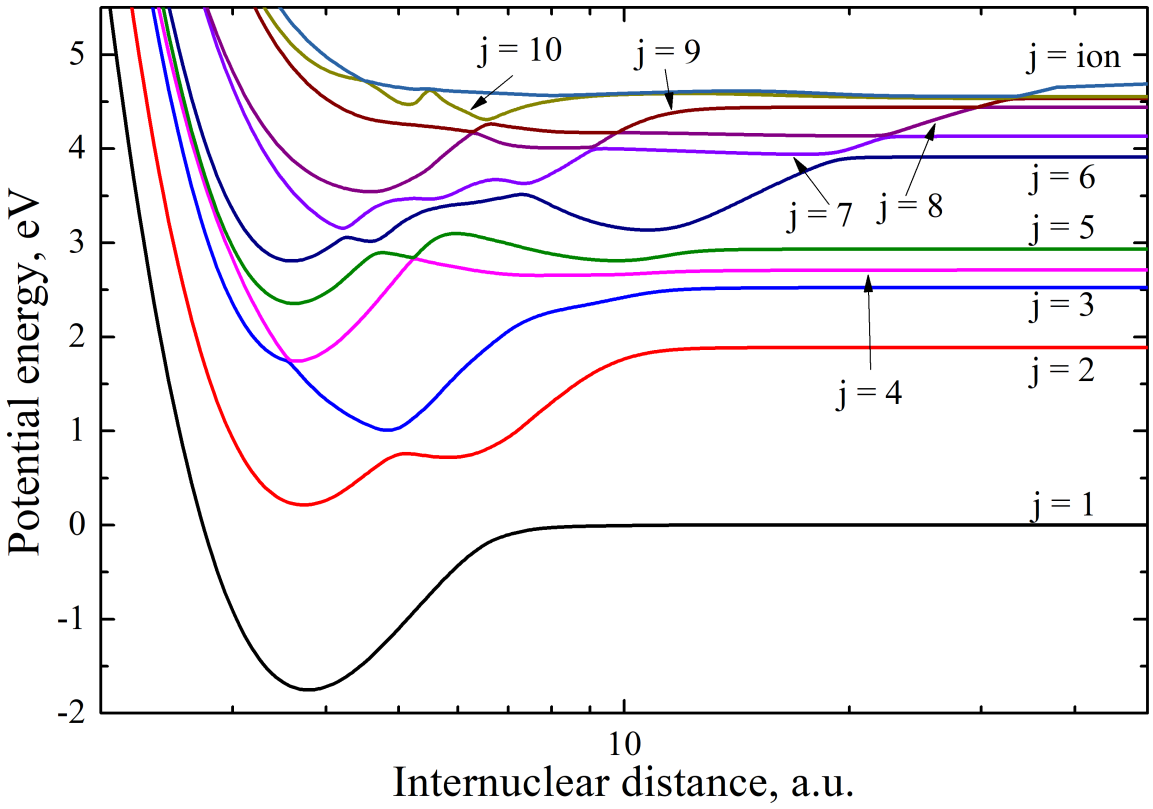

Figure 25. Adiabatic potential energies U_j of a CaH quasimolecule as a function of the internuclear distance R for molecular symmetry $^2\Sigma^+$, calculated in [126]. See the notation in the Table 6.

Table 6. Molecular states of a CaH quasimolecule in molecular symmetry $^2\Sigma^+$, corresponding scattering channels, asymptotic energies calculated from the ground state $\mathrm{Ca}(4s^2\ ^1S) + \mathrm{H}(1s\ ^2S)$, as well as statistical weights, characterizing populations of molecular states $^2\Sigma^+$.

j	Scattering channel	Asymptotic energy (eV)	p_j^{stat}
1	$\mathrm{Ca}(4s^2\ ^1S) + \mathrm{H}(1s\ ^2S)$	0.0	1.0
2	$\mathrm{Ca}(4s4p\ ^3P^\circ) + \mathrm{H}(1s\ ^2S)$	1.88585	0.11111
3	$\mathrm{Ca}(3d4s\ ^3D) + \mathrm{H}(1s\ ^2S)$	2.52317	0.06667
4	$\mathrm{Ca}(3d4s\ ^1D) + \mathrm{H}(1s\ ^2S)$	2.70920	0.2
5	$\mathrm{Ca}(4s4p\ ^1P^\circ) + \mathrm{H}(1s\ ^2S)$	2.93215	0.33333
6	$\mathrm{Ca}(4s5s\ ^3S) + \mathrm{H}(1s\ ^2S)$	3.91022	0.33333
7	$\mathrm{Ca}(4s5s\ ^1S) + \mathrm{H}(1s\ ^2S)$	4.13066	1.0
8	$\mathrm{Ca}(3d4p\ ^3F^\circ) + \mathrm{H}(1s\ ^2S)$	4.44114	0.04762
9	$\mathrm{Ca}(4s5p\ ^3P^\circ) + \mathrm{H}(1s\ ^2S)$	4.53218	0.11111
10	$\mathrm{Ca}(4s5p\ ^1P^\circ) + \mathrm{H}(1s\ ^2S)$	4.55395	0.33333
ionic	$\mathrm{Ca}^+(4s\ ^2S) + \mathrm{H}^-(1s^2\ ^1S)$	5.36308	1.0

from a given initial state to all possible final states, a GPU-based program was used, which allowed for an acceptable time (several weeks) calculate the dynamics of $N^{tot} = 122{,}880$ probability currents for each individual launch in the collision energy range from 0.01 to 100 eV with variable step ($\Delta\mathrm{E} = 0.01$ eV in the range [0.01,0.1) eV, $\Delta\mathrm{E} = 0.1$ eV in the range [0.1,1.0) eV, $\Delta\mathrm{E} = 1.0$ eV in the range [1.0,10.0) eV, $\Delta\mathrm{E} = 10.0$ in the range [10.0,100.0) eV) for each value of the quantum number of the total angular momentum J (in the range from 0 to several thousand in increments of $\Delta J = 2$ to speed up calculations, for more information, see §1.4.3). This allows us to calculate the full probability of an inelastic transition with a minimum value of the order of 8.1×10^{-6}. The accuracy of determining the total probability of a non-adiabatic transition from some initial state to some final one is $\frac{1}{\sqrt{N^{tot}}} \approx 0.003$.

Since the probability current method is based on the Landau-Zener model [64–66] to determine the probability of a single passage of a non-adiabatic region, then data on the parameters of all non-adiabatic regions are needed for calculations. For all non-adiabatic regions, all necessary parameters are obtained from adiabatic potential energies, such as the position of the center of the non-adiabatic region, the energy splitting in the center of the region, the average energy and the Landau-Zener parameter ξ (see the formula (1.53)).

Knowing the full probability of a non-adiabatic transition $P^{tot}_{in\to out}$, the cross sections of all inelastic processes in the entire considered range of collision energies were calculated using the formulas (1.70) and (1.72). Then the rate coefficients were calculated in the temperature range 1000 – 10000 K in increments of $\Delta T = 1000$ K according to the formula (1.74) for exothermic processes and according to the balance equation (1.75) for endothermic processes.

4.2.3 Analysis of cross sections and rate coefficients of inelastic processes

A total of 110 inelastic processes have been investigated by the probability current method. The Figure 26 shows a comparison of the cross sections of mutual neutralization $\mathrm{Ca}^+ + \mathrm{H}^- \to \mathrm{Ca}^* + \mathrm{H}$ as a function of the collision energy calculated by the probability current method (this study) and within the framework of the reprojection method in the paper [18]. It can be seen that the largest cross sections correspond to the neutralization processes in the scattering channels $\mathrm{Ca}(4s5s\ ^3S) + \mathrm{H}(1s\ ^2S), \mathrm{Ca}(4s5s\ ^1S) + \mathrm{H}(1s\ ^2S), \mathrm{Ca}(4s5p\ ^3P^\circ) + \mathrm{H}(1s\ ^2S), \mathrm{Ca}(4s5p\ ^1P^\circ) + \mathrm{H}(1s\ ^2S)$. At the same time, the cross sections obtained by two different methods for these processes agree with each other very well. Also, the cross sections of neutralization processes $\mathrm{Ca}^+ + \mathrm{H}^- \to \mathrm{Ca}(3\mathrm{d}4\mathrm{s}\ ^1\mathrm{D}) + \mathrm{H}(1\mathrm{s}\ ^2\mathrm{S}), \mathrm{Ca}(3\mathrm{d}4\mathrm{p}\ ^3\mathrm{F}^\circ) + \mathrm{H}(1\mathrm{s}\ ^2\mathrm{S})$ have a good agreement, the cross sections of the processes $\mathrm{Ca}^+ + \mathrm{H}^- \to \mathrm{Ca}(4\mathrm{s}^2\ ^1\mathrm{S}) + \mathrm{H}(1\mathrm{s})\ ^2\mathrm{S}), \mathrm{Ca}(4\mathrm{s}4\mathrm{p}\ ^3\mathrm{P}^\circ) + \mathrm{H}(1\mathrm{s}\ ^2\mathrm{S}), \mathrm{Ca}(3\mathrm{d}4\mathrm{s}\ ^3\mathrm{D}) +$

$H(1s\ ^2S), Ca(4s4p\ ^1P^\circ) + H(1s\ ^2S)$ are somewhat less consistent. For most cross sections in almost the entire range of collision energies, the difference in the values of the cross sections obtained by two different methods does not exceed $\approx 30\%$, the largest differences do not exceed one order of magnitude for neutralization processes in the lower three scattering channels.

Figure 27 shows a graphical representation of the rate coefficients of the processes of excitation, de-excitation, ion-pair formation and mutual neutralization at a temperature T = 6000 K, calculated from the cross sections obtained by the probability current method. The calculated rate coefficients can be divided into three groups, according to their values:

- group I: the processes with a rate coefficient exceeding 10^{-8} cm^3/s;
- group II: the processes with a rate coefficient lying in the range $10^{-8} - -10^{-12}$ cm^3/s;
- group III: the processes with a rate coefficient smaller than 10^{-12} cm^3/s.

Let's consider which groups the various processes belong to among all inelastic processes at temperature T = 6000 K, as well as at some other temperatures. The processes of mutual neutralization of $Ca^+ + H^- \rightarrow Ca(4s5s\ ^3S) + H(1s\ ^2S), Ca(4s5s\ ^1S) + H(1s\ ^2S), Ca(4s5p\ ^3P^\circ) + H(1s\ ^2S), Ca(4s5p\ ^1P^\circ) + H(1s\ ^2S)$ belong to the I group of processes with characteristic values of rate coefficients lying in the range $(2.4\text{-}5.5) \times 10^{-8}$ cm^3/s (in the Figure 27 are marked by red).

The second group of processes includes many processes of excitation, de-excitation, ion-pair formation and mutual neutralization. The largest values of the cross sections correspond to some processes of mutual neutralization and ion-pair formation (at temperatures exceeding 4000 K), as well as the process of de-excitation $7 \rightarrow 6$, with values of rate coefficients at a temperature T = 6000 K, lying in the range $(1.1\text{-}8.5) \times 10^{-9}$ cm^3/s. In the Figure 27, the processes belonging to group II are marked by orange, yellow, green and blue.

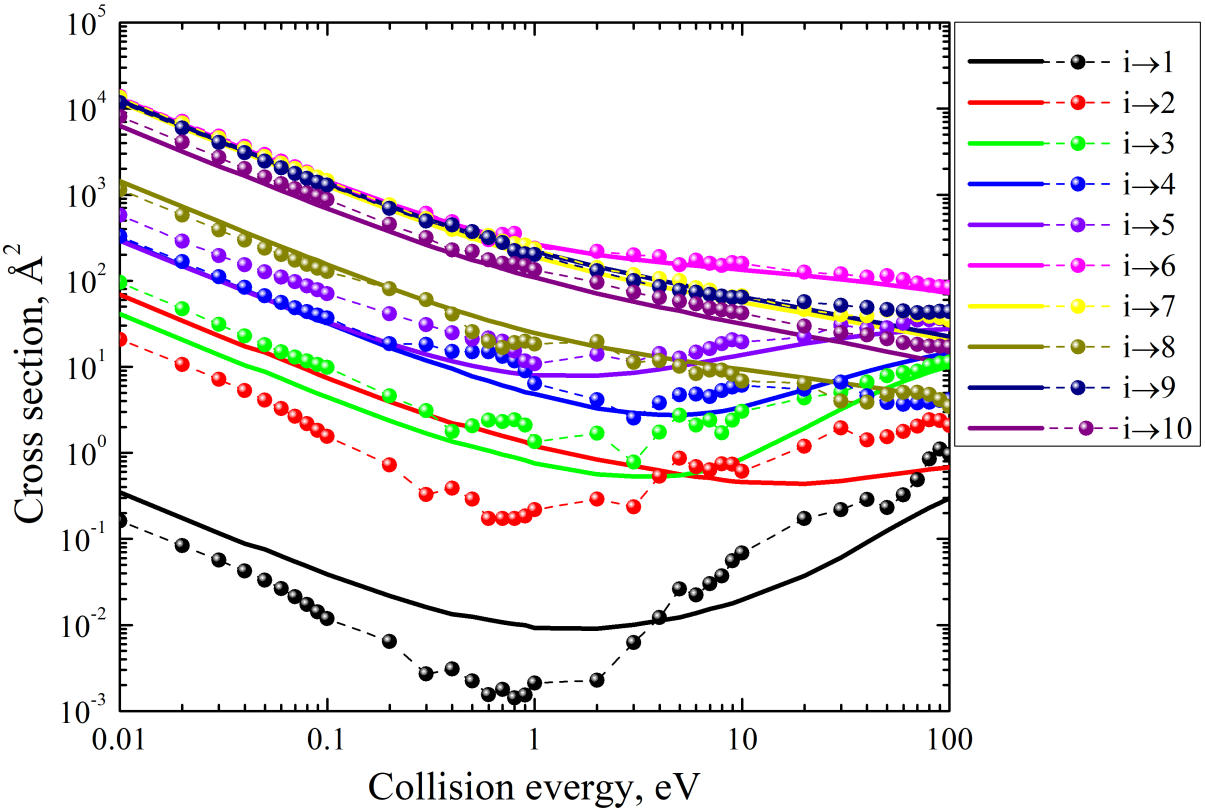

Figure 26. Cross sections of mutual neutralization processes $Ca^+ + H^- \to Ca^* + H$ as a function of the collision energy obtained by the probability current method and by the reprojection method in the paper [18]. Solid lines represent cross sections obtained by the probability current method, symbols with a dotted line represent cross sections obtained within the framework of the reprojection method. For the notation, see the Table 6.

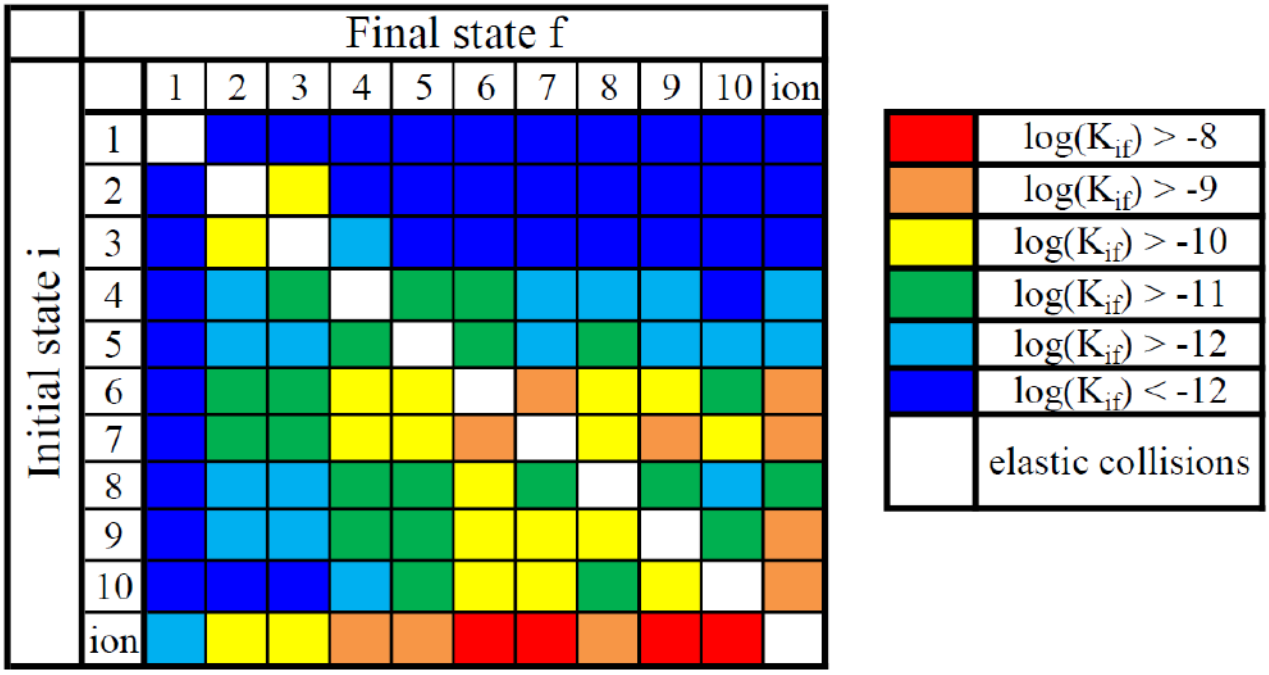

Figure 27. Graphical representation of the rate coefficients of the processes of excitation, de-excitation, ion-pair formation and mutual neutralization at a temperature T = 6000 K. For the notation, see the Table 6.

Group III at the temperature T = 6000 K includes the processes of excitation, de-excitation and several processes of ion-pair formation, mainly involving three low-lying states, as well as most of the processes of ion pair formation at temperatures below 3000-4000 K. In the Figure 27, the processes belonging to group III are marked by blue. Taking into account the processes belonging to groups I and II is most important when modelling gas and plasma media, in particular, the photospheres of stars.

Let us compare the rate coefficients of inelastic processes calculated from cross sections obtained by various methods. Figure 28 shows the dependence of the values of the rate coefficients of neutralization processes on the excitation energy of the calcium atom for the temperature T = 6000 K. It can be seen that the rate coefficients obtained by both the probability current method and the reprojection method agree very well with each other, as well as with predictions of a simplified model. The rate coefficients obtained by the probability current method for most processes ($ionic \rightarrow 3-10$) differ from the rate coefficients obtained by the reprojection method by less than two times. However, for neutralization processes in scattering channels 1 and 2, the difference is 4.02 and 5.60 times, respectively.

Such a large discrepancy in the values of cross sections and rate coefficients of neutralization processes into low-lying scattering channels is due to the fact that for non-adiabatic regions between these channels, the Landau-Zener model does not describe the probability of non-adiabatic transition very well, while for higher-lying states, non-adiabatic transitions in non-adiabatic regions between these high-lying channels can be described with good accuracy within this model. This is confirmed by comparing the cross sections of inelastic processes obtained by the probability current method, taking into account the probability of a non-adiabatic transition in each non-adiabatic region according to the Landau-Zener model, with the cross sections obtained by calculating a system of coupled equations by the reprojection method taking into account the radial matrix elements of non-adiabatic coupling obtained by the *ab initio* quantum chemical calculations.

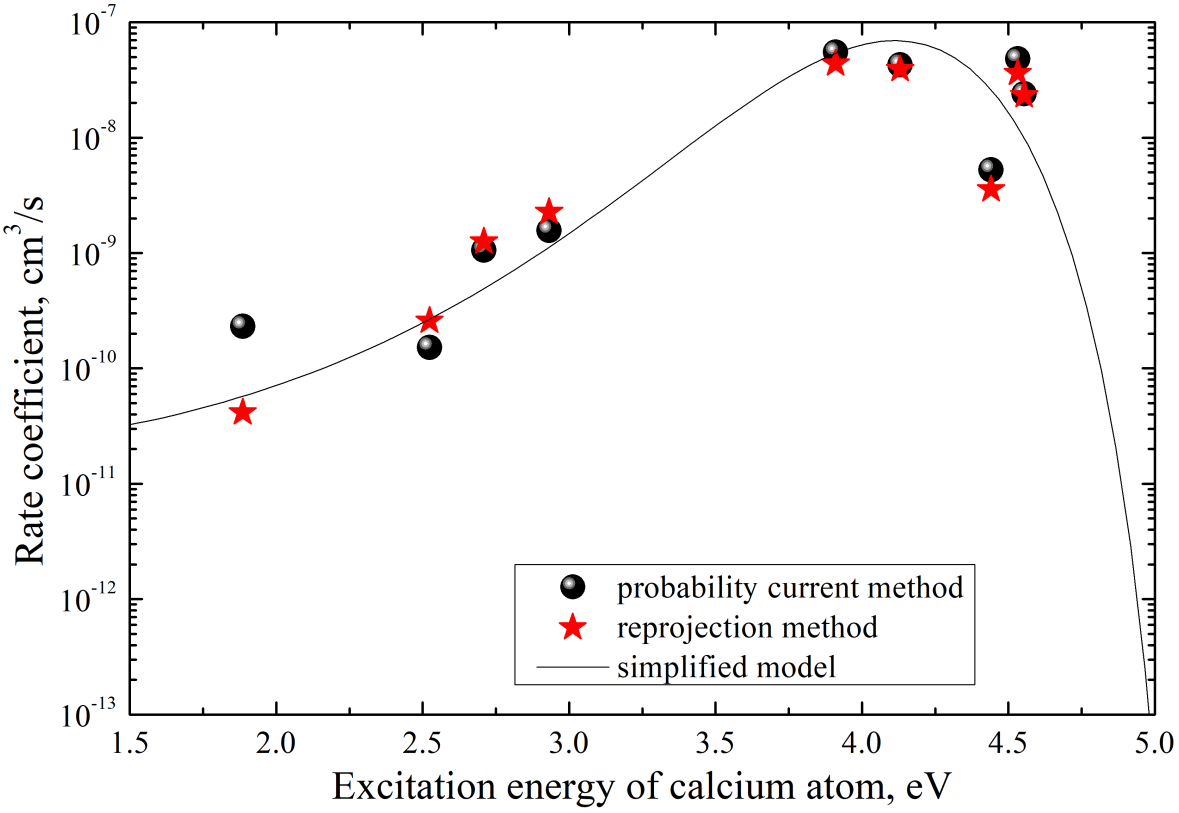

Figure 28. The rate coefficients of the mutual neutralization processes $Ca^+ + H^- \to Ca^* + H$ as a function of the excitation energy of the calcium atom for the temperature T = 6000 K, obtained by the probability current method and the reprojection method in the paper [18]. Balls represent rate coefficients calculated from cross sections obtained by the probability current method, asterisks represent rate coefficients calculated from cross sections obtained by the reprojection method, the solid line corresponds to the predictions of the simplified model [107, 108]. For the notation, see the Table 6.

The results of the comparison suggest that for most inelastic processes, the probability current method reproduces the results of accurate quantum calculations with good accuracy. At the same time, the probability current method has a number of advantages, such as less demanding of computational resources, less computing time, and no need for data on matrix elements of non-adiabatic couplings.

The Figures 29 and 30 show the temperature dependences of the rate coefficients of the processes of mutual neutralization and ion-pair formation, respectively. It can be seen that the data obtained by the probability current method agree very well with the data obtained within the framework of the reprojection method. Also, for processes $ionic \leftrightarrow 6$, 7, 9, 10, these data agree well with the data obtained by the multichannel formula (1.68). However, rate coefficient of the process $ionic \leftrightarrow 8$ obtained by the multichannel formula differ by about seven orders of magnitude from the rate coefficients obtained by the probability current method and the reprojection method. This suggests that the cross sections of these processes are strongly influenced by non-adiabatic transitions at small internuclear distances, since the non-adiabatic region due to ion-covalent interaction between states 8 and 9 is quite narrow (the energy splitting in the center of this non-adiabatic region is very small). This is due to the fact that processes involving state 8 correspond to two-electron transitions within the $^2\Sigma^+$ molecular symmetry, and the passage of this region by the system has a diabatic character. In this case, the total probability of a non-adiabatic transition from any j channel to this one (the $j \rightarrow 8$ process) has a small value when taking into account only the non-adiabatic region due to the ion-covalent interaction. Additional consideration of the non-adiabatic region at short distances, caused primarily by covalent-covalent interaction, can lead to a significant increase in the total probability of non-adiabatic transition to this state, which will eventually lead to a significant increase in the cross sections of inelastic processes, which is observed in this situation.

From the above analysis, the following conclusions can be drawn:

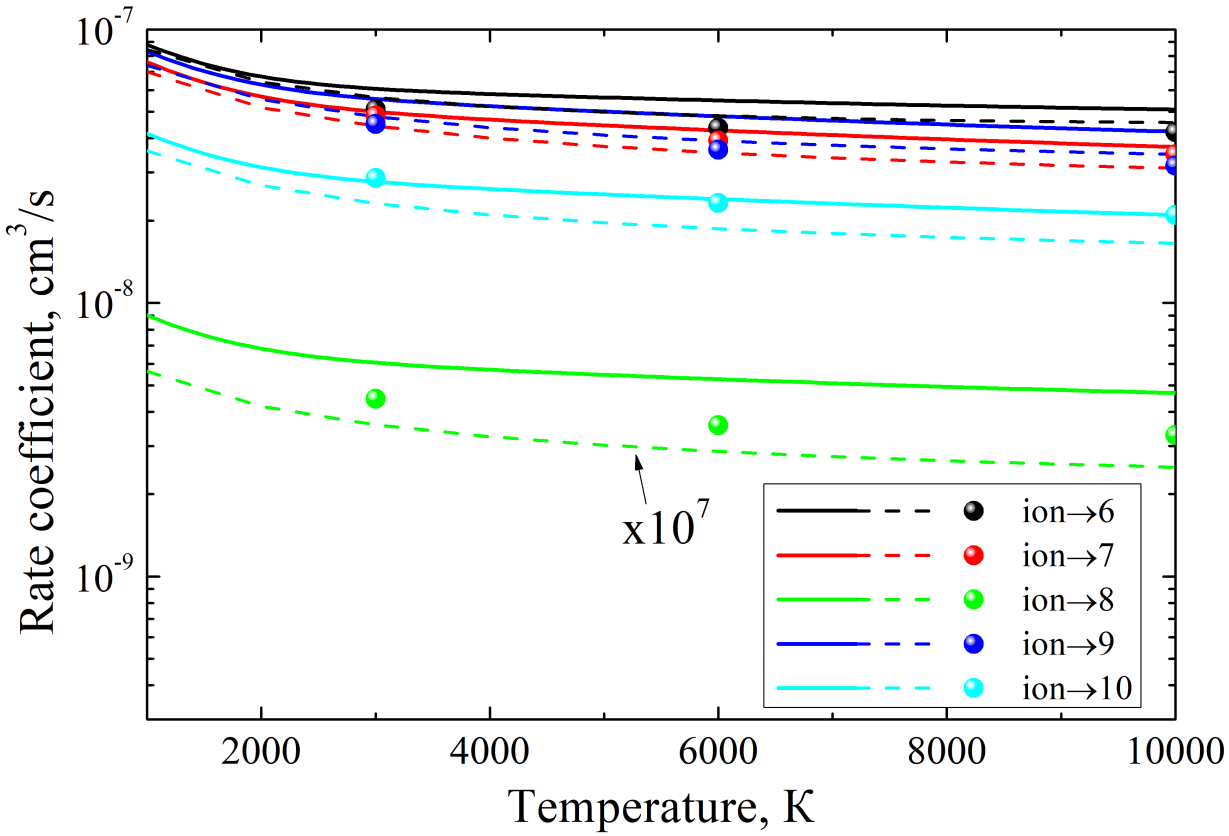

Figure 29. The rate coefficients of the mutual neutralization processes $Ca^+ + H^- \to Ca^* + H$ as a function of temperature. Solid lines correspond to rate coefficients calculated from cross sections obtained by the probability current method, dotted lines – rate coefficients obtained from cross sections calculated by the multichannel formula, symbols – rate coefficients calculated from cross sections obtained by the reprojection method in [18]. For the notation, see the Table 6. The value of the $ion \to 8$ process rate coefficient obtained by the multichannel formula are multiplied by 10^7.

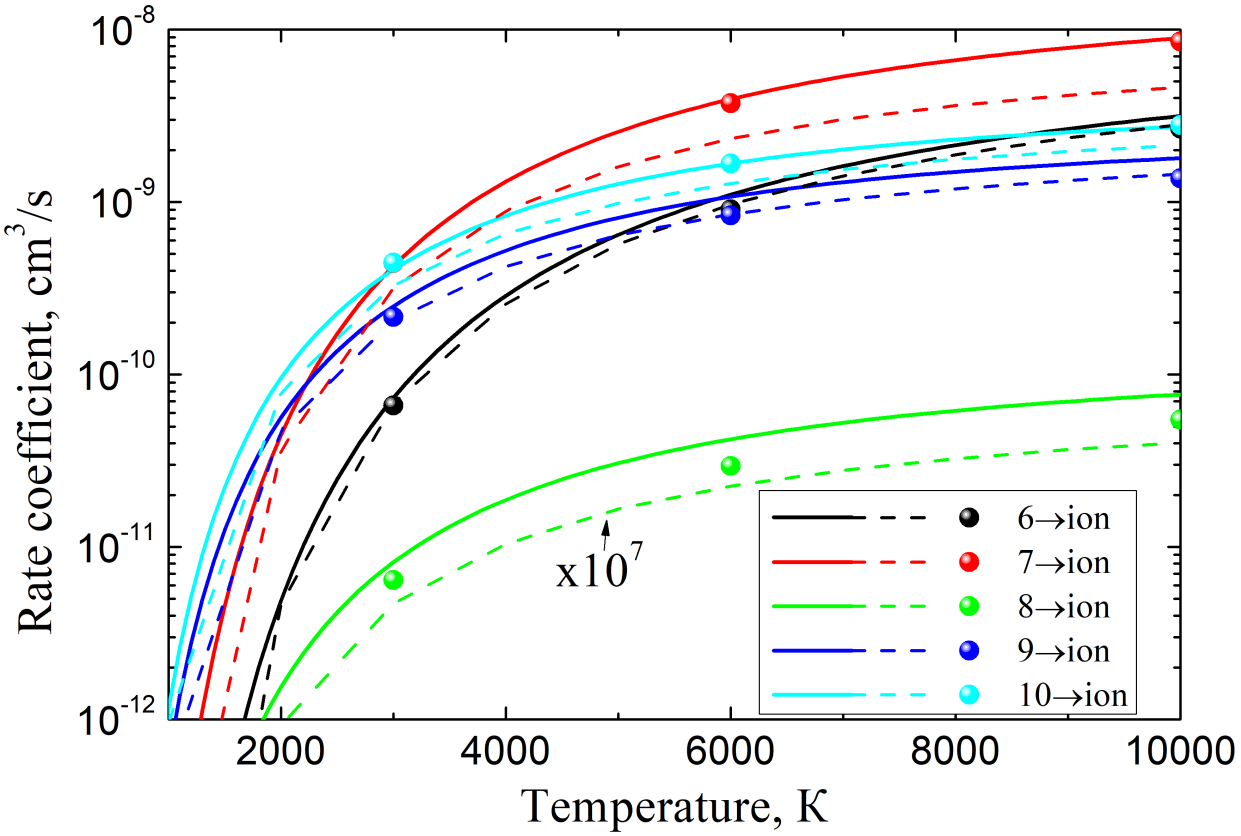

Figure 30. The rate coefficients of the ion-pair formation processes $Ca^* + H \to Ca^+ + H^-$ as a function of temperature. Solid lines correspond to rate coefficients calculated from cross sections obtained by the probability current method, dotted lines – rate coefficients obtained from cross sections calculated by the multichannel formula, symbols – rate coefficients calculated from cross sections obtained by the reprojection method in [18]. For the notation, see the Table 6. The value of the $ion \to 8$ process rate coefficient obtained by the multichannel formula are multiplied by 10^7.

1. For collisions of calcium with hydrogen, the probability current method gives values of cross sections and rate coefficients that differ little from the results obtained in the framework of *ab initio* quantum calculations by the reprojection method: for most processes, the difference in the values of cross sections and rate coefficients lies in the range of 30-50%, for all processes, the difference in the values of rate coefficients does not exceed two orders of magnitude.

2. Taking into account non-adiabatic regions at small distances practically does not affect the final values of cross sections and rate coefficients of processes with large values, while for processes characterized by small values of cross sections and rate coefficients, taking into account these non-adiabatic regions can affect the values of cross sections and rate coefficients significantly, which can be seen, for example, when comparing cross sections and rate coefficients of the neutralization process $ionic \leftrightarrow 8$ obtained by the multichannel formula (taking into account only the non-adiabatic regions due to ion-covalent interaction) and by the probability current method: the difference in the values of the rate coefficients reaches more than seven orders of magnitude. At the same time, the values of cross sections and rate coefficients for the same process obtained by the probability current method are in good agreement with the results obtained by the quantum reprojection method.

§ 4.3 Investigation of inelastic processes in ion-atomic collisions $Ca^+ + H$, $Ca + H^+$, as well as ion-ion collisions $Ca^{2+} + H^-$

Let's consider inelastic processes in atom-ion collisions of calcium and hydrogen, namely $Ca^+ + H$, $Ca + H^+$ and $Ca^{2+} + H^-$. The electronic structure of the molecular ion CaH^+, used in this work in the study of nuclear

dynamics, was obtained by the method of configuration interaction (full CI) for a system of two valence electrons, taking into account the non-empirical pseudopotential of the core of the ion $Ca^{2+}(3s^23p^6)$ in the paper [115], initially the potentials were obtained in the diabatic representation in the paper [114]. Nuclear dynamics is investigated by the probability current method (stochastic version of the algorithm). The cross sections of all inelastic processes are calculated in the collision energy range 0.01 –100 eV according to the formulas (1.70) and (1.72). The rate coefficients are calculated in the temperature range 1000 – 10000 K according to the formula (1.74) for exothermic processes and according to the balance equation (1.75) for endothermic processes.

4.3.1 Adiabatic potential energies of the molecular ion CaH^+

Adiabatic molecular potential energies for 17 molecular states in the molecular symmetry $^1\Sigma^+$ were obtained in [114] by the configuration interaction method (full CI) for a system of two valence electrons: one on a hydrogen atom, the second on a calcium ion $Ca^+(4s)$. The pseudopotential of the core $Ca^{2+}(3s^23p^6)$ was calculated for the calcium atom, which was taken into account in the calculations. Initially, the potentials were calculated in the diabatic representation, then adiabatic potential energies were obtained from these potentials (see [115]), which are used in this study of nuclear dynamics. All 17 considered states are shown in the Table 7. Figure 31 shows the adiabatic molecular potential energies of all the considered states, as a function of the internuclear distance. It can be seen that there is an extremely large energy splitting between the third and fourth terms, about 3 eV in the center of the non-adiabatic region. Because of this, it is expected that the cross sections of inelastic processes involving the three lower channels will have extremely low values, with the possible exception of transitions between these three channels.

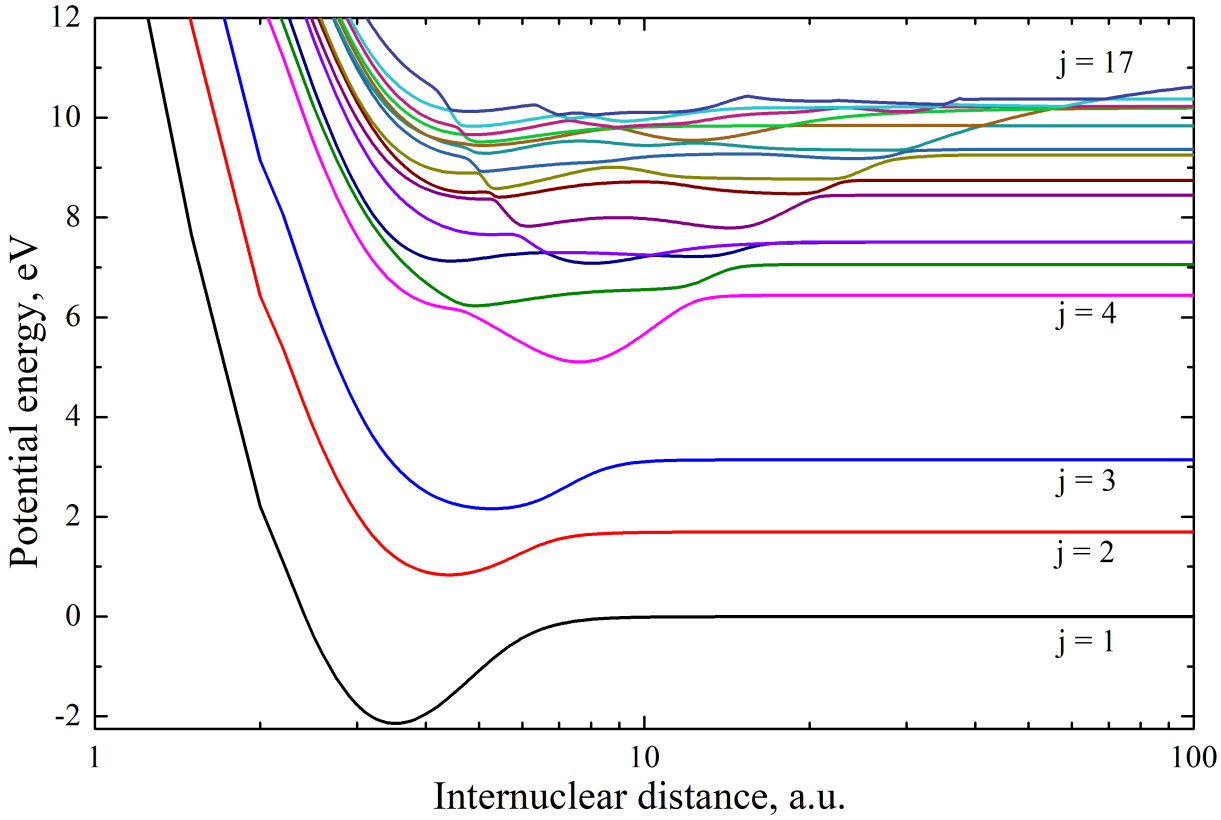

Figure 31. Adiabatic potential energies U_j of the molecular ion CaH^+ as a function of the internuclear distance R for the molecular symmetry $^1\Sigma^+$, calculated in [115]. See the notation in the Table 7.

Table 7. Molecular states of the molecular ion CaH^+ in molecular symmetry $^1\Sigma^+$, corresponding scattering channels, asymptotic energies calculated from the ground state $Ca^+(4s\ ^2S) + H(1s\ ^2S)$ and statistical weights characterizing populations of molecular states in $^1\Sigma^+$ symmetry.

j	Scattering channel	Asymptotic energy (eV)	p_j^{stat}
1	$Ca^+(4s\ ^2S) + H(1s\ ^2S)$	0.0	0.25
2	$Ca^+(3d\ ^2D) + H(1s\ ^2S)$	1.69682	0.05
3	$Ca^+(4p\ ^2P^\circ) + H(1s\ ^2S)$	3.14173	0.0833
4	$Ca^+(5s\ ^2S) + H(1s\ ^2S)$	6.44250	0.25
5	$Ca^+(4d\ ^2D) + H(1s\ ^2S)$	7.05761	0.05
6	$Ca^+(5p\ ^2P^\circ) + H(1s\ ^2S)$	7.50988	0.0833
7	$Ca(4s^2\ ^1S) + H^+$	7.51040	1.0
8	$Ca^+(4f\ ^2F^\circ) + H(1s\ ^2S)$	8.44472	0.035714
9	$Ca^+(6s\ ^2S) + H(1s\ ^2S)$	8.74708	0.25
10	$Ca^+(5d\ ^2D) + H(1s\ ^2S)$	9.01708	0.25
11	$Ca^+(6p\ ^2P^\circ) + H(1s\ ^2S)$	9.23838	0.0833
12	$Ca^+(7s\ ^2S) + H(1s\ ^2S)$	9.85033	0.05
13	$Ca^+(4s\ ^2S) + H(2s\ ^2S)$	10.20165	0.25
14	$Ca^+(4s\ ^2S) + H(2p\ ^2P)$	10.20505	0.0833
15	$Ca(3d4s\ ^1D) + H^+$	10.22470	0.2
16	$Ca(4s4p\ ^1P) + H^+$	10.37681	0.3333
17	$Ca^{2+}(3p^6\ ^1S) + H^-(1s^2\ ^1S)$	11.16617	1.0

4.3.2 Investigation of nonadiabatic nuclear dynamics by the hopping probability current method

Non-adiabatic nuclear dynamics in this study is investigated by the probability current method (see §1.4.3), namely the stochastic version of the algorithm. To calculate the full probabilities of a non-adiabatic transition from a given initial state to all possible final states, a GPU-based program was used, which allowed for an acceptable time (several weeks)

calculate the dynamics of $N^{tot} = 65{,}536$ probability currents for each individual launch in the collision energy range from 0.01 to 100 eV with variable step ($\Delta E = 0.01$ eV in the range [0.01,0.1) eV, $\Delta E = 0.1$ eV in the range [0.1,1.0) eV, $\Delta E = 1.0$ eV in the range [1.0,10.0) eV, $\Delta E = 10.0$ in the range [10.0,100.0) eV) for each value of the quantum number of the total angular momentum J (in the range from 0 to several thousand in increments of $\Delta J = 2$ to speed up calculations, for more information, see §1.4.3). This allows us to calculate the full probability of an inelastic transition with a minimum value of the order of 1.526×10^{-5}. The accuracy of determining the total probability of a non-adiabatic transition from some initial state to some final one is $\frac{1}{\sqrt{N^{tot}}} \approx 0.004$.

In the course of further research, it turned out that such accuracy is not enough to describe processes involving the three lower states. The program for calculating cross sections by the method of probability currents has been upgraded:

1) the algorithm for calculating the dynamics of probability currents has been upgraded: an adaptive step along the internuclear distance has been taken into account, which significantly accelerates the calculation of the dynamics of each probability current;

2) the program for calculating the full probabilities of a non-adiabatic transition from a given initial state to all final ones has been upgraded using GPU calculation capabilities: now not only different threads and blocks are used, but also several grids, which allows to multiply the number of simultaneously calculated probability currents; also, in addition, for greater accuracy, several sequentially launched calculations are now being launched on the video card, which, together with the modernization of the algorithm, allows for more than an order of magnitude improvement in the accuracy of calculations with approximately the same calculation time.

As a result, the total probabilities of non-adiabatic transitions, cross sections and rate coefficients of inelastic processes were recalculated with the number of probability currents $N^{tot} = 104{,}857{,}600$, which gives a minimum probability of 9.53×10^{-9} and an accuracy of the order of $\frac{1}{\sqrt{N^{tot}}} \approx 10^{-4}$. Further comparison will be carried out with the second, recalculated data set (cross sections and rate coefficients). For all non-adiabatic regions, all the parameters necessary for the application of the Landau-Zener model are obtained from adiabatic potential energies (the position of the center of the non-adiabatic region R_C, the energy splitting in the center of the non-adiabatic region, the value of the average energy and the Landau-Zener parameter ξ, see (1.53)).

4.3.3 Analysis of cross sections and rate coefficients of inelastic processes

Figure 32 shows cross sections of neutralization processes $Ca^{2+} + H^- \rightarrow Ca^+/Ca^* + H^*/H^+$ as a function of the collision energy, calculated by the probability current method. Solid lines correspond to the cross sections obtained by the modernized probability current method, symbols and dotted lines correspond the cross sections obtained by the old version of the probability current method. It can be seen that for almost all the cross sections presented, both versions give the same result, however, for cross sections of neutralization processes into scattering channels 4, 5, 6 at low collision energies (less than a few eV), the new version of the program gives smoother cross sections, without fluctuations. The cross sections of the neutralization processes into three lower channels not shown in this figure, the old version of the program gave reasonable values of the cross sections (estimated by the multichannel formula) only at very large values of the collision energy (exceeding 30-40 eV). At lower energies, due to artifacts of numerical calculations, the cross sections were overestimated by several orders of magnitude. At the same time, it was not possible to obtain cross sections with both versions of the programs

for collision energies less than 1 eV, there was not enough accuracy. For this reason, for processes involving the three lower channels, it is better to use estimates obtained by the multichannel formula, since there are no non-adiabatic regions located at short distances for these states.

Figure 33 shows the dependence of the rate coefficients values of neutralization processes on the excitation energy of the calcium ion Ca^+ at a temperature T = 6000 K, obtained by the probability current method and by the multichannel formula. It can be seen that for most processes, the results obtained by two different methods agree very well with each other, which suggests that the main contribution to the cross sections of these processes is made by inelastic transitions in the non-adiabatic regions due to ion-covalent interaction. However, it is also seen that for neutralization processes involving highly excited molecular states, the results calculated by the multichannel formula differ from the results obtained by the probability current method. This suggests that for processes involving highly excited states, transitions in the non-adiabatic regions located at short distances can have a significant effect on the values of the final cross sections and rate coefficients.

Figure 34 shows a graphical representation of the values of the rate coefficients of all the studied inelastic processes for temperature T = 6000 K. We divide, as before, all the rate coefficients into three groups, according to their values:

- group I: the processes with a rate coefficient exceeding 10^{-8} cm^3/s (marked by red squares in the Figure 34);
- group II: the processes with a rate coefficient lying in the range $10^{-8} - -10^{-12}$ cm^3/s (marked by orange, yellow, green and light blue squares in the Figure 34;
- group III: the processes with a rate coefficient smaller than 10^{-12} cm^3/s (marked by blue squares in the Figure 34).

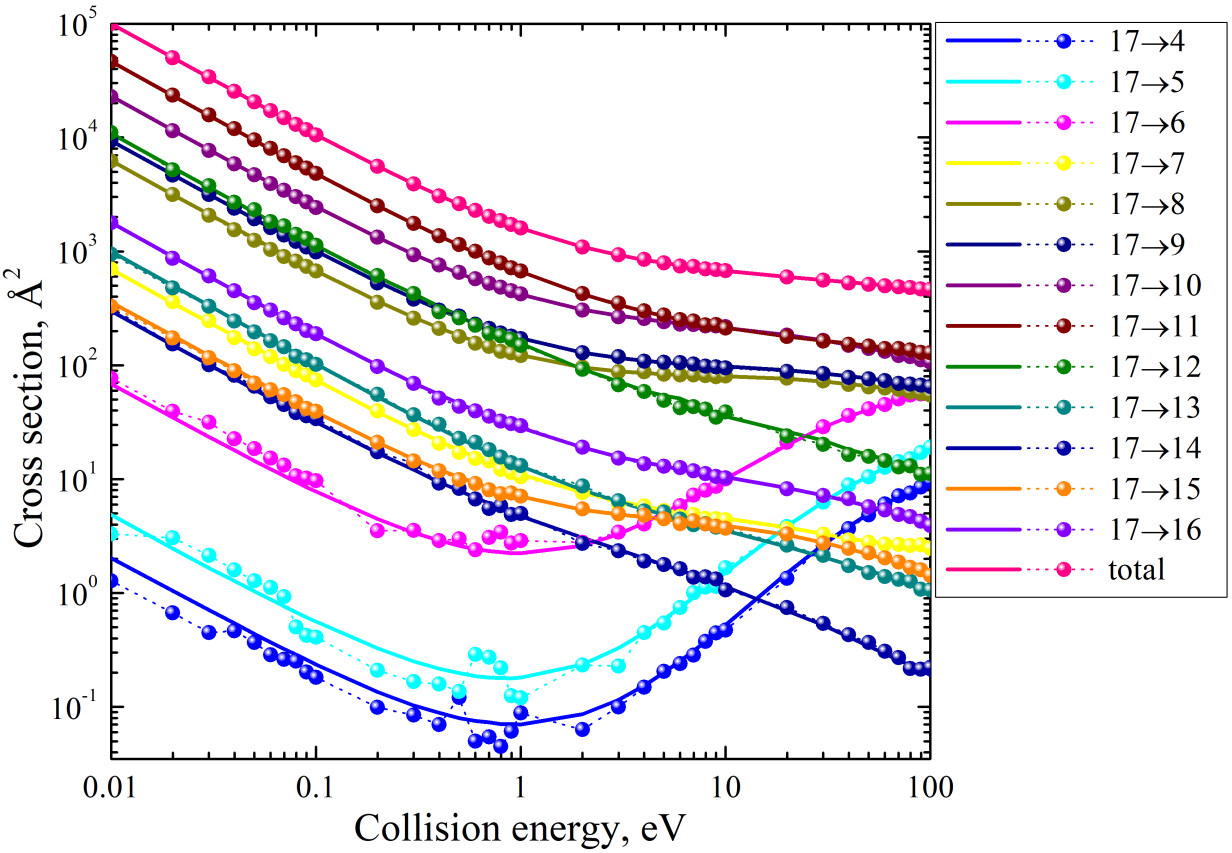

Figure 32. Cross sections of neutralization processes $Ca^{2+} + H^- \to Ca^+/Ca^* + H^*/H^+$ as a function of the collision energy calculated by the probability current method. Solid lines represent cross sections obtained by the modernized probability current method, symbols with a dotted line represent cross sections obtained by the probability current method without optimization and modernization. For the notation, see the Table 7.

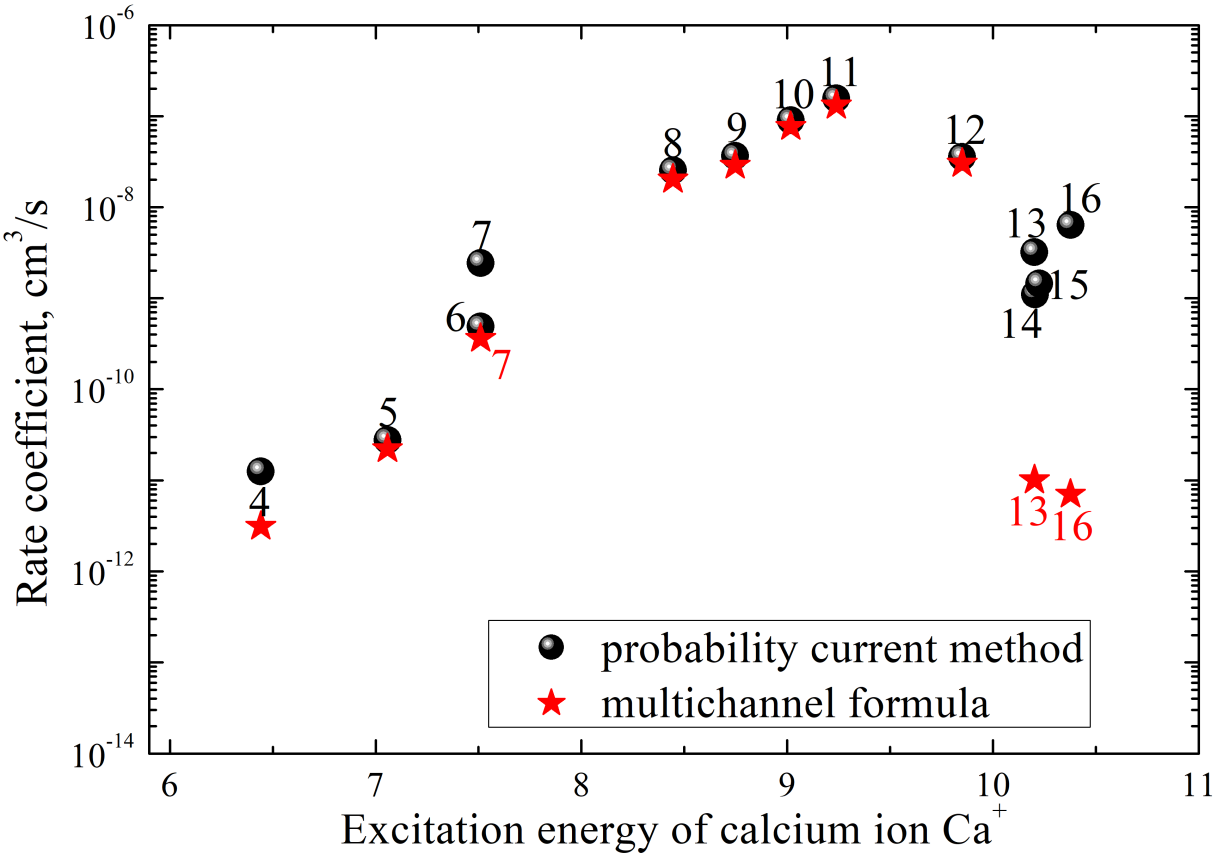

Figure 33. Rate coefficients of neutralization processes $Ca^{2+} + H^- \to Ca^+/Ca^* + H^*/H^+$ as a function of the excitation energy of calcium ion Ca^+ for a temperature T = 6000 K, obtained by the upgraded probability current method and by the multichannel formula. Balls represent rate coefficients calculated from cross sections obtained by the probability current method, asterisks represent rate coefficients calculated from cross sections obtained by the multichannel formula. The rate coefficients of the processes $17 \to 6$, 14, 15 obtained by the multichannel formula have values less than $10^{-15}\,\mathrm{cm}^3/\mathrm{s}$, therefore they are not represented on this figure. For the notation, see the Table 7.

At a temperature of T = 6000 the neutralization processes $17 \rightarrow 8$, 9, 10, 11, 12 belong to the I group of processes as well as the process of de-excitation $16 \rightarrow 13$ with values of rate coefficients lying in the range $(1.79\text{-}15.6) \times 10^{-8}$ cm^3/s.

Group II of processes includes many processes of excitation, de-excitation, recharge, ion-pair formation and neutralization. The largest cross sections correspond to some processes of neutralization, ion-pair formation, de-excitation, excitation and recharge with characteristic values of rate coefficients at a temperature T = 6000 K, lying in the range $(1.22\text{-}9.57) \times 10^{-9}$ cm^3/s.

Group III includes almost all processes involving the three lower states (with the exception of one process of de-excitation $4 \rightarrow 3$), as well as many processes of excitation, de-excitation, recharge and some processes of ion-pair formation (involving states 4, 5, 6).

From the above analysis, the following conclusions can be drawn:

1. The rate coefficients of processes involving the three lower states, namely $\mathrm{Ca}^+(4s\ ^2S) + \mathrm{H}(1s\ ^2S)$, $\mathrm{Ca}^+(3d\ ^2D) + \mathrm{H}(1s\ ^2S)$ and $\mathrm{Ca}^+(4p\ ^2P^\circ) + \mathrm{H}(1s\ ^2S)$ have extremely small values, which is caused by a large energy splitting between the third and fourth molecular states.

2. Taking into account non-adiabatic regions at short distances can have a significant impact on the final values of cross sections and rate coefficients, especially this is typical for high-lying states.

3. For most processes, the dominant mechanism of non-adiabatic transitions is the ion-covalent interaction, which forms non-adiabatic regions at medium and large internuclear distances.

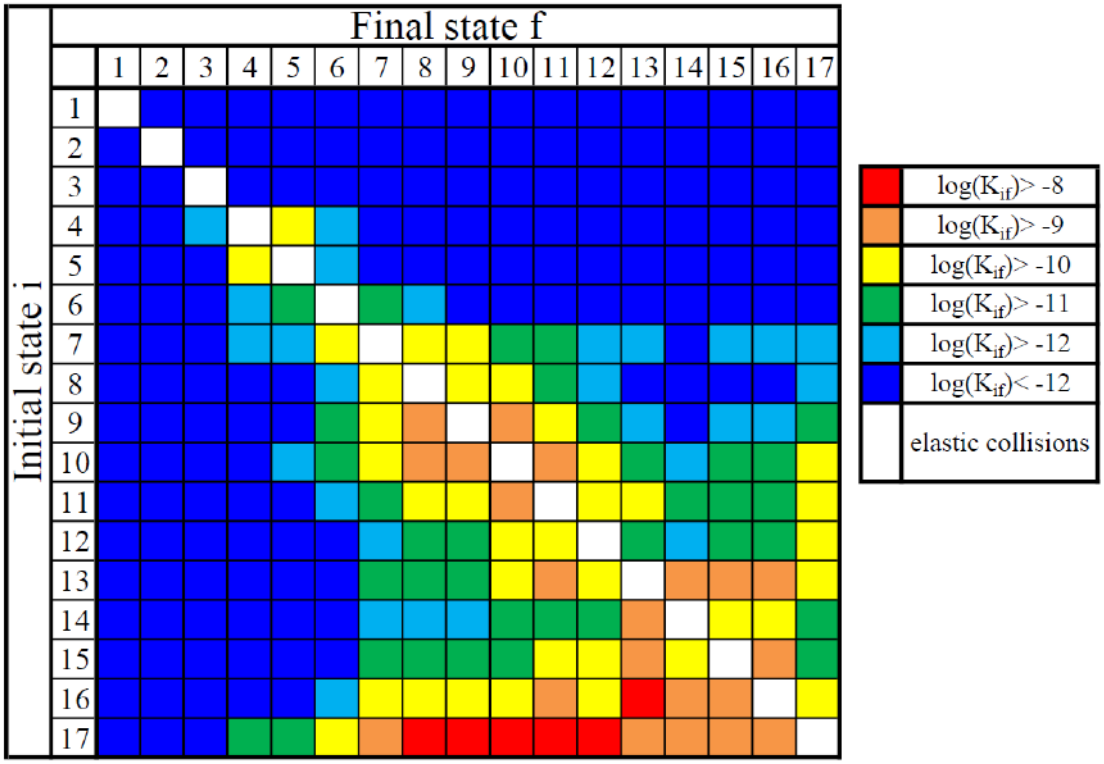

Figure 34. Graphical representation of the rate coefficients of the processes of charge exchange, excitation and de-excitation at a temperature of T = 6000 K. See the notation in the Table 7.

§ 4.4 Investigation of inelastic processes in collisions of calcium cations with hydrogen atoms and anions $Ca^{+}+H$ and $Ca^{2+}+H^{-}$ taking into account the fine structure of energy levels

The method of accounting for the fine structure of alkali metal atoms proposed in papers [23, 24] (see also Chapter 2), is also suitable for accounting for the fine structure of alkaline earth metal ions. The following questions are of interest: how much consideration of the fine structure of an atom/ion in collisions with hydrogen can affect the final values of the cross sections and rate coefficients of inelastic processes? And how the rate coefficients obtained in the LS representation (without taking into account the fine structure) and in the JJ representation (taking into account the fine structures), summed up over all levels of the fine structure, correlate with each other? The study of collisions of calcium ions with hydrogen atoms provides answers to these questions.

Within the framework of this study, atomic terms in JJ representation were obtained from quantum chemical adiabatic potential energies and all parameters of the non-adiabatic regions necessary for the application of the Landau-Zener model were determined. Only the non-adiabatic regions due to ion-covalent interaction were taken into account, since the method proposed in [23], allows us to correctly take into account only such non-adiabatic regions. In the case of collisions of $Ca^{+}+H$ and $Ca^{2+}+H^{-}$, as was shown in the previous part of this Chapter, the main mechanism of non-adiabatic transitions is the ion-covalent interaction. Nuclear dynamics was investigated by the multichannel formula. The cross sections are calculated in the collision energy range 0.001 – 100 eV, the rate coefficients are calculated in the temperature range 1000 – 10000 K according to the same formulas as before.

4.4.1 Adiabatic potential energies of a quasimolecular ion CaH^+ in the JJ representation

At the paper [115] the adiabatic potential energies of the quasimolecular ion CaH^+ were presented in the LS representation. In recent work [23] the asymptotic method for taking into account the fine splitting of energy levels has been proposed. This method was applied to the original terms of the quasimolecular ion CaH^+ in the LS representation, resulting in the terms in the JJ representation. These topics are shown in the Figure 35, all the considered states are listed in the Table 8.

As can be seen from the Figure 35, the result is adiabatic potential energies, between which there are regions where terms going closer to each other (non-adiabatic regions) due to the ion-covalent interaction of molecular terms. At the same time, the non-adiabatic regions caused by covalent-covalent interaction cannot be correctly described within the framework of the method proposed in the paper [23], since this method is asymptotic. At the same time, these non-adiabatic regions are arranged in a certain order, which allows the use of the multichannel formula (1.68) to calculate the total probability of a non-adiabatic transition from some initial state to some final one.

4.4.2 Investigation of non-adiabatic nuclear dynamics in the framework of the multichannel approach

In this study, non-adiabatic nuclear dynamics in collisions of $Ca^+ + H$ and $Ca^{2+} + H^-$ is investigated within the framework of the multichannel approach based on the Landau-Zener model. For all non-adiabatic regions, the parameters necessary for the application of the Landau-Zener model were determined (see more details (1.53)). Using the multichannel formula (see §1.4.4), the total probabilities of non-adiabatic transitions from all initial states to all final ones are calculated. According to the calculated probabilities, the cross sections of all inelastic processes are calculated ac-

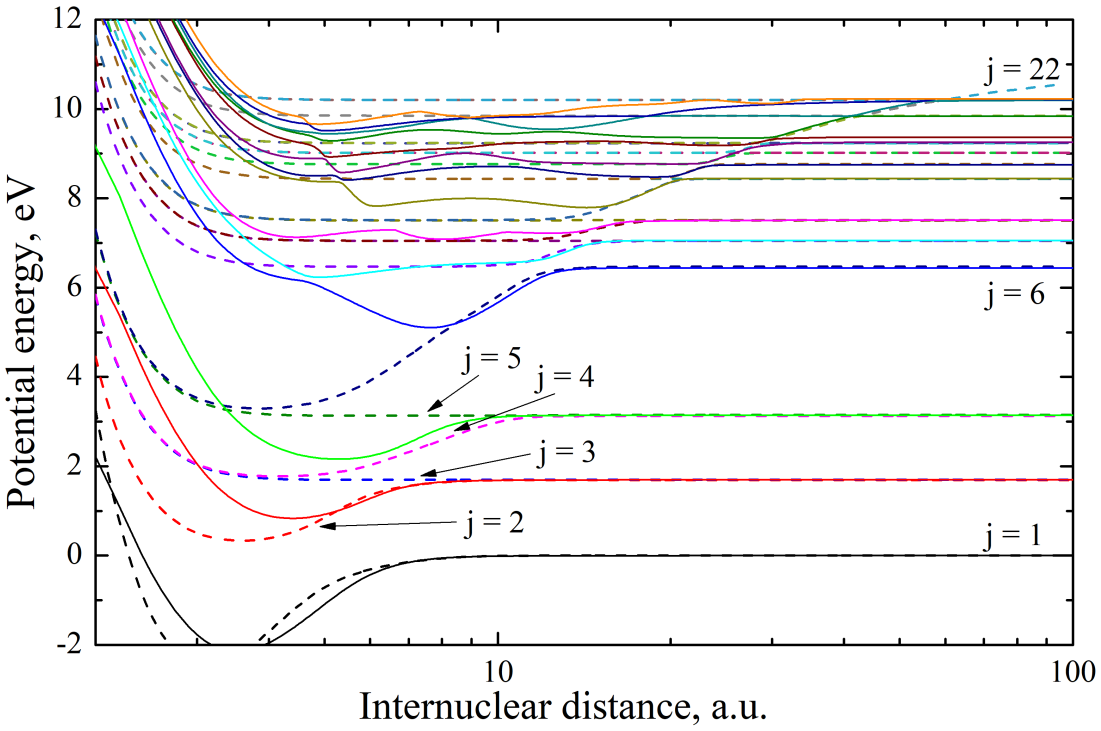

Figure 35. The potential energies of the molecular ion CaH^+, taking into account the fine structure, obtained within the framework of the method described in the paper [23] from the adiabatic potential energies calculated in the work [115]. Solid lines denote the original adiabatic potential energies, dotted lines represent the potential energies obtained by the asymptotic method of taking into account the fine structure [23]. See the notation in the Table 8.

Table 8. Molecular states $CaH^+(j\ 0^+)$ in the JJ representation, corresponding scattering channels, asymptotic energies calculated from the ground state $Ca^+(4s\ ^2S_{1/2}) + H(1s\ ^2S_{1/2})$ (data taken from the NIST database [109]) and statistical populations p_j^{stat} of molecular states 0^+.

j	Scattering channel	Asymptotic energy (eV)	p_j^{stat}
1	$Ca^+(4s\ ^2S_{1/2}) + H(1s\ ^2S_{1/2})$	0.0	0.25
2	$Ca^+(3d\ ^2D_{3/2}) + H(1s\ ^2S_{1/2})$	1.692408	0.125
3	$Ca^+(3d\ ^2D_{5/2}) + H(1s\ ^2S_{1/2})$	1.699932	0.0833
4	$Ca^+(4p\ ^2P^\circ_{1/2}) + H(1s\ ^2S_{1/2})$	3.123349	0.25
5	$Ca^+(4p\ ^2P^\circ_{3/2}) + H(1s\ ^2S_{1/2})$	3.150984	0.125
6	$Ca^+(5s\ ^2S_{1/2}) + H(1s\ ^2S_{1/2})$	6.467875	0.25
7	$Ca^+(4d\ ^2D_{3/2}) + H(1s\ ^2S_{1/2})$	7.047169	0.125
8	$Ca^+(4d\ ^2D_{5/2}) + H(1s\ ^2S_{1/2})$	7.049551	0.0833
9	$Ca^+(5p\ ^2P^\circ_{1/2}) + H(1s\ ^2S_{1/2})$	7.505138	0.25
10	$Ca^+(5p\ ^2P^\circ_{3/2}) + H(1s\ ^2S_{1/2})$	7.514841	0.125
11	$Ca^+(4f\ ^2F^\circ_{5/2}) + H(1s\ ^2S_{1/2})$	8.437981	0.0833
12	$Ca^+(4f\ ^2F^\circ_{7/2}) + H(1s\ ^2S_{1/2})$	8.437981	0.0625
13	$Ca^+(6s\ ^2S_{1/2}) + H(1s\ ^2S_{1/2})$	8.762908	0.25
14	$Ca^+(5d\ ^2D_{3/2}) + H(1s\ ^2S_{1/2})$	9.016407	0.125
15	$Ca^+(5d\ ^2D_{5/2}) + H(1s\ ^2S_{1/2})$	9.017486	0.0833
16	$Ca^+(6p\ ^2P^\circ_{1/2}) + H(1s\ ^2S_{1/2})$	9.234953	0.25
17	$Ca^+(6p\ ^2P^\circ_{3/2}) + H(1s\ ^2S_{1/2})$	9.239519	0.125
18	$Ca^+(7s\ ^2S_{1/2}) + H(1s\ ^2S_{1/2})$	9.850331	0.25
19	$Ca^+(4s\ ^2S_{1/2}) + H(2s\ ^2S_{1/2})$	10.20165	0.25
20	$Ca^+(4s\ ^2S_{1/2}) + H(2p\ ^2P_{1/2})$	10.20505	0.25
21	$Ca^+(4s\ ^2S_{1/2}) + H(2p\ ^2P_{3/2})$	10.20505	0.125
22	$Ca^{2+}(3p^6\ ^1S_0) + H^-(1s^2\ ^1S_0)$	11.11772	1.0

cording to the formulas (1.70) and (1.72) in the collision energy range 0.0001 – 100 eV, then the rate coefficients in the temperature range 1000 – 10000 K are calculated according to the formulas (1.74) and (1.75) for exothermic and endothermic processes, respectively.

4.4.3 Analysis of cross sections and rate coefficients of inelastic processes

One of the main questions in this study is the following: how will taking into account the fine structure of energy levels eventually affect the values of cross sections and rate coefficients? To answer it, let's compare the rate coefficients obtained by the same method – namely, the multichannel formula – for the same set of potentials in LS and JJ representations, respectively.

Figure 36 shows the dependences of the values of the rate coefficients of neutralization processes on the excitation energy of the calcium ion Ca^+ at a temperature T = 6000 K, while the rate coefficients obtained taking into account the fine structure of energy levels are not summed over the fine structure levels. It can be seen from this figure that practically all the rate coefficients obtained in the JJ coupling approximation do not individually exceed the values of the rate coefficients obtained in the LS coupling approximation, with rare exceptions, as expected, since one scattering channel in the LS representation corresponds to one or more scattering channels in the JJ representation.

Therefore, it is also of interest to compare the rate coefficients summed over all levels of the fine structure, which is shown in Figure 37. In this case, the comparison can also be carried out with the rate coefficients obtained by the probability current method in the previous part of this Chapter. It can be seen from this figure that the rate coefficients with the largest values (exceeding $10^{-10}\,cm^3/s$) do not differ much, no matter what method they are calculated.

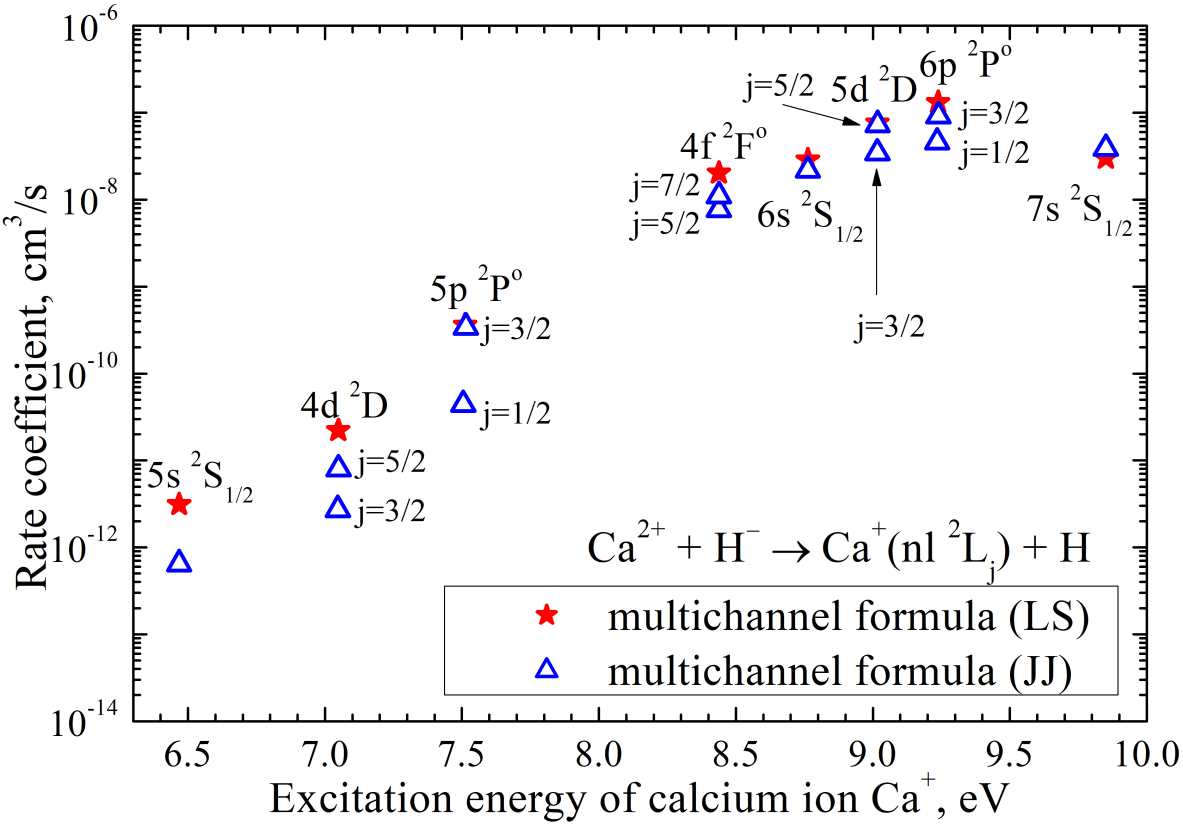

Figure 36. The rate coefficients of neutralization processes at a temperature T = 6000 K, as a function of the excitation energy of the calcium ion in the final state (calculated from the energy of the ground state). Asterisks correspond to rate coefficients obtained without taking into account the fine structure (in LS representation), triangles correspond to rate coefficients obtained taking into account the fine structure (in JJ representation). Both data sets are calculated by the multichannel formula.

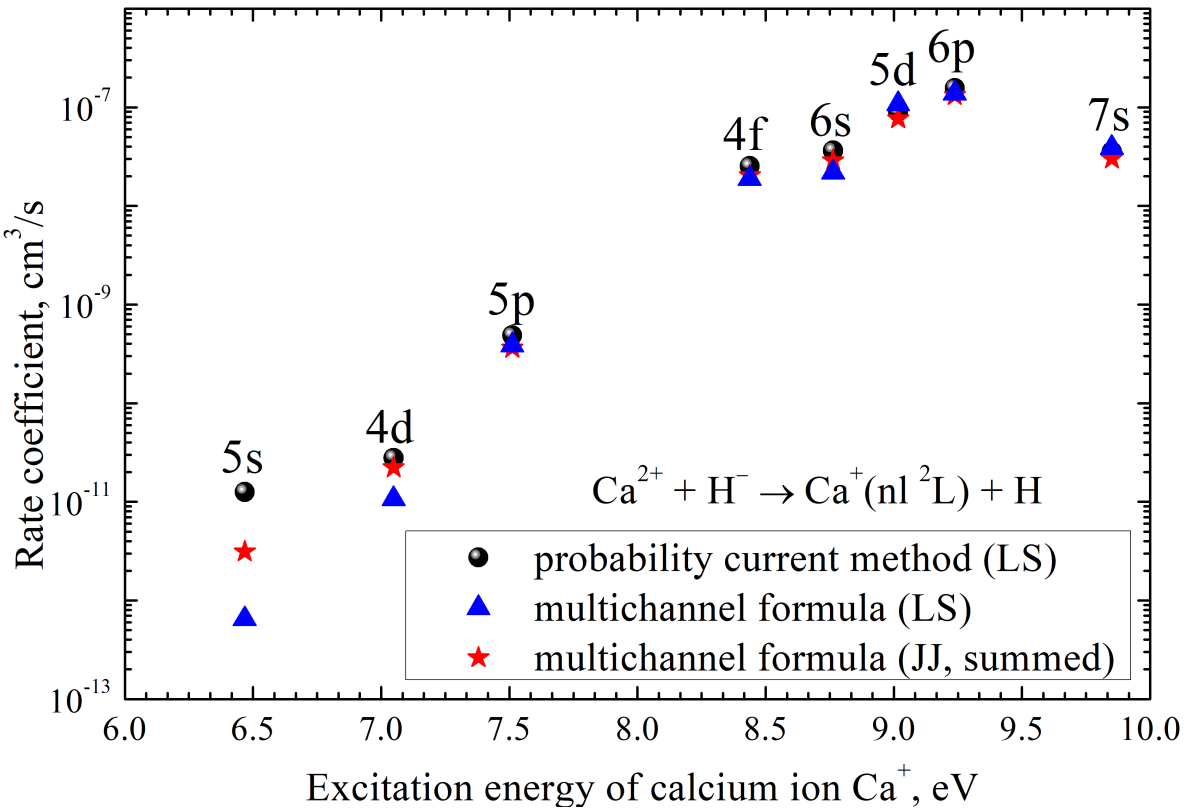

Figure 37. The rate coefficients of neutralization processes at a temperature T = 6000 K, as a function of the excitation energy of the calcium ion in the final state (calculated from the energy of the ground state). Balls correspond to rate coefficients obtained by the probability current method (in LS representation), asterisks – rate coefficients obtained by the multichannel formula without taking into account the fine structure (in LS representation), triangles – rate coefficients obtained by the multichannel formula taking into account the fine structure (in JJ representation), summed over fine structure levels.

Let us analyze the values of the total rate coefficients of neutralization processes obtained by different methods. The total rate coefficient of the neutralization process, obtained from calculations by the probability current method, is $3.48 \times 10^{-7}\,\mathrm{cm}^3/\mathrm{s}$, by the multichannel formula without taking into account the fine structure – $2.88 \times 10^{-7}\,\mathrm{cm}^3/\mathrm{s}$, by the multichannel formula taking into account the fine structure – $3.26 \times 10^{-7}\,\mathrm{cm}^3/\mathrm{s}$. As can be seen, the difference in values does not exceed 20%. At the same time, taking into account the fine structure in this case increases the total rate coefficient of the neutralization process relative to the calculation by the multichannel formula without taking into account the fine structure and approximates its value to the value of the rate coefficient obtained by the more accurate probability current method.

From all of the above, several conclusions can be drawn:

1. The rate coefficients of neutralization processes into low-lying scattering channels obtained taking into account the fine structure are almost always smaller in magnitude than the rate coefficients obtained without taking into account the fine structure, see Figure 37, processes in the vicinity of the excitation energy of the final state of the calcium ion ≈ 7 eV and less.

2. The rate coefficients of neutralization processes obtained by the multichannel formula taking into account the fine structure, with values exceeding $\approx 10^{-10}\,\mathrm{cm}^3/\mathrm{s}$, differ both in the higher and lower direction relative to the rate coefficients obtained also by the multichannel formula but without taking into account the fine structure. This suggests that taking into account the fine structure of energy levels leads to a non-trivial redistribution of the values of the rate coefficients, which cannot be reproduced using any simple formulas.

§ 4.5 Concluding remarks

In this paper, inelastic processes in collisions of calcium atoms and ions with hydrogen atoms and ions, namely the processes of excitation, de-excitation and charge exchange, were investigated.

It is shown that:

1. For collisions Ca + H and $Ca^+ + H^-$, the probability current method gives values of cross sections and rate coefficients that differ little from the results obtained in the framework of *ab initio* quantum calculations by the reprojection method: for most processes, the difference in the values of cross sections and rate coefficients lies in the range of 30-50%, for all processes, the difference in the values of the rate coefficients does not exceed two orders of magnitude.

2. Taking into account non-adiabatic regions at short distances practically does not affect the final values of cross sections and rate coefficients of processes with large values, while for processes characterized by small values of cross sections and rate coefficients, taking into account these regions can significantly affect the values of cross sections and rate coefficients, especially this is typical for highly excited states.

3. For most of the processes considered in collisions Ca + H, $Ca^+ + H^-$, Ca^+ + H, Ca + H^+ and $Ca^{2+} + H^-$ the dominant mechanism of non-adiabatic transitions is the ion-covalent interaction, which forms non-adiabatic regions at medium and large internuclear distances.

4. Taking into account the fine structure of energy levels leads to a non-trivial redistribution of the values of the rate coefficients, which cannot be reproduced using any simple formulas.

The results obtained in this Chapter are published in the following articles:

- Belyaev A. K. Atomic Data on Inelastic Processes in Calcium–Hydrogen Collisions / A. K. Belyaev, **Ya. V. Voronov**, S. A. Yakovleva, A. Mitrushchenkov, M. Guitou, N. Feautrier // The Astrophysical Journal. – 2017. – Vol. 851. – No. 1. – P. 59.

- Belyaev A. K. Data on Inelastic Processes in Low-energy Calcium–Hydrogen Ionic Collisions / A. K. Belyaev, **Ya. V. Voronov**, F. X. Gadéa // The Astrophysical Journal. – 2018. – Vol. 867. – No. 2. – P. 87.

- Belyaev A. K. Inelastic processes in calcium-hydrogen ionic collisions with account for fine structure / A. K. Belyaev, **Ya. V. Voronov**, S. A. Yakovleva // Physical Review A. – 2019. – Vol. 100. – No. 6. – P. 062710.

Also, the results of this study were presented at the following conferences:

- «Stars, planets and their magnetic fields» (17–21 September, 2018, Saint-Petersburg, Russia). Poster "**Calculations of atomic data on inelastic processes in collisions of various chemical elements with hydrogen**".

- XXI Mendeleev Congress on General and Applied Chemistry, Symposium "The Periodic Table through Space and Time" (9-13 September, 2019, Saint-Petersburg, Russia). Poster "**Application of the probability current method to nuclear dynamical calculations in collisions with hydrogen**";

- Physics of Stars and Planets: atmospheres, activity and magnetic fields (16-20 September, 2019, N. Tusi Shamakhi Astrophysical Observatory, Shamakhi, Azerbaijan). Poster "**Application of the probability current method to nuclear dynamical calculations in collisions with hydrogen**".

This research was supported by grants:

- the Ministry of Science and Higher Education grant No. 3.1738.2017/PCH 2017-2019, the head of Prof. Belyaev A. K.
- RSF grant No. 17-13-01144, the head of Prof. Belyaev A. K.

Chapter 5. Investigation of inelastic processes in collisions of lithium atoms and ions with hydrogen atoms and ions

§ 5.1 Preliminary remarks

Lithium is a fairly common chemical element in the Universe. Lithium was the third most common element formed during primary nucleosynthesis. Determining the lithium abundance in the photospheres of stars of various spectral classes is an very important task of modern astrophysics for several reasons. Firstly, the most accurate determination of the lithium abundance allows us to build more accurate models of primary nucleosynthesis (see, for example, [127]). Secondly, the lithium abundance, as well as beryllium and boron, makes it possible to understand the mixing processes inside stars (see, for example, [127], and references therein). Thirdly, the precise determination of lithium abundance makes it possible to better understand the processes of stellar evolution. In cosmology, there are so-called primary lithium problem [128] and the Spite plateau problem (or the secondary lithium problem) [129, 130], also see [131].

One of the important problems is also the problem of the primary nucleosynthesis of the isotope ^{7}Li (see, for example, [132]), which consists in the fact that the amount of the isotope ^{7}Li predicted by the standard theory of the Big Bang nucleosynthesis exceeds three to four times the amount observed in the oldest stars, although the known abundance of deuterium ^{2}H and helium ^{4}He are good consistent with the predictions of the theory of primary nucleosynthesis (see [128, 133–139], and references therein).

The study of the effect of the substitution of isotopes of both lithium and hydrogen on the values of cross sections and rate coefficients is also important for the reason that it is easier to investigate collisions with deuterium rather than hydrogen in an experiment (see, for example, [7–

9]). But, since collisions with hydrogen are of interest for astrophysical applications, it is necessary to understand well how the replacement of hydrogen with deuterium will affect the values of cross sections and rate coefficients.

The importance of taking into account inelastic collisions of lithium with hydrogen for lithium thermalization was first noted in [13]. The first estimates of the rate coefficients of excitation processes were obtained in the same work using the Dravin formula. Since then, many studies of the photospheres of stars of various spectral classes have been carried out within the framework of deviation from local thermodynamic equilibrium (see, for example, [131, 140–143] and references therein). These studies were based on various sets of data on rate coefficients. It should be noted separately that in the work [144] it was shown that, in addition to the excitation processes, the processes of mutual neutralization and ion-pair formation are of great importance, especially for stars with low metallicity.

It should also be noted that for lithium-hydrogen collisions, theoretical calculations are not the only source of information on the characteristics of inelastic collisions to date. Various scientific teams have conducted many experimental studies of the processes of mutual neutralization of $Li^+ + H^-/D^- \rightarrow Li^* + H/D$ for different collision energies (see, for example, [7, 8, 145, 146]). This state of affairs allows for a detailed comparison of the results of theoretical calculations and experimental data and to improve the models used.

Studies of the electronic structure of the LiH molecule have been carried out in such works as [7, 147, 148] and others. Nuclear dynamics studies have also been conducted as part of the most accurate quantum reprojection method [15], and within the multichannel formula (for example, [7]). At the paper [15] the nuclear dynamics study within the framework of the reprojection method was carried out for the four lower lithium states Li(2s, 2p, 3s, 3p), while the excitation cross section into the Li(3p) state was considered as the total cross section into this state and all the overlying

ones. The partial cross sections in these overlying states were estimated using a multichannel formula.

The research to which this Chapter of the dissertation is devoted was carried out in order to more accurately assess partial cross sections involving lithium states Li(3p, 3d, 4s, 4p), as well as to identify the effect of lithium and hydrogen isotope substitution in collisions on the values of cross sections and rate coefficients. For this purpose, the potential energies obtained in [148] were used, as well as the hopping and branching probability current method. This Chapter will present the results of studies of inelastic processes in collisions of lithium and hydrogen. Cross sections of inelastic processes are calculated in the collision energy range 0.001 – 100 eV, rate coefficients in the temperature range 1000 – 10000 K.

§ 5.2 Adiabatic potential energies of the LiH molecule

The electronic structure of the LiH molecule used in this study was calculated by the pseudopotential method in [148]. These data are an improved version of the potentials calculated in [147,149]. At the paper [148] Croft et al. not only calculated the electronic structure of the LiH molecule, but also compared their results with the experimentally obtained spectroscopic data on the vibrational levels of the ground and first excited states of LiH and obtained good agreement. In the Table 9 presents a comparison of the results obtained in [7, 148] with experimentally known data on the asymptotic energies of the LiH molecule [109] (Table 9a), as well as a comparison of the positions of the centers of the non-adiabatic regions caused by ion-covalent interaction and located at relatively large internuclear distances, and the maximum values of the matrix elements of the non-adiabatic coupling H_{jk} in the centers of the corresponding non-adiabatic regions R_c (Table 9b). It can be seen that all data sets agree well with each other, with the exception of non-adiabatic coupling for the last two high-lying non-adiabatic regions. Thus, it can be concluded that the potential energies

presented in [148] are sufficiently accurate and suitable for the study of non-adiabatic nuclear dynamics in lithium-hydrogen collisions.

Table 9. a) comparison of the asymptotic energies of the scattering channels (in eV) of the quasimolecule LiH($^1\Sigma^+$); b) comparison of the positions of the centers of the non-adiabatic regions R_c (in atomic units) caused by ion-covalent interaction and located at relatively large internuclear distances, as well as the maximum values of the corresponding matrix elements of the non-adiabatic coupling H_{jk} in the centers of the non-adiabatic regions R_c (in atomic units).

a) asymptotic energies, eV

No.	Scattering channel	NIST	Croft et al. [148]	Launoy et al. [7]
1	Li(2s) + H(1s)	0.0	0.0	0.0
2	Li(2p) + H(1s)	1.8478	1.8480	1.8495
3	Li(3s) + H(1s)	3.3731	3.3738	3.3721
4	Li(3p) + H(1s)	3.8343	3.8343	3.8357
5	Li(3d) + H(1s)	3.8786	3.8795	3.8770
6	Li(4s) + H(1s)	4.3409	4.3416	4.3561
7	Li(4p) + H(1s)	4.5216	4.5223	——
8	$Li^+ + H^-$	4.6377	4.6377	4.639

b) Parameters R_c and H_jk, a.u.

No.	j-k	R_c, a.u.		H_{jk}, a.u.	
		Croft et al. [148]	Launoy et al. [7]	Croft et al. [148]	Launoy et al. [7]
1	Li(2s)-Li(2p)	7.20	7.19	0.22	0.21
2	Li(2p)-Li(3s)	11.30	11.41	0.17	0.18
3	Li(3s)-Li(3p)	22.05	22.12	0.47	0.50
4	Li(3p)-Li(3d)	34.40	34.05	1.08	1.24
5	Li(3d)-Li(4s)	35.90	35.97	3.69	2.04

The Figure 38 shows the potential energies of the LiH molecule. In total, 7 covalent states and one ionic state were taken into account. The Table 10 shows all the states taken into account in this study in $^1\Sigma^+$ symmetry. All other molecular symmetries were not considered, because, as

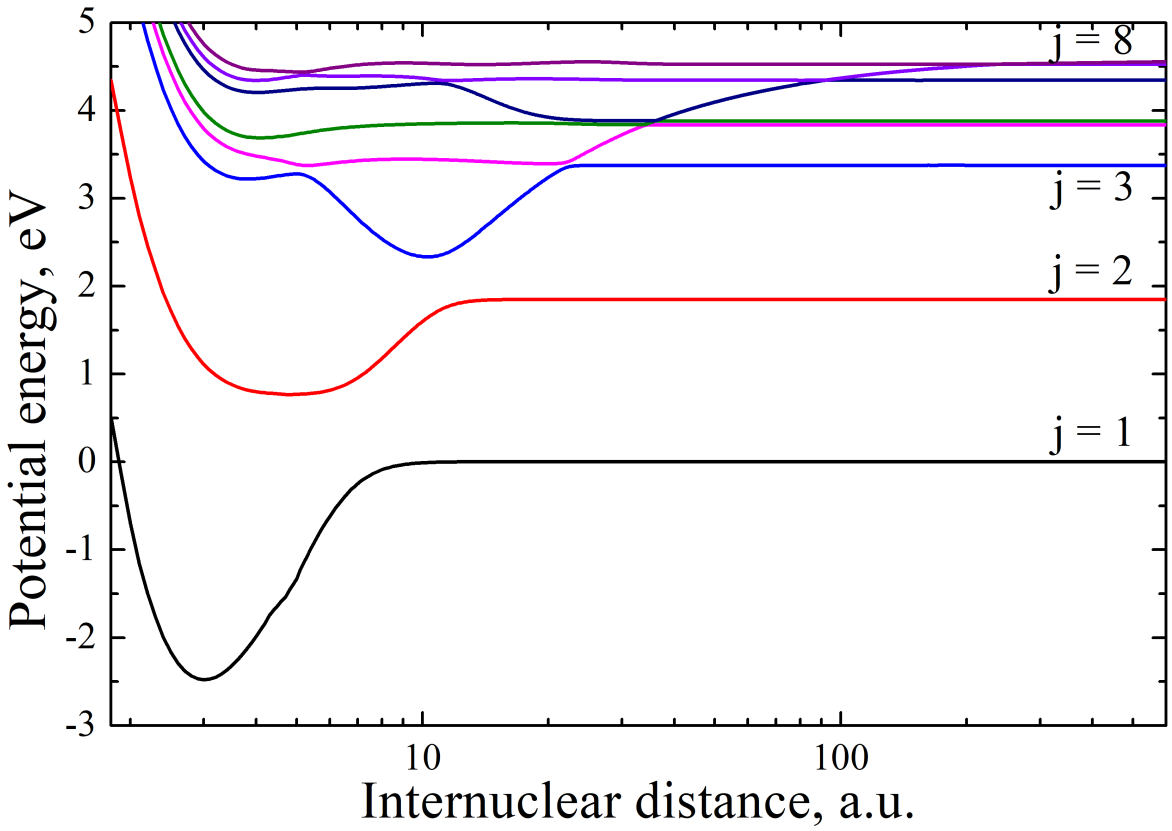

Figure 38. Adiabatic potential energies U_j of a quasimolecule LiH as a function on the internuclear distance R for molecular symmetry $^1\Sigma^+$, calculated in [148]. For the notation, see the Table 10.

discussed earlier in Chapters 3, 4, and also mainly confirmed in Chapter 3, the main contribution to the values of cross sections and rate coefficients make transitions within the molecular symmetry of the ionic channel. Transitions between different molecular symmetries were also not considered for the reasons outlined in Chapter 3.

Table 10. The molecular states of the quasimolecule LiH in $^1\Sigma^+$ symmetry, corresponding scattering channels, asymptotic energies (in eV) calculated from the ground state, and statistical populations of molecular states in $^1\Sigma^+$ symmetry.

j	Scattering channels	Asymptotic energies (eV)	p_j^{stat}
1	$\mathrm{Li}(2s\ ^2S) + \mathrm{H}(1s\ ^2S)$	0.0	0.2500
2	$\mathrm{Li}(2p\ ^2P) + \mathrm{H}(1s\ ^2S)$	1.8480	0.0833
3	$\mathrm{Li}(3s\ ^2S) + \mathrm{H}(1s\ ^2S)$	3.3738	0.2500
4	$\mathrm{Li}(3p\ ^2P) + \mathrm{H}(1s\ ^2S)$	3.8343	0.0833
5	$\mathrm{Li}(3d\ ^2D) + \mathrm{H}(1s\ ^2S)$	3.8795	0.0500
6	$\mathrm{Li}(4s\ ^2S) + \mathrm{H}(1s\ ^2S)$	4.3416	0.2500
7	$\mathrm{Li}(4p\ ^2P) + \mathrm{H}(1s\ ^2S)$	4.5223	0.0833
ionic	$\mathrm{Li}^+(1s^2\ ^1S) + \mathrm{H}^-(1s^2\ ^1S)$	4.6377	1.0

§ 5.3 Investigation of non-adiabatic nuclear dynamics in the LiH molecule with averaging over the masses of lithium isotopes. Analysis of cross sections and rate coefficients

Usually, when calculating inelastic processes in collisions of various elements with hydrogen, the mass of various isotopes of the element that is the partner of the collision with hydrogen is not taken into account. The mass of an element is considered the weighted average mass of all isotopes, taking into account the prevalence of these isotopes. This paragraph is devoted to a calculations, where the weighted average mass of lithium isotopes ^{6}Li and ^{7}Li, equal to 6.9675 au, was taken into account.

The total probabilities of non-adiabatic transitions from all initial states to all final ones were calculated by the hopping probability current method (see § 1.4.3). At the same time, the total number of probability currents for

each calculation over the quantum number of the total angular momentum was equal to $N^{tot} = 163{,}840$, which gives the minimum probability of $\approx 6.1 \times 10^{-6}$ and the accuracy of calculating the total probability of a non-adiabatic transition $\frac{1}{\sqrt{N^{tot}}} \approx 2.5 \times 10^{-3}$. The cross sections of all inelastic processes were calculated in the range of collision energies 0.01 – 100 eV according to the formulas (1.70) and (1.72), the rate coefficients – in the temperature range 1000 – 10000 K according to the formulas (1.74) and (1.75) for exothermic and endothermic processes, respectively.

Figure 39 shows cross sections of mutual neutralization processes obtained in this work by the hopping probability current method, in comparison with the results of calculations by Belyaev and Barklem [15]. The figure shows that for processes with the largest cross sections, namely processes $\mathrm{Li}^+ + \mathrm{H}^- \to (\mathrm{Li(3s)}, \mathrm{Li(3p)}, \mathrm{Li(3d)}) + \mathrm{H(1s)}$, cross sections agree very well with each other. There is also a good agreement for the process $\mathrm{Li}^+ + \mathrm{H}^- \to \mathrm{Li(2p)} + \mathrm{H(1s)}$. At the same time, for processes $\mathrm{Li}^+ + \mathrm{H}^- \to (\mathrm{Li(4s)}, \mathrm{Li(4p)}) + \mathrm{H(1s)}$ values of the cross sections agree somewhat worse, especially at low collision energies, but the difference in general does not exceed two orders of magnitude in the range [0.01, 10.0] eV. It is worth noting that with an increase of the collision energy, there is a better agreement of the cross sections. The worst agreement is observed for the process $\mathrm{Li}^+ + \mathrm{H}^- \to \mathrm{Li(2s)} + \mathrm{H(1s)}$. However, it is the processes $\mathrm{Li}^+ + \mathrm{H}^- \to (\mathrm{Li(3s)}, \mathrm{Li(3p)}, \mathrm{Li(3d)}) + \mathrm{H(1s)}$ make a dominant contribution to the total cross section of mutual neutralization, from 99.98% to 98.93% in the range [0.001,10.0] eV according to [15] and in the range from 99.62% to 98.61% according to the results obtained by the probability current method in the same energy range. This suggests that the results obtained by the probability current method reproduce with good accuracy the results obtained by *ab initio* quantum methods for processes with the largest cross sections.

Let us now analyze the values of the rate coefficients. Figure 40 shows the rate coefficients of mutual neutralization processes at a tem-

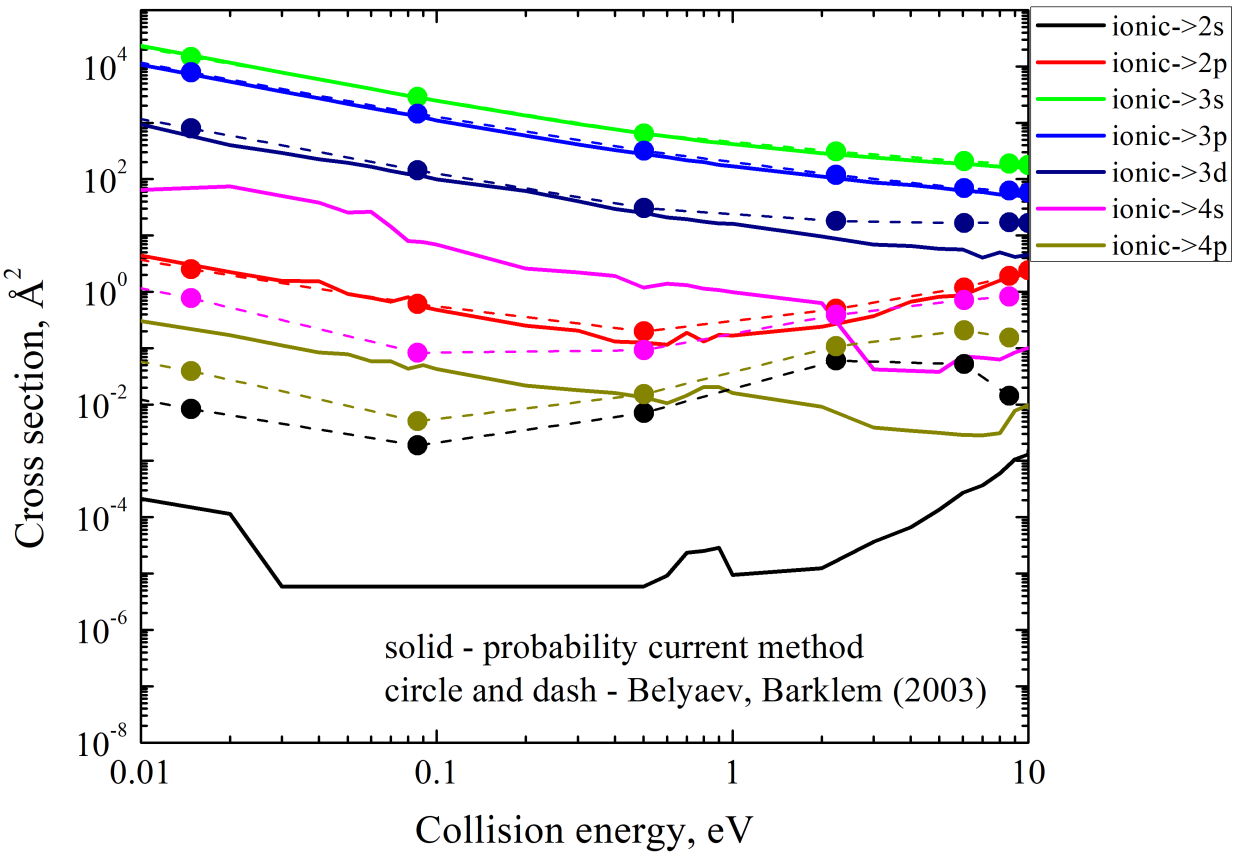

Figure 39. Cross sections of mutual neutralization as a function on the collision energy. Solid lines correspond to calculations carried out by the probability current method, symbols and dotted lines correspond to calculations by Belyaev and Barklem [15].

perature T = 6000 K obtained by various methods. The rate coefficients obtained by the probability current method and by the multichannel formula were calculated in the present study. The figure shows that, in general, the agreement of all three data sets is very good for the processes $Li^+ + H^- \rightarrow (Li(2p), Li(3s), Li(3p), Li(3d)) + H(1s)$. For the process $Li^+ + H^- \rightarrow Li(4s) + H(1s)$ the rate coefficients obtained by the probability current method and by the multichannel formula agree well, but both of these rate coefficients are about an order of magnitude higher than the value of the rate coefficient obtained by more rigorous *ab initio* quantum methods. At the same time, for the process $Li^+ + H^- \rightarrow Li(4p) + H(1s)$ the rate coefficients obtained by *ab initio* quantum method and the probability current method agree well, and the rate coefficient obtained by the multichannel formula has a value more than an order of magnitude higher than these two rate coefficients. This result suggests that the final values of the rate coefficients obtained by the probability current method reproduce well the results of more rigorous quantum calculations for quantities with large and intermediate values of the rate coefficients, that is, in the range $10^{-12} - 10^{-8}$ cms, with an accuracy of about one order of magnitude. But, unlike quantum *ab initio* calculations of nuclear dynamics, the probability current method does not require knowledge of the matrix elements of non-adiabatic coupling, and is also generally less resource- and time-consuming.

Figure 41 shows a graphical representation of all calculated rate coefficients of inelastic processes by the probability current method at the temperature T = 6000 K. All calculated rate coefficients can be divided into three groups, according to their values:

- group I: the processes with a rate coefficient exceeding 10^{-8} cm^3/s;
- group II: the processes with a rate coefficient lying in the range $10^{-8} - -10^{-12}$ cm^3/s;
- group III: the processes with a rate coefficient smaller than 10^{-12} cm^3/s.

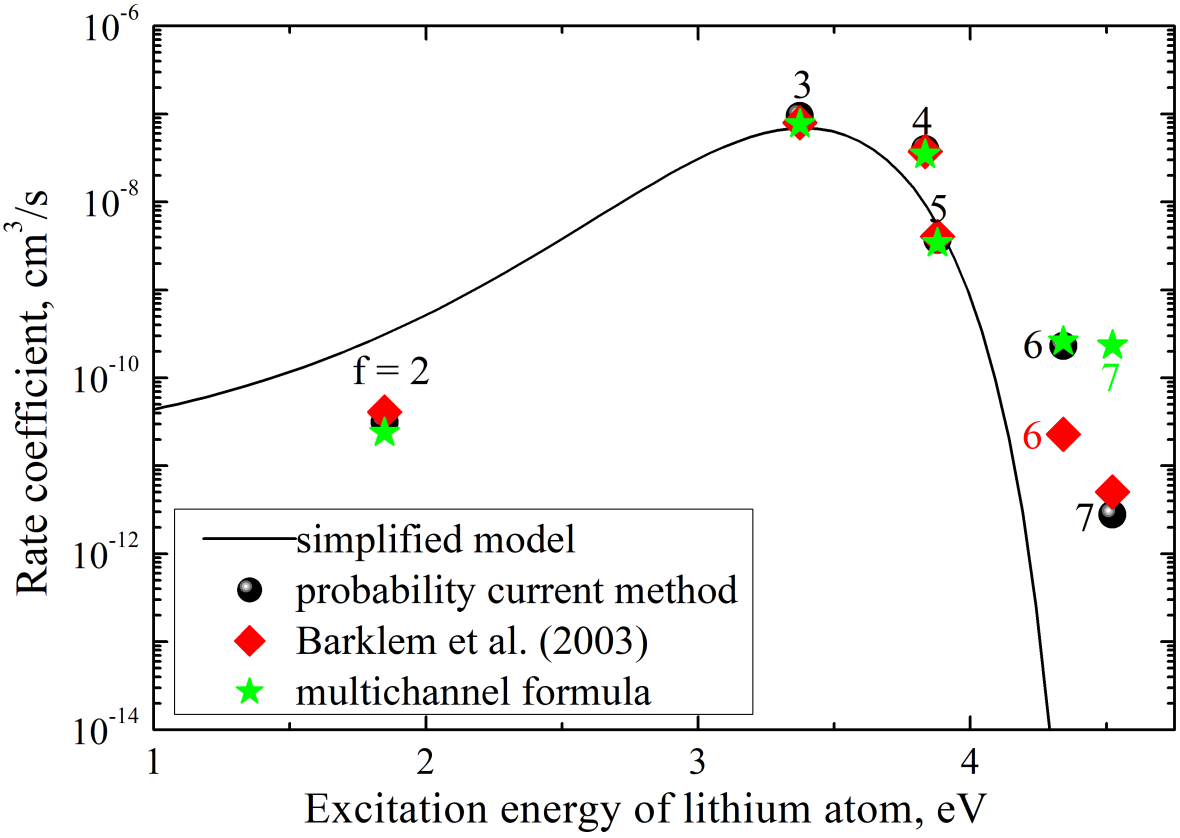

Figure 40. The dependence of the values of the rate coefficients of the mutual neutralization processes on the excitation energy of the lithium atom. Black balls denote the rate coefficients obtained by the hopping probability current method, red diamonds are the rate coefficients presented in [144] (calculated from the cross sections obtained in [15]), green asterisks are the rate coefficients obtained within the multichannel formula, the solid line corresponds to the simplified model curve. For the notation, see the Table 10.

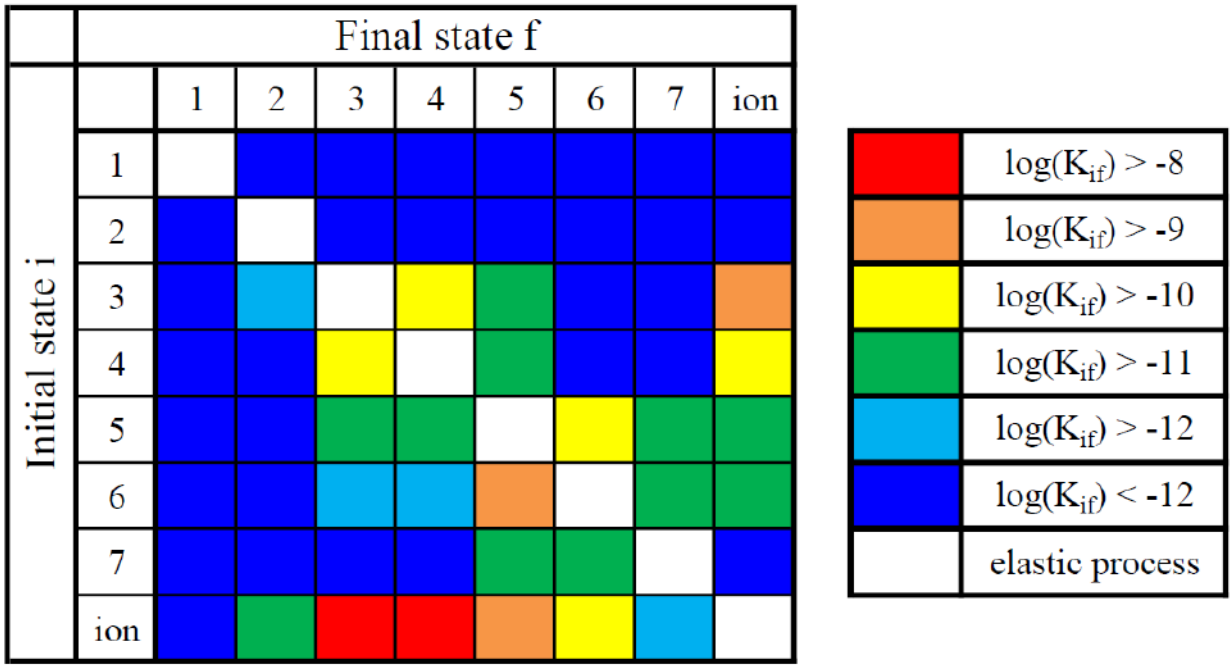

Figure 41. Graphical representation of the rate coefficients of all inelastic processes calculated by the hopping probability current method at the temperature T = 6000 K. For the notation, see the Table 10.

Group I includes only the processes of mutual neutralization $Li^+ + H^- \to (Li(3s), Li(3p)) + H(1s)$ with the values of the rate coefficients (9.47, 4.00) $\times 10^{-8}\,cm^3/s$ respectively. These processes are marked by red squares in the Figure 41.

Group II includes 23 inelastic processes (approximately 40% of the total), the largest values of the rate coefficients correspond to mutual neutralization process $Li^+ + H^- \to Li(3d) + H(1s)$, ion-pair formation process $Li(3s) + H(1s) \to Li^+ + H^-$ and de-excitation process $Li(4s) + H(1s) \to Li(3d) + H(1s)$ with values (3.71, 2.05, 1.60) $\times 10^{-9}\,cm^3/s$ respectively. These processes are marked by orange squares in the Figure 41. Other processes belonging to group II are marked by yellow, green and blue squares in the Figure 41.

Group III includes all processes involving the ground state, almost all processes involving the first excited state $Li(2p)$ (with the exception of two processes), as well as several other processes of excitation, de-excitation and

ion-pair formation, a total of 31 processes (or $\approx$55% of the total number of considered inelastic processes). Taking into account the processes belonging to groups I and II is most important when modelling the photospheres of stars under conditions of deviation from local thermodynamic equilibrium.

§ 5.4 Investigation of the effect of isotope substitution on the cross sections and rate coefficients of inelastic processes in collisions $^{6/7}$Li+H/D/T

Consider the effect of different masses of lithium and hydrogen isotopes on the values of cross sections and rate coefficients. This study was conducted in the same way as the previous one, within the framework of the probability current method, but with significantly greater accuracy. Firstly, when calculating by the hopping probability current method, the number of probability currents calculated for each value of the quantum number of the total angular momentum J has been increased to N^{tot} =2,621,440,000, since an algorithm using parallel calculations on the GPU has been applied. This resulted in a minimal probability $\approx 3.8 \times 10^{-10}$ and accuracy $\frac{1}{\sqrt{N^{tot}}} \approx 2 \times 10^{-5}$. Secondly, this was not enough for individual processes, and in this case the algorithm of branching probability currents with an accuracy of $\approx 10^{-10}$ was used.

The potential energies were used the same as in the previous study. This is justified by the fact that the potential energies calculated within the framework of the Born-Oppenheimer approach are calculated under the assumption of frozen nuclei at each value of the internuclear distance. The replacement of the masses of a particular nucleus will affect the matrix elements of non-adiabatic coupling, which are not taken into account in the framework of the Landau-Zener model, which underlies the probability current method. Thus, within the framework of the chosen approach, the isotopic effect will manifest itself only in the second part within the frame-

work of the Born-Oppenheimer approach, that is, in the study of nuclear dynamics.

As part of the assessment of the probability of a single non-adiabatic transition in the non-adiabatic region according to the Landau-Zener model, it is possible to make assumptions about exactly how different masses of nuclei will affect the cross-sections:

(I) for a given collision energy E_{col}, the velocity of radial motion v will be the smaller the greater the reduced mass of the nuclei μ; with a constant Landau-Zener parameter ξ^{LZ}, the probability of a non-adiabatic transition with a single passage through the non-adiabatic region will decrease (see the formula (1.53)), which will lead to a decrease in cross section values and rate coefficients;

(II) an increase in the reduced mass μ leads to a slower growth of the centrifugal term $\frac{\hbar^2 J(J+1)}{2\mu R^2}$ and the effective potential $\mathrm{U}^{eff}(R)$ as a function of the quantum number of the total angular momentum (see formula (1.25)); this leads to the fact that the upper limit of summation by J increases for the cross section (see the formula (1.70)), which in turn leads to an increase in cross sections and rate coefficients.

It should be noted that the first effect is more contributed at low collision energies not exceeding ≈ 1 eV. It turns out that there are two effects that lead to opposite results. Predicting the effect of both effects on the cross sections of inelastic processes is a non-trivial task, which is unambiguously uncertain for an arbitrary collision system. Therefore, for each pair of colliding particles, it is necessary to carry out its own calculation of nuclear dynamics.

First of all, we will compare the results obtained with known experimental and theoretical data. Figure 42 shows the proportions of partial cross sections of mutual neutralization from the total cross section of mutual neutralization for processes $^7\mathrm{Li}^+ + \mathrm{D}^- \rightarrow^7 \mathrm{Li}(3s, 3p, 3d) + \mathrm{D}(1s)$ as

a function on the collision energy. Presented as experimental data [7, 8], and *ab initio* quantum theoretical calculations [148]. It can be seen from the figure that the agreement of the *ab initio* calculations with model calculations using the probability current method is almost perfect, the only discrepancy occurs for the process $^7\mathrm{Li}^+ + \mathrm{D}^- \to^7 \mathrm{Li}(3d) + \mathrm{D}(1s)$ for collision energies exceeding $\approx$4 eV. Comparison of theoretical calculations by the probability current method with experimental data also shows a fairly good agreement, especially in the range of collision energies [0.1, 1.0] eV. At lower collision energies, discrepancies are observed that do not exceed $\approx$10% of the total neutralization cross section. It is also worth noting that the discrepancy between experimental and theoretical calculations for the process $^7\mathrm{Li}^+ + \mathrm{D}^- \to^7 \mathrm{Li}(3d) + \mathrm{D}(1s)$ at low collision energies (<0.02 eV) is quite significant: the proportion of the cross section of this process from the total cross section obtained by the probability current method is $\approx$3% versus $\approx$10% according to the data from the paper [7]. Nevertheless, the contribution of this process to the total cross section of mutual neutralization does not exceed 10%, so it can be concluded that in general there is a very good agreement of the results obtained by the probability current method with the experimentally obtained results. It is also worth noting that in the paper [150] Figure 2 shows a comparison of various theoretical calculations and experimental data, and shows that the results obtained by the probability current method (PC) have the best agreement with the experiment for the process $^7\mathrm{Li}^+ + \mathrm{D}^- \to^7 \mathrm{Li}(3s) + \mathrm{D}(1s)$.

Let us now analyze the influence of different isotope masses on the cross-sections of inelastic processes. Let us first consider the effect of the masses of various lithium isotopes on the cross sections. Since the cross sections of the mutual neutralization processes have the largest values among all inelastic processes, we will mainly consider them in the future. Let us give the values of the reduced masses for the case when different lithium isotopes collide with the same hydrogen isotopes:

- $\mu^{^6LiH} = 0.863197$ a.u., $\mu^{^7LiH} = 0.881238$ a.u.;

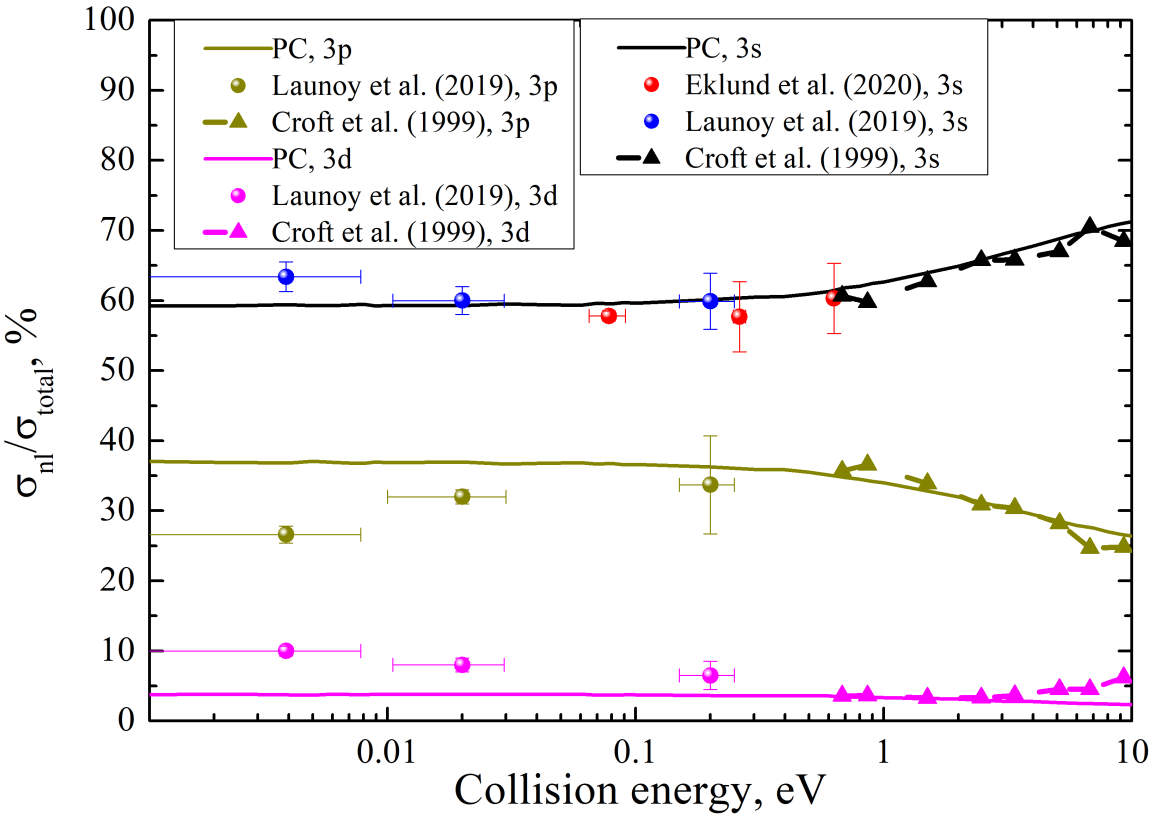

Figure 42. The branching fractions of partial mutual neutralization cross sections σ_{nl} of the total neutralization cross section σ_{total}, expressed in %, in collisions $^7\mathrm{Li}^+ + \mathrm{D}^- \rightarrow ^7\mathrm{Li}(3s, 3p, 3d) + \mathrm{D}(1s)$ as a function of the collision energy. Solid lines correspond to the results obtained by the probability current method (PC), red circles correspond to experimental data from the paper [8], blue, pink and brown circles correspond to experimental data from the paper [7], triangles and dotted lines correspond to theoretical calculations from the paper [148].

- $\mu^{^6LiD} = 1.508872$ a.u., $\mu^{^7LiD} = 1.564870$ a.u.;
- $\mu_{^6LiT} = 2.008810$ a.u., $\mu^{^7LiT} = 2.109300$ a.u.

It can be seen that the values of the reduced masses are quite close to each other (in each row), so the difference in the values of the cross sections will be small. This can be seen from the Figures 43 and 44. Comparing dotted lines with solid lines of the same colour, one can be seen that there is practically no difference for processes with the largest cross sections (Figure 43). For the processes ^{6}Li/^{7}Li + H and ^{6}Li/^{7}Li + D, the difference in cross section values ranges from 1-3% to 25-40%. At low collision energies (< 1.0 eV), the difference is systematically greater than at high collision energies. For example, cross section of the resonance process ^{6,7}Li$(2p)$ + H(1s) $\rightarrow$ ^{6,7}Li(2s) + H(1s) at collision energy $E_{col} = 100$ eV equals $\sigma_{2\rightarrow1}^{^6LiH} = 0.2561464$ Å^2 and $\sigma_{2\rightarrow1}^{^7LiH} = 0.2508187$ Å^2 respectively, and the difference it is only $\approx 2\%$. On the other hand, for the same process at the collision energy $E_{col} = 0.1$ eV, the cross sections are $\sigma_{2\rightarrow1}^{^6LiH} = 2.74831 \times 10^{-7}$ Å^2 and $\sigma_{2\rightarrow1}^{^7LiH} = 2.26535 \times 10^{-7}$ Å^2, and the difference is $\approx 20\%$.

From the Figure 43 it is also clear that the dotted lines are slightly lower or almost coincide with solid lines, that is, the cross sections of processes involving the lithium isotope ^{7}Li are systematically no less than the cross sections of processes involving the lithium isotope ^{6}Li. At the same time, from the Figure 44 it can be seen that for processes $\mathrm{Li}^+ + \mathrm{H}^- \rightarrow \mathrm{Li}(2s, 2p) + \mathrm{H}(1s)$ dotted lines are systematically no less than solid lines, that is, the opposite situation takes place. This suggests that for the processes of mutual neutralization when replacing lithium isotopes ^{6}Li $\leftrightarrow ^7$Li, the values of which are not the largest, the effect (I) has the greatest effect, while for the largest cross sections, effect (II) has a slight influence superior to (I). Nevertheless, for the cross sections with the largest values, the isotopic effect is quite small.

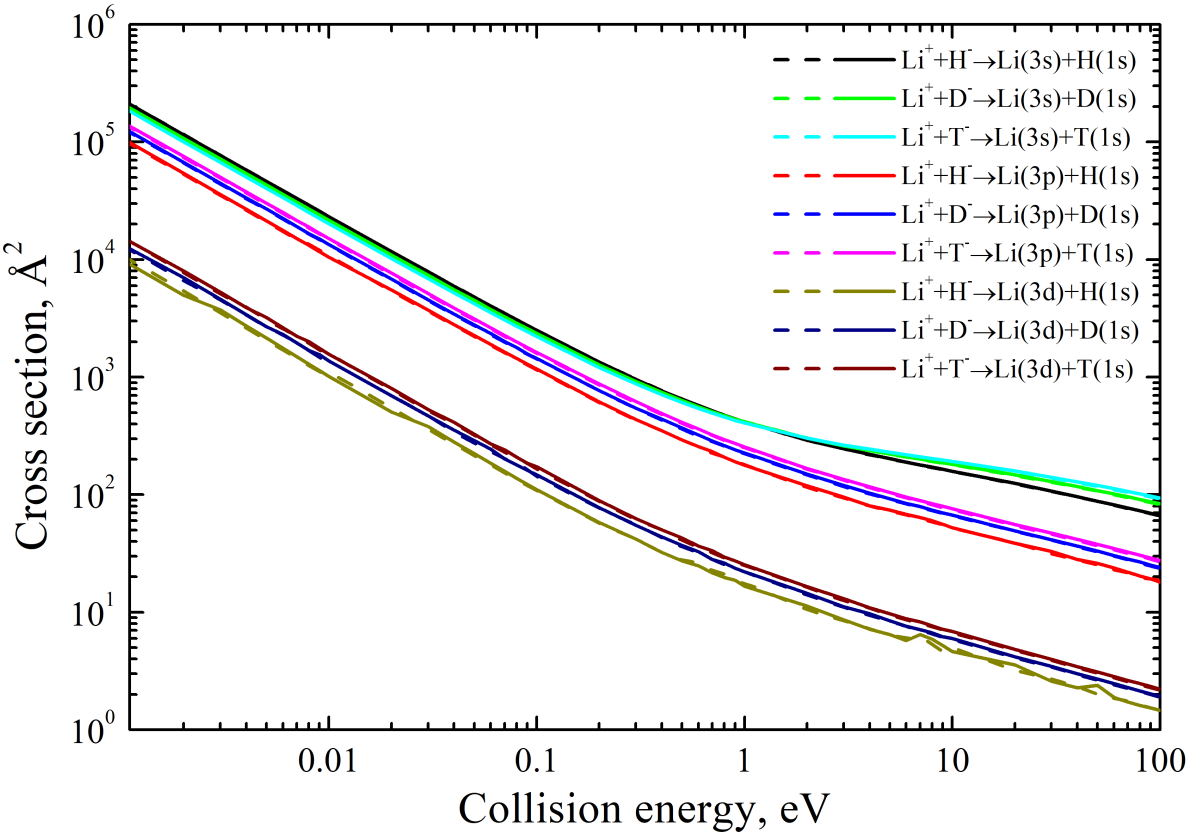

Figure 43. Cross sections of mutual neutralization processes $\mathrm{Li}^+ + \mathrm{H}^- \to \mathrm{Li}(3s, 3p, 3d) + \mathrm{H}(1s)$ in collisions of lithium isotopes $^{6/7}$Li with hydrogen isotopes H/D/T as a function of the collision energy. Solid lines correspond to processes involving the lithium isotope ^{7}Li, dotted lines correspond to processes involving the lithium isotope ^{6}Li. Collisions with hydrogen isotopes H/D/T are indicated by different colours.

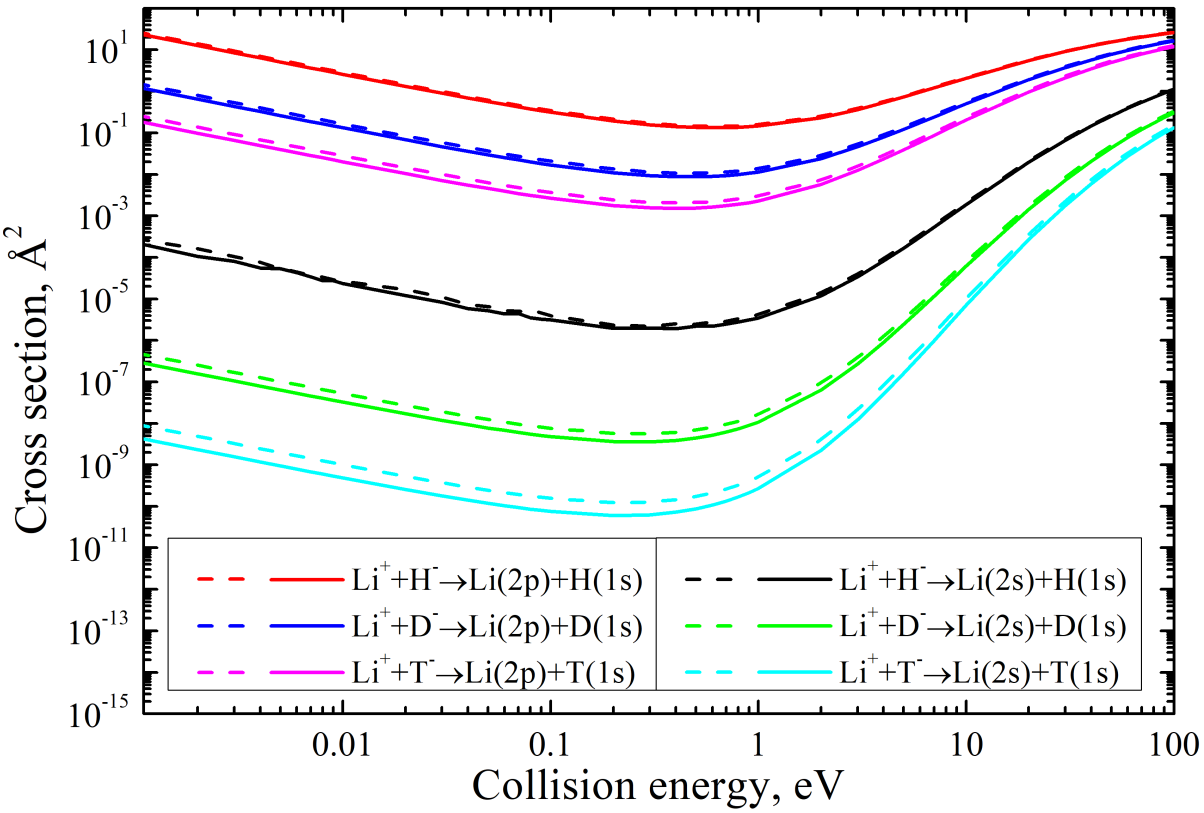

Figure 44. Cross sections of mutual neutralization of processes $\mathrm{Li}^+ + \mathrm{H}^- \to \mathrm{Li}(2s, 2p) + \mathrm{H}(1s)$ in collisions of lithium isotopes $^{6/7}$Li with hydrogen isotopes H/D/T as a function of the collision energy. Solid lines correspond to processes involving the lithium isotope ^{7}Li, dotted lines correspond to processes involving the lithium isotope ^{6}Li. Collisions with hydrogen isotopes H/D/T are indicated by different colours.

Let us now consider the influence of the masses of various hydrogen isotopes on the cross sections values. The situation is different here. Let us give the values of the reduced masses for this case:

- $\mu^{^6LiH} = 0.863197$ a.u., $\mu^{^6LiD} = 1.508872$ a.u., $\mu^{^6LiT} = 2.008810$ a.u.;
- $\mu^{^7LiH} = 0.881238$ a.u., $\mu^{^7LiD} = 1.564870$ a.u., $\mu^{^7LiT} = 2.109300$ a.u.

It can be seen that in this case the difference in the values of the reduced masses is significant (in each row) and reaches more than twice when replacing $\mathrm{H} \leftrightarrow \mathrm{T}$. From the figure 44 it can be seen that for the process $\mathrm{Li}^+ + \mathrm{H}^- \rightarrow \mathrm{Li}(2p) + \mathrm{H}(1s)$ at low collision energies (<1 eV), the difference in cross section values reaches one order of magnitude in collisions $^{6/7}\mathrm{Li}+\mathrm{H}$ and $^{6/7}\mathrm{Li} + \mathrm{D}$ and two orders of magnitude in collisions of $^{6/7}\mathrm{Li} + \mathrm{H}$ and $^{6/7}\mathrm{Li} + \mathrm{T}$. For the process $\mathrm{Li}^+ + \mathrm{H}^- \rightarrow \mathrm{Li}(2s) + \mathrm{H}$ the difference in cross section values at low collision energy is even stronger: two orders of magnitude in collisions $^{6/7}\mathrm{Li}+\mathrm{H}$ and $^{6/7}\mathrm{Li}+\mathrm{D}$ and four orders of magnitude in collisions $^{6/7}\mathrm{Li} + \mathrm{H}$ and $^{6/7}\mathrm{Li} + \mathrm{T}$. But on the other hand, from the Figure 43 it can be seen that for mutual neutralization processes $\mathrm{Li}^+ + \mathrm{H}^- \rightarrow \mathrm{Li}(3s, 3p, 3d) + \mathrm{H}(1s)$ the difference reaches no more than two times. Moreover, it can be noted that, for example, for the process $\mathrm{Li}^+ + \mathrm{H}^- \rightarrow \mathrm{Li}(3p) + \mathrm{H}\,(1\mathrm{s})$, the largest cross section corresponds to collisions $^{6/7}\mathrm{Li}+\mathrm{T}$, the slightly smaller cross section corresponds to collisions $^{6/7}\mathrm{Li} + \mathrm{D}$ and the smallest corresponds to collisions $^{6/7}\mathrm{Li} + \mathrm{H}$. Based on this, it can be concluded that for processes with the largest cross sections, effect (II) makes a significantly greater contribution than (I). For processes with small cross sections, effect (I) has a greater influence. It is also worth noting that for processes $\mathrm{Li}^+ + \mathrm{H}^- \rightarrow \mathrm{Li}(2s, 2p) + \mathrm{H}(1s)$ with increasing collision energy, the difference in cross section values becomes smaller, while as for processes $\mathrm{Li}^+ + \mathrm{H}^- \rightarrow \mathrm{Li}(3s, 3p, 3d) + \mathrm{H}$ this cannot be said.

For a clearer understanding of exactly how both effects (I) and (II) affect the final values of the cross sections, it is worth looking at the Figure 45, where the dependences of the full probabilities of the non-

adiabatic transition of mutual neutralization processes to the states of $\mathrm{Li}(2s, 2p, 3s, 3p, 3d) + \mathrm{H}(1s)$ for collisions of lithium isotope $^7\mathrm{Li}$ with hydrogen isotopes H/D/T are presented. The figure shows that the processes $\mathrm{Li}^+ + \mathrm{H}^- \to \mathrm{Li}(2s, 2p) + \mathrm{H}(1s)$ are characterized by small values of the total probabilities of a non-adiabatic transition, not exceeding 0.001. At the same time, processes $\mathrm{Li}^+ + \mathrm{H}^- \to \mathrm{Li}(3s, 3p, 3d) + \mathrm{H}(1s)$ are characterized by the values of the total probabilities of a non-adiabatic transition exceeding the value of 0.001 in the entire range of J. The essence of the effect (I) is in changing the total probability of a non-adiabatic transition, while the effect (II) is to increase the maximum value of J_{max}, at which the probability of a non-adiabatic transition is still non-zero. From the Figure 45 it is clearly seen that for processes with the highest total probabilities of a non-adiabatic transition (processes $\mathrm{Li}^+ + \mathrm{H}^- \to \mathrm{Li}(3s, 3p, 3d) + \mathrm{H}(1s)$) the values of the total probabilities do not change very much (in the range of $\approx 50\%$ in both directions) depending on which hydrogen isotope collide with lithium. But the heavier the hydrogen isotope, the more terms in the sum in the cross section calculation formula (see formula (1.70)), and for the above processes, J_{max} increases significantly in collisions with heavier hydrogen isotopes, up to $\approx .50\%$ when replacing hydrogen with tritium:

- $\mathrm{Li}^+ + \mathrm{H}^- \to \mathrm{Li}(3s) + \mathrm{H}(1s)$: $J_{max}^{^7\mathrm{LiH}} = 278, J_{max}^{^7\mathrm{LiD}} = 369, J_{max}^{^7\mathrm{LiT}} = 428$;
- $\mathrm{Li}^+ + \mathrm{H}^- \to \mathrm{Li}(3p) + \mathrm{H}(1s)$: $J_{max}^{^7\mathrm{LiH}} = 352, J_{max}^{^7\mathrm{LiD}} = 467, J_{max}^{^7\mathrm{LiT}} = 542$;
- $\mathrm{Li}^+ + \mathrm{H}^- \to \mathrm{Li}(3d) + \mathrm{H}(1s)$: $J_{max}^{^7\mathrm{LiH}} = 362, J_{max}^{^7\mathrm{LiD}} = 482, J_{max}^{^7\mathrm{LiT}} = 560$;

For processes $\mathrm{Li}^+ + \mathrm{H}^- \to \mathrm{Li}(2s, 2p) + \mathrm{H}(1s)$ the situation is such that the full probability of a non-adiabatic transition decreases by an order of magnitude, or even several orders of magnitude, with an increase in the mass of the hydrogen isotope. In this case, the increase in the number of summands in the formula for calculating the cross section of the inelastic process plays a significantly smaller role.

Let us now proceed to consider the effect of isotope substitution in lithium-hydrogen collisions on the rate coefficients of inelastic processes.

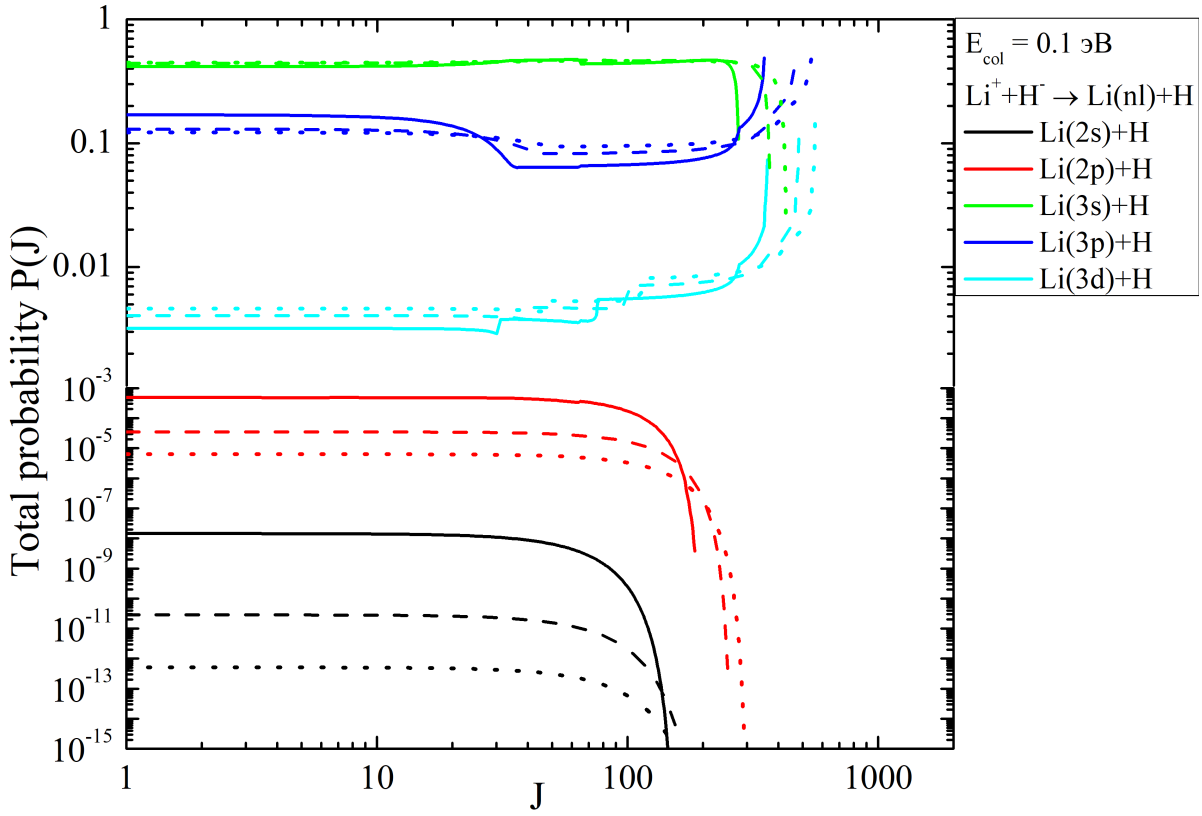

Figure 45. The total probability of non-adiabatic transition of mutual neutralization processes $^7\mathrm{Li}^+ + \mathrm{H}^-/\mathrm{D}^-/\mathrm{T}^- \rightarrow ^7\mathrm{Li}(2s, 2p, 3s, 3p, 3d) + \mathrm{H/D/T}$ as a function of the quantum number of the total angular momentum at the collision energy $\mathrm{E}_{col} = 0.1$ eV. Solid lines correspond to collisions $^7\mathrm{Li}^+ + \mathrm{H}^-$, dotted lines correspond to collisions $^7\mathrm{Li}^+ + \mathrm{D}^-$, dotted lines correspond to collisions $^7\mathrm{Li}^+ + \mathrm{T}^-$.

Table 11. The rate coefficients (in cm^3/s) of mutual neutralization at the temperature T = 6000 K, calculated in this work by the probability current method, as well as presented in [7, 144, 151]. The number in square brackets denotes the power of ten.

	Collision partners	Li(3s)	Li(3p)	Li(3d)	total rate coefficient
Probability current method	$^7Li^+ + H^-$	8.50[-8]	3.74[-8]	3.53[-9]	1.26[-7]
	$^7Li^+ + D^-$	6.30[-8]	3.54[-8]	3.51[-9]	1.02[-7]
	$^6Li^+ + H^-$	8.59[-8]	3.74[-8]	3.60[-9]	1.27[-7]
	$^6Li^+ + D^-$	6.43[-8]	3.54[-8]	3.49[-9]	1.04[-7]
experiment [7]	$^7Li^+ + H^-$	7.43[-8]	2.72[-8]	7.72[-9]	1.10[-7]
	$^7Li^+ + D^-$	5.54[-8]	2.57[-8]	7.48[-9]	8.90[-8]
Croft et al. [151]	$^7Li^+ + H^-$	-	-	-	1.18[-7]
Barklem et al. [144]	$^7Li^+ + H^-$	7.95[-8]	3.74[-8]	4.05[-9]	1.21[-7]

The Table 11 shows the values of the partial rate coefficients of the mutual neutralization processes $Li^+ + H^- \to Li(3s, 3p, 3d) + H(1s)$ calculated by various methods. It can be seen that the comparison of the total rate coefficients of the mutual neutralization process shows a good agreement of all available results with each other. Both for collisions $^7Li + H$ and for collisions $^7Li + D$, the total rate coefficients agree within $\approx 15\%$. At the same time, the maximum difference in the values of the partial rate coefficients is approximately 2 times for the process $Li^+ + H^- \to Li(3d) + H(1s)$.

Consider separately the resonance process $Li(2p) + H(1s) \to Li(2s) + H(1s)$ corresponding to the 670.776/670.791 nm doublet, which is extremely important for astrophysical applications. The cross sections of this process, and also the rate coefficients, have small values, see Figure 46. These cross sections are strongly affected by the (I) effect, which is also seen in the Figure 46. In general, the cross section of this process is more

strongly affected by collisions with various hydrogen isotopes, leading to a difference of more than two orders of magnitude for collisions $\mathrm{Li} + \mathrm{H}$ and $\mathrm{Li} + \mathrm{D}$ and more than four orders of magnitude for collisions $\mathrm{Li} + \mathrm{H}$ and $\mathrm{Li} + \mathrm{T}$ at collision energies less than 0.1 eV. While collisions of different lithium isotopes with the same hydrogen isotopes lead to the maximum difference for collisions of $^6\mathrm{Li} + \mathrm{T}$ and $^7\mathrm{Li} + \mathrm{T}$, not exceeding twice at low energies collision and decreasing with increasing collision energy.

Figure 47 shows the dependence of the the rate coefficients values of the mutual neutralization processes on the excitation energy of the lithium atom at a temperature $\mathrm{T} = 6000$ K. From this figure it can be seen that for processes $\mathrm{Li}^+ + \mathrm{H}^- \to \mathrm{Li}(3s, 3p, 3d, 4s, 4p) + \mathrm{H}(1s)$ the difference in the values of all six different combinations of collision partners is small and does not exceed $\approx 60\%$. In other words, for these processes, the effect of isotope substitution is weakly expressed. For processes $\mathrm{Li}^+ + \mathrm{H}^- \to \mathrm{Li}(2s, 2p) + \mathrm{H}(1s)$ the difference in the values of the rate coefficients can reach several orders of magnitude when the same lithium isotopes collide with different hydrogen isotopes and only ≈ 2 times when different lithium isotopes collide with the same hydrogen isotopes (compare the black, red and blue symbols in Fig. 47 and rhombuses with circles, squares with asterisks and triangles with crosses).

Figure 48 shows the dependence of the values of the total rate coefficients of the mutual neutralization processes for all six combinations of collision partners on temperature. It can be seen that in the entire temperature range studied, the replacement of lithium isotopes in collisions with the same hydrogen isotopes has practically no effect on the value of the total rate coefficient. However, for collisions of $^6\mathrm{Li}$, the value of the rate coefficient is systematically higher (but not more than 2.2But the replacement of hydrogen isotopes leads to a more significant change in the values of the rate coefficients:

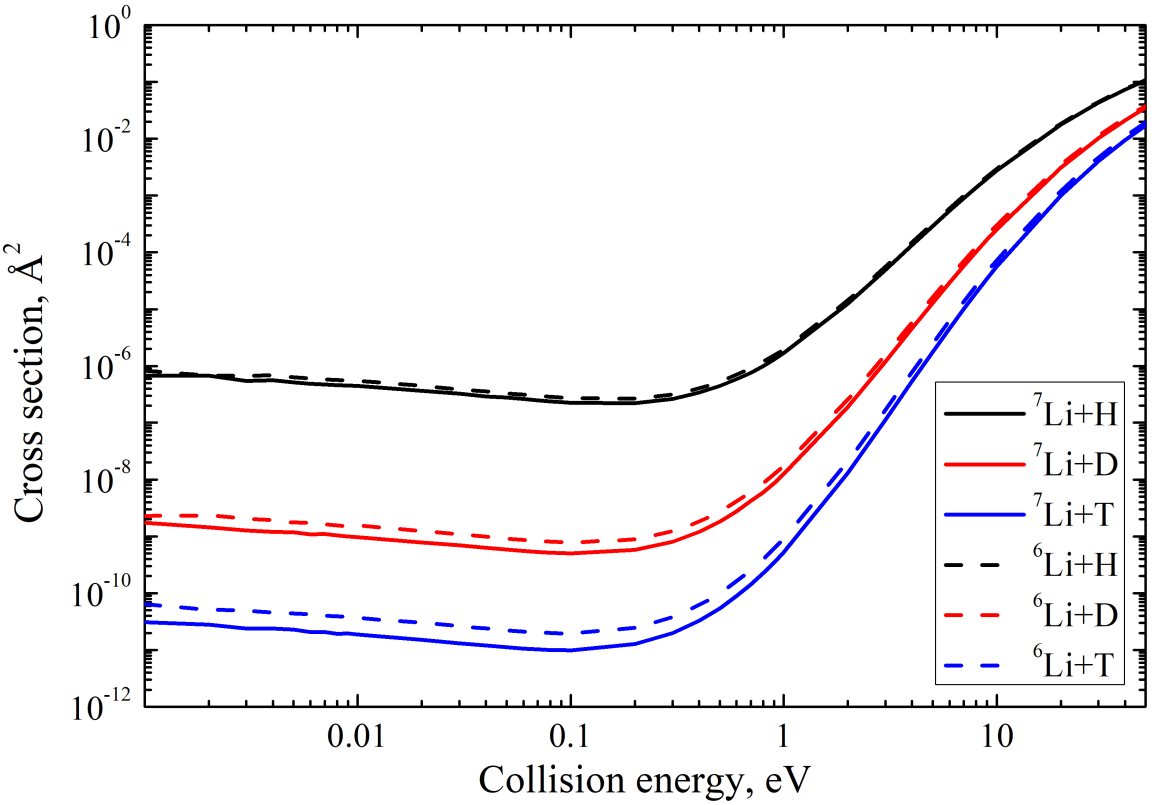

Figure 46. The cross section of the resonance de-excitation process $\mathrm{Li}(2p) + \mathrm{H} \to \mathrm{Li}(2s) + \mathrm{H}$ as a funtion of the collision energy. Solid lines correspond to collisions of the lithium isotope ^{7}Li with various hydrogen isotopes, dotted lines correspond to collisions of the lithium isotope ^{6}Li with various hydrogen isotopes.

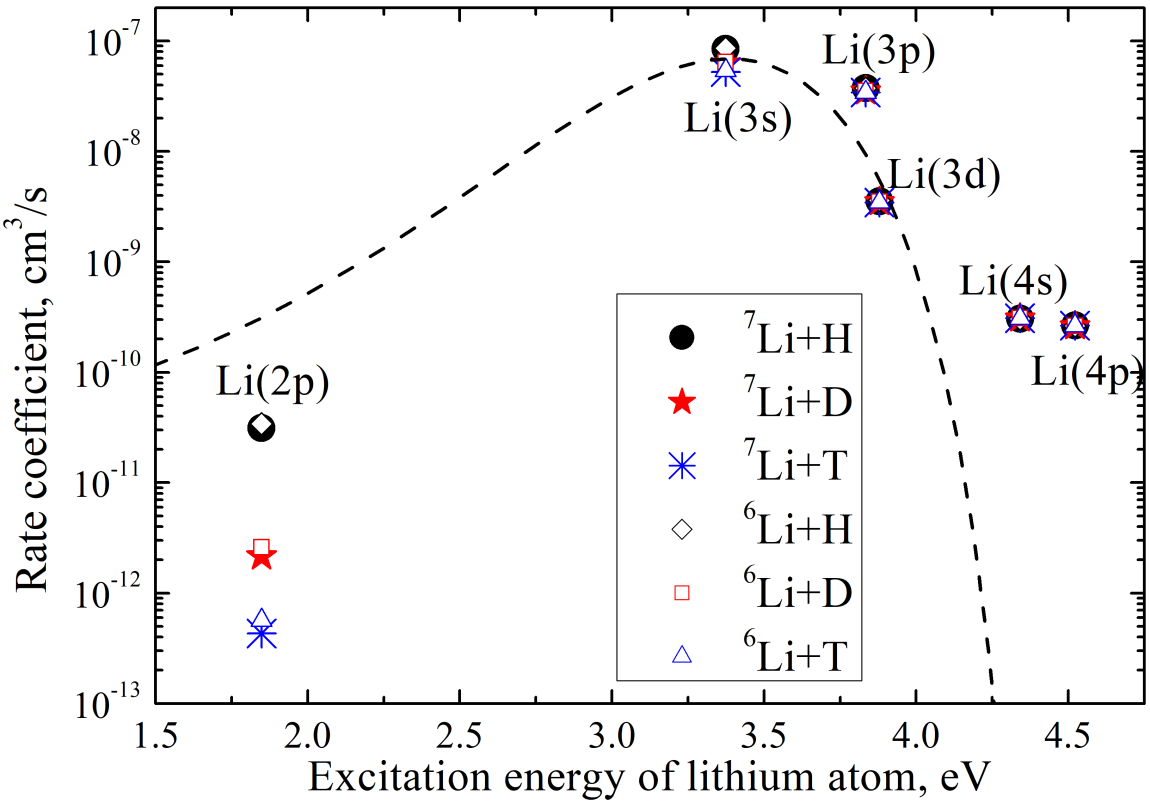

Figure 47. The rate coefficients of the mutual neutralization processes as a functions of the excitation energy of the lithium atom at a temperature of T = 6000 K. Black circles indicate the rate coefficients corresponding to collisions $^7\mathrm{Li} + \mathrm{H}$, red asterisks – collisions $^7\mathrm{Li} + \mathrm{D}$, blue crosses – collisions $^7\mathrm{Li} + \mathrm{T}$, black hollow rhombuses – collisions $^6\mathrm{Li} + \mathrm{H}$, red hollow squares – collisions $^6\mathrm{Li} + \mathrm{D}$, blue hollow triangles – collisions $^6\mathrm{Li} + \mathrm{T}$.

- when replacing $H \to D$, the values of the total rate coefficients vary in the range from 30 to 20% at the temperatures 1000 and 10000 K respectively;

- when replacing $D \to T$, the values of the total rate coefficients vary in the range from 14 to 12% at the temperatures 1000 and 10000 K respectively;

- when replacing $H \to T$, the values of the total rate coefficients vary in the range from 46 to 35% at the temperatures 1000 and 10000 K respectively;

From all of the above, the following conclusions can be drawn:

1. In collisions of lithium and hydrogen, there is practically no difference which of the isotopes of lithium collides with hydrogen;

2. Collisions of the same lithium isotopes with different hydrogen isotopes can be well distinguished for some processes;

3. resonance process $\mathrm{Li}(2p) + \mathrm{H}(1s) \to \mathrm{Li}(2s) + \mathrm{H}(1s)$ is quite sensitive to the replacement of hydrogen isotopes at low collision energies;

4. the total rate coefficients of the mutual neutralization process in collisions $^{6/7}\mathrm{Li} + \mathrm{H}$ are approximately 25% higher than the rate coefficients of the mutual neutralization process in collisions $^{6/7}\mathrm{Li} + \mathrm{D}$ in the temperature range [1000, 10000] K.

§ 5.5 Concluding remarks

In this Chapter, inelastic processes in collisions of lithium atoms and cations with hydrogen atoms and anions are investigated by the probability current method. It is shown that the results obtained by the model probability current method are in good agreement with the results of the most accurate *ab initio* quantum calculations.

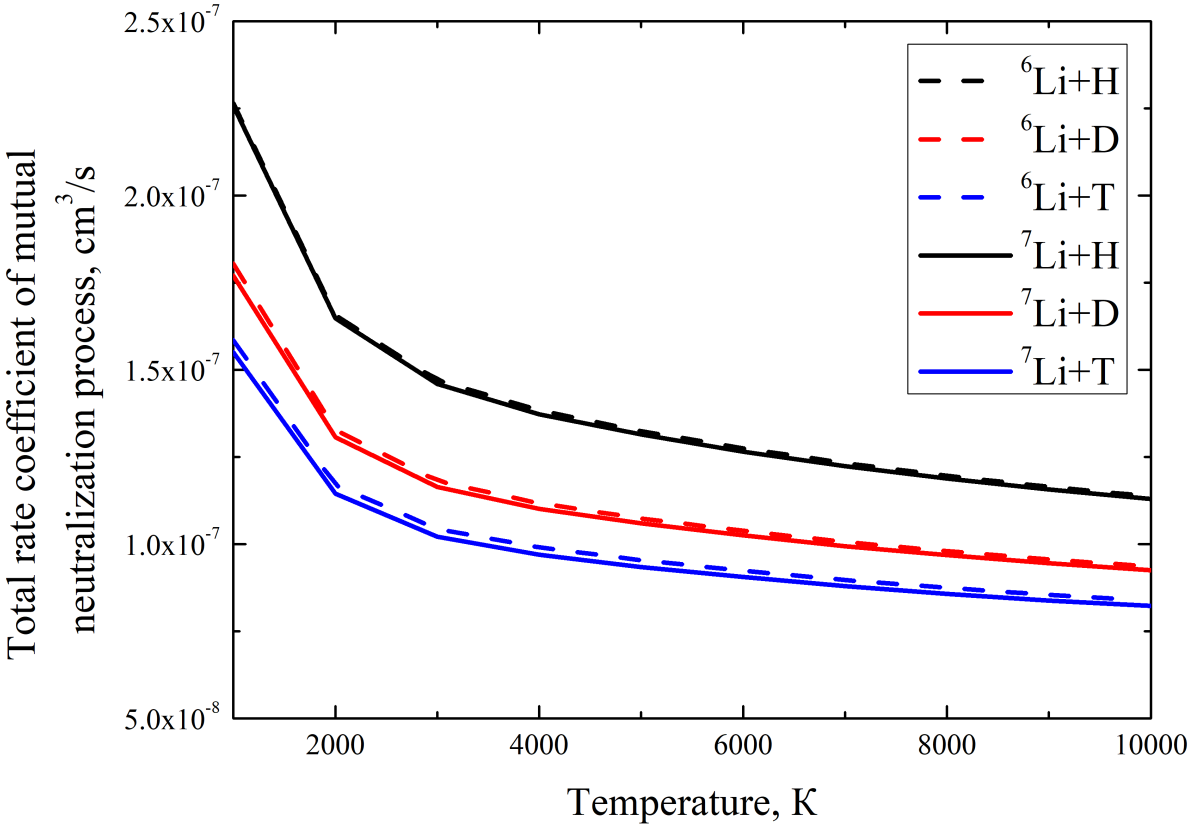

Figure 48. The total rate coefficients of mutual neutralization processes as a function of temperature. Solid lines marked collisions of the lithium isotope ^{7}Li with various hydrogen isotopes, dotted lines marked collisions of the isotope ^{6}Li with various hydrogen isotopes. Collisions with hydrogen H are indicated in black, collisions with deuterium D in red, collisions with tritium T in blue.

The influence of different masses of lithium and hydrogen isotopes on the cross sections and rate coefficients of inelastic processes has also been studied. It is shown that the replacement of lithium isotopes in collisions with the same hydrogen isotopes has a weak effect on the values of cross sections and rate coefficients, while the replacement of hydrogen isotopes in collisions with the same lithium isotopes leads to noticeable changes in the values of cross sections and rate coefficients for some processes, up to several orders of magnitude. Resonance process cross section $\mathrm{Li}(2p) + \mathrm{H}(1s) \rightarrow \mathrm{Li}(2s) + \mathrm{H}(1s)$ is sensitive to the substitution of hydrogen isotopes at low collision energies, up to several orders of magnitude. It is shown that the total rate coefficients of the mutual neutralization process in collisions $^{6/7}\mathrm{Li} + \mathrm{H}$ are approximately 25% higher than the values of the rate coefficients of the mutual neutralization process in collisions $^{6/7}\mathrm{Li} + \mathrm{D}$ in the temperature range [1000, 10000] K. It is also shown that the results obtained by the probability current method are in good agreement with the available experimental data.

The results obtained in this Chapter are published in the following articles:

- Belyaev A. K., **Voronov Ya. V.** Atomic Data on Inelastic Processes in Low-energy Lithium–Hydrogen Collisions / A. K. Belyaev, Ya. V. Voronov // The Astrophysical Journal. – 2018. – Vol. 868. – No. 2. – P. 86.

- Belyaev A. K., **Voronov Ya. V.** Isotopic effects in low-energy lithium-hydrogen collisions / A. K. Belyaev, Ya. V. Voronov // Physical Review A. – 2021. – Vol. 104. – No. 2. – P. 022812.

The results were also presented at the following conferences:

- XXI Mendeleev Congress on General and Applied Chemistry, Symposium "The Periodic Table through Space and Time" (9-13 September, 2019, Saint-Petersburg, Russia). Poster "**Application of the**

probability current method to nuclear dynamical calculations in collisions with hydrogen";

- Physics of Stars and Planets: atmospheres, activity and magnetic fields (16-20 September, 2019, N. Tusi Shamakhi Astrophysical Observatory, Shamakhi, Azerbaijan). Poster "**Application of the probability current method to nuclear dynamical calculations in collisions with hydrogen**".

This research was supported by grants:

- the Ministry of Science and Higher Education grant No. 3.1738.2017/PCH 2017-2019, the head of Prof. Belyaev A. K.

- the Ministry of Education grant No. 2020-0026 2020-2022, the head of Prof. Belyaev A. K.

Conclusion

In conclusion, let us present the main results obtained in this dissertation:

1. A modified asymptotic method that allows taking into account the fine structure of energy levels in collisions of alkali metal atoms and alkali-like ions with hydrogen, proposed in [23,24], received a further generalization for the case of collisions of alkaline earth metal atoms with hydrogen. Using the example of collisions of calcium ions with hydrogen $Ca^+ + H$, it is shown that taking into account the fine structure of energy levels leads to a non-trivial redistribution of the values of the rate coefficients, which cannot be reproduced using any simple formulas.

2. The processes of excitation, de-excitation, ion-pair formation and mutual neutralization in collisions of oxygen atoms and ions with hydrogen atoms and ions are investigated. Inelastic processes for 11 covalent states and two ionic states in six molecular symmetries have been studied by the hopping probability current method (stochastic version), for a total of 240 processes. By the multichannel formula, processes for 16 covalent states and two ionic ones for three molecular symmetries were studied, a total of 292 processes. In the study of nuclear dynamics, molecular adiabatic potential energies obtained in [28] by the MRCI method for 11 lower covalent states and two ionic ones were used, as well as obtained within the framework of the asymptotic method for 5 high-lying covalent states. It is shown that the largest rate coefficients correspond to the processes of mutual neutralization $O^+(2p^3\ ^4S^\circ) + H^-(1s^2\ ^1S) \to O(2p^3 4s\ ^5S^o) + H(1s\ ^2S)$, $O^-(2p^5\ ^2P) + H^+ \to O(2p^4\ ^3P) + H(2p\ ^2P)$ and $O^+(2p^3\ ^4S^\circ) + H^-(1s^2\ ^1S) \to O(2p^3 3p\ ^3P) + H(1s\ ^2S)$. These processes, as well as processes with rate coefficients values greater than 10^{-12} cm^3/s, are most important to take into account when mod-

elling stellar spectra under conditions of deviation from local thermodynamic equilibrium. It is also shown that taking into account non-adiabatic transitions in molecular symmetries not generated by ionic states practically does not affect the values of cross sections and rate coefficients of processes belonging to group I, but can significantly affect processes belonging to groups II and III. In particular, for some processes, the cross sections at low collision energies are mainly determined by the contribution of non-adiabatic transitions in molecular symmetries not generated by ionic states.

3. Inelastic processes in collisions of calcium atoms and ions with hydrogen atoms and ions, namely the processes of excitation, de-excitation and charge exchange, are investigated. It is shown that for collisions Ca+H and $Ca^{+}+H^{-}$, the probability current method gives values of cross sections and rate coefficients that differ little from the results obtained in the framework of the *ab initio* quantum calculations by the reprojection method: for most processes, the difference in the values of cross sections and rate coefficients lies in the range of 30-50%, for all processes, the difference in the values of the rate coefficients does not exceed two orders of magnitude. As in the case of oxygen, in the case of calcium, taking into account non-adiabatic regions at short distances practically does not affect the final values of cross sections and rate coefficients of processes with large values, while for processes with small values of cross sections and rate constants, taking into account these regions can affect the values of cross sections and rate coefficients significantly, especially this is typical for highly excited states. For most of the processes considered in collisions Ca+H, $Ca^{+}+H^{-}$, Ca^{+}+H, Ca+H^{+} and $Ca^{2+}+H^{-}$, the dominant mechanism of non-adiabatic transitions is ion-covalent interaction forming non-adiabatic regions at medium and large internuclear distances.

4. Inelastic processes in collisions of lithium atoms and cations with hydrogen atoms and anions by the probability current method are investigated. It is shown that the results obtained by the model probability current method are in good agreement with the results of the most accurate *ab initio* quantum calculations. The dependence of the cross sections and rate coefficients of inelastic processes on the replacement of lithium and hydrogen isotopes in collisions is also investigated. It is shown that the replacement of lithium isotopes in collisions with the same hydrogen isotopes has a weak effect on the values of cross sections and rate coefficients, while the replacement of hydrogen isotopes in collisions with the same lithium isotopes leads to noticeable changes in the values of cross sections and rate coefficients for some processes, up to several orders of magnitude. Resonance process cross section $\mathrm{Li}(2p) + \mathrm{H}(1s) \to \mathrm{Li}(2s) + \mathrm{H}(1s)$ is quite sensitive to the substitution of hydrogen isotopes at low collision energies, up to several orders of magnitude. It is shown that the total rate coefficients of the mutual neutralization process in collisions $^{6/7}\mathrm{Li} + \mathrm{H}$ are approximately 25% higher in magnitude than the rate coefficients of the mutual neutralization process in collisions $^{6/7}\mathrm{Li} + \mathrm{D}$ in the temperature range [1000, 10000] K. It is also shown that the results obtained by the probability current method are in good agreement with the available experimental data for neutralization processes $\mathrm{Li}^+ + \mathrm{H}^- \to \mathrm{Li}(3s, 3p, 3d) + \mathrm{H}(1s)$.

All the goals and objectives set out in the Introduction have been fully achieved. The author expresses gratitude to his supervisor, Professor Andrey Konstantinovich Belyaev, for setting tasks, fruitful discussions and consultations, attentive and sensitive leadership of research activities, as well as the active involvement of the author in research activities at the international level. The author also expresses gratitude to Svetlana Anatolyevna Yakovleva for the active involvement of the author in research activities, for conducting interesting joint research, for consultations and

assistance in research, as well as for creating a creative atmosphere that contributed to fruitful scientific work. The author thanks Dmitry Sergeyevich Rodionov for consultations and discussions on the subject of the conducted research, for joint research work, for technical assistance on various issues, as well as for creating a creative atmosphere that contributed to fruitful scientific work. The author thanks the staff of the Department of Theoretical Physics and Astronomy of the A. I. Herzen State Pedagogical University, especially Professors Alexander Zurabovich Devdariani, Evgeny Dmitrievich Trifonov, Alexander Sergeevich Troshin, Andrey Anatolyevich Grib, Associate Professor Igor Viktorovich Ryzhov, researcher at the Research Institute of Physics Vitaly Dmitrievich Vertogradov, as well as associate Professor of the Department of Methods of Teaching Physics Artemy Nikolaevich Krushelnitsky for useful discussions and the interest shown in the work. The author thanks the foundations of the RSF, RFBR, BASIS, as well as the Ministry of Science and Higher Education and the Ministry of Education for funding the research. The author expresses special gratitude to Natalia Sergeevna Shabanova for moral support throughout the work on the conducted research and all the research activities of the author, as well as to Galina Petrovna Voronova, who at one time insisted on continuing the author's studies at the university.

References

1. Korotin S., Kučinskas A. Abundance of beryllium in the Sun and stars: The role of non-local thermodynamic equilibrium effects // Astronomy & Astrophysics. 2022. Vol. 657. P. L11.

2. Popa S. A., Hoppe R., Bergemann M. et al. NLTE analysis of the methylidyne radical (CH) molecular lines in metal-poor stellar atmospheres // arXiv preprint arXiv:2212.06517. 2022.

3. Asplund M. New Light on Stellar Abundance Analyses: Departures from LTE and Homogeneity // Annual Review of Astronomy and Astrophysics. 2005. Vol. 43, no. 1. Pp. 481–530.

4. Proc. IAU Symp. 298, Setting the Scene for Gaia and LAMOST. Cambridge Univ. Press, Cambridge, 2014.

5. Barklem P. S. Accurate abundance analysis of late-type stars: advances in atomic physics // The Astronomy and Astrophysics Review. 2016. Vol. 24, no. 1. Pp. 1–54.

6. Ralchenko Yu. Application of large datasets to analysis of spectra from highly-charged high-Z ions // Book of Abstract of the 9th International Conference on Atomic and Molecular Data and Their Applications (September 21-25, 2014, Jena, Germany). 2014.

7. Launoy T., Loreau J., Dochain A. et al. Mutual Neutralization in Li^+-D^- Collisions: A Combined Experimental and Theoretical Study // The Astrophysical Journal. 2019. "— sep. Vol. 883, no. 1. P. 85. URL: https://doi.org/10.3847/1538-4357/ab3346.

8. Eklund G., Grumer J., Rosén S. et al. Cryogenic merged-ion-beam experiments in DESIREE: Final-state-resolved mutual neutralization of Li^+ and D^- // Phys. Rev. A. 2020. "— Jul. Vol. 102. P. 012823. URL: https://link.aps.org/doi/10.1103/PhysRevA.102.012823.

9. Grumer J., Eklund G., Amarsi A. M. et al. State-Resolved Mutual Neutralization of Mg^+ and D^- // Phys. Rev. Lett. 2022. "— Jan. Vol. 128. P. 033401. URL: https://link.aps.org/doi/10.1103/PhysRevLett.128.033401.

10. Eklund G., Grumer J., Barklem P. S. et al. Final-state-resolved mutual neutralization of Na+ and D- // Physical Review A. 2021. Vol. 103, no. 3. P. 032814.

11. Drawin H. W. On the analytical expression of the ionization cross section for atom-atom collisions and on the ion-electron recombination in dense neutral gases // Zeitschrift für Physik. 1968. Vol. 211. Pp. 404–417.

12. Drawin H. W. Influence of atom-atom collisions on the collisional-radiative ionization and recombination coefficients of hydrogen plasmas // Zeitschrift für Physik. 1969. Vol. 225. Pp. 483–493.

13. Steenbock W., Holweger H. Statistical equilibrium of lithium in cool stars of different metallicity // Astronomy and Astrophysics. 1984. Vol. 130. Pp. 319–323.

14. Barklem P. S., Belyaev A. K., Guitou M. et al. On inelastic hydrogen atom collisions in stellar atmospheres // Astronomy & Astrophysics. 2011. Vol. 530. P. A94.

15. Belyaev A. K., Barklem P. S. Cross sections for low-energy inelastic H + Li collisions // Physical Review A - Atomic, Molecular, and Optical Physics. 2003. Vol. 68, no. 6. P. 062703.

16. Belyaev A. K. Inelastic aluminium-hydrogen collision data for non-LTE applications in stellar atmospheres // Astronomy & Astrophysics. 2013. Vol. 560. P. A60.

17. Guitou M., Spielfiedel A., Rodionov D. S. et al. Quantum chemistry and nuclear dynamics as diagnostic tools for stellar atmosphere modeling // Chemical Physics. 2015. Vol. 462. P. 94–103.

18. Belyaev A. K., Vlasov D. V., Mitrushchenkov A., Feautrier N. Quantum study of inelastic processes in low-energy calcium–hydrogen collisions // Monthly Notices of the Royal Astronomical Society. 2019. Vol. 490, no. 3. Pp. 3384–3391.

19. Born M., Oppenheimer R. Zur Quantentheorie der Molekeln // Annalen der Physik. 1927. Vol. 389, no. 20. Pp. 457–484.

20. Belyaev A. K., Barklem P. S., Dickinson A. S., Gadéa F. X. Cross sections for low-energy inelastic H + Na collisions // Physical Review A - Atomic, Molecular, and Optical Physics. 2010. Vol. 81. P. 032706.

21. Belyaev A. K., Yakovleva S. A., Barklem P. S. Inelastic silicon-hydrogen collision data for non-LTE applications in stellar atmospheres // Astronomy & Astrophysics. 2014. Vol. 572. P. A103.

22. Yakovleva S.A. Model'nye podhody v issledovaniyah neuprugih processov pri medlennyh atomnyh stolknoveniyah: Kandidatskaya dissertaciya / RGPU im. A.I. Gercena. 2015.

23. Yakovleva S. A., Voronov Ya. V., Belyaev A. K. Uchet tonkoj struktury atomov shchelochnyh metallov pri neuprugih stolknoveniyah s vodorodom // Optika i spektroskopiya. 2019. Vol. 127, no. 2.

24. Belyaev A. K., Voronov Ya. V., Yakovleva S. A. Inelastic processes in calcium-hydrogen ionic collisions with account for fine structure // Physical Review A. 2019. Vol. 100, no. 6. P. 062710.

25. Voronov Ya. V., Yakovleva S. A., Belyaev A. K. Atomic data on inelastic processes in boron-hydrogen collisions with accounting for fine

structure // Monthly Notices of the Royal Astronomical Society. 2023. Vol. 520, no. 1. Pp. 107–112.

26. Belyaev Andrey K, Voronov Yaroslav V. Isotopic effects in low-energy lithium-hydrogen collisions // Physical Review A. 2021. Vol. 104, no. 2. P. 022812.

27. Bergemann M., Hoppe R., Semenova E. et al. Solar oxygen abundance // Monthly Notices of the Royal Astronomical Society. 2021. Vol. 508, no. 2. Pp. 2236–2253.

28. Mitrushchenkov A., Guitou M., Belyaev A. K. et al. Inelastic excitation and charge transfer processes for oxygen in collision with H atoms // Journal of Chemical Physics. 2019. Vol. 150. P. 064312.

29. Belyaev A. K., Voronov Ya. V., Mitrushchenkov A. et al. Inelastic processes in oxygen–hydrogen collisions // Monthly Notices of the Royal Astronomical Society. 2019. Vol. 487, no. 4. Pp. 5097–5105.

30. Belyaev A. K., Voronov Ya. V., Gadéa F. X. Data on Inelastic Processes in Low-energy Calcium–Hydrogen Ionic Collisions // The Astrophysical Journal. 2018. Vol. 867, no. 2. P. 87.

31. Belyaev Andrey K, Voronov Yaroslav V. Atomic Data on Inelastic Processes in Low-energy Lithium–Hydrogen Collisions // The Astrophysical Journal. 2018. Vol. 868, no. 2. P. 86.

32. Belyaev A. K., Voronov Ya. V., Yakovleva A., S. A. Mitrushchenkov et al. Atomic Data on Inelastic Processes in Calcium–Hydrogen Collisions // The Astrophysical Journal. 2017. Vol. 851.

33. Rodionov D.S. Neadiabaticheskie perekhody pri medlennyh atomnyh stolknoveniyah: Kandidatskaya dissertaciya / RGPU im. A.I. Gercena. 2015.

34. Belyaev A. K., Egorova D., Grosser J., Menzel T. Electron translation and asymptotic couplings in low - energy atomic collisions // Physical Review A - Atomic, Molecular, and Optical Physics. 2001. Vol. 64. P. 052701.

35. Hartree D. R. The wave mechanics of an atom with a non-coulomb central field. Part II. Some results and discussion // Mathematical Proceedings of the Cambridge Philosophical Society / Cambridge University Press. Vol. 24. 1928. Pp. 111–132.

36. Fock V. „Selfconsistent field “mit Austausch für Natrium // Zeitschrift für Physik. 1930. Vol. 62. Pp. 795–805.

37. Townsend J., Kirkland J. K., Vogiatzis K. D. Chapter 3 - Post-Hartree-Fock methods: configuration interaction, many-body perturbation theory, coupled-cluster theory // Mathematical Physics in Theoretical Chemistry / Ed. by S. M. Blinder, J. E. House. Elsevier, 2019. Developments in Physical & Theoretical Chemistry. Pp. 63–117.

38. Tihonov D.S. Sovremennaya teoreticheskaya himiya v sovremennom izlozhenii: Vazhnejshie koncepcii kvantovoj himii pod odnoj oblozhkoj. URSS, 2022. P. 512.

39. Dreizler R., Gross E. Density Functional Theory. Plenum Press, New York, 1995. P. 676.

40. Koch W., Holthausen M. C. A chemist’s guide to density functional theory. John Wiley & Sons, 2015. P. 294.

41. Smirnov B. M. Asimptoticheskie metody v teorii atomnyh stolknovenij. Atomizdat, 1973. P. 296.

42. Yakovleva S., Voronov Ya., Belyaev A. Atomic data on inelastic processes in low-energy beryllium-hydrogen collisions // Astronomy & Astrophysics. 2016. Vol. 593. P. A27.

43. Olson R. E., Smith F. T., Bauer E. Estimation of the Coupling Matrix Elements for One-Electron Transfer Systems // Appl. Optics. 1971. Vol. 10. P. 1848.

44. Olson R. E. Absorbing-Sphere Model for Calculating Ion—Ion Recombination Total Cross Sections // The Journal of Chemical Physics. 1972. Vol. 56, no. 6. Pp. 2979–2984.

45. Hedberg H. M., Nkambule S., Larson Å. Landau-Zener studies of mutual neutralization in collisions of $H^+ + H^-$ and $Be^+ + H^-$ // Journal of Physics B: Atomic, Molecular and Optical Physics. 2014. Vol. 47.

46. Smirnov B. M. Formation and decay of negative ions // Soviet Physics Doklady. Vol. 10. 1965. P. 218.

47. Smirnov B. M. Negative-Ion Gas Laser // Soviet Physics Doklady. Vol. 12. 1967. P. 242.

48. Janev R. K. Nonadiabatic transitions between ionic and covalent states // Advances in atomic and molecular physics. Elsevier, 1976. Vol. 12. Pp. 1–37.

49. Belyaev A. K., Voronov Ya. V. Atomic Data on Inelastic Processes in Low-Energy Manganese-Hydrogen Collisions // Astronomy & Astrophysics. 2017. Vol. 606. P. A106.

50. Barklem P. S. Excitation and charge transfer in low-energy hydrogen-atom collisions with neutral atoms: Theory, comparisons, and application to Ca // Physical Review A - Atomic, Molecular, and Optical Physics. 2016. Vol. 93. P. 042705.

51. Barklem P. S. Erratum: Excitation and charge transfer in low-energy hydrogen-atom collisions with neutral atoms: Theory, comparisons, and application to Ca [Phys. Rev. A 93, 042705 (2016)] // Physical

Review A - Atomic, Molecular, and Optical Physics. 2017. Vol. 95. P. 069906.

52. Grice R., Herschbach D. R. Long-range configuration interaction of ionic and covalent states // Molecular Physics. 1974. Vol. 27, no. 1. Pp. 159–175.

53. Adelman S. A., Herschbach D. R. Asymptotic approximation for ionic-covalent configuration mixing in hydrogen and alkali hydrides // Molecular Physics. 1977. Vol. 33, no. 3. Pp. 793–809.

54. Nikitin E.E., Umanskij S.Ya. Neadiabaticheskie perekhody pri medlennyh atomnyh stolknoveniyah. Atomizdat, 1979. P. 272.

55. Yakovleva S. A., Belyaev A. K., Kraemer W. P. Inelastic processes in low-energy iron-hydrogen collisions // Chemical Physics. 2018. Vol. 515. Pp. 369–374.

56. Yakovleva S. A., Belyaev A. K., Bergemann M. Cobalt-hydrogen atomic and ionic collisional data // Atoms. 2020. Vol. 8, no. 3. P. 34.

57. Sitnova T.M., Yakovleva S.A., Belyaev A.K., Mashonkina L.I. Vliyanie stolknovenij s vodorodom na opredelenie soderzhaniya titana v holodnyh zvezdah // Pis'ma v Astronomicheskij zhurnal: Astronomiya i kosmicheskaya astrofizika. 2020. Vol. 46, no. 2. Pp. 122–132.

58. Voronov Ya. V., Yakovleva S. A., Belyaev A. K. Inelastic Processes in Nickel–Hydrogen Collisions // The Astrophysical Journal. 2022. Vol. 926, no. 2. P. 173.

59. Grosser J. Angular momentum coupling in atom-atom collisions // Zeitschrift fur Physik D Atoms, Molecules and Clusters. 1986. Vol. 3, no. 1. Pp. 39–58.

60. Grosser J., Menzel T., Belyaev A. K. Approach to electron translation in low - energy atomic collisions // Physical Review A - Atomic, Molecular, and Optical Physics. 1999. Vol. 59. Pp. 1309–1316.

61. Belyaev A.K., Vlasov D.V., Kas'yanova A.M. K voprosu o neadiabaticheskih perekhodah pri atomnyh stolknoveniyah // Optika i spektroskopiya. 2007. Vol. 103. Pp. 956–960.

62. Yakovlev S. L., Yarevskij E. A., Elander N., Belyaev A. K. Ob asimptoticheskom reshenii mnogokanal'noj zadachi rasseyaniya s neadiabaticheskoj svyaz'yu kanalov // Teoreticheskaya i matematicheskaya fizika. 2018. Vol. 195, no. 3. Pp. 437–450.

63. Bates D. R., McCarroll R. Electron Capture in Slow Collisions // Proceedings of The Royal Society A. 1958. Vol. 245. Pp. 175–183.

64. Landau L. D. Zur Theorie der Energieübertragung bei Stößen // Physikalische Zeitschrift der Sowjetunion. 1932. Vol. 1, no. 2. Pp. 46–51.

65. Landau L. D. Zur Theorie der Energieübertragung bei Stößen // Physikalische Zeitschrift der Sowjetunion. 1932. Vol. 1, no. 1. Pp. 88–98.

66. Zener C. Non-adiabatic crossing of energy levels // Proceedings of the Royal Society of London. Series A, Containing Papers of a Mathematical and Physical Character. 1932. Vol. 137, no. 833. Pp. 696–702.

67. Nikitin E. E. Veroyatnost' neadiabaticheskih perekhodov v sluchae neraskhodyashchihsya termov // Optika i spektroskopiya. 1962. Vol. 13, no. 6. Pp. 761–765.

68. Nikitin E. E. Resonance and non-resonance intermolecular energy exchange in molecular collisions // Discussions of the Faraday Society. 1962. Vol. 33. Pp. 14–21.

69. Demkov Yu.N. Perezaryadka pri malom defekte rezonansa // Zhurnal eksperimental'noj i teoreticheskoj fiziki. 1963. Vol. 45, no. 2. Pp. 195–201.

70. Stüeckelberg E. C. G. Theorie der unelastischen Stößen zwischen Atomen // Helvetica Physica Acta. 1932. Vol. 5. Pp. 369–422.

71. Nikitin E. E. Teoriya elementarnyh atomno-molekulyarnyh reakcij. CHast' I. – Metody. Izd-vo Novosibirskogo gos. un-ta, 1971.

72. Child M. S. Molecular collision theory. Courier Corporation, 1996. P. 300.

73. Nikitin E. E. Theory of non-adiabatic transitions. recent developement of the Landau-Zener (Linear) model. 1968.

74. Belyaev A. K., Lebedev O. V. Nonadiabatic nuclear dynamics of atomic collisions based on branching classical trajectories // Physical Review A - Atomic, Molecular, and Optical Physics. 2011. Vol. 84, no. 1. P. 014701.

75. Belyaev A. K. Model approach for low-energy inelastic atomic collisions and application to Al + H and $Al^+ + H^-$ // Physical Review A - Atomic, Molecular, and Optical Physics. 2013. Vol. 88, no. 5. P. 052704.

76. Tully J. C. Molecular dynamics with electronic transitions // The Journal of Chemical Physics. 1990. Vol. 93, no. 2. Pp. 1061–1071.

77. Bjerre A., Nikitin E. E. Energy transfer in collisions of an excited sodium atom with a nitrogen molecule // Chemical Physics Letters. 1967. Vol. 1, no. 5. Pp. 179–181.

78. Tully J. C., Preston R. K. Trajectory surface hopping approach to nonadiabatic molecular collisions: the reaction of H+ with D2 // The Journal of Chemical Physics. 1971. Vol. 55, no. 2. Pp. 562–572.

79. Fermanian Kammerer C., Lasser C. Single switch surface hopping for molecular dynamics with transitions // The Journal of Chemical Physics. 2008. Vol. 128, no. 14. P. 144102.

80. Demkov Yu. N., Osherov V. I. Stationary and nonstationary problems in quantum mechanics that can be solved by means of contour integration // Soviet Journal of Experimental and Theoretical Physics. 1968. Vol. 26, no. 5. Pp. 916–921.

81. Vikipediya. CUDA — Vikipediya, svobodnaya enciklopediya [Elektronnyj resurs]. 2018. URL: https://ru.wikipedia.org/wiki/CUDA.

82. Vikipediya. OpenCL — Vikipediya, svobodnaya enciklopediya [Elektronnyj resurs]. 2018. URL: https://ru.wikipedia.org/wiki/OpenCL.

83. Belyaev A.K. Peredacha vozbuzhdeniya v sluchae trekh vzaimodejstvuyushchih termov // Himicheskaya fizika. 1985. Vol. 4. Pp. 750–758.

84. Landau L.D., Lifshic E.M. Kurs teoreticheskoj fiziki. Tom III. Kvantovaya mekhanika (nerelyativistskaya teoriya). FIZMATLIT, 2002. P. 808.

85. Neretina M. D., Mashonkina L. I., Sitnova T. M. et al. Influence of Collisions with Hydrogen Atoms on Non-LTE Effects for K I and Ca II in Stellar Atmospheres // Astronomy Letters. 2020. Vol. 46, no. 9. Pp. 621–629.

86. Belyaev A. K., Voronov Ya. V. Atomic Data on Inelastic Processes in Boron–Hydrogen Collisions // Astronomy Letters. 2022. Vol. 48, no. 3. Pp. 178–184.

87. Steffen M., Prakapavičius D., Caffau E. et al. The photospheric solar oxygen project. IV. 3D-NLTE investigation of the 777 nm triplet lines // Astronomy & Astrophysics. 2015. Vol. 583. P. A57.

88. Berg D. A., Skillman E. D., Henry R. B. C. et al. Carbon and Oxygen Abundances in Low Metallicity Dwarf Galaxies // Astrophysical Journal. 2016. Vol. 827. P. 126.

89. Bertran de Lis S., Allende Prieto C., Majewski S. R. et al. Cosmic variance in [O/Fe] in the Galactic disk // Astronomy & Astrophysics. 2016. Vol. 590. P. A74.

90. Brewer J. M., Fischer D. A. C/O and Mg/Si Ratios of Stars in the Solar Neighborhood // Astrophysical Journal. 2016. Vol. 831. P. 20.

91. Wilson D. J., Gänsicke B. T., Farihi J., Koester D. Carbon to oxygen ratios in extrasolar planetesimals // Monthly Notices of the Royal Astronomical Society. 2016. Vol. 459. Pp. 3282–3286.

92. Sitnova T. M., Mashonkina L. I. Influence of Inelastic Collisions with Hydrogen Atoms on Non-LTE Oxygen Abundance Determinations // Astronomy Letters. 2018. Vol. 44, Issue 6. Pp. 411–419.

93. Matteucci F., Francois P. Oxygen abundances in halo stars as tests of galaxy formation // Astronomy & Astrophysics. 1992. Vol. 262. Pp. L1–L4.

94. Gratton R. G., Carretta E., Matteucci F., Sneden C. Abundances of light elements in metal-poor stars. IV. [Fe/O] and [Fe/Mg] ratios and the history of star formation in the solar neighborhood // Astronomy & Astrophysics. 2000. Vol. 358. Pp. 671–681.

95. Barklem P. S. Electron-impact excitation of neutral oxygen // Astronomy & Astrophysics. 2007. Vol. 462, no. 2. Pp. 781–788.

96. Israelian G., López R. J. G., Rebolo R. Oxygen abundances in unevolved metal-poor stars from near-ultraviolet OH lines // The Astrophysical Journal. 1998. Vol. 507, no. 2. P. 805.

97. Boesgaard A. M., King J. R., Deliyannis C. P., Vogt S. S. Oxygen in unevolved metal-poor stars from keck ultraviolet hires spectra // The Astronomical Journal. 1999. Vol. 117, no. 1. P. 492.

98. Nissen P. E., Primas F., Asplund M., Lambert D. L. O/Fe in metal-poor main sequence and subgiant stars // Astronomy & Astrophysics. 2002. Vol. 390, no. 1. Pp. 235–251.

99. Pérez A. E. G., Asplund M., Primas F. et al. Oxygen abundances in metal-poor subgiants as determined from [O i], O i and OH lines // Astronomy & Astrophysics. 2006. Vol. 451, no. 2. Pp. 621–642.

100. Pazira H., Kiselman D., Leenaarts J. Solar off-limb emission of the O I 7772 Å line // Astronomy & Astrophysics. 2017. Vol. 604. P. A49.

101. Amarsi A. M., Barklem P. S., Asplund M. et al. Inelastic O+H collisions and the O I 777 nm solar centre-to-limb variation // Astronomy & Astrophysics. 2018. Vol. 616. P. A89.

102. Qin X., Zhang S. D. Low-lying electronic states of the OH radical: Potential energy curves, dipole moment functions, and transition probabilities // Journal of the Korean Physical Society. 2014. Vol. 65, no. 12. Pp. 2017–2022.

103. van Dishoeck E. F., Langhoff S. R., Dalgarno A. The low-lying 2Σ-states of OH // The Journal of Chemical Physics. 1983. Vol. 78, no. 7. Pp. 4552–4561.

104. van der Loo M. P. J., Groenenboom G. C. Ab initio calculation of (2+1) resonance enhanced multiphoton ionization spectra and lifetimes of

the (D, 3) Σ- 2 states of OH and OD // The Journal of chemical physics. 2005. Vol. 123, no. 7. P. 074310.

105. Li L., Nikiforov A., Xiong Q. et al. Measurement of OH radicals at state X 2Π in an atmospheric-pressure micro-flow dc plasma with liquid electrodes in He, Ar and N2 by means of laser-induced fluorescence spectroscopy // Journal of Physics D: Applied Physics. 2012. Vol. 45, no. 12. P. 125201.

106. Barklem P. S. Excitation and charge transfer in low-energy hydrogen atom collisions with neutral oxygen // Astronomy & Astrophysics. 2018. Vol. 610. P. A57.

107. Belyaev A. K., Yakovleva S. A. Estimating Inelastic Heavy-Particle-Hydrogen Collision Data. I. Simplified Model and Application to Potassium-Hydrogen Collisions // A&A. 2017. Vol. 606. P. A147.

108. Belyaev A. K., Yakovleva S. A. Estimating Inelastic Heavy-Particle-Hydrogen Collision Data. II. Simplified model for ionic collisions and application to barium-hydrogen ionic collisions // A&A. 2017. Vol. 608. P. A33.

109. Kramida A., Ralchenko Yu., Reader J., Team NIST ASD. NIST Atomic Spectra Database (version 5.10), [Online]. 2022. URL: https://physics.nist.gov/asd.

110. Hörnquist J., Hedvall P., Larson Å., Orel A. E. Mutual neutralization in $H^+ + H^-$ collisions: An improved theoretical model // Phys. Rev. A. 2022. "— Dec. Vol. 106. P. 062821. URL: https://link.aps.org/doi/10.1103/PhysRevA.106.062821.

111. Drake J. J. A non-LTE study of neutral calcium in late-type stars with special reference to Pollux // MNRAS. 1991. Vol. 251. Pp. 369–378.

112. Korn A. J., Richard O., Mashonkina L. et al. HE 1327–2326, an unevolved star with [Fe/H] < –5.0. III. Does its atmosphere reflect its natal composition? // The Astrophysical Journal. 2009. Vol. 698, no. 1. P. 410.

113. Mashonkina L., Sitnova T., Belyaev A. K. Influence of inelastic collisions with hydrogen atoms on the non-LTE modelling of Ca I and Ca II lines in late-type stars // Astronomy & Astrophysics. 2017. Vol. 605. P. A53.

114. Habli H., Dardouri R., Oujia B., Gadéa F. X. Ab Initio Adiabatic and Diabatic Energies and Dipole Moments of the CaH^+ Molecular Ion // The Journal of Physical Chemistry A. 2011. Vol. 115. Pp. 14045–14053.

115. Habli H., Ghalla H., Oujia B., Gadéa F. X. Ab initio study of spectroscopic properties of the calcium hydride molecular ion // The European Physical Journal D. 2011. Vol. 64. Pp. 5–19.

116. Mashonkina L., Korn A. J., Przybilla N. A non-LTE study of neutral and singly-ionized calcium in late-type stars // Astronomy & Astrophysics. 2007. Vol. 461, no. 1. Pp. 261–275.

117. Sitnova T. M., Mashonkina L. I., Ryabchikova T. A. A NLTE line formation for neutral and singly ionized calcium in model atmospheres of BF stars // Monthly Notices of the Royal Astronomical Society. 2018. Vol. 477, no. 3. Pp. 3343–3352.

118. Nissen P. E., Schuster W. J. Two distinct halo populations in the solar neighborhood-Evidence from stellar abundance ratios and kinematics // Astronomy & Astrophysics. 2010. Vol. 511. P. L10.

119. Bensby T., Yee J. C., Feltzing S. et al. Chemical evolution of the Galactic bulge as traced by microlensed dwarf and subgiant stars-V.

Evidence for a wide age distribution and a complex MDF // Astronomy & Astrophysics. 2013. Vol. 549. P. A147.

120. Nomoto K., Kobayashi C., Tominaga N. Nucleosynthesis in stars and the chemical enrichment of galaxies // Annual Review of Astronomy and Astrophysics. 2013. Vol. 51. Pp. 457–509.

121. Keller S. C., Bessell M. S., Frebel A. et al. A single low-energy, iron-poor supernova as the source of metals in the star SMSS J031300. 36- 670839.3 // Nature. 2014. Vol. 506, no. 7489. Pp. 463–466.

122. Starkenburg E., Hill V., Tolstoy E. et al. The NIR Ca ii triplet at low metallicity-Searching for extremely low-metallicity stars in classical dwarf galaxies // Astronomy & Astrophysics. 2010. Vol. 513. P. A34.

123. Merle T., Thévenin F., Pichon B., Bigot L. A grid of non-local thermodynamic equilibrium corrections for magnesium and calcium in late-type giant and supergiant stars: application to Gaia // Monthly Notices of the Royal Astronomical Society. 2011. Vol. 418, no. 2. Pp. 863–887.

124. Zhao G., Mashonkina L., Yan H. L. et al. Systematic non-LTE study of the- 2.6?[Fe/H]? 0.2 F and G dwarfs in the solar neighborhood. II. Abundance patterns from Li to Eu // The Astrophysical Journal. 2016. Vol. 833, no. 2. P. 225.

125. Belyaev A. K., Yakovleva S. A., Guitou M. et al. Model estimates of inelastic calcium-hydrogen collision data for non-LTE stellar atmospheres modeling // Astronomy & Astrophysics. 2016. Vol. 587. P. A114.

126. Mitrushchenkov A., Guitou M., Belyaev A. K. et al. Calcium-hydrogen interactions for collisional excitation and charge transfer // Journal of Chemical Physics. 2017. Vol. 146. P. 014304.

127. Randich S., Magrini L. Light Elements in the Universe // Front. Astron. Space Sci. 2021. Vol. 8. P. 6.

128. Fields B. D. The Primordial Lithium Problem // Annual Review of Nuclear and Particle Science. 2011. "— Nov. Vol. 61, no. 1. Pp. 47–68. URL: http://dx.doi.org/10.1146/annurev-nucl-102010-130445.

129. Spite Fr., Spite M. Abundance of lithium in unevolved halo stars and old disk stars-Interpretation and consequences // Astronomy and Astrophysics. 1982. Vol. 115. Pp. 357–366.

130. Steffen M., Cayrel R., Caffau E. et al. ^{6}Li detection in metal-poor stars: can 3D model atmospheres solve the second lithium problem? // Memorie della Società Astronomica Italiana (Mem. S.A.It.). 2008. Vol. 75. Pp. 282–293.

131. Wang E. X., Nordlander T., Asplund M. et al. 3D NLTE spectral line formation of lithium in late-type stars // Monthly Notices of the Royal Astronomical Society. 2021. Vol. 500, no. 2. Pp. 2159–2176.

132. Varshalovich D. A., Ivanchik A. V., Balashev S. A., Petitjean P. Big Bang nucleosynthesis of deuterium and HD/H2 molecular abundances in interstellar clouds of 12 Gyr ago // Physics-Uspekhi. 2010. "— jul. Vol. 53, no. 4. Pp. 397–401.

133. Pitrou C., Coc A., Uzan J.-P., Vangioni E. Precision Big Bang nucleosynthesis with improved Helium-4 predictions // Physics Reports. 2018. Vol. 754. Pp. 1–66.

134. Hernández J. I. G., Bonifacio P., Caffau E. et al. The 6Li/7Li isotopic ratio in the metal-poor binary CS22876–032 // Astronomy & Astrophysics. 2019. Vol. 628. P. A111.

135. Fields B. D. A deeper look at a cosmic nuclear reaction // Nature. 2020. Vol. 587. Pp. 203–204.

136. Fields B. D., Olive K. A., Yeh T.-H., Young C. Big-Bang Nucleosynthesis after Planck // Journal of Cosmology and Astroparticle Physics. 2020. Vol. 2020, no. 3. P. 010.

137. Gai M., Kading E. E., Hass M. et al. The Interaction of Neutrons with ^{7}Be at BBN Temperatures: Lack of Standard Nuclear Solution to the "Primordial ^{7}Li Problem" // European Physical Journal Web of Conferences. Vol. 227 of European Physical Journal Web of Conferences. 2020. P. 01007.

138. Molaro P., Cescutti G., Fu X. Lithium and beryllium in the Gaia-Enceladus galaxy // Monthly Notices of the Royal Astronomical Society. 2020. Vol. 496, no. 3. Pp. 2902–2909.

139. Starrfield S., Bose M., Iliadis C. et al. Carbon-Oxygen Classical Novae Are Galactic ^{7}Li Producers as well as Potential Supernova Ia Progenitors // Astrophysical Journal. 2020. Vol. 895, no. 1. P. 70.

140. Carlsson M., Rutten R. J., Bruls J. H. M. J, Shchukina N. G. The non-LTE formation of Li I lines in cool stars // Astronomy & Astrophysics. 1994. Vol. 288. Pp. 860–882.

141. de La Reza R., da Silva L. Lithium abundances in strong lithium K giant stars: LTE and non-LTE analyses // The Astrophysical Journal. 1995. Vol. 439. Pp. 917–927.

142. Lind K., Asplund M., Barklem P. S. Departures from LTE for neutral Li in late-type stars // Astronomy & Astrophysics. 2009. Vol. 503, no. 2. Pp. 541–544.

143. Lind K., Melendez J., Asplund M. et al. The lithium isotopic ratio in very metal-poor stars // Astronomy & Astrophysics. 2013. Vol. 554. P. A96.

144. Barklem P. S., Belyaev A. K., Asplund M. Inelastic H + Li and H^- + Li^+ collisions and non-LTE Li in line formation in stellar atmospheres // Astronomy & Astrophysics. 2003. Vol. 409, no. 2. Pp. L1–L4.

145. Peart B., Foster S. J. Measurements of mutual neutralisation of Li+ with H-ions and of Na+ with O-ions // Journal of Physics B: Atomic and Molecular Physics. 1987. Vol. 20, no. 21. P. L691.

146. Peart B., Hayton D. A. Merged beam measurements of the mutual neutralization of He+/H-and Li+/D-ions // Journal of Physics B: Atomic, Molecular and Optical Physics. 1994. Vol. 27, no. 12. P. 2551.

147. Boutalib A., Gadéa F. X. Ab initio adiabatic and diabatic potential-energy curves of the LiH molecule // The Journal of chemical physics. 1992. Vol. 97, no. 2. Pp. 1144–1156.

148. Croft H., Dickinson A. S., Gadéa F. X. A theoretical study of mutual neutralization in Li^+ + H^- collisions // Journal of Physics B: Atomic, Molecular and Optical Physics. 1999. Vol. 32, no. 1. Pp. 81–94.

149. Gadéa F. X., Boutalib A. Computation and assignment of radial couplings using accurate diabatic data for the LiH molecule // Journal of Physics B: Atomic, Molecular and Optical Physics. 1993. Vol. 26, no. 1. P. 61.

150. Schmidt-May A. F., Eklund G., Rosén S. et al. Experimental confirmation of the isotope effect on the branching in mutual neutralization // Proceedings of the DESIREE Symposium. 2022. P. 23.

151. Croft H., Dickinson A. S., Gadéa F. X. Rate coefficients for the Li^+/H^- and Li^-/H^+ mutual neutralization reactions // MNRAS. 1999. Vol. 304. Pp. 327–329.